LAMINARISATION IN STRONGLY ACCELERATED BOUNDARY LAYERS

by

William Philip Jones B.Sc., D.I.C., M.Sc.

Thesis submitted for the degree of
Doctor of Philosophy
in the Faculty of Engineering
University of London

September 1971

ABSTRACT

Three accelerated turbulent boundary layers have been set up in a plane convergent channel and studied experimentally. The accelerations considered correspond to values of K ($\equiv \nu/U_{1,G}^2 \frac{dU_{1,G}}{dx_1}$) equal to 1.5×10^{-6}, 2.5×10^{-6} and 3.0×10^{-6} and encompass the range over which laminarisation of the turbulent boundary layer is known to occur. Mean velocity profile measurements in the three boundary layers showed a deviation from a fully turbulent solution towards that appropriate to a laminar flow as K was increased. Measurements of fluctuating quantities made with a constant temperature hot-wire anemometer served to emphasize some of the differences between the turbulence structure of low Reynolds number accelerated boundary layers and that normally observed in high Reynolds number flows.

The main outcome of the theoretical programme has been the provision of a new model of turbulence which is applicable to both the fully turbulent and the viscous sublayer regions of the boundary layer. The model involves solution of partial differential rate equations for turbulence kinetic energy and dissipation rate of turbulence energy together with the mean momentum, thermal energy (for heat transfer predictions) and continuity equations.

The model has been applied to the prediction of wall boundary layer flows in which the accelerations are so severe that the boundary layer reverts partially towards laminar. In all cases, the predicted hydrodynamic and heat transfer development of the boundary layers is in close agreement with the measured behaviour.

Acknowledgements

The author wishes to express his gratitude to his supervisor, Dr. B.E. Launder, who initiated the work described in this thesis, for his advice, guidance and assistance throughout all stages of the project.

The author is also indebted to the members of his thesis committee, Dr. J.H. Whitelaw and Dr. R.G. Taylor for their constant interest, advice and suggestions.

Thanks are also due to other colleagues, librarian and technical staff who have contributed at various stages to the successful completion of this work.

All the numerical computations reported in this thesis were performed with the aid of digital computers under the control of the University of London computing centre.

Contents

CHAPTER 1

INTRODUCTION

1.1 General Background

The behaviour of turbulent boundary layers in accelerating flows is a subject which has attracted a number of experimental examinations in recent years. The most important finding to be established by these studies is that, when the acceleration is severe enough, the originally turbulent boundary layer undergoes a reversion towards laminar (refs. 2, 49, 50, 63 and 80). The phenomenon has been variously termed 'laminarisation', 'reverse transition', 'inverse-transition' and 're-laminarisation'; the first of these will be adopted for the present work.

The majority of the measurements of strongly accelerated boundary layers have been of highly non-equilibrium flows; that is, of flows where the structure undergoes rapid evolution in the direction of flow. In these cases it is not possible to ascribe a single parameter to denote precisely when laminarisation will occur. However Launder (49), Moretti and Kays (63), Patel and Head (68) and Schraub and Kline (80) found experimentally that the parameter $K \left[= \frac{\nu}{U_{1,G}^2} \frac{dU_{1,G}}{dx_1}\right]$ provided a useful if rough guide as to when an accelerated turbulent boundary layer would undergo reversion to laminar. If a turbulent boundary layer is subjected to an acceleration of magnitude

so that K exceeds a value of approximately 3×10^{-6} then reversion to laminar flow will eventually ensue.

Accelerations giving rise to values of K at least an order of magnitude larger than the above commonly arise in rocket nozzles and in flow over turbine blades. Values of K of the order 10^{-6} may arise in many other fluid flow devices, e.g. in wind tunnel contractions and in closely packed heat exchanger tube banks. The problem is thus one of substantial practical significance.

'Constant-K' Boundary Layers

The flow which develops in a plane convergent channel gives rise to boundary layers which are completely similar for both laminar and turbulent flow. In turbulent flow, it is the only flow configuration with varying free stream velocity in which the characteristic viscous and turbulence length scales may develop at the same rate; thus it is the only case where complete similarity of the turbulent boundary layer may exist. For these boundary layers the acceleration parameter K, skin friction coefficient and any local Reynolds number are invariant with x_1.

The work of Schraub and Kline (80) first indicated that the study of 'constant-K' boundary layers might be of special relevance to the problem of laminarisation. They examined the sublayer structure of accelerated turbulent boundary layers by means of dye injection and hydrogen bubble techniques. They found that the sinuous low momentum sublayer streaks which are a feature of

turbulent boundary layers on smooth surfaces did not suddenly cease to form above a certain level of acceleration. Instead they suffered a progressive diminution as the value of K was steadily increased. On the basis of their results Schraub and Kline suggested that the boundary layers could be placed in three categories.

(1) $K < 10^{-6}$: no detectable effects of the acceleration on the sublayer structure of the boundary layer.

(2) $10^{-6} \leq K < 3.5 \times 10^{-6}$: sublayer structure of the boundary layer markedly affected by the acceleration but the layer remains essentially turbulent.

(3) $K \geq 3.5 \times 10^{-6}$: a complete degeneration to laminar flow occurs if the acceleration continues for sufficient time.

Although Schraub and Kline's experiments were performed in boundary layer flows in which K varied in the x_1 direction the measurements suggested that it would be possible to set up a family of constant K similar boundary layers which would exhibit a progressive shift from turbulent to laminar as K was increased. That this was indeed the case was demonstrated by Launder and Stinchcombe (51). They investigated experimentally turbulent boundary layers at three constant values of acceleration parameter K (0.7×10^{-6}, 1.3×10^{-6}, 3.0×10^{-6}). As K was increased

their mean velocity profiles exhibited a continuous shift towards those appropriate to a laminar flow. Acceleration eliminated the wake and made less definite any division between the viscous sublayer and the fully turbulent regions of the layer. In addition, Launder and Stinchcombe made hot wire measurements showing high turbulence intensities, which indicated that the boundary layers were all essentially turbulent. However Launder and Stinchcombe acknowledged that their measurements suffered from substantial three-dimensional effects and that their measurements thus served to indicate qualitative trends only.

Support for the above conclusion also arises from experimental heat transfer studies. Moretti and Kays (63) have noted a substantial reduction in Stanton number on the application of a negative pressure gradient (acceleration) and a subsequent rise on its removal. However their data showed detectable dips in Stanton number even for accelerations where K did not exceed 10^{-6}; that is barely one third of that required to cause complete degeneration of a turbulent flow to laminar.

1.2 Prediction of Laminarisation

In view of the practical importance of the phenomena in question, a means of predicting both its occurrence and consequences is clearly desirable. Now, recent years have seen a significant advance in the development of means of predicting both laminar and, most especially, turbulent flow.

This advance has been brought about by the advent of the high speed digital computer which has made possible the development of a number of numerical schemes for solution of the time averaged forms of the partial differential equations which govern fluid motion e.g. references (1) and (31). However, for turbulent flow, averaging results in a loss of information to the point where the equations of motion are not closed. Unknown velocity correlations arise and these must be approximated in terms of known quantities to produce a closed set of equations before solution can be attempted. Such an approximation is here termed a 'turbulence model'.

For steady turbulent boundary layer flows a number of authors (e.g. ref. (69)) have made use of the Prandtl mixing-length model of turbulence to obtain predictions. More recently more complex turbulence models have also been utilised e.g. references (62) and (65). Generally the results obtained provide predictions of sufficient accuracy for practical engineering purposes over a wide range of boundary layer flows. However to the knowledge of the writer these models all fail to predict the main properties of boundary layers undergoing laminarisation. For example the predictions of Moretti and Kay's data presented by Patankar and Spalding (69) fail to display any dip in Stanton number in the region of acceleration and as a result the predicted heat transfer rates at the end of the acceleration were typically twice as high as the measured values.

1.3 The present contribution

The foregoing sections have pointed to the absence of a reliable means of predicting the development of the turbulent boundary layer in an acceleration. Also, from the experimental viewpoint, it is evident that the majority of measurements of accelerated boundary layers have been of highly non-equilibrium flows; that is flows where the turbulence structure undergoes rapid evolution in the direction of flow. In these cases it is difficult, if not impossible to separate the effects of flow 'history' from those of acceleration. With the aforementioned points in mind the present work was embarked upon: its purpose was twofold:-

(1) To study experimentally the hydrodynamic behaviour of a turbulent boundary layer when subjected to strong acceleration. This was carried out by means of an examination of the similar turbulent boundary layers which arise from flow in a plane convergent channel. These boundary layers have special relevance to the phenomenon of laminarisation since they have a turbulence structure which is 'frozen' in the flow direction. The effects of acceleration may thus be considered in isolation from those of flow 'history'. The accelerations considered covered the range over which laminarisation was known to occur i.e. $10^{-6} < K < 3.0 \times 10^{-6}$. The experiments included measurements of mean and fluctuating quantities and may thus help to provide a better understanding of laminarisation.

(2) To develop a reliable means of predicting the behaviour of the turbulent boundary layer when subject to strong acceleration, i.e. laminarisation. The procedure must be capable of predicting the development of both the hydrodynamic and thermal boundary layers and thus provide predictions of local heat transfer rates and skin friction coefficients. It is desirable that the method be as general as possible so that it may be easily extended to handle flow situations where, in addition to acceleration, large fluid property variations and surface mass transfer are present. At the same time the procedure must be economical and easy to use.

1.4 Outline of Thesis

This thesis is divided into five chapters of which this introduction is the first.

The second chapter introduces the reader to the relevant equations of fluid motion. Included are the partial differential equations which govern the development of the boundary layer. Also presented are the ordinary differential equations to which the above stated partial differential equations reduce for the similar boundary layer.

Chapter three contains a description of the writer's experimental work. It begins with a review of previous relevant experimental work by other workers. This is followed by a description of the experimental apparatus, instrumentation and experimental technique. Finally the

results obtained are presented and discussed. Comparisons are made with other data where appropriate.

Chapter four contains the writer's theoretical contribution to the present work. The chapter is split into four main sections:-

(1) The chapter begins with a review of existing models of turbulence. The review covers a range from the 'simple' models which attempt a description of turbulence purely in terms of the mean velocity to the more complex types in which turbulence is described in terms of various (and many) properties.

(2) Section two is concerned with predictions of accelerated boundary layers obtained through numerical solution of the boundary layer equations with an 'augmented' mixing length model of turbulence. The path followed in devising the model is outlined together with the checks made on the numerical accuracy of the solutions. The section ends with some comments on the mixing length model.

(3) Section three is devoted to a turbulence model which is based on the solution of a partial differential rate equation for turbulence kinetic energy together with an algebraic length scale distribution. Comparisons between prediction and experiment are made.

(4) Finally in section four a new turbulence model is presented in which characteristic velocity and length scales of the turbulence are obtained from the solution of partial

differential rate equations for turbulence kinetic energy and dissipation rate of turbulence kinetic energy. The section and Chapter ends with a comparison between predicted and experimental hydrodynamic and heat transfer results.

Finally in Chapter five the achievements of chapters three and four are summarised and re-appraised. Suggestions are made for future theoretical and experimental work.

CHAPTER II

THE EQUATIONS OF MOTION

2.1 Introductory Remarks

The purpose of this chapter is both to provide the reader with an introduction to the mathematical description of the motion of a fluid continuum and to provide a foundation for the presentation and discussion of the results of the present study. The motion of any fluid is governed by the physical laws of conservation of mass and momentum (Newton's 2nd Law) which in this case may be expressed through the continuity and Navier-Stokes equations. The chapter begins with a statement of these equations. For turbulent flows it is not practicable to attempt solution of the equations and the approach commonly adopted for their treatment is that of averaging the equations. The averaged Navier-Stokes equation is therefore next to be presented. The remaining part of the chapter is concerned with the equations of the boundary layer to which the present work is restricted. The boundary layer forms of the averaged Navier-Stokes equation are presented together with various integral equations which may be derived therefrom. Finally, the chapter ends with a presentation of the ordinary differential equation to which the partial differential boundary layer equation reduces for the similar boundary layer with which part of the present work is concerned.

2.2 The Navier Stokes and continuity equations

The spatial distribution of velocity with time of a fluid continuum is represented by the Navier-Stokes equation. For an incompressible, Newtonian fluid this may be written in cartesian tensor notation as:-

$$\rho\frac{\partial U_i}{\partial t} + \rho\, U_j \frac{\partial U_j}{\partial x_j} = -\frac{\partial P}{\partial x_i} + \mu \frac{\partial^2 U_i}{\partial x_j \partial x_j} \qquad (2.1)$$

To this must be added the continuity equation

$$\frac{\partial U_i}{\partial x_i} = 0 \qquad (2.2)$$

(repeated suffices imply summation over the three values of the repeated suffix).

The above equations together with boundary conditions represent a closed set, the solution of which would in principle provide a complete description of any turbulent flow. However these equations are extremely complex and for turbulent flow appear impossibly difficult to solve. Turbulent motion is three-dimensional in nature and has appreciably variations in velocity over times and lengths which are small (typically of the order 10^{-2} secs and 10^{-3} m. respectively); numerical solution of the equations is therefore not practicable. Therefore the approach adopted here is that followed by the vast majority of workers in the field of turbulent flow: the equations are averaged to convert them into equations for the variation of statistical quantities. This treatment was first used by O. Reynolds (74) and is perhaps the only practical approach to the problem of turbulent motion.

The total velocity and pressure are each separated into mean and fluctuating components:-

$$P = \bar{P} + p \; ; \quad U_i = \bar{U}_i + u_i \qquad (2.3)$$

where $\bar{P}$ and $\bar{U}_i$, the time* mean values of P and U_i respectively are defined by:-

$$\bar{P} = \lim_{T\to\infty} \frac{1}{T} \int_0^T P \, dt \; ; \quad \overline{U_i} = \lim_{T\to\infty} \frac{1}{T} \int_0^T U_i \, dt$$

The fluctuating components thus have zero mean values.

On substituting (2.3) and averaging the Navier-Stokes equation the following result is obtained:-

$$\rho \, \bar{U}_j \frac{\partial \bar{U}_i}{\partial x_j} = -\frac{\partial \bar{P}}{\partial x_i} + \frac{\partial}{\partial x_j} \{ \mu \frac{\partial \bar{U}_i}{\partial x_j} - \rho \, \overline{u_i u_j} \} \qquad (2.4)$$

where the overbars denote averaged values: for brevity they will be dropped from the means $\bar{U}$ and $\bar{P}$ from hereon. Equation (2.4) is known as the Reynolds equation. It contains the unknown velocity correlation, $\overline{u_i u_j}$ which represents the mean rate of transfer of momentum by turbulent movements. The velocity correlation $\overline{u_i u_j}$ has been traditionally termed the Reynolds stress tensor; if it could be determined then the mean motion would be known.

An equation for $\overline{u_i u_j}$ may be derived by further manipulation of the Navier-Stokes equation. It may be written:-

---

* In general the only meaningful average is the probability (or ensemble) average. However for flows with mean values stationary in time, to which the present work is restricted, the probability and time average are identical.

$$\frac{DR_{ij}}{Dt} = -R_{im}\frac{\partial U_j}{\partial x_m} - R_{jm}\frac{\partial U_i}{\partial x_m} - \frac{\partial}{\partial x_m}\{\overline{u_i u_j u_m}\}$$

$$- \frac{1}{\rho}\left[\frac{\partial}{\partial x_i}\overline{u_j p} + \frac{\partial}{\partial x_j}\overline{u_i p}\right] + \overline{\frac{p}{\rho}\left[\frac{\partial u_i}{\partial x_j} + \frac{\partial u_j}{\partial x_i}\right]}$$

$$+ \nu\frac{\partial^2 R_{ij}}{\partial x_m \partial x_m} - 2\nu\,\overline{\frac{\partial u_i}{\partial x_m}\cdot\frac{\partial u_j}{\partial x_m}} \qquad (2.5)$$

where $R_{ij} \equiv \overline{u_i u_j}$

As may be readily observed, further unknown quantities appear on the R.H.S. of equation (2.5).

Equation (2.5) may be contracted to yield an equation for the turbulence kinetic energy:-

$$\frac{Dk}{Dt} = \frac{\partial}{\partial x_m}\left\{\frac{\partial k}{\partial x_m} - \overline{u_m\left(\frac{u_j u_j}{2} + P/\rho\right)}\right\}$$

$$- \overline{u_i u_j}\,\frac{\partial U_i}{\partial x_j} - \nu\,\overline{\left(\frac{\partial u_i}{\partial x_j}\right)^2} \qquad (2.6)$$

where $k \equiv \overline{\frac{u_j u_j}{2}}$

2.3 The boundary layer equations

For the boundary layer, where there is one predominant direction of mean flow, equation (2.4) is much simplified. For the steady incompressible plane two-dimensional boundary layer the equation may be reduced to:-

$$\rho U_1 \frac{\partial U_1}{\partial x_1} + \rho U_2 \frac{\partial U_1}{\partial x_2} = - \frac{\partial P}{\partial x_1} + \frac{\partial}{\partial x_2} \{\mu \frac{\partial U_1}{\partial x_2} - \rho \overline{u_1 u_2} \}$$

$$- \frac{\partial}{\partial x_1} \{\overline{u_1^2} - \overline{u^2}_2 \} \qquad (2.7)$$

and the continuity equation becomes:-

$$\frac{\partial U_1}{\partial x_1} + \frac{\partial U_2}{\partial x_2} = 0 \qquad (2.8)$$

The last term on the right hand side of equation (2.7), the normal stress term, is usually small and is normally neglected.

A section of the present study is concerned with heat transfer to the boundary layer. It is therefore appropriate to introduce the thermal energy equation. An equation describing the enthalpy distribution in the two-dimensional plane boundary layer may be derived in a manner similar to that in which equation (2.7) is derived.* It may be stated:

$$\rho U_1 \frac{\partial \Theta}{\partial x_1} + \rho U_2 \frac{\partial \Theta}{\partial x_2} = \frac{\partial}{\partial x_2} \{\alpha \frac{\partial \Theta}{\partial x_2} - \rho \overline{u_2 \theta}\} \qquad (2.9)$$

In equation (2.9) a term analogous to the normal stress term of equation (2.7) has been neglected.

Integral equations of the boundary layer

For constant property two-dimensional plane boundary layer flows equations (2.7) and (2.9) may be integrated with respect to x_2 whereupon the following results:-

$$\frac{\nu}{U_{1,G}} \frac{dR_2}{dx_1} = \frac{C_f}{2} - KR_2 \{H+1\} + F \qquad (2.10)$$

*For a more detailed discussion of the equations 2.1 to 2.9 the reader is directed to ref. (38).

$$\frac{\nu}{U_{1,G}}\left\{\frac{dR_\Delta}{dx_1}+\frac{R_\Delta}{[\Theta_W-\Theta_G]}\frac{d}{dx_1}[\Theta_W-\Theta_G]\right\}=St+F \qquad (2.11)$$

2.4 The similar boundary layer

The similar boundary layers which arise from flow in a plane convergent channel are the subject of the experimental part of the present study. In this flow the acceleration parameter K is constant from station to station and the equations (2.7), (2.8) and (2.9) may thus be reduced to ordinary differential equations in terms of a similarity variable proportional to $[U_{1,G}\, x_{2/}]$ with the following normalisations:

$$f(\eta)=\frac{U_1}{U_{1,G}}\;;\; S(\eta)=\frac{\overline{u_1u_2}}{U^2_{1,G}}\;;\; \eta=\frac{U_{1,G}x_2}{}$$

equations (2.7) and (2.8) may be expressed*:-

$$f''+K(1-f^2)-Ff'-S'=0 \qquad (2.12)$$

(where the primes denote differentiation with respect to η) with boundary conditions: $f(0)=0$ and $f(\infty)=1$.

With the above choice of variables it is easily demonstrated that:-

$$R_2=\int_o^\infty f(1-f)\,d \qquad \text{and } Cf/_2=f''(0)$$

and thus the local skin friction coefficient and any local length scale Reynolds number are invariant with x_1. The two-dimensional momentum integral equation then reduces to:-

$$Cf/_2=R_2K(H+1)-F \qquad (2.13)$$

* For a fuller discussion of equation (2.12) the reader is directed to refs. (51) and (83).

Now for the laminar flow, i.e. S = 0 with zero surface mass transfer parameter, F equation (2.12) may be integrated analytically to yield:-

$$\frac{U_1}{U_{1,G}} = 3 \tanh^2 \left\{\sqrt{\frac{K}{2}} - \tanh^{-1}\sqrt{\frac{2}{3}}\right\} - 2.0 \qquad (2.14)$$

This solution yields the following results:-

$$R^2{}_2K = .120; \; H = 2.0$$

However, for turbulent flows analytic approaches to the integration of equation (2.12) are not likely to be fruitful and numerical methods of solution must be adopted.

Equation (2.12) may also be used to determine the Reynolds stress distribution in a similar boundary layer from the measured mean velocity profile. The equation may be integrated to yield:-

$$-S(\eta) = K\int_{\eta}^{\infty}(1 - f^2)\,d\eta - f'(\eta) + F\{f(\eta) - 1\} \qquad (2.15)$$

and thus the velocity profile may be used to determine the Reynolds stress $-\overline{u_1u_2}$.

CHAPTER III

THE EXPERIMENTAL INVESTIGATION

3.1 Introductory Remarks

In this chapter the results of the writer's experimental study of strongly accelerated turbulent boundary layers are presented. The study entailed a detailed examination of the similar turbulent boundary layers which arise from flow in a plane convergent channel and included measurements of both mean and fluctuating hydrodynamic quantities. The chapter also includes a review of the results of previous related experimental investigations.

The chapter comprises three main sections the first of which is concerned with a review and discussion of the results of previous hydrodynamic and heat transfer (experimental) studies relating to accelerated turbulent boundary layers and laminarisation. Sections II and III are concerned with the present experimental study. In section II the apparatus used is described and this is followed by a description of the technique adopted to perform the measurements. Finally in section III the results of the current experimental study are presented, discussed and finally compared with the findings of other workers where appropriate.

3.2 SECTION I - A review of previous experimental studies of accelerated turbulent boundary layers

In reviewing the existing experimental studies of accelerated turbulent boundary layers it is desirable to distinguish between those properties normally associated with the turbulent boundary layer in mild and zero pressure gradient and those peculiar to accelerated flows. Therefore, before proceeding with the discussion of previous experimental work, it is appropriate to mention briefly some of the properties normally associated with the turbulent boundary layer developing in mild or zero pressure gradient.

3.21 The turbulent boundary layer in mild and zero pressure gradients

The turbulent boundary layer developing in zero pressure gradient over a smooth, impermeable plane surface has, over the years been the subject of many experimental investigations A careful examination of the results of these experimental studies led Coles (21) to conclude that the mean velocity profile of a turbulent boundary layer developing in zero pressure gradient could be described by a two parameter family of the form

$$\frac{U_1}{U_\tau} = f\left(\frac{x_2 U_\tau}{\nu}\right) + \frac{2\pi}{\kappa}\, w\left(\frac{x_2}{x_{2,G}}\right) \qquad (3.1)$$

The functions f and w which are supposed universal are known as the law of the wall and the law of the wake respectively. The parameter π characterises the 'strength' of the wake component.

In the viscous region in the immediate vicinity of the wall (say $x_2^+ < 5$) the law of the wall reduces to the linear form:-

$$U_1^+ = x_2^+ \qquad (3.2)$$

In the fully turbulent regime of the near wall region, i.e. $x_2^+ > 30$ the law of the wall reduces to the well known semi-logarithmic law:-

$$U_1^+ = \frac{1}{\kappa} \ln x_2^+ + C \qquad (3.3)$$

where κ and C are universal constants having values, recommended by Coles, of 0.41 and 5.0, respectively.

The law of the wake was presented in tabulated form by Coles and the 'strength' parameter π given as a unique function of momentum Reynolds number R_2. The function is such that π which is zero for values of R_2 less than 500, increases steadily between 500 and 3000 and is sensibly constant for all higher Reynolds numbers.

The velocity profile family of Coles has also been found to provide an adequate description of the velocity profiles measured in turbulent boundary layers developing in a wide range of arbitrary pressure gradients. Here, however the 'strength' of the wake parameter π must be allowed to vary in the flow direction; its value will not be given by a unique function of R_2 as in the constant pressure case.

3.22 Laminarisation - the early experimental evidence

The phenomenon of laminarisation seems to have been first observed by Sternberg (81) in 1954. He found that an initially turbulent boundary layer underwent reversion to laminar flow around the shoulder of a projectile in a Prandtl Meyer type expansion. Subsequently possible examples of laminarisation were noticed by Senoo (78), 1954 and by Sergienko and Gretsov (79) 1959. Senoo found the boundary layer on the end wall of a turbine nozzle cascade to be laminar in the region of the throat in spite of the upstream layer being turbulent. Sergienko and Gretsov took measurements at inlet to and exit from a supersonic wind tunnel, the boundary layer at the former being turbulent and at the latter laminar.

The above results prompted Launder (49) and (50) to undertake a detailed hydrodynamic study of the incompressible turbulent boundary layer under the influence of strong acceleration. Launder obtained both mean profile and fluctuating quantity data. His conclusions may be summarised as follows:-

(1) The effect of the acceleration is to reduce an initially turbulent boundary layer to laminar providing the acceleration is sufficiently strong and is applied for sufficient time. The pressure gradient parameter K is important in the determination of whether laminarisation will occur.

(2) Important features of laminarisation are the thickening of the sublayer in normalised x_2^+ co-ordinates and a deviation of the velocity profile from the law of the wall.

A pertinent study of laminarisation was performed by Schraub and Kline (80) who utilised dye-injection and hydrogen bubble techniques to study the sublayer structure of accelerated turbulent boundary layers. As we have already seen they were the first to provide a description of the stages by which laminarisation occurs.

In 1965 Moretti and Kays (63) published surface heat flux data for accelerated boundary layers with K between 0 and 4×10^{-6}. However, no hydrodynamic or temperature profile data was furnished. Moretti and Kays concluded that for K greater than 3.0×10^{-6} the heat transfer rate rapidly approached the laminar boundary-layer level, suggesting that laminarisation was occurring. Their data also indicated substantial dips in heat transfer rates for lower accelerations.

3.23 Further hydrodynamic studies

A number of hydrodynamic studies of accelerated boundary layers followed the aforementioned experiments. The studies were mainly of equilibrium* (or at least near equilibrium) boundary layers which represent a simpler case than arbitrarily developing flows. Equilibrium boundary layers have a turbulence structure which is 'frozen' (or only slowly changing) in the flow direction and therefore allow the effects of flow history to be eliminated.

---

* An equilibrium boundary layer is one in which all of the velocity profile outside the viscous sublayer is similar when plotted in velocity defect co-ordinates. For these flows the pressure gradient parameter β is invariant in the flow direction. Similar boundary layers therefore constitute a special subgroup of equilibrium boundary layers.

Herring and Norbury (37) studied experimentally high Reynolds number equilibrium boundary layers in mild acceleration. Velocity defect profiles were established corresponding to values of the pressure gradient parameter β ($\equiv {}^{\delta_1}/_{\tau_W} \, {}^{dP}/_{dx_1}$) of - 0.35 and - 0.53. Their data agreed well with the theoretical predictions of Mellor and Gibson (61) which were based on a high Reynolds number 'equilibrium' theory.

The experiments of Launder and Stinchcombe (51) were concerned with the determination of the effects and onset of laminarisation. They made an experimental study of the similar (constant K) turbulent boundary layers which occur from flow in a plane convergent channel. Three constant values of the parameter K were considered ($K = 0.7 \times 10^{-6}$, 1.3×10^{-6} and 3.0×10^{-6}). As K was increased, the mean velocity profiles exhibited a continuous shift from a typically fully turbulent form to one more akin to that of a laminar boundary layer. Acceleration eliminated the wake and a thickening (in x_2^+ co-ordinates) of the viscous sublayer as K was increased was evident. Launder and Stinchcombe also performed measurements of longitudinal turbulence intensity with a constant temperature anemometer. For the three boundary layers it was found that there existed a large self-preserving turbulence intensity, thus indicating that the boundary layers were <u>all</u> essentially turbulent. Launder and Stinchcombe however acknowledge that their results suffered from substantial three dimensional effects. When they applied the two-dimensional momentum integral equation (2.10) implausibly low values of

$Cf/_2$ were obtained; at $K = 0.7 \times 10^{-6}$ the skin friction coefficient, $Cf/_2$ calculated with equation (2.10) was estimated to be about 35% low. This behaviour was attributed to streamline divergence which worsened as K was increased. The experimental findings of Launder and Stinchcombe can therefore only be regarded as qualitative.

Badri Narayanan and Ramjee (2) investigated, in a hydrodynamic study, the accelerated turbulent boundary layer. Included in their experiments were four 'constant-K' accelerations ($K = 0.75 \times 10^{-6}$, 2.8×10^{-6}, 5.2×10^{-6} and 7.2×10^{-6}). Both mean velocity and longitudinal turbulence intensity data were obtained with a constant current hot wire anemometer. For those cases where $K \geq 2.8 \times 10^{-6}$ their measurements indicated that the mean velocity profiles had almost reached a fully laminar form at the end of the acceleration. In these cases, a substantial decay in the turbulence intensity $\sqrt{\overline{u_1^2}}/U_{1,G}$ was also noted. The measurements are, however, not as accurate as one would like. It is also doubtful whether the boundary layers reached equilibrium by the end of the acceleration.

Patel and Head (68) studied experimentally strongly accelerated turbulent boundary layers in the entry region of a pipe. The favourable pressure gradients were created in the entry length of the pipe by mounting a centre-body symmetrically in the pipe. Mean velocity profiles were obtained with a flattened tip pitot tube and wall shear stress with a sublayer fence approximately .003 ins high. This sublayer fence was calibrated in zero pressure gradientsagainst a Preston tube. In the region of strong acceleration the velocity profiles when plotted semi-logarithmically in $U_1^+ - x_2^+$ co-ordinates indicate

that:-

(1) The velocity profile in the wall region departs substantially from the inner semi-logarithmic law; the profiles lie above the inner law.

(2) The wake is eliminated by the acceleration

(3) The division between the viscous sublayer and the fully turbulent regions becomes less pronounced.

(4) The sublayer becomes thicker (in x_2^+ co-ordinates) in the region of acceleration.

3.24 Heat transfer to the accelerated turbulent boundary layer

In a hydrodynamic and heat transfer study, Zaric (90) appears to have detected laminarisation in what would, at first glance, seem an unsuitable environment; namely flow through a roughened passage. The roughened surface was a continuous symetric saw-tooth form with an apex angle of 148°.

The flow near the rough surface was alternately accelerated and retarded due to the profile of the rough surface. Towards the end of each accelerated region the local Stanton number dropped significantly and the measured velocity profiles were laminar-like in form.

Experimental studies of flow in rocket nozzles have also been concerned with laminarisation. Boldman, Schmidt and Gallagher (9) obtained heat transfer and mean profile data in the convergent section of a conical supersonic nozzle. To perform their experiments they utilised two nozzles of included angles 60 and 120 degrees which resulted in average values of K

up to approximately 30 x 10^{-6}. The measured surface heat transfer rates exhibited large deviations below a fully turbulent correlation and approached values more appropriate to a laminar flow. At the nozzle exits the mean velocity profiles were also laminar-like in form.

Back, Cuffel and Massier (3) performed a series of tests on a supersonic convergent nozzle. Their measurements included surface heat transfer data, mean velocity profiles and mean temperature profiles within the nozzle. The accelerations were such that K changed rapidly along the nozzle axis with averaged values of K ranging from 10^{-6} to 10^{-5}. A reduction in surface heat transfer below a fully turbulent correlation was observed above a value of K of about 2 x 10^{-6}. At the highest accelerations the surface heat transfer rate was reduced to a value approximately 50% below that given by the fully turbulent correlation. Both temperature and velocity profiles approached laminar forms at the highest values of K.

3.25 The 'Stanford continuing programme with mass transfer'

A substantial experimental research effort into the hydrodynamic and heat transfer aspects of the accelerated turbulent boundary layer is being undertaken at the University of Stanford, U.S.A. The programme includes studies of the turbulent boundary layer with surface mass transfer and is proceeding under the direction of Professor W. M. Kays.

As a part of the aforementioned investigation Julien et al (43) and Thielbahr et al (82) studied the effects of surface mass transfer on turbulent boundary layers undergoing

moderate accelerations. The experiments were conducted in parallel, and with identical flow conditions on the same apparatus. Julien et al present the results of a hydrodynamic study and Thielbahr et al heat transfer measurements. The constant values of acceleration parameter K considered were 0.57×10^{-6}, 0.77×10^{-6} and 1.45×10^{-6}. For each acceleration a range of values of mass transfer parameter was investigated from F = -0.004 (suction) to +0.006 (blowing). Julien et al obtained mean velocity profile data by use of a flattened pitot tube. From this data they calculated the wall shear stress by (a) the application of the two-dimensional momentum integral equation (2.10) and by (b) a sublayer method based on extrapolating the measured velocity profiles to the wall. For the zero mass transfer case the measured profiles identical trends to those found previously by other workers; namely a progressive 'overshoot' of the semi-logarithmic law of the wall and an elimination of the wake region as K is increased. The main effect of mass transfer was, in the case of suction, to augment the effects of the acceleration and, in the case of blowing to reduce them. Similar results were noted by Thielbahr et al in the heat transfer study. At a particular acceleration the Stanton number was reduced by suction and increased by blowing at the surface; a contrary behaviour to that normally associated with the turbulent boundary layer. The temperature-profile measurements also showed that the thermal boundary layer penetrated far outside the velocity layer by the end of the acceleration.

Strongly accelerated turbulent boundary layers with and without surface mass transfer were studied by Loyd et al (56)

and Kearney et al (45). The work was concerned with both hydrodynamic and heat transfer aspects of the turbulent boundary layer; the results of the hydrodynamic study being presented by Loyd et al and those of the heat transfer investigation by Kearney et al. The experiments, which relate to two constant values of the acceleration parameter K (namely $K = 2.0 \times 10^{-6}$ and 2.5×10^{-6}) were performed in parallel under identical flow conditions on the same apparatus. The measurements covered a range of mass transfer parameter F between 0 and +0.004 (blowing). Loyd et al made mean velocity profile measurements with a flattened tip pitot tube and also performed longitudinal turbulence intensity measurements with a constant temperature hot wire anemometer. The wall shear stress along the test plate was calculated by estimating the slope of the measured mean velocity profiles at the wall and by application of the two-dimensional momentum integral equation (2.10) to the velocity profiles. At the end of the acceleration Loyd found that the measured mean velocity profiles approached those appropriate to a similar laminar boundary layer as K was increased but progressively deviated therefrom as the mass transfer parameter F was increased. The effect of varying the Reynolds number R_2 at the beginning of the acceleration was also considered. It was found that the further the initial R_2 was above the asymptotic similar value the more rapid was the response of the boundary layer to the acceleration. For all cases a large turbulence intensity was present at the end of the acceleration although in some cases a decay (when plotted in normalised form) was evident through the acceleration.

Kearney et al present the results of the heat transfer study in which both surface heat transfer rates and temperature profiles were measured. The measurements indicated that the local surface heat transfer rate fell below that appropriate to a fully turbulent layer by an amount which increased progressively (with or without blowing) as K was increased. Further heat transfer measurements were performed to investigate the effects of (1) various conditions at the start of the acceleration and (2) step changes in blowing within the region of acceleration. The distribution of 'turbulent Prandtl number' across the boundary layer was calculated from the measured profile data. The results suggested that the 'turbulent Prandtl number' correlation for constant pressure turbulent flow may also be valid for accelerated boundary layer flows.

3.3 SECTION II - Experimental apparatus and technique

3.31 Experimental apparatus

The experiments to be described were carried out in the working section of an open circuit wind tunnel, shown schematically in figure (3.1). The working fluid, air is supplied by a centrifugal fan powered by a 10 b.h.p variable speed motor. The fan is capable of delivering a volume of 3,300 ft^3/min at a pressure of 10 inches of water.

The air enters the fan via a filter box of dimensions 3 ft. x 3 ft. x 4 ft. From the fan the air passes into a settling chamber of cross section 4 ft. wide x $2\frac{1}{4}$ ft. high via a diffuser. The settling chamber and diffuser contains five

wire mesh screens and a honeycomb section of aluminium foil the purpose of which is to minimise the turbulence intensity in the working section. In designing the mesh screens, the recommendations of refs. (11) and (14) were followed. Of critical importance is the open area ratio, which if less than .57 in the final screen can cause vortices which randomly affect the boundary layer in the transverse direction. Finally the air enters the working section through a 9:1 contraction.

The working section is a 16 in x 9 in rectangular duct constructed from $\frac{1}{2}$ in thick perspex (plexiglass) sheet, a section of the roof of which can be set at any inclination to the lower wall. The roof and lower wall, the test plate thus form a 2-dimensional plane convergent channel. Throughout the present study the roof was set at approximately 10 degrees to the test plate. Measurements performed with a constant temperature hot-wire-anemometer indicated that in the working section the longitudinal turbulence intensity was about 0.1%. No swirl component of velocity could be detected.

The test plate was constructed from a 16 ins x 60 ins x 0.5 ins thick section of perspex (plexiglass) sheet. It rests on rails attached to the side of the working section and thus its position relative to the convergent section is readily adjustable. Static pressure holes of .022 ins. diameter are spaced at 2.0 ins. intervals along the centre line of the plate. Access holes of diameter 2.875 ins. through which the probes could be inserted are located at 4.0 in. centres along a line parallel to but offset by a distance of 4.0 in from the centre-line of the plate. These holes were plugged when not in use.

3.32 INSTRUMENTATION

(1) Pitot boundary layer probe

Mean velocity profiles were obtained with a flattened tip pitot tube. The probe is illustrated in fig. (3.3). The probe tip is .011 ins. high by a .120 ins. wide with a wall thickness of .002 ins. The probe was constructed so that, although it was inserted into the working section at a distance from the centre line the transverse could be made with the pitot tube tip along the centre line of the test plate.

(2) Pressures

All pressures were measured with a null reading tilting U-tube micromanometer. This instrument contains a silicon fluid of specific gravity .822. It can be used in the pressure range 0 - 1.5 ins. of fluid with an accuracy of $\pm 10^{-4}$ ins. of fluid. The manometer is fully described in ref. (12).

(3) Boundary layer traversing gear

The probes were manually positioned relative to the wall with a traversing gear which utilises two standard micrometers the scales of which are divided into increments of .001 inches. The gear was such that two probes could be traversed simultaneously if necessary.

(4) Stanton tubes

Stanton tubes were produced from Gillette stainless steel razor blades of thickness .004". They were glued to the test surface with Evostik Contact adhesive and could easily be removed on completion of the measurement.

(5) Hot Wire Equipment

The hot wire measurements were performed using the equipment listed below:-

i) 2 DISA constant temperature anemometers type 55A01

ii) 2 DISA lineariser units type 55D10

iii) 1 DISA R.M.S. Voltmeter type 55D35

iv) 1 DISA Random signal indicator and correlator type 55A06

v) 1 Solatron Digital Voltmeter type LM 1420.2

vi) 1 Telequipment Oscilloscope type D53

vii) 1 Bruel & Kjær spectrum analyser type 2112

The longitudinal turbulence intensity measurements were performed using a standard DISA gold plated boundary layer hot wire probe type 55F04. Shear stress measurements were performed by use of a standard DISA miniature hot wire X-probe type 55A38.

3.33 Qualification of the rig

The sloping roof of the working section was raised so that a uniform free stream velocity was obtained. The resulting constant pressure boundary layers were then measured at 4" intervals along the centre line of the test plate with the flattened tip pitot tube.

The criterion used to determine whether the boundary layer profiles so obtained were similar to those normally found in constant pressure plane flow were as follows.

(1) The value of Cf/2 found by Clauser chart should agree with the Cf/2 - R_2 correlation of Coles (21).

(2) That the strength of the wake found should also agree with the correlation of ref. (21). Coles designated a turbulent boundary layer as normal if the wake strength is within ± 20% of the value given by:-

$$\frac{\Delta U}{u_\tau} = 2.65 \left[1 - \exp\left\{- \frac{(R_2 - 500)}{850}\right\}\right] \qquad (3.4)$$

for $R_2 > 500$

The constant pressure data obtained satisfied the above criteria to a reasonable accuracy and the apparatus was deemed satisfactory. A typical measured mean velocity profile is displayed in figure (3.4).

3.34 Experimental technique

(1) Distances

In all cases traverses were started at the wall position. The position of the probe relative to the wall was determined by moving the probe into contact with the wall and then adjusting the micrometer screw by increments of.0003 ins. until a gap was visible. The reflection of the probe could be observed in the polished surface of the test plate and it is therefore estimated that the position of the wall can be determined to within .0005 ins.

(2) Mean velocity

Mean velocities were obtained by measurement of the difference between the total pressure P_{tot} and the static pressure P_s with a flattened tip pitot tube. The velocity is given by:-

$$U = \left\{ \rho \frac{(P_{tot} - P_s)}{2} \right\}^{\frac{1}{2}} \qquad (3.5)$$

As there is considerable disagreement as to the effect of turbulence on pitot tubes no correction was made for this effect.

For a flattened pitot tube of dimensions similar to those used in the present study, the effect of viscosity is found to be negligible (ref. (60)) for a Reynolds number (based on the tip height) greater than 30, For the measurements presented here the minimum Reynolds number always exceeded 30 and thus no correction was needed.

The only correction made to the velocity measurements was a displacement correction, similar to that proposed by McMillan (59), which was added to the distance from the wall. The correction applied was 0.15 times the probe tip height. It is intended to account for the effect of a mean velocity gradient on the probe reading: for the probe used in the present study the displacement amounted to about .002 ins. and is therefore only significant in the region very close to the wall.

(3) Wall shear stress measurement

The wall shear stress was measured by use of Stanton tubes. These were glued to the test plate when required and removed on completion of the measurement. The Stanton tube is a sublayer device which must be of dimensions such that it lies within the linear ($U_1^+ = X_2^+$) velocity profile region immediately adjacent to the wall; because of its (small) physical dimensions calibration is always necessary In the present study the Stanton tubes were calibrated in situ against a Preston tube. The Preston tube, a total head device, is found to have a fairly universal calibration in flows where the mean velocity profile in the fully turbulent near wall region is described by the semi-logarithmic wall law (equation (3.3)); an essential requirement for its use. It was therefore used to calibrate the Stanton tubes in the constant pressure flows which resulted when the roof of the test section was raised. The Preston tube calibration of Patel (67) was used. A typical Stanton tube calibration was:-

$$\frac{\tau_w d^2}{4\rho\nu^2} = .34 \left[\frac{\Delta p d^2}{4\rho\nu^2} \right]^{.736} \qquad (3.6)$$

No pressure gradient corrections were added to the Stanton tube measurements.

An estimate of the wall shear stress was also obtained by application of the two-dimensional momentum integral equation (2.10) to the measured mean velocity profiles. The skin friction was then given by:-

$$Cf/2 = R_2 K (H + 1) + \frac{\nu}{U_{1,G}} \frac{dR_2}{dx_1} \qquad (3.7)$$

where for a similar boundary layer the last term on the right hand side of (3.7) is zero. The constant K boundary layers considered here only asymptotically approached their similar solutions. The term $\frac{\nu}{U_{1,G}} \frac{dR_2}{dx_1}$ was therefore estimated graphically whereby it was found to contribute negligibly to the skin friction coefficient.

(4) Hot-wire-anemometer measurements

By suitable choice of the lineariser exponent a calibration curve of the following form was obtained:-

$$E = P + QU \qquad (3.8)$$

For each probe a value of exponent was chosen by trail and error and then retained throughout the experiments.

The hot wires were calibrated in the test section of the tunnel against a pitot tube. In all cases a calibration was carried out prior to each profile measurement. This calibration was found to change by less than 2% over the time it took to perform a complete boundary layer traverse. The tangential cooling correction of Champagne (17) was applied to the X-wire measurements. No other corrections were applied. The method of reduction of the raw hot-wire-anemometer data is described in appendix 1 . A typical calibration curve is displayed in figure (3.5).

(5) Spectrum Measurements

The spectrum measurements were performed with a Bruel and Kjar frequency analyser operating with a bandwith of 1/3 of octave. The normalised frequency spectrum is then given by:-

$$G(f) = \frac{e^2(f)}{e^2_{total}\Delta f} \qquad (3.9)$$

where $\int_0^\infty G(f)\, df = 1$

This frequency spectrum was transformed into a wave number spectrum $F(n_1)$ by use of the identities:-

$$n_1 \equiv \frac{2\pi f}{U_{1,c}}$$

$$F(n_1) \equiv \frac{U_c}{2\pi} G(f) \qquad (3.10)$$

where $U_{1,c}$ (the convective velocity) was assumed equal to U_1 the local mean velocity. This assumption is known to be only approximate in shear flow; the convective velocity may differ significantly from the local mean velocity and is also a function of wave number. The assumption has nevertheless been used by a majority of workers and, in the absence of more precise knowledge of the convective velocity, must be utilised here. It should be of sufficient accuracy for present purposes.

(6) Setting up an Asymptotic boundary layer

(i) Estimation of the Acceleration parameter K

The velocity outside the boundary layer for flow in a convergent plane channel is given by:-

$$U_1 = \frac{U_o \ell}{\ell - x'_1} \qquad (3.11)$$

where U_o is the velocity at $x_1' = 0$ and where ℓ is the distance between the line of intersection of the channel planes and $x'_1 = 0$. With the aid of the continuity equation it may be deduced that:-

$$K = \frac{\nu \tan \alpha}{U_o h_o} \qquad (3.12)$$

where h_o is the channel height at $x'_1 = 0$ and α is the angle between the channel planes.

In practice the above expression is only approximate but its use does result in a value of K reasonably close to that desired.

(ii) Positioning the test plate

A similar boundary layer is most easily obtained if the boundary layer at the beginning of the constant K acceleration is as close as possible to its asymptotic similar form. In the experiments described here the conditions at the channel entrance were controlled by the position of the test plate, which was variable relative to the convergent channel.

The method adopted in setting up similar boundary layer utilised an iterative technique the outline of which is

is as follows:-

a) Estimate a value of R_2 appropriate to a similar boundary layer arising at the value of acceleration parameter K being considered and position the test plate so that this estimated value is achieved at the channel entrance.

b) Measure with a pitot tube the mean velocity profiles at the convergent channel entrance and exit

c) Compare the resulting values of R_2 and re-position the test plate accordingly

The procedures (b) and (c) were repeated until the values of R_2 at the channel entrance and exit were approximately equal. The only limitation on the above method is that the boundary layer at the channel inlet must be fully turbulent; a fully turbulent boundary layer in zero pressure gradient with R_2 less than about 400 is difficult to obtain.

(iii) Calculation of the acceleration parameter K

At the end of each test the acceleration parameter K was calculated accurately from the measured variation of free stream velocity along the test plate. The free stream velocity was measured with the pitot tube at 4 in. intervals along the test plate and a least squares polynomial then fitted through the data points. Finally K was obtained by differentiation of the polynomial.

3.4 Experimental Results

In this section the measurements performed during the present experimental study are presented and discussed. The turbulent boundary layers under consideration are those which arise from flow in a plane convergent channel. As noted in Chapter II the above boundary layers will asymptotically approach similar form. This asymptotic similar boundary layer will have mean velocity profiles which are similar when plotted in normalised co-ordinates, and acceleration parameter K and local length Reynolds numbers which are invariant with x_1.

Laminarisation is known to occur over the range $10^{-6} < K > 3.5 \times 10^{-6}$. For this reason three values of K equal to 1.5×10^{-6}, 2.5×10^{-6} and 3.0×10^{-6} have been studied experimentally during the present work. The quantities measured, in each case consist of mean velocity profiles, wall shear stress, longitudinal turbulence intensity and spectra of longitudinal turbulence intensity. For the lowest value of K, ie $K = 1.5 \times 10^{-6}$ measurements have also been performed of normal and transverse turbulence intensities and Reynolds shear stress. The boundary layers at the other values of K were considered to be too thin for the latter measurements to be performed with any degree of accuracy. Various integral parameters have also been calculated from the measured mean velocity profiles.

3.41 Mean Quantities - Integral parameters

Figures 3.6, 3.7 and 3.8 show the variation through the plane convergent channel of momentum-deficit thickness Reynolds

number, R_2, shape factor H, skin friction coefficient $C_f/2$ and acceleration parameter K. It may be observed that, for the three cases, K reaches its constant value at a distance of approximately 8 ins from the convergent channel entrance and is maintained constant to within about 5% over a distance of approximately 20 ins. In each case both R_2, H and $C_f/2$ are maintained sensibly constant in the region of constant K. The values of $C_f/2$ obtained by use of the two-dimensional integral equation and directly by Stanton tube agree to a reasonable accuracy (approximately $\pm$ 5%). This provides evidence to support the view that a two-dimensional flow has been attained.

At $K=1.5 \times 10^{-6}$ (figure 3.6) R_2, H and $C_f/2$ have constant values of about 680, 1.50 and .0025 respectively throughout the region of constant K. Figure 3.7 (where $K = 2.5 \times 10^{-6}$) shows the variation of R_2 and H through the acceleration for two different initial values of R_2 at the convergent channel entrance. At the beginning of the constant K region, the two values of R_2 are 340 and 390 respectively. In the case of the lower value, R_2 is maintained sensibly constant and H shows a small but perceptible rise to a constant value of 1.6. However, for the higher initial value, R_2 decreases and the shape factor rises slowly through the acceleration. At the end of the channel R_2 and H have values equal to 340 and 1.6 respectively; values identical to those resulting from the lower initial R_2 value. The estimated asymptotic values of R_2, H and $C_f/2$ are 340, 1.6 and .0023 respectively.

The variation of R_2, H and $C_f/2$ through the acceleration

for $K = 3.0 \times 10^{-6}$ is shown in figure 3.8. The behaviour of R_2 and H is shown for three initial values of R_2 at the channel entrance. At the beginning of the constant K region of acceleration the values are 470, 390 and 340 respectively. The two highest initial values of R_2 give rise to boundary layers with decreasing values of R_2 through the constant K acceleration. The boundary layers arising from the lowest initial value of R_2 also display a very small though progressive decrease in R_2 through the acceleration. The shape factor increases slowly and does not appear to reach a constant value. The changes in R_2 and H are small and probably fall within the error bounds of the measurements. However it is not possible in this case to conclude from examination of R_2 and H whether or not the boundary layer has reached similarity conditions by the end of the acceleration.

3.42 Mean velocity profiles

For the three values of K presently considered the mean velocity profiles at various x_1 stations covering the constant K portion of the acceleration are displayed in figures 3.9, 3.10 and 3.11. On linear scales the normalised velocity $U_{1}/U_{1,G}$ is plotted with abscissa the similarity variable $\eta \left(= \frac{U_{1,G}\, X_2}{\nu}\right)$ On each figure the velocity profile appropriate to a laminar similar boundary layer is also shown. The velocity profiles shown in figures 3.9, 3.10 and 3.11 all exhibit small changes in shape from channel entrance to exit. These small changes in profile shape are of course to be expected since the boundary layers at the beginning of the constant

acceleration are not likely to be in equilibrium but will approach asymptotically their respective similar solution as the acceleration proceeds to take effect.

The velocity profiles for $K = 1.5 \times 10^{-6}$ and $K = 2.5 \times 10^{-6}$ shown in figures 3.9 &3.10 are closely similar for $[U_1/U_{1,G}]$ less than about 0.5, i.e. in the vicinity of the wall. The main changes in profile shape occur in the region $.75 < [U_1/U_{1,G}] < .9$ where a slight filling out, i.e. increase in velocity, of the profile takes place through the acceleration. The velocity profiles corresponding to $K = 3.0 \times 10^{-6}$ (figure 3.11) show slightly different behaviour from those of the other accelerations in that changes, again small, take place in the vicinity of the wall for $\eta < 10^3$ where the velocity profiles appear to become less steep through the acceleration. There is also some slight filling out of the velocity profile in the outer region.

On comparison of the measured velocity profiles (figures* 3.9 3.10 & 3.11) for the three constant K accelerations presently considered it may be observed that boundary layer velocity profiles approach progressively nearer to those appropriate to a similar laminar boundary layer as K is increased.

---

* The velocity profiles displayed in figures 3.10 and 3.11 and which correspond to $K = 2.5 \times 10^{-6}$ and $K = 3.0 \times 10^{-6}$ respectively are those measured, in each case for the lowest initial values of R_2 at the channel entrance.

The extent to which the mean velocity profiles are similar is shown in figures 3.12, 3.13 and 3.14 which correspond to $K \simeq 1.5 \times 10^{-6}$, 2.5×10^{-6} and 3.0×10^{-6} respectively. On semi-logarithmic axes, the normalised velocity $U_1/U_{1,G}$ is plotted against η at x_1 stations covering the final 8 ins of the accelerations. Although there is a small amount of scatter in the profiles they are clearly similar (or self-preserving) with respect to the chosen axes. Also shown on the figures 3.12 - 3.14 are the stress lines which would result from the measured wall shear stress values if the mean velocity profiles were described by the semi-logarithmic wall law.* On comparison of figures 3.12 - 3.14 it is evident that, for the three cases the measured velocity profiles lie above the line; the deviation increasing progressively as K is increased.

---

* The logarithmic law of the wall may be written

$$\frac{U_1}{U_\tau} = \frac{1}{\kappa} \ln \left[\frac{x_2 U_\tau}{\nu} \right] + C$$

where, by definition $U_\tau = U_{1,G}\sqrt{C_{f/2}}$
and thus we may also write

$$\frac{U_1}{U_{1,G}} = \frac{C_{f/2}}{\kappa} \ln \left[\frac{x_2 \, U_{1,G}\sqrt{C_{f/2}}}{\nu} \right] + C$$

Clearly if $U_1/U_{1,G}$ is plotted against $\frac{x_2 \, U_{1,G}}{\nu}$ on semi-logarithmic axes then, for every constant value of $C_{f/2}$ a straight line will result. This plot is called a Clauser chart and is often used for the estimation of wall shear stress co-efficient $C_{f/2}$. It will obviously only provide accurate estimations of $C_{f/2}$ of there exists a region of mean velocity profile which is represented by the law of the wall.

In figures 3.15 - 3.17 mean velocity profiles are plotted on semi-logarithmic axes in U^+, x_2^+ co-ordinates. The measured values of $C_{f/2}$ are used in the normalisation. For each value of K a typical mean velocity profile, measured near the end of the acceleration is plotted. Figure 3.15 refers to $K = 1.5 \times 10^{-6}$, figure 3.16 to $K = 2.5 \times 10^{-6}$ and figure 3.17 to $K = 3.0 \times 10^{-6}$ respectively. Also shown on each figure is the straight line corresponding to the logarithmic law of the wall.

On comparison and examination of the figures three main features concerning the velocity profiles become evident. Firstly the mean profiles, for the three values of K, have no wake i.e. no portion whcih may be represented by the law of the wake, ref (21). Secondly the velocity profiles show a deviation from the law of the wall. The profiles lie above (overshoot) the wall law by an amount which increases progressively as K is increased. Thirdly it is difficult to distinguish any clear division between the viscous sublayer and fully turbulent regions of the velocity profiles. Indeed Indeed at the two highest values of K i.e. $K = 2.5 \times 10^{-6}$ and $K = 3.0 \times 10^{-6}$ a division seems completely absent.

3.43 Fluctuating Quantities

(1) Longitudinal turbulence intensities

Longitudinal turbulence intensities $\frac{\sqrt{\overline{u_1^2}}}{U_{1,G}}$ are shown in figures 3.18, 3.19 and 3.20 with similarity variable η as abscissa. In figure 3.18 the turbulence intensity profiles for

$K = 1.5 \times 10^{-6}$ are shown at various x_1 stations through the constant K region of the acceleration. The maximum intensity of about .11 occurs near the wall at η equal to approximately 3×10^2 and from this value the intensity falls of rapidly with increasing η in a smooth concave fashion. A small decay in turbulence intensity in the inner half of the boundary layer, through the acceleration may be observed and in the initial part of the acceleration some slight growth (in η co-ordinates) in the thickness of the layer is evident. The profiles do however exhibit a fair degree of similarity from station to station throughout the acceleration.

In figure 3.19 the turbulence intensity profiles for $K = 2.5 \times 10^{-6}$ at various stations through the acceleration are displayed. The maximum intensity again occurs close to the wall at $\eta \approx 3 \times 10^2$ where it has a value between .11 and .12. From its maximum value, the intensity falls off rapidly (as for $K = 1.5 \times 10^{-6}$) with increasing η. Through the constant K region of the acceleration a decay of about 8% in maximum turbulence intensity may be noted and in the initial part of the acceleration a slight thickening of the layer occurs. In other respects however the profiles display an excellent degree of similarity throughout the acceleration.

The turbulence intensity profiles for $K = 3.0 \times 10^{-6}$ are displayed in figure 3.20. As for the other values of K, the peak intensity occurs in the immediate vicinity of the wall at $\eta = 3 \times 10^{\frac{1}{2}2}$ approximately. and falls off rapidly with increasingη. However figure 3.20 shows a more substantial decay in turbulence intensity through the constant K acceleration

than that occurring for the other values of K. This decay is most pronounced in the maximum intensity in which a decrease of about 25-30% occurs between the beginning and end of the acceleration. It thus seems likely that the turbulence intensity $\sqrt{\overline{u^2}}_{1}/U_{1,G}$ profile does not reach its similar or self-preserving form by the end of the acceleration.

(2) Turbulent shear and normal stress measurements

For the lowest value of K considered in the present study (i.e. $K = 1.5 \times 10^{-6}$) hot-wire-anemometer measurements were performed with an X-wire. The results are shown in figures 3.21, 3.23, 3.24, 3.25, & 3.26. By traversing the boundary layer at x_1 = 12ins with the X-wire first in the $x_1 - x_3$ plane and then in the $x_1 - x_2$ plane profiles of both Reynolds normal and shear (non-zero) stresses were obtained. In the constant K acceleration the boundary layer becomes thinner in physical co-ordinates as x_1 and thus the stream velocity is increased and by the end of the acceleration is too thin for X-wire measurements to be performed. However at x_1 = 12ins the boundary layer was approximately .5ins thick and it was thus possible to make X-wire measurements. Because of the greater physical dimensions of the X-wire it is not possible to obtain turbulence measurements as close to the wall as with the single normal hot wire used for the longitudinal turbulence intensity measurements.

The Reynolds shear stress $(-\overline{u_1 u_2})$ distribution through the boundary later (measured with the X-wire) is shown in figure 3.21 with abscissa η. The shear stress falls off smoothly with increasing distance from the wall and has its greatest value at the measuring station nearest the wall

where $-\overline{u_1u_2}/U^2_{1,G}$ is about .0008; a value which is only about 30% of the measured wall shear stress. This result is not unexpectedhowever, since it may easily be shown that the shear stress will decrease rapidly with increasing distance from the wall in a strongly accelerated flow. Also shown is the Reynolds stress distribution obtained from the measured mean velocity profile at x_1 = 12.0 ins with the aid of the integrated similarity equation (equation (2.15)). The agreement between the distributions of $\overline{u_1u_2}$ obtained by the two methods is not particularly good: although both profiles have maximum values considerably less than the wall shear stress there is considerable discrepancy in the detailed profile shapes. Some part of this discrepancy may be due to the fact that the boundary layer may not have reached its asymptotic similar form at x_1 = 12.0 ins and thus use of equation (2.15) would have been inappropriate.

The Reynolds shear stress distributions obtained from the mean velocity profiles with the aid of equation (2.15) for the three values of K considered are shown in figure 3.22. It may be readily observed that, in the three cases the shear stress $(-\overline{u_1u_2})$ falls off smoothly with increasing distance from the wall. As expected* both the maximum

---

* The boundary layer equations in the limit as the wall is approached reduce to:

$$\frac{\partial \tau}{\partial x_2} = dP/dx_1$$

which on normalisation may be written as:-

$\frac{d\bar{S}}{\partial \eta} = -K$ where $\bar{S} = \tau/\rho U^2_{1,G}$

and where τ = total (turbulent + viscous) shear stress

values and overall levels of shear stress ($-\overline{u_1u_2}$) fall with increasing K; at $K = 1.5 \times 10^{-6}$ the maximum value of ($-\overline{u_1u_2}$) is about 70% of the wall values whereas for $K = 3.0 \times 10^{-6}$ it is only about 30% of the wall value.

In figure 3.23 the Reynolds normal stresses $\sqrt{\overline{u_1^2}}/U_{1,G}$, $\sqrt{\overline{u_3^2}}/U_{1,G}$ and $\sqrt{\overline{u^2}}_{3/U_{1,G}}$ (measured with the X-wire) for $K = 1.5 \times 10^{-6}$ are shown. The intensities all have maximum values in the immediate vicinity of the wall but fall off as the distance from the wall is increased. Near the wall the longitudinal turbulence intensity $\sqrt{\overline{u^2}}_{1/U_{1,G}}$ is by far the greatest, being about twice the magnitude of the transverse intensity which is in turn about 30% larger than the normal component $\sqrt{\overline{u^2}}_{2/U_{1,G}}$. At the outer edge of the boundary layer the three intensities become equal. The normal stress measurements shown in figure 3.23 are in roughly the same proportion to each other as those found in a constant pressure, high Reynolds number turbulent boundary layer, e.g. Klebanoff (46). However, the intensities of figure 3.23 fall off more rapidly than in the constant pressure case. This difference corresponds to the relative differences in shear stress distribution arising in constant pressure and strongly accelerated flows. In a constant pressure flow the shear stress in the vicinity of the wall is approximately constant whereas in a strongly accelerated flow the shear stress decreases rapidly with distance from the wall.

In figure 3.24 the turbulence kinetic energy $k/U_{1,G}^2$ and the structure parameter $-\overline{u_1u_2}/k$ profiles are plotted with abscissa η. The turbulence kinetic energy profile follows the expected form, decreasing smoothly with increasing

distance from the wall. The structure parameter - $\overline{u_1 u_2}/k$ is approximately constant over roughly 75% of the boundary layer as is the case in high Reynolds number flows. However, its magnitude (about 0.22) is about 25% less than the value found in high Reynolds number boundary layer flows, e.g. ref (46).

The co-efficient of correlation $\frac{\overline{u_1 u_2}}{\sqrt{\overline{u_1^2}}\sqrt{\overline{u_2^2}}}$ is displayed in figure 3.25. A roughly constant value of approximately .35 may be observed over 75% of the layer with the co-efficient going to zero at the wall and the outer edge of the boundary layer. This result is similar to that found in high Reynolds number turbulent flow. However the value of correlation co-efficient is less than the value of approximately 0.5 which is that obtained in high Reynolds number boundary layers e.g. Klebanoff (46).

Some measure of the accuracy of the X-probe measurements may be obtained from figure 3.26. Displayed is the longitudinal intensity $\sqrt{\overline{u_1^2}}/U_{1,G}$ measured with (a) the single normal wire boundary layer probe (DISA gold plated) (b) the X-probe in the $x_1 - x_2$ plane (c) the X-probe in the $x_1 - x_3$ plane. The agreement of the profiles obtained by the three methods, it may be observed is very good. The two X-probe profiles are essentially co-incident and lie slightly above the single wire measurements. Any differences may be accounted for by the fact that the X-probe, which utilises two wires, is likely to lead to results slightly less accurate than the single normal wire. In X-probe measurements small errors may be introduced by the interaction of the two wires and by the fact that the two wires are a finite distance apart and thus do not measure at the same point in space.

3.44 Spectra of Longitudinal turbulence intensity

For each of the three values of K presently considered, the spectra of longitudinal turbulence intensity were measured at two x_1 stations for various positions in the boundary layer. The results of these measurements are shown in figures 3.27 - 3.38.

(1) $K = 1.5 \times 10^{-6}$

The spectral measurements obtained for $K = 1.5 \times 10^{-6}$ at station $x_1 = 12$ins are displayed in non-dimensional form in figure 3.27; the length $\nu/U_{1,G}$, which is here proportional to the boundary layer thickness has been used to perform normalisation. For values of η covering the range $10^3 \leq \eta \leq 9 \times 10^3$, the spectrum measurements fall, to a fair approximation onto a single curve. This is a slightly surprising result since high Reynolds number turbulent-boundary layer data e.g. ref (46) would lead one to expect the proximity of the wall to influence the shape of the spectrum at the inner most position (which corresponds to $x_2/x_{2,G} \approx 0.1$). As expected, the spectra decrease smoothly with increasing wave number.

Figure 3.28 shows, again for $K = 1.5 \times 10^{-6}$ the spectral distributions obtained at station $x_1 = 20$ ins at the same values of η as for station $x_1 = 12$. The measurements show identical results to those displayed in figure 3.27.

The variation in spectra along lines of constant n through the acceleration is illustrated in figure 3.29; the spectral distribution at $n = 10^3$ for $x_1 = 12.0$ ins and $x_1 = 20.0$ ins is shown. It is evident that the normalised spectra do not appreciably change either shape or level and are thus similar in the region 12 ins $\leq x_1 \leq$ 20 ins. This result provides strong evidence to support the view that the boundary layer set up at 1.5×10^{-6} is very close to its asymptotic form.

(2) $\underline{K = 2.5 \times 10^{-6}}$

Figures 3.30, 3.31, 3.32, 3.33 and 3.34 show the longitudinal intensity spectrum measurements for the boundary layer arising at $K = 2.5 \times 10^{-6}$. The spectra at various positions in the boundary layer covering the range $.5 \times 10^3 \leq n \leq 4.8 \times 10^3$ at station $x_1 = 16$ are shown in figure 3.30. The spectra fall off with increasing wave number smoothly but more rapidly than for $K = 1.5 \times 10^{-6}$. For $n < 1.6 \times 10^3$ the spectra at various positions in the layer lie on one curve with some deviation occuring in the low wave number range. There is some evidence of influence of the wall on the spectrum measured at the position nearest to the wall, $n = 0.5 \times 10^3$. The results of spectrum measurements performed at station $x_1 = 24$ ins and at the same values of n as for $x_1 = 16$ are displayed in figure 3.31. The measurements show exactly the same trends as those obtained for $x_1 = 16$ ins differing only in level.

The variation of normalised spectral distribution of intensity through the acceleration is illustrated in figures 3.32 and 3.33. Displayed is a typical variation, at constant n, of the spectrum with distance through the acceleration;

figures 3.32 and 3,33 corresponding to $n = 0.5 \times 10^3$ and $n = 4.8 \times 10^3$ respectively. A quite large decay in normalised spectra through the acceleration may be observed in both figures 3.32 and 3.33. The curves however appear to be of similar shape and seem to differ mainly in level i.e. a scaling difference. That this is the case may be observed from figure 3.34 where both spectra at $x_1 = 16$ and $x_1 = 24$ are normalised with the same length $[\nu/U_{1,G}]_{x_1 = 16}$. The spectra measured at constant but at two values of x_1 may now be observed to lie, to a fair approximation on a single curve. Two explanations of this fact seem possible and they are:

(a) The length on which the spectra scale remains constant between $x_1 = 16$ and $x_1 = 24$. This implies that the physical dimensions of the turbulent eddies remains constant and changes occur in intensity level only.

(b) The assumption (utilised to transform the measured frequency distributions into wave number spectra, see p 41) that the velocity at which turbulent eddies are convected passed a fixed point in space is equal to the local mean velocity is in error. The turbulent eddies are convected with a constant velocity proportional to the velocity at $x_1 = 16$ ins and changes occur in both turbulent scale and intensity.

The present measurements do not enable distinction to be drawn between either of the above explanations; either or some combination of both remains plausible.

(3) $K = 3.0 \times 10^{-6}$

The spectrum measurements performed for $K = 3.0 \times 10^{-6}$ for various positions in the layer at two x_1 stations are shown in figures 3.35, 3.36, 3.37 and 3.38. These measurements display almost identical behaviour to those obtained for $K = 2.5 \times 10^{-6}$. The discussion and interpretation of the spectra of longitudinal intensity for $K = 2.5 \times 10^{-6}$ may thus be taken equally to apply to those obtained at $K = 3.0 \times 10^{-6}$.

The spectrum measurements performed at the three values of acceleration parameter K presently considered exhibit both similarities to and differences from the results obtained in high Reynolds number flows e.g. ref (46). An important difference is the absence, in all three cases, of any region of the spectrum which varies as $n_1^{-5/3}$.* This is not an unexpected result since the occurrence of a -5/3 law depends on the existence of an inertial subrange which in turn depends on a large separation in wave number space between the energy containing eddies and the eddies responsible for the dissipation of turbulent energy. This separation is not likely to occur in low Reynolds number flows and in fact an overlap between energy containing and dissipation eddies is more likely. The latter suposition is supported to some extent by the similarities between the present spectrum measurements and those obtained at the edge of the viscous sublayer in high Reynolds number boundary layers e.g. ref (20). In both cases a very sudden fall in the spectrum with increasing wave number is to be noted.

---

* For a more detailed discussion the reader is directed to ref (38)

The scale of the turbulent motion may also be estimated from spectrum measurements. The longitudinal integral scale* of the turbulence is given approximately by:

$$L_{x_1} = \lim_{n_1 \to 0} F(n_1) \qquad (3.13)$$

(for a fuller discussion see Hinze (38))

For the present measurements the spectra show some scatter in the low wave number region and it is not possible to extrapolate the spectral density $F(n_1)$ to zero wave number with any high degree of accuracy. The expression (3.13) may however be used to obtain an order of magnitude estimation of the integral scale. On performing this we obtain $L_{x_1}/\delta \approx 1$ for all the boundary layers presently considered. This result indicates the presence of large turbulent eddies of physical dimensions comparable with boundary layer thickness.

---

* The longitudinal integral scale is properly defined as

$$\Lambda_1 \equiv \int_{-\infty}^{+\infty} \frac{\overline{u_i(\underline{x})\, u_i(\underline{x}+\underline{r})}}{u_j(\underline{x})\, u_j(\underline{x})}\, dr_1$$

and thus represents a distance over which the velocities are correlated. It provides a measure of the physical dimensions of the largest eddies of the turbulent motion. The length L_{x_1} is approximately proportional to the integral scale Λ_1

3.45 Comparison with other similar turbulent boundary layer data

The data obtained during the present experimental study are compared with the constant K boundary-layer data of other workers in figures 3.39 and 3.40 which display the variation* of R_2 and H and K. Included in the figures are the constant K boundary layer data of Launder and Stinchcombe (51), Badri Narayanan and Ramjee (2), Julien et al (43), Loyd et al (56) together with the present data. The data of Julien et al and Loyd et al were obtained in the same experimental apparatus. Their results represent part of a much larger experimental investigation into the effects of heat and mass transfer and pressure gradient on the turbulent boundary layer which is proceeding under the direction of Professor W M. Kays and his associates at the University of Stanford, U.S.A. Also shown in figures 3.39 and 3.40 is the

---

* The reader is reminded that a turbulent boundary layer developing in a constant K acceleration will asymptotically approach a similar solution for which R_2 and H will be invariant with x_1. For this similar flow both R_2 and H will be given by unique functions of K.

equilibrium boundary layer data of Herring and Norbury for which $\beta = -.53$ (where $\beta \equiv \delta_1/\tau_w \, dp/dx_1$). Launder and Stinchcombe (51) showed that equilibrium boundary layers where $\beta < -.5$ would approach asymptotically the similar constant K boundary layer solution. Furthermore they estimated that the Herring and Norbury data was very close to similar at the last measuring station. It is thus appropriate to include the data in this discussion of similar turbulent boundary layers. To facilitate discussion of the various data the similar theoretical solution appropriate to laminar flow is shown together with the 'fully turbulent standard' mixing length solution of ref. (52).

The results of Herring and Norbury, Julien et al ($K = .57 \times 10^{-6}$ $K = .77 \times 10^{-6}$) and Badri Narayanan and Ramjee ($K = .6 \times 10^{-6}$) are representative of similar boundary layers arising in a mild acceleration. For these layers the momentum deficit thickness Reynolds number R_2 and shape factor H, lie very close to the 'theoretical' fully turbulent solution. This is not an unexpected result since the Reynolds numbers are relatively large; we should also not expect a mild pressure gradient to distort the turbulence structure of the boundary layer to any appreciable extent.

Boundary layers in strong accelerations are represented by the data of Launder and Stinchcombe, Julien et al ($K = 1.45 \times 10^{-6}$), Loyd et al, Badri Narayanan and Ramjee ($K = 2.8 \times 10^{-6}$) and the present measurements. The experimental results of the present study display a smooth shift in measured values of R_2 and H from those appropriate to a 'fully turbulent' boundary layer towards those of a

laminar flow as K is increased.

The data of Launder and Stinchcombe also display a similar trend but their values of R_2 are substantially lower than those of the present study. The experiments of Launder and Stinchcombe however were, as they acknowledge markedly affected by three-dimensionality of the mean flow which, they estimated, produced values of R_2 too low by approximately 30%. However, as they again point out, the shape factor measurements are less effected by lack of two-dimensionality and their values agree fairly well with the shape factors measured in the present study.

The experiments of Badri Narayanan and Ramjee ($K = 2.8 \times 10^{-6}$) result in a value of R_2 which is in very close agreement with the present data and a shape factor which is estimated to be about 6% higher than the value implied by the present data.

The constant K boundary layer data of Julien et al (for $K = 1.45 \times 10^{-6}$) and Loyd et al is presented by them as being representative of layers which have reached 'similar conditions'. Their data however differ from the present data by quite a large amount. The discrepancies between the values of R_2 and H measured in the present study and those obtained by Julien et al and Loyd et al appear to increase with K; at $K = 2.5 \times 10^{-6}$ Loyd's value of R_2 is about 30% higher and the shape factor is approximately 8% lower compared with 15% higher and 7½% lower at $K = 1.45 \times 10^{-6}$. The reason for this discrepancy may be readily observed in fig.3.41 where the variation of R_2 and H along the test section in the experiments of Julien and

Loyd is shown. The physical dimensions of their apparatus resulted in values of R_2 at the beginning of the acceleration which were much larger than the asymptotic similar values. Thus, although in other respects their experiments are of a high quality, the boundary layers at the end of the acceleration have clearly not reached their asymptotic form; both R_2 and H are still changing quite appreciably.

3.46 Concluding Remarks

Three constant K turbulent boundary layers have been set up in a plane convergent channel and studied experimentally. The values of K considered i.e. $K = 1.5 \times 10^{-6}$, $K = 2.5 \times 10^{-6}$ and $K = 3.0 \times 10^{-6}$ cover the range over which laminarisation occurs.

The boundary layers have mean velocity profiles which asymptotically approach those of similar boundary layers at their respective value of K. For the three values of K the boundary layers have over the final stages of the acceleration, mean velocity profiles which are 'similar' to a high degree and thus values of R_2 and H which are essentially constant from station to station. The measured values of skin friction coefficient are also constant (to within the experimental error) throughout the acceleration. The mean velcoity profiles display a relative shift from those appropriate to a 'fully turbulent' boundary layer towards those of a similar laminar boundary layer as K is increased. For the highest value of acceleration i.e. $K = 3.0 \times 10^{-6}$ the mean velocity profiles have values of R_2 and H which approach those of a similar laminar boundary layer. These results are in broad agreement

with the results of other experimentalists.

Longitudinal turbulence intensity profiles were measured at 4 in intervals through the constant K region of the accelerations. The profiles show some decay of intensity through the acceleration although for $K = 1.5 \times 10^{-6}$ and $K = 2.5 \times 10^{-6}$ the amount is small. For $K = 3.0 \times 10^{-6}$ a larger decay is evident; being most noticeable in the maximum intensity near the wall in which a decay of about 30% occurs. It should be noted that a changing longitudinal intensity profile (normalised) in the acceleration is not inconsistent with a similar mean velocity profile. Any very large scale fluctuation will contribute to the longitudinal intensity but at the same time is unlikely to contribute appreciably to the Reynolds stress $[- \overline{u_1 u_2}]$ and as a result the mean velocity will remain unaffected. Also turbulence quantities e.g. $\overline{u_1^2}$, $\overline{u_1 u_2}$, respond to the effects of pressure gradient, in general more slowly than the mean velocity and in addition provide a more sensitive indication of the structure of the turbulent boundary layer. The approach of profiles of fluctuating quantities to their similar form will proceed more slowly than the mean velocity profile. The longitudinal turbulence intensity profiles thus provide a very sensitive test of the'closeness to similarity' of the boundary layers.

However, for $K = 3.0 \times 10^{-6}$, in addition to the decay in longitudinal turbulence intensity there is a small but perceptable increase in shape factor through the acceleration. At the end of the acceleration the resulting values of R_2 and H of 275 and 1.75 respectively are quite close to the values

of 220 and 2.0 which are appropriate to a similar laminar boundary layer at $K = 3.0 \times 10^{-6}$. In view of this it seems possible that for $K = 3.0 \times 10^{-6}$ a similar turbulent boundary layer may not exist; that is, an initially turbulent boundary layer if subjected to an acceleration of $K = 3.0 \times 10^{-6}$ will eventually decay to laminar. The above remarks however remain conjective only, since in the present study it was not possible to maintain the acceleration for a sufficient distance for either a fully similar turbulent boundary layer to arise or for complete degeneration to laminar to occur at $K = 3.0 \times 10^{-6}$.

For the three accelerations presently considered the spectra of longitudinal turbulence intensity were measured at various positions in the boundary layer and at two x_1 stations. These spectra differ from those obtained in high Reynolds number flows in that a [-5/3] law was absent. The spectra do, however indicate the presence of large eddies of wave length comparable with the boundary layer thickness; a result also obtained in high Reynolds number flows.

At the lowest acceleration, i.e. $K = 1.5 \times 10^{-6}$ measurements of the Reynolds shear and normal stresses were made with an X-wire hot wire probe. The measurements indicate that the normal stresses are roughly in the same proportion to each other as in high Reynolds number flows. The structure parameter $[\frac{\overline{u_1 u_2}}{k}]$ and correlation coefficient $\frac{\overline{u_1 u_2}}{\sqrt{\overline{u_1^2}}\sqrt{\overline{u_2^2}}}$ are also, as in high Reynolds number flows, approximately constant over a large part of the boundary layer but have values which are less than those found in high Reynolds number flows. It thus seems plausible to conjecture that the Reynolds shear stress

approaches zero more rapidly than the turbulence kinetic energy in a turbulent boundary layer which is undergoing degeneration to laminar; the turbulence becoming more disorganised and random in nature.

CHAPTER IV

THEORETICAL CONTRIBUTION

4.1 Introductory Remarks

The design of equipment for practical applications requires, in a large number of cases, the calculation of various fluid flow phenomena. Some idea of the importance of this requirement may be obtained if mention is made of some of the many situations where accurate prediction of the flow is needed. Prior knowledge of the flow is required for the design of aircraft, heat exchangers, rocket nozzles, gas turbines, compressors and combustion chambers; for example the aircraft designer needs to be able to predict drag and the efficient design of heat exchangers requires prediction of local heat transfer rates. To meet the needs of the designer a calculation or prediction method must fulfil certain requirements, namely that it provides accurate and reliable solutions and that it is economical to use.

The motion of any fluid continuum is described by the Navier-Stokes equation. However, fluid motion has traditionally, and for very good reason, been divided into two categories, namely laminar and turbulent flows. For laminar flow, the numerical solution of the equations of motion is at present possible, although in general not a trivial task, and solutions have been obtained for a number of cases. However, most practically occurring

flows are turbulent and solution of the Navier-Stokes equation is not, in this case, a feasible proposition. In order to make the turbulent flow problem tractable, it is necessary to separate the mean and fluctuating motion and then average the Navier-Stokes equation. Averaging, however, results in a loss of information to the point where the equations are not closed. In the equation of mean motion unknown velocity correlations of the fluctuating motion arise in the form of apparent stresses traditionally termed the Reynolds stresses. Additional equations for these Reynolds stresses may be derived by manipulation of the Navier-Stokes equation but further unknown correlations are then introduced. Of course equations may be derived for these further unknowns and so on. However the number of independent unknowns increases at a greater rate than the number of equations and so rigorous closure is just not possible. Thus any treatment of turbulent flow in which averaged equations are utilised will, of necessity, involve approximation. At some stage it is necessary to curtail derivation of further equations and to approximate the unknown correlations in terms of known quantities. Such approximations have been individually termed 'closure assumptions' and when taken collectively to form a closed set of equations constitute a 'turbulence model'. The calculation of turbulent flow thus involves the devising of (a) a model of turbulence and (b) an efficient and economical means of solving the resulting equations. Clearly the development of (a) and (b) are closely related.

The calculation of turbulent flow was in the past, for the most part,restricted to the calculation of steady two-dimensional turbulent boundary layers for which procedures based on the ordinary differential integrated equations of motion were developed. However these lacked generality and over the past decade have been largely superseded by methods based on solution of the partial differential boundary layer equations. The past five years have also seen the development of numerical schemes for solving the averaged partial differential (elliptic) equations for two-dimensional steady flow e.g. ref (31), and for two-dimensional unsteady (or time dependent) flow e.g. ref (1). The two-dimensional turbulent boundary layer remains, however, an important sub-class of turbulent flow and provides a close approximation of many important practical applications e.g. flow in ducts and pipes and flow over turbine and compressor blades.

The present work is concerned with devising a procedure for calculating the development of the turbulent boundary layer with particular reference to strongly accelerated flows and laminarisation. However before introducing the present contribution it is appropriate to review the various turbulence models which have been proposed by other workers. The remainder of this Chapter is thus divided into four main sections, the first of which is concerned with a review of existing turbulence models. In sections II, III and IV the present contribution is described. Section II is concerned with predictions

made with the aid of a mixing length turbulence model. Presented in Section III are some predictions obtained with a turbulence model based on an approximated form of the turbulence kinetic energy equation together with an algebraic length scale distribution. Finally in Section IV a new turbulence model is presented. The model provides for a description of turbulence in terms of two scalar turbulence properties for which differential rate equations are solved. The model is applied to the calculation of a range of accelerated flows and comparisons made with experiment.

4.2 SECTION I - A brief survey of existing turbulence models

All the models to be reviewed here have the common aim of calculation of the Reynolds stress tensor Rij ($\equiv\overline{u_i u_j}$) which appears in the averaged equation of mean motion:

$$\frac{DU_i}{Dt} = -\frac{1}{\rho}\frac{\partial P}{\partial x_i} + \frac{\partial}{\partial x_j}\{\nu\frac{\partial U_i}{\partial x_j} - R_{ij}\} \qquad (4.1)$$

A large number of models have been proposed in order to obtain a closed set of equations and these vary both in principle and in complexity and sophistication. It is thus necessary before surveying the models to adopt a method of classification. The one chosen here is that of categorising the closure assumptions into two basic groups depending on whether (a) the Reynolds stress is assumed directly proportional to the mean rate of strain, or (b) the rate of change of Reynolds stress is specified in terms of local flow parameters. Models which fall into

the former class will be called 'turbulent viscosity' models. Those of the latter group involve solution of a partial differential rate equation for the Reynolds stress and will therefore be termed differential rate models.

(1) 'Turbulent Viscosity' Models

Models of this group represent the simplest level of approximation and involve representation of the Reynolds stress in terms of a function of the mean rate of strain. All models of this type may be written in the general form:-

$$\overline{u_i u_j} = {}^2/_3 k\,\delta_{ij} - \nu_T S_{ij} \qquad (4.2)$$

where $S_{ij} \equiv \frac{\partial U_i}{\partial x_j} + \frac{\partial U_j}{\partial x_i}$

and where ν_T is a 'turbulent viscosity' which must be specified in terms of either the mean velocity field or some properties of the turbulence.

(2) Differential Rate Models

Models which fall within this group have the common feature of requiring solution of a differential equation for the Reynolds stress. By manipulation of the Navier-Stokes equation (see ref (38)) an equation for R_{ij} may be derived:-

$$\frac{DR_{ij}}{Dt} = - R_{im}\frac{\partial U_j}{\partial x_m} - R_{jm}\frac{\partial U_i}{\partial x_m} - \frac{\partial}{\partial x_m}\{\overline{u_i u_j u_m}\}$$

$$- \frac{1}{\rho}\left[\frac{\partial}{\partial x_j}\overline{u_i p} + \frac{\partial}{\partial x_i}\overline{u_j p}\right] + \overline{p/\rho\left\{\frac{\partial u_i}{\partial x_j} + \frac{\partial u_j}{\partial x_i}\right\}}$$

$$+ \nu\frac{\partial^2 R_{ij}}{\partial x_m \partial x_m} - 2\nu\,\overline{\frac{\partial u_i}{\partial x_m}\,\frac{\partial u_j}{\partial x_m}} \qquad (4.3)$$

The unknown terms appearing on the right of the above equation may be either approximated in terms of R_{ij}, the mean velocity field and various length scales or obtained from solution of differential rate equations for those quantities. Of course these equations will contain further unknowns for which approximations must be made. Models at this level of closure usually include one or more equations for turbulence length scales. For the simplest case, (where only an equation for R_{ij} is utilised), the models in general involve solution of a minimum of six differential equations in addition to the mean momentum and continuity equations.

The two basic groups defined above may be subdivided still further. Thus we differentiate between simple 'turbulent viscosity' models in which the viscosity is specified purely in terms of flow geometry and local mean velocity and more elaborate turbulent viscosity models in which turbulence is recognised explicitly; ν_T is specified in terms of some turbulence properties for which differential rate equations are solved.

Similarly, models of the differential rate group are subdivided into those in which closure assumptions are made to the R_{ij} equation, here termed Reynolds stress Closures, and those for which closure is effected at a higher order. A number of higher order models have

been proposed but they are extremely complex and uncertain in nature and at present do not represent a practical solution to turbulent flow. Therefore they will be classified collectively under the subgroup heading higher order models.

4.21 'Turbulent Viscosity' Models

(1) Simple 'Turbulent Viscosity' Models

This model has been used extensively in the calculation of turbulent boundary layer flows for which it reduces to:

$$\overline{u_1 u_2} = - \nu_T \frac{\partial U_1}{\partial x_2} \qquad (4.4)$$

The turbulent viscosity is specified either (i) in terms of the flow geometry or by (ii) the Prandtl mixing length hypothesis.

An example of (i) is the constant turbulent viscosity model proposed by Prandtl (71) for free jet flows:

$$\nu_T = C \, \delta \, (U_{1_{MAX}} - U_{1_{MIN}}) \qquad (4.5)$$

where C is a constant and δ is the jet width.

The Prandtl mixing length hypothesis results in:

$$\nu_T = \ell_m^2 \left| \frac{\partial U_1}{\partial x_2} \right| \quad \text{(or in general} \quad \nu_T = \ell_m^2 \sqrt{S_{mn} S_{mn}} \text{)} \qquad (4.6)$$

where ℓ_m is the mixing length which must be specified in terms of flow geometry. The mixing length model has been used with considerable success for the calculation of a wide range of both free and wall boundary layer flows, see e.g. ref (69). The model has also been used to a lesser extent

for the calculation of 'recirculating flows' (see e.g. ref (31)) although the success is here limited. However the degree of success obtained depends directly on the correctness of the mixing length specification and thus some prior knowledge of the flow is required before calculation can be made. Many appraisals of the validity and implications of the mixing length model are available in the literature (e.g. refs (38) and (84)) and so detailed discussion is not warranted here. Suffice it to say that the model appears to be a good approximation if confined to self-preserving flows which can be described by single time and length scales and flows in local equilibrium where the spatial and time development proceeds slowly.

(2) More Elaborate 'Turbulent Viscosity' Models

Models of this group have the common feature that the viscosity is assumed to depend on turbulence rather than mean flow properties. They represent an improvement over the 'simple viscosity models' in that turbulence is recognised explicitly; the evolution of the turbulence field being incorporated through differential equations for one or more properties of the turbulence. At the same time the models involve only a small amount of additional effort for solution over the 'simple viscosity models' and considerably less than the closures at the Reynolds stress level.

The 'turbulent viscosity' may now be written:-

$$\nu_T = k^{\frac{1}{2}}L \qquad (4.7)$$

where L is a turbulence length scale which may either be specified algebraically in terms of flow geometry or obtained from solution of a differential equation. k is the turbulence kinetic energy which is obtained from the solution of a differential rate equation. The model was proposed independently by Kolmogorov (47), Prandtl (72) and Emmons (27). With an algebraic scale distribution, the model has been used in the calculation of various boundary layer flows by a number of workers, some examples of whom are Weighardt (72), Glushko (30), Beckwith and Bushnell (8) and Mellor and Herring (62). The model has also, to a lesser extent, been applied to the calculation of two-dimensional recirculating flows, e.g. ref (87).

Specification of an algebraic scale distribution in terms of flow geometry requires some prior knowledge of the flow to be predicted. The desire to dispense with this constraint led a number of workers to propose differential equations from which the turbulence length scale could be obtained. Kolmogorov (47) appears to have made the first suggestion of this kind in proposing a turbulent viscosity model based on solution of equations for turbulence kinetic energy and frequency of turbulence. Harlow et al (35) postulated an equation for L (later replaced by an equation for dissipation rate of turbulence energy)as part of a viscosity model and applied it to the prediction of turbulent pipe flow. The agreement between calculation and experiment was however poor. (Harlow's group have now discarded 'turbulent viscosity' models in favour of those based on approximation

and solution of the Reynolds stress equations.)

Rotta (77) derived a differential equation for an integral scale of the turbulence as a component of a turbulence model in which closure assumptions were made for the unknown terms in the Reynolds stress equations. Recently Rodi and Spalding (76) and Ng and Spalding (65) have utilised Rotta's length scale equation in a turbulent viscosity model to obtain predictions for a range of boundary layer flows; Rodi and Spalding present predictions for quasi-parallel free flows and Ng and Spalding predictions for wall boundary layers.

A slightly different approach was recently adopted by Nee and Kovasznay (64) who proposed a differential rate equation for the 'turbulent viscosity' itself. With an algebraic length scale distribution the model was applied to the calculation of a number of wall boundary layer flows.

4.22 Differential Rate Models

(1) Reynolds Stress Closures

A rigorous approach to the calculation of the Reynolds stress tensor $\overline{u_i u_j}$ necessitates approximation and solution of the Reynolds stress equations. It is unlikely that a truly universal general turbulence model will be found which does not involve closure at least at this level of approximation. However the difficulties in both closing the equations and then subsequently solving the resultant set deterred most earlier workers - at least those with any intention of using their models - from proposing closure

at the Reynolds stress level. A contributing factor was that most workers were concerned with boundary layer flows only for which the simpler models in most cases suffice.

Recent interest in the development of general turbulence models has resulted in a good deal of attention being attracted to closure at the Reynolds stress level. The first turbulence model based on closure at this level of approximation was given by Rotta (77). The closed set of equations with a turbulence scale distribution given by Nikuradse's (66) mixing length expression was solved for the case of a plane channel (outside the viscous sublayer only). In a subsequent paper (77) Rotta derived, from the Navier-Stokes equation an equation for an integral scale of the turbulence which was to be used in place of the mixing length expression. More recently, Donaldson and Rosenbaum (25) have effected closure of the Reynolds stress equations by a method of invariant modelling. An algebraic scale distribution was utilised and the equation set was applied to the calculation of the constant pressure plane boundary layer. An attempt was also made to predict natural transition.

Harlow et al (32) have also considered models based on the Reynolds stress equations. They proposed a model which involves solution of an equation for dissipation rate of turbulence kinetic energy as well as the Reynolds stress equations. The model has been tested in a number of situations. Harlow and Romero (33) used the model with moderate success to study the distortion of isotropic

turbulence and Daly and Harlow (22) obtained predictions for flow in a plane channel. At present the model is not accurate near walls and is still under development.

A different approach to the closure of the R_{ij} equation was recently adopted by Bradshaw et al (10) who proposed a boundary layer calculation method which was based on a differential rate equation for the shear stress $[-\overline{u_1 u_2}]$. Use was made of Townsend's (84) proposal that, for boundary layer flows, the ratio $\{\overline{u_1 u_2}/k\}$ might be constant in regions of persistent shear. Bradshaw et al extended this proposal by hypothesizing that the ratio $[\overline{u_1 u_2}/k]$ was a well behaved function of the cross stream co-ordinate for boundary layer flows. The assumption was then used by Bradshaw et al to convert the turbulent kinetic energy equation into one for shear stress $[\overline{u_1 u_2}]$ and with an algebraic dissipation length scale formed the basis of a boundary layer calculation procedure. For the purposes of demonstration, the ratio $[\overline{u_1 u_2}/k]$ was assumed constant. The method was used for the successful prediction of a range of constant property wall boundary layer flows and has also been used for the prediction of compressible boundary layers. The method has also been extended so that certain types of three dimensional flows may be calculated. However the model in its present form has certain restrictive features: it is unsuitable for the prediction of flows in which the shear stress changes sign or for which an axis of symmetry exists e.g. pipe flow. Extension of the model to handle almost any boundary layer flow is in principle possible but

considerable prior knowledge of the flow would be required for specification of the variation of $[\overline{u_1 u_2}/k]$ and dissipation length across the layer. The model is thus not as general as the various turbulent viscosity models.

Hanjalic (36) has recently presented boundary layer predictions obtained with a turbulence model based on the simultaneous solution of the equations for turbulence kinetic energy, dissipation rate of turbulence energy, and Reynolds shear stress $[\overline{u_1 u_2}]$. Calculations were performed for a wide range of high Reynolds number flows which included wall boundary layers, turbulent pipe and channel flow, and various assymetric and free turbulent flows. The agreement of the predictions with experiment was in almost all cases excellent. This is of particular note since the calculations were performed using a single set of empirical constants; the model is thus extremely general.

(2) Higher Order Models

There have been a number of proposals for turbulence models in which closure assumptions are made at a higher level of approximation than for models at the Reynolds stress level. However the models are of necessity complex in form and usually involve large numbers of differential equations and assumptions which are extremely uncertain in nature. They do not, at present, represent a practical approach to the calculation of turbulent flow and so only a few examples will be discussed here.

Chou (18) proposed a turbulence model in which

closure assumptions were made in the equation for triple velocity correlation. The pressure fluctuation terms were approximated by consideration of Poisson's equation for the fluctuating pressure and an additional equation was derived for the vorticity decay. From this latter quantity the micro-scale of turbulence, which was utilised in the approximations, was obtained. The closed set of equations was applied to the calculation of turbulent flow in a plane channel for which quite good agreement was achieved with the small amount of data available in 1945.

More complex models based on approximation of the triple velocity correlation equations have also been proposed by Davidov (23) and Kolovandin and Vatutin (48). However no applications of the models have been presented.

Another approach to the problem of closure has recently been proposed by Lundgren (58). Closure was effected by making assumptions regarding the multipoint probability distribution functions for velocity rather than the velocity moments. However no applications of the model have so far been presented.

An approach which may provide information regarding turbulence structure was that adopted by Deardoff (24) For flow in a channel, a time dependent, three dimensional, numerical solution of the Navier-Stokes equation was performed for the large scale motion. For turbulent motion of scale smaller than the computational mesh a 'turbulent viscosity' closure approximation was used. While models of this type will not for many years provide

a practical general solution for turbulent flow, the results of a few such calculations may provide useful information and guidance for the framing of lower order turbulence models.

4.3 SECTION II - Early attempts at the prediction of Laminarisation

4.31 Determination of the Onset of Laminarisation

Initial theoretical work into the phenomenon of laminarisation was directed into devising a parameter which would determine its onset. This work yielded parameters which may all be written in the form $K.(Cf/_2)^{-n}$ and for which values of the exponent n equal to $\frac{1}{2}$, 1 and 3/2 were separately proposed e.g. ref (4), (51). Of these exponents the value 3/2 is probably the most appropriate. However if parameters of the above type are to provide an indication of the onset of laminarisation, then it is necessary that the acceleration be applied for some appreciable time and be changing only slowly in the flow direction. The reason for this is that the mean velocity and, especially, the turbulence structure i.e. $[\overline{u_1 u_2}]$ will not respond instantaneously to the effects of acceleration. Moreover, in the case of a slowly changing acceleration, the skin friction coefficient $[Cf/_2]$ will also vary slowly and be related to the acceleration parameter K. $Cf/_2$ is usually an inaccurately known parameter in accelerating flows and as a result there is little experimental evidence to prefer parameters of the

general form $K.(Cf/_2)^{-n}$ over the simpler parameter K. The parameter K has the benefit of containing only external flow parameters which are usually well specified in practically occurring flows.

A conceptual improvement over parameters of the type $K.(Cf/_2)^{-n}$ was made by Patel and Head (68) who proposed that the onset of laminarisation was controlled by the parameter $\nu/u_\tau^3 \overline{\partial\tau}/_{\partial x_2}$ where $\overline{\partial\tau}/_{\partial x_2}$ is an average shear stress gradient over the inner region. The parameter was used by Patel and Head to correlate the departures from the law of the wall which occur in low Reynolds number turbulent flow in pipes and channels and in accelerated boundary layers. The parameter, although an improvement over earlier ones, suffers from the defect that the inner fraction over which the shear stress gradient should be averaged must be chosen in some arbitrary fashion. Moreover, from the experimental viewpoint it is a formidable task to measure shear stress gradients near walls in accelerating flows.

Recently Bradshaw (13) has formulated a model which is purported to determine the onset of laminarisation. Bradshaw argued that turbulent flow would be directly dependent on viscosity when the shear-stress-producing and dissipating range of eddy sizes overlapped and that laminarisation would thus occur when the viscosity independent region disappeared. As a measure of the overlap region, an eddy Reynolds number $({}^{\tau}t/_{\rho})^{\frac{1}{2}} L/_{\nu}$ was introduced (where L is a length scale associated with the

shear-stress-producing eddies). By putting L equal to the mixing length (κx_2) and from consideration of high Reynolds number constant pressure flows a critical value of this Reynolds number was deduced. Laminarisation would thus occur if the maximum value of the Reynolds number $(\tau t/\rho)^{\frac{1}{2}}L/\nu$ was below the critical value through the layer. Bradshaw demonstrated that his model was consistent with Preston's (73) value of the minimum Reynolds number necessary for the existence of a turbulent boundary layer in zero pressure gradient and the Patel-Head shear stress gradient parameter. He also attempted to demonstrate that his criteria would account for laminarisation of a boundary layer over a porous surface with suction. The model of Bradshaw suffers, however, from two shortcomings: firstly it allows only the determination of the onset of laminarisation and provides no information regarding the types of flow which will arise under the influence of laminarisation. It is known that in moderate accelerations boundary layers may arise which exhibit features intermediate between those of fully turbulent and laminar boundary layers, e.g. the dips in Stanton number shown in the experiments of Moretti and Kays: the model does not provide a means of predicting these features. Secondly, when applied to flows with suction the model gives rise to a laminarisation criteria in which the boundary layer thickness δ appears. It is difficult to envisage, however, that transpiration induced laminarisation could be influenced by events far from the surface (which is the implication of including δ).

4.32 Some Predictions of Laminarisation with a Mixing Length Model

Early attempts at the prediction of laminarisation centred around use of the Van Driest (26) near wall mixing length specification*:-

$$\ell_m = \kappa x_2\{1 - \exp\left[\frac{-x_2\sqrt{\tau/\rho}}{\nu A^+}\right]\} \qquad (4.8)$$

This expression was found by Van Driest (with the constants κ and A^+ assigned the values 0.40 and 26.0 respectively) to lead to predictions of mean velocity profiles in turbulent pipe flow which were in excellent agreement with measured values throughout the sublayer and semi-logarithmic regions of the flow. Now, an important observed feature of boundary layers undergoing strong acceleration is a thickening (in x_2^+ co-ordinates) of the viscous sublayer. The parameter A^+ may be interpreted as a measure of the thickness of the sublayer. Thus if A^+ is allowed to vary then a means exists for modelling the observed behaviour of the sublayer of accelerated boundary layers.

In papers by Launder and Jones (52) and (53) and Jones and Launder (42) proposals were made for the specification of A^+ in terms of a function of p^+ which was to be used in conjunction with a simple empirical

---

* In Van Driest's original proposal, the wall shear stress appeared in the argument of the exponential. The expression was generalised by Patankar and Spalding (69) who replaced the wall shear stress with the local value.

lag equation. Since then a number of other workers have proposed models for the determination of A^+. Kays et al (44) correlated the Stanford experimental data to obtain A^+ as a function of the local dimensionless pressure gradient, p^+ and surface mass transfer rate m^+. They then used the correlation together with a lag equation similar to that proposed by Launder and Jones (53) to obtain predictions of their data. An 'A^+ model' which was intended to be applicable to accelerated flows with surface mass transfer was also proposed by Launder and Jones (54). The laminarisation criteria of Bradshaw (13) was re-interpreted by utilising the Van Driest mixing length formula to obtain an expression for A^+. The model displayed the correct qualitative trends for variations of sublayer thickness caused by acceleration or suction through a porous surface. 'A^+ models' which purport to be applicable to accelerated flows with surface mass transfer have also been proposed by Cebeci and Mosinskis (16) and Powell and Strong (70).

While a number of the above proposals do represent an improvement over the 'standard' Van Driest formula (equation (4.8)) there appears no evidence that a wholly satisfactory prescription of near wall mixing length has yet been devised; indeed, later in this section it will be argued that such a prescription is not achievable.

The remaining part of this section is concerned with some mixing length predictions of strongly accelerated flows obtained by the writer. Much of this work is

described in papers by Launder and Jones (52) and (53) and Jones and Launder (41). It is included here mainly to provide the reader with some idea of the limitations of a mixing length model when applied to the calculation of accelerated flows.

4.33 The Model Considered

Hydrodynamic predictions were performed through solution of the continuity and mean momentum equations (equations (2.7) and (2.8)). The Reynolds stress ($\overline{u_1 u_2}$) was obtained by use of a simple turbulent viscosity model in which the viscosity was assumed given by the Prandtl mixing length hypothesis:-

$$\nu_T = \ell_m^2 \left| \frac{\partial U_1}{\partial x_2} \right| \qquad (4.9)$$

where the mixing length, ℓ_m was given by a ramp function modified in the near wall region by a Van Driest (26) formulation:

$$\left.\begin{aligned} \ell_m &= \kappa x_2 D_v \qquad 0 < x_2 \leq \frac{\lambda}{\kappa} \delta_{.99} \\ \ell_m &= \lambda \delta_{.99} M \qquad x_2 > \lambda/\kappa \delta_{.99} \\ D_v &= 1. - \exp\left\{\frac{-x_2\sqrt{\tau/\rho}}{\nu A^+}\right\} \end{aligned}\right\} \qquad (4.10)$$

where κ and λ are constants of values .40 and .09 respectively. $\delta_{.99}$ is the normal distance (from the surface) at which the velocity differs by 1% from the free stream value and where M is chosen to give a continuous shear stress at the ramp join.

Such a ramp mixing length distribution seems to have been first used by Hudimoto (39) and was substantiated by Escudier (28) in an examination of a diversity of experimental data. The mixing length model defined by equations (4.9) and (4.10) with A^+ having a constant value of 26 will be here termed the 'standard mixing length model'.

For flows with heat transfer it is necessary to calculate the development of the thermal boundary layer. This may be achieved through solution of the thermal energy equation (equation (2.9)).

The term $\overline{u_j \theta}$ which represents the transfer of thermal energy by turbulent motions was approximated in a manner analogous to the turbulent viscosity model for momentum. It may be written:-

$$\overline{u_j \theta} = -\nu_T / \sigma_T \frac{\partial \Theta}{\partial x_j} \qquad (4.11)$$

where σ_T is a turbulent Prandtl number whose value was taken to be 0.9 throughout the boundary layer.

Patankar and Spalding (69) used their finite-difference procedure for the solution of the boundary layer equations to apply a mixing length model similar to that given by equation (4.10) to the prediction of a diversity of flows. Their finite difference solution was patched near the wall at x_2^+ about 100 onto a one dimensional solution obtained once and for all by use of the Van Driest expression and the molecular viscosity did not appear explicitly in the finite difference equations.

Reasonable agreement with experiment was achieved for a range of high Reynolds number flows. The model however completely failed to predict the effects of laminarisation on the boundary layer.

In the present work the finite difference procedure was extended so that the complete boundary layer equations were solved for all the layer including the near wall viscous sublayer region. This circumvented the need for the one dimensional approximation in the near wall region but necessitated the use of a larger number of cross stream grid lines. There were several reasons for this decision:

a) It was felt that the one dimensional approximation was unlikely to be satisfied over any appreciable region in strongly accelerated flows. This conjecture has subsequently been shown to be correct by Loyd et al (56) who found from an examination of their profile data that the one dimensional relation $\tau^+ = 1 + m^+U_1^+ + p^+x_2^+$ was inadequate beyond $x_2^+>5$ for strongly accelerated flows.

b) Earlier experimental studies (49) and (68) had suggested that the principal effects of strong acceleration on the turbulent boundary layer were displayed in the sublayer. One such feature was the increase in thickness (in x_2^+ co-ordinates) of the viscous sublayer with increasing acceleration. In view of this it was anticipated that successful prediction of laminarisation might be accomplished if some means could be found for predicting the thickness of the sublayer. As noted previously, this variation in sublayer thickness may be incorporated in the mixing

length model if A^+ is allowed to vary.

However, predictions based on a variable A^+ model necessitated either the carrying out of a one dimensional calculation after each forward step or extension of the finite difference scheme to cover all the layer including the near wall region; the latter of these was clearly to be preferred.

c) In a boundary layer undergoing laminarisation, the region of significant viscous stresses would ultimately extend to cover all the layer and not, as in high Reynolds number flows, be confined to a region in the immediate vicinity of the wall. Thus part of the reasoning behind the introduction of one dimensional solutions no longer applied.

4.34 Similar Boundary Layers

Attention was first focussed on the prediction of the similar turbulent boundary layers which arise from flow in a plane convergent channel; we have seen that these layers have special relevance to the problem of laminarisation. However before predictions could be made it was necessary to check the accuracy of solutions obtained with the modified version of the finite difference procedure. Similar boundary layers were particularly convenient for this purpose also, since here the partial differential boundary layer and continuity equations reduced to a single ordinary differential equation. Thus it was possible to solve this ordinary differential, 'similarity' equation numerically and compare the resulting

solution with that obtained with the finite difference procedure. Details of the numerical solution of the 'similarity' equation and a discussion of the results obtained are given by Launder and Jones (52).

Initially some difficulties were experienced with the finite difference procedure, first in obtaining similar solutions and then in achieving agreement with the solution of the ordinary-differential 'similarity' equation. However these were resolved with the removal of a number of small inconsistencies* from the finite difference procedure. A comparison of the two solutions then revealed excellent agreement with only small differences between profiles and values of R_2 and H which agreed to within about 4%. These small differences could be accounted for at least in part by the small discrepancies in mixing length specification between the two solutions; these were associated mainly with the definition of boundary layer thickness and could not easily be removed. The finite difference solutions satisfied the 2-dimensional momentum integral equation (2.10) to within 2%. As an additional check on the accuracy of the finite difference procedure solutions were obtained for laminar similar boundary layers for which an exact analytic solution existed. The calculated mean velocity profiles were practically indistinguishable from the exact profiles and the predicted values of R_2 and H were within 2% of their exact values.

---

* These inconsistencies do not appear in later versions of the Patankar-Spalding finite difference procedure.

4.35 Constant A^+ Solutions - Comparison with Experiment

A comparison of predicted similar boundary layer mean velocity profiles with experimental data is displayed in figures 4.1(a) and 4.1(b). The predicted profiles are those obtained by use of the mixing length model defined by equations (4.9) and (4.10). Figure 4.1(a) shows the mean velocity $U_1/U_{1,G}$ plotted with abscissa $(\frac{U_{1,G}}{\nu} x_2)K^{\frac{1}{2}}$. The experimental data are those of Herring and Norbury* (37), ($\beta = -0.53$), and Jones (40); the exact laminar solution is also shown. It may be observed that the data of Herring and Norbury are, indeed, well predicted by the theoretical solution. Agreement is less satisfactory, however, with Jones' data at $K=2.2 \times 10^{-6}$. The discrepancy between measurement and prediction is greatest near the wall, where the slope of the theoretical profile is considerably greater than the measured.

The above discrepancy is shown in sharper relief in figure 4.1(b) where theoretical and experimental profiles are plotted semi-logarithmically on U_1^+, x_2^+ axes. The laminar solution and universal profile

$$U_1^+ = 1/.40 \ln x_2^+ + 5.3 \qquad (4.12)$$

are also plotted. At $K=2.4 \times 10^{-7}$, the predicted profile and the data of Herring and Norbury lie close to equation (4.12) At $K=2.2 \times 10^{-6}$ the predicted profile lies somewhat below

---

* The data of Herring and Norbury is of equilibrium rather than similar boundary layers. However, as is remarked elsewhere in this thesis, p. 61, the data is, in fact also closely representative of a similar boundary layer at $K=2.4 \times 10^{-7}$.

equation (4.12) but the measured solution lies considerably above it; that is, the effective sublayer thickness of the measured profile is significantly thicker than that of the theoretical solution.

Further evidence of the respective successes and shortcomings of the predicted solutions is presented in figures 4.1(c)and 4.2(b). Since R_2 and H are constant for a given value of K, a single point on these graphs corresponds to a particular similar boundary layer. Here, attention is focussed on the predicted solution for $A^+=26$ marked by a dashed line. In figure 4.1(c) the Herring and Norbury data and those of Badri Narayanan and Ramjee (2) for their mildest acceleration lie very close to the predicted turbulent solution. Jones' data, however, lie midway between the turbulent and laminar solutions as do those of Badri Narayanan and Ramjee for their steeper accelerations (though, with the latter data, it seems doubtful whether the boundary layers had truly reached an asymptotic form). The data of the present experimental study, although not available at the time the calculations were performed, are also shown; a shift of the measured boundary layers from turbulent to laminar as K is increased is clearly displayed.

The predicted and measured variation of the shape factor, H, with K is shown in figure 4.2(b). Because the viscous sublayer has been included in the theoretical solution the shape factor increases with K. The rise in H, however, is not nearly as rapid as that of the measured

solutions.

4.36 Variable A^+ Solutions

The above comparisons with data have shown the predicted solutions to be in close agreement with measurements for values of K upto about 10^{-6}. For higher values of K, the data show a progressive shift towards the laminar boundary layer solution. Indeed, the data on figure 4.2(b)would seem to suggest that no non-laminar solution exists for a value of K in excess of approximately 4×10^{-6}. Figure 4.1(b)had shown clearly that one important shortcoming of the theoretical solution was that no means were incorporated to allow the region over which viscous effects were important to grow as K increased. Thus it seemed worth investigating whether by increasing A^+ one could obtain solutions in tolerable agreement with experiment. Hence a finite difference solution of the similar boundary layer at $K=2.2 \times 10^{-6}$ was obtained with A^+ chosen (by trial and error) so that the predicted profile had the same value of R_2 as Jones' measured solution i.e. $R_2=430$. (This latter result was obtained by the writer in an earlier experimental study (40) and was the only data available at the time the calculations were performed; the results of the present experimental study and those of Julien et al (43) and Loyd et al (56) did not become available until later). The required value of A^+ was 61 and in figures 4.1(b) and 4.2(a)the theoretical and measured velocity

profiles are plotted. The result surpassed expectations for the complete experimental profile was indistinguishable from that predicted with $A^+ = 61$. However one data point did not provide sufficient information to determine the variation of A^+ with K for all similar boundary layers. In the absence (at the time) of more experimental data it was necessary to speculate how A^+ depended on K. The hypothesis used was that, for similar boundary layers, A^+ varied with K at a rate just sufficient to prevent the skin friction co-efficient exceeding some maximum value. The value chosen was that implied by Jones' data; namely $[C_{f/2}]_{max} = \cdot 0024$. It is of interest to note that this was the same value of skin friction which Coles (21) suggested was the maximum a turbulent boundary layer in zero pressure gradient could attain. [An examination of the present experimental results and the data of Julien et al (43) and Loyd et al (56) reveals that the above hypothesis was not far removed from the truth.]

The required value of A^+ for a particular value of K was determined by solving the boundary layer equations for a range of A^+ and by interpolation, selecting the value which gave the desired skin friction coefficient. As a result A^+ could be expressed as a function of K. In fact A^+ was correlated in terms of p^+ since one dimensional theoretical arguments (ref (51)) had suggested that it would be a better indicator of the onset of laminarisation than K alone*. The variation of A^+ with p^+ found from

---

* The parameter p^+ may be written as $-K\,(C_{f/2})^{-3/2}$. Hence for similar boundary layers, since $C_{f/2}$ is uniquely related to K, it is immaterial whether K or p^+ is used.

the maximum $C_{f/2}$ hypothesis was closely described by:-

$$A_s^+ = 26 \qquad p^+ > -5.36 \times 10^{-3}$$
$$A_s^+ = 11 - 2800\, p^+ \qquad p^+ \leq -5.36 \times 10^{-3} \tag{4.13}$$

where the subscript 's' denotes a value of A^+ appropriate to a similar boundary layer.

The predicted variations of R_2 and H with K, with A_s^+ calculated from (4.13) are represented by the broken lines in figures 4.1(c) and 4.2(b). The predictions display a plausible shift from the turbulent to the laminar solution as K is increased.

4.37 Non-Similar Boundary Layers

So far a method has been proposed for determining the effective sublayer thickness A^+ for the similar boundary layers which occur from flow in a plane convergent channel. However, in practical applications, the boundary conditions are very rarely, if ever, such that similar layers arise. It is thus necessary, for the successful calculation of practically occurring flows, to have a means of determining A^+ for non-similar (non-equilibrium) flows. At this point it should be noted that the method proposed for similar boundary layers, if applied to non-equilibrium situations, implies an instant response of the sublayer to changes in p^+; a totally implausible behaviour which leads to predicted laminarisation effects which occur much too rapidly.

For non-similar flows it was thus proposed that

the local rate of change of A^+ was proportional to the 'amount' the layer was out of equilibrium; a measure of which was taken to be the difference between the local value of A^+ and the hypothetical value that A^+ would attain if local conditions prevailed everywhere, i.e. if the value of p^+ was constant and equal to its local value. Hence this may be written:

$$\frac{dA^+}{dx} = c \frac{U_\tau}{\nu}[A_s^+ - A^+] \qquad (4.14)$$

where c is an empirical constant whose value must be chosen by recourse to experiment and where the value of A_s^+ is determined from equation (4.13) with the locally prevailing value of p^+. The length $[\nu/U_\tau]$ was taken as a representative sublayer scale.

It should be added that equation (4.14), although appealing in view of its simplicity, has little physical justification. It does however provide a simple and convenient method of introducing an essential lag in the effects of changes in boundary conditions on the predictions.

4.38 Heat Transfer Predictions

Predictions of the heat transfer data of Moretti and Kays (63) were obtained by simultaneous solution of the mean momentum and thermal energy equations, (2.7) and (2.9) in conjunction with the above quoted turbulence model. In the version of the finite difference programme used by Patankar and Spalding (69) the rate of spread of the finite difference grid was controlled by the calculated

rate of entrainment of fluid into the momentum boundary layer. However in strongly accelerated flows it is possible for the thermal boundary layer to extend beyond the velocity layer, e.g. ref (45). For the calculations presented here the grid control was such that this latter behaviour was possible; values of entrainment were calculated from consideration of both the momentum and thermal energy equations and the larger value used for grid control. The value of the constant c, appearing in the lag equation (4.14) was chosen by trial and error whereby two values were found to be necessary. They were:-

$$c = 3 \times 10^{-4} \qquad A^+ \geq A_s^+$$

$$c = 3 \times 10^{-5} \qquad A^+ < A_s^+ \qquad (4.15)$$

Figures 4.3(a) - 4.3(c) show experimental and predicted Stanton numbers for three tests in which a virtually constant value of K is applied for a distance of 2 ft starting at about 4 ft from the start of the test section. In each of the tests the experimental Stanton numbers decrease rapidly in the accelerated region and then rise again when acceleration falls to zero. In the acceleration region the Stanton number variation is generally well predicted by the model. At the start of the acceleration and just upstream therefrom the predicted Stanton numbers consistently lie below the measured value. However, much of this discrepancy would appear to be attributable to experimental error in this region for many of Moretti

and Kays runs display a virtually constant Stanton number between x_1 = 3.0 and x_1 = 4.0 ft irrespective of the position where the acceleration begins. A discrepancy which cannot be attributed to experimental uncertainty is that which appears downstream of the acceleration. The experimental Stanton numbers rise considerably more quickly than the predicted.

Figures 4.3(d) & 4.3(f) show predicted and measured Stanton numbers in flows where the acceleration parameter, K, varies roughly sinusoidally with distance, the acceleration occurring over a length of about 1 ft. In each case the acceleration was preceded by a development of 5 ft in zero pressure gradient and a step change in wall temperature was imposed at 2 ft from the entry to the test section. Despite this close similarity between these three tests upstream of the contraction, there is no concurrence between the relative behaviour of the experimental and predicted solutions in the region of zero pressure gradient. In figure 4.3(d) the predicted Stanton number is about 10% higher than the data; in figure 4.3(f) about 4% higher and in figure 4.3(e) about 6% lower. In each case the boundary layer predictions were started upstream of the step in wall temperature with estimated initial velocity and temperature profiles. These estimates, especially for the temperature profile, may have been significantly in error. It was found, however, that making changes in these profiles upstream of the step in temperature had a negligible effect on the Stanton number a foot or so

downstream of it. Moreover, it is very difficult to see how imperfections in the model used in the calculations could account for the inconsistency of the predicted solution relative to the measurements.

Because of the above discrepancies in the zero-pressure gradient regions, it is less easy to draw conclusions about the accelerated region than would otherwise be the case. However certain patterns are evident. Firstly, up to the peak value of K the predicted Stanton number follows the trend of the data faithfully even though, in figures 4.3(d) and 4.3(e), the predicted Stanton numbers are too high. As K falls away to zero the predicted Stanton numbers rise sharply whereas the measured values continue to fall for a while before rising. As a result, the predicted minimum Stanton numbers are some 75% higher than the measured. The discrepancy between experiment and prediction is rather larger for figure 4.3(f) than for the other two runs, and it is noted, for this test K reached a maximum value of about 6×10^{-6}. This value is almost twice as large as the maximum acceleration in which a turbulent boundary layer may persist. The fact that the measured Stanton numbers only begin to rise someway downstream of the predicted minimum is thus to be expected. The mixing length model used here however implies that the boundary layer is still essentially turbulent and therefore cannot plausibly be expected to display this feature. The lack of agreement in figures 4.3(d) and 4.3(e)may also be partly attributable to the same

reason.

There are however a number of other possible sources for the disagreement between predictions and experiment, all of which are related to defects in the model. Firstly, the model supposes that the major effects of laminarisation on the boundary layer are restricted to the sublayer. Some evidence exists that suggests that this is the case for similar boundary layers but it may not be so for arbitrarily developing accelerated flows. For example the mixing length model may be expected to predict values of Reynolds stress which are greatly in error in the outer region. However the model was retained since it was felt that events in the outer region (where the Reynolds stress is small in accelerated flows) would not have appreciable effect on the skin friction or Stanton number. In an attempt to substantiate this supposition, modifications to the specification of turbulent viscosity in the outer region of the boundary layer were considered.

Firstly the constant mixing length model of the outer region was replaced by a constant turbulent viscosity modified by on intermittancy factor. This may be written:-

$$\nu_T = N\delta_1 U_{1,G}\gamma \qquad (4.16)$$

where N is a constant whose value was assumed to be ·018.*

---

* This value of constant N was chosen to give agreement with high Reynolds number constant pressure boundary layer data.

The distribution of intermittancy γ across the layer was taken from the measurements of Klebanoff (46) in zero pressure gradient.

Secondly the constant mixing length of the outer region was modified by the inclusion of a generalised form of the Van Driest damping function all across the boundary layer. This modified mixing length specification may be written:-

$$\left.\begin{aligned} \ell_m &= \kappa x_2 D_v \qquad x_2 \leq \frac{\lambda}{\kappa}\delta_{.99} \\ \ell_m &= \lambda \delta_{.99} D_v \qquad x_2 > \frac{\lambda}{\kappa}\delta_{.99} \\ D_v &= 1 - \exp\left\{ \frac{-[\nu_{eff}\,\nu_T']^{\frac{1}{2}}}{\kappa A^+ \nu} \right\} \end{aligned}\right\} \qquad (4.17)$$

where $\nu_{eff} = \nu + \nu_T$

and $\nu_T' = \left\{\frac{\ell_m}{D_v}\right\}^2 \left|\frac{\partial U_1}{\partial x_2}\right|$

In the inner wall region the above expression is identical with the original mixing length specification described by equation (4.10).

When predictions were obtained with the two models given by equations (4.16) and (4.17), the results were negligibly different from those obtained with the original outer model; that is in spite of the fact that the models each lead to very different distributions of turbulent viscosity for the outer layer. This result lends support to the original contention that events in the outer region (where Reynolds stress is small) do not contribute appreciably to the development

of strongly accelerated boundary layers; the evolution of the strongly accelerated boundary layer is dominated by the inner wall region.

The question also arises as to whether p^+ is an adequate parameter with which to correlate the effects of laminarisation on the sublayer in non-similar boundary layers*. The need for the empirical lag equation (4.14) to obtain passable predictions clearly suggests that it is not. This may also be expected to apply to all other parameters which result from a one-dimensional analysis.

The empirical lag equation (4.14) may be interpreted as a means of correcting the inadequacies of p^+ as a general laminarisation criterion. However, use of the equation cannot be expected, in general to lead to reliable prediction of accelerating flows. Of course passable agreement with experiment could always be obtained for particular types of acceleration by adjustment of the lag constant 'c'; this is however tantamount to feeding in the answer.

Some efforts were made towards removing the above defects by considering alternative variations of the model. The effects of laminarisation on the sublayer thickness parameter A^+ were correlated against various other parameters which were intended to be unrestrained by one-dimensional considerations. The method adopted for the

---

* For similar boundary layers the parameter p^+ is of course adequate since it and all other local parameters are invariant in the flow direction.

determination of the p^+ function i.e. the maximum $C_{f/2}$ hypothesis, was utilised to express A^+ first in terms of the Head-Patel shear stress gradient parameter $[\frac{\nu}{\rho u_\tau^3}\frac{\partial \tau}{\partial x_2}]$ and secondly in terms of a maximum eddy Renolds number $\{(\tau/\rho)^{\frac{1}{2}} \ell_m / \nu\}$ across the layer. Both these models were then utilised to obtain predictions of the heat transfer data of Moretti and Kays (63). Calculations were also performed with A^+ determined by use of a model proposed by Launder and Jones (54). This latter model was based on extension of Bradshaw's (13) critical eddy Reynolds number hypothesis for laminarisation. However the three above A^+ models all gave rise to heat transfer predictions which, although varying in detail, were in no better agreement with experiment than the simpler original $A^+(p^+)$ model. For this reason detailed consideration of the results should not be necessary.

At this point it is as well to consider the more fundamental question as to whether it is possible to extend a local equilibrium (simple 'turbulent viscosity') turbulence model to cover situations which, as in strongly accelerated flows, are far from equilibrium. There is no reason to believe that this is possible and in fact there is evidence to suggest that the converse is true. For example it seems reasonable to assume, in the light of both experimental and computational results, that in general no local mean flow parameters exist which may be used to ascribe the effects of strong acceleration on the mixing length constants. Thus

augmented simple turbulent viscosity turbulence models are likely to be of restricted applicability and may be used with confidence only for the prediction of flows similar to those from which they were derived. In the opinion of the author any further work into the specification of mixing length is unwarranted; future effort can well be more fruitfully directed towards devising higher order turbulence models.

It was therefore decided that effort would be directed towards the task of devising a turbulence model in which the 'turbulent viscosity' was specified purely in terms of local properties of the turbulence for which differential rate equations were to be solved. The simple viscosity models previously described make use of the single velocity scale $\left|\overline{u_1 u_2}\right|^{\frac{1}{2}}$ and a length scale specified in terms of flow configuration to describe the turbulence. Neither of these scales are entirely satisfactory. The velocity scale $\left|\overline{u_1 u_2}\right|^{\frac{1}{2}}$ although a turbulence property may be zero when, for example, k or $\overline{u_{2A}}$ are finite. The length scale specification in terms of flow geometry (or boundary layer thickness) is even less satisfactory for this is not a property of the turbulent motions but rather a scale of the mean motion. Thus we may anticipate that if any substantial improvements in prediction are to be achieved then differential rate equations for <u>both</u> characteristic velocity <u>and</u> length scales of the turbulence must be solved.

4.4 SECTION III - A More Elaborate Turbulent Viscosity Model

This section is concerned with predictions of turbulent flows obtained with the aid of a turbulence model based on approximation and solution of the differential rate equation for turbulence kinetic energy in conjunction with an algebraic length scale distribution.

4.41 The Model Considered

The model makes use of the turbulence energy equation:-

$$U_1\frac{\partial k}{\partial x_1} + U_2\frac{\partial k}{\partial x_2} = \frac{\partial}{\partial x_2}\left[\nu\frac{\partial k}{\partial x_2} - \overline{\frac{u_2(u_ju_j + 2p/\rho)}{2}}\right] - \overline{u_1u_2}\frac{\partial U_1}{\partial x_2} - \nu\overline{\left(\frac{\partial u_i}{\partial x_j}\right)^2} \qquad (4.18)$$

with the following approximations:-

$$-\overline{u_1u_2} = \nu_T\frac{\partial U_1}{\partial x_2}$$

$$\nu\overline{\left(\frac{\partial u_i}{\partial x_j}\right)^2} = C_D\frac{k^{3/2}}{\ell_D}$$

$$-\overline{u_2(u_ju_j + p/\rho)} = \frac{\nu_T}{\sigma_k}\frac{\partial k}{\partial x_2} \qquad (4.19)$$

where $\nu_T = C_\mu k^{\frac{1}{2}}\ell\,[1 - \exp\{-A_\mu R_t'\}]$

$\ell_D = \ell[1 - \exp\{-A_D R_t'\}]$

and $R_t' = \dfrac{k^{\frac{1}{2}}\ell}{\nu}$

The values of the constants C_D, C_μ, σ_k, A_μ and A_D

were assumed to be 0·416, 0·22, 1·53, 0·016 and 0·263 respectively; these values and the forms of the functions of Reynolds number R_t' were recommended by Wolfshtein (86).

The length scale ℓ was specified in terms of the boundary layer thickness by the following algebraic function:-

$$\frac{\ell}{\delta_{\cdot 99}} = \frac{x_2}{\delta_{\cdot 99}} \qquad \frac{x_2}{\delta_{\cdot 99}} \leq \frac{a_1}{1-a_2}$$

$$\frac{\ell}{\delta_{\cdot 99}} = a_1 + a_2\left(\frac{x_2}{\delta_{\cdot 99}}\right) \qquad \frac{a_1}{1-a_2} < \frac{x_2}{\delta_{\cdot 99}} \leq \frac{a_3-a_1}{a_2+a_4} \qquad (4.20)$$

$$\frac{\ell}{\delta_{\cdot 99}} = a_3 - a_4\left(\frac{x_2}{\delta_{\cdot 99}}\right) \qquad \frac{x_2}{\delta_{\cdot 99}} > \frac{a_3-a_1}{a_2+a_4}$$

where $\delta_{\cdot 99}$ is the distance from the solid wall to the point where the mean velocity differs by 1% from its free stream value. The constants a_1, a_2, a_3 and a_4 have the value ·17, ·29, ·565 and ·42 respectively. The above length scale distribution is similar to that given by Glushko (30) from consideration of constant pressure, high Reynolds number boundary layer measurements. In retrospect the function seems unnecessarily complicated and a simple ramp function, similar to that used for the mixing length specification, would probably have sufficed. The function, when used in conjunction with the approximations given by equation (4.19) results in predictions which are in good agreement with measurements for high Reynolds number constant pressure flows.

The turbulence energy equation with approximations

given by equations (4.18) through (4.20), the mean momentum and continuity equations together with boundary conditions form a closed set which may be solved.

(1) Boundary conditions for the turbulence energy equation

The following boundary conditions were imposed on the equation for turbulence energy:-

$$x_2 = o \qquad k = o$$
$$x_2 = x_{2,G} \qquad k = o \tag{4.21}$$

where the subscript G denotes the outer 'edge' of the boundary layer. The 'edge' of the boundary layer is here defined as the surface beyond which all quantities considered are constant; it does not necessarily coincide with the 'edge' of the velocity boundary layer. It should also be noted that a zero free stream turbulence energy never arises in reality. Nevertheless for the calculations presented here we assume k_G is zero; most experimentalists have endeavoured to achieve this condition.

(2) Solution of the equations

The above-described partial differential equation for turbulence energy together with the mean momentum and continuity equations were solved by means of the finite-difference procedure of Patankar and Spalding (69). One hundred cross-stream grid lines were employed with the grid compressed near the wall so that about half were distributed within the region x_2^+ less than 100. The forward x_1 step was typically taken to be 0·3 times the boundary layer thickness. The modifications outlined in Section I were

embodied in the version of the procedure used and so the 'growth' of the finite difference grid was not tied uniquely to the velocity layer.

(3) Discussion of results

The predictions obtained with the above turbulence energy model were, in all cases considered,* practically identical with those obtained with the conventional ($A^+ = 26$) mixing length model of Section I. For accelerated boundary layers the predictions are therefore in conflict with measurements. This latter conclusion is in agreement with the work of Caldwell and Seban (15) who found that the use of a turbulence energy model (with algebraic scale) brought no improvement in the prediction of strongly accelerated flows. Caldwell and Seban also made numerous unsuccessful attempts to modify their model in order to procure agreement of predictions with experiment for strongly accelerated flows. A similar result has also been achieved by Mellor and Herring (62) for arbitrarily developing plane boundary layers (excluding strongly accelerated flows). They found that predictions obtained with a turbulence energy model (with algebraic scale) were indistinguishable from those obtained with the aid of a simple mixing length-viscosity model.

In view of the above findings a detailed examination of the predictions obtained with the aid of the above-described model is not thought necessary here. Some results, typical of those obtained are shown in figures 3.39 and 3.40, where, for similar boundary layers the predicted

---

* Predictions were made for constant pressure and accelerated boundary layer flows.

variation of R_2 and H with K is displayed. Also shown in the figures are the predictions obtained with the standard ($A^+ = 26{\cdot}0$) mixing length model of Section I. As may be readily observed, the curves obtained with the aid of the two models are practically indistinguishable.

4.5 SECTION IV - An Energy-Dissipation Turbulence Model

This section is concerned with the formulation and presentation of a more elaborate turbulent viscosity model in which length and velocity scales are determined from the solution of partial differential rate equations for turbulence kinetic energy and dissipation rate of turbulence energy. The model differs from others of its type in that viscous terms have been included so that the model may be applied both to the fully turbulent and sublayer regions of the boundary layer. Thus the procedure of patching a fully turbulent finite difference solution onto a one-dimensional 'law of the wall' solution is avoided; a feature of the model which is essential to the successful prediction of laminarisation. The proposed model contains a number of empirical constants and functions but it is emphasised that these have all been obtained by reference to high Reynolds number constant pressure boundary layer data only.

4.51 The Proposed Model

(1) The starting point for the derivation of the model is Rotta's (77) approximation of the Reynolds stress

equation. This may be written in the following form:-

$$\frac{DR_{ij}}{Dt} + \overline{u_\ell u_j}\frac{\partial U_i}{\partial x_\ell} + \overline{u_\ell u_j}\frac{\partial U_i}{\partial x_\ell} + c_1\frac{\varepsilon}{k}\left[\overline{u_i u_j} - {}^2/_3\,\delta_{ij}k\right]$$

$$- \left[a^{mi}_{\ell j} + a^{mj}_{\ell i}\right]\frac{\partial U_\ell}{\partial x_m} - \frac{\partial}{\partial x_m}\left[\nu\frac{\partial R_{ij}}{\partial x_m} - \overline{u_m u_i u_j}\right] \qquad (4.22)$$

$$- \frac{1}{\rho}\left[\frac{\partial}{\partial x_i}\overline{u_j p} + \frac{\partial}{\partial x_j}\overline{u_i p}\right] + (1 - c_2)\,\delta_{ij}\frac{\varepsilon}{3} + c_2\varepsilon\,\frac{\overline{u_i u_j}}{k} = 0$$

where c_1 and c_2 are functions of Reynolds number R_T ($\equiv {}^{k^2}/_{\varepsilon\nu}$) which approach constant values at large R_T. The function c_2 takes a value of unity at low R_T and approaches zero for large values of R_T. The coefficients $a^{mi}_{\ell j}$, $a^{mj}_{\ell i}$ are functions of the turbulence which must be estimated. ε is the dissipation rate of turbulence kinetic energy.

If consideration is now restricted both to plane boundary layer flows and to the stress component R_{12} there results:

$$\frac{DR_{12}}{Dt} + \overline{u_2^2}\frac{\partial U_1}{\partial x_2} + c_1\frac{\varepsilon}{k}\overline{u_1 u_2} - \left\{a^{21}_{12} + a^{22}_{11}\right\}\frac{\partial U_1}{\partial x_2} \qquad (4.23)$$

$$- \frac{\partial}{\partial x_2}\left\{\nu\frac{\partial R_{12}}{\partial x_2} - \overline{u_2^2 u_1} - \frac{\overline{u_1 p}}{\rho}\right\} + c_2\varepsilon\,\frac{\overline{u_1 u_2}}{k} = 0$$

Furthermore, if the terms representing the transport of R_{12} are now neglected, we obtain:-

$$\left\{\overline{u_2^2} - \left(a^{21}_{12} + a^{22}_{11}\right)\right\}\frac{\partial U_1}{\partial x_2} + \frac{\varepsilon}{k}\overline{u_1 u_2}\,(c_1 + c_2) = 0 \qquad (4.24)$$

Some justification for this latter approximation arises from the considerable success which has been achieved with mixing length turbulence models; they also imply the neglect of transport of R_{12}. This leads us to suppose that for many flows the transport terms are indeed negligible.

The values of the coefficients a^{21}_{12} and a^{22}_{11} were estimated by Rotta to be given by:

$$a^{21}_{12} = -0{\cdot}2 \quad \overline{u_1^2} \qquad a^{22}_{11} = 0{\cdot}8 \quad \overline{u_2^2} \tag{4.25}$$

On substituting the above values and re-arranging equation (4.24), there results the following relation:

$$-\overline{u_1 u_2} = \frac{0{\cdot}2k[\overline{u_1^2} + \overline{u_2^2}]}{\epsilon[c_1 + c_2]} \quad \frac{\partial U_1}{\partial x_2} \tag{4.26}$$

Now for boundary layer flows $[\overline{u_1^2} + \overline{u_2^2}]$ may plausibly be assumed proportional to the turbulence energy k. With this assumption equation (4.26) may be recast as:-

$$-\overline{u_1 u_2} = F_\mu \; k^2/\epsilon \; \frac{\partial U_1}{\partial x_2} \tag{4.27}$$

where F_μ is a function of Reynolds number R_T ($\equiv k^2/\nu\epsilon$) which has a constant value for large values of R_T.

An estimate of the high R_T value of F_μ may be obtained if it is first noted that:-

$$F_{\mu_\infty} = \frac{0{\cdot}2}{c_1} \quad \{\frac{\overline{u_1^2} + \overline{u_2^2}}{k}\} \approx \frac{0{\cdot}2}{c_1} \tag{4.28}$$

The constant c_1 may be estimated by consideration (of the c_1 may be estimated by consideration) of the experimental data of Tucker and Reynolds (85) on the return of an initially anistropic turbulent flow to isotropy in the absence of strain or shear. An examination of the data in conjunction with equation (4.28) leads to a value of c_1 equal to 2.5 (see ref (75)) which in turn gives $F_{\mu_\infty} \approx \cdot 08$. Such a value of F_μ will later be shown to be appropriate to the successful prediction of boundary layer flows. The low R_T form of the function F_μ cannot at this stage be estimated since there is a total absence of data concerning low Reynolds number turbulence.

If a dissipation length scale is now introduced i.e. $\ell_\epsilon \equiv k^{3/2}/\epsilon$ then the relation (4.27) may be re-written as:

$$-\overline{u_1 u_2} = F_\mu k^{\frac{1}{2}} \ell_\epsilon \frac{\partial U_1}{\partial x_2} \qquad (4.29)$$

which will be recognised as a 'turbulent viscosity' model with

$$\nu_T = F_\mu k^{\frac{1}{2}} \ell_\epsilon \qquad (4.30)$$

Here it should be emphasized that the above result is not peculiar to Rotta's approximation of the R_{ij} equation. For boundary layer flows, a 'turbulent viscosity' relation will result from any approximation of the R_{12} equation on neglect of the terms describing the transport of R_{12}, providing that the remaining terms are approximated by linear combinations of $\partial U_1/\partial x_2$, R_{ij}, k and L (where L is any turbulence length scale).

Nevertheless the above derivation does emphasize some essential requirements which must be fulfilled if a 'turbulent viscosity' model is to provide accurate predictions of flow development. Firstly it is clear that 'turbulent viscosity' models are appropriate only to boundary layer flows (to which the present work is restricted). Secondly, 'turbulent viscosity' models may be expected to lead to accurate predictions only if the transport of $\overline{u_1 u_2}$ is negligible. This latter requirement is unlikely to be fulfilled in general: there are undoubtedly boundary layer flows in which the transport of $\overline{u_1 u_2}$ plays a significant role. Nevertheless, the degree of error which the neglect of the transport of $\overline{u_1 u_2}$ entails may only be determined by application of the model to the calculation of boundary layer development and comparison of the results with experiment.

To complete the model a means of calculating both the turbulence energy and the dissipation rate of turbulence energy is required. Here their values will be obtained by solution of approximated forms of the exact partial differential transport equations for turbulence energy and dissipation rate of turbulence energy. The approximation proceeds as follows:

(2) The Turbulence Energy Equation

An exact equation for the turbulence kinetic energy may be derived by manipulation of the Navier-Stokes equation (2.1), e.g. see reference (38). For boundary layer flows the equation may be written:-

$$\frac{Dk}{Dt} = \frac{\partial}{\partial x_2}\{\nu\frac{\partial k}{\partial x_2} - \overline{u_2(u_j u_j + p/\rho)}\} - \overline{u_1 u_2}\ \frac{\partial U_1}{\partial x_2} - \epsilon \quad (4.31)$$

where $\epsilon = \nu\ \overline{(\frac{\partial u_i}{\partial x_j})^2}$

The first term on the right of equation (4.31) represents the transport of turbulence energy by pressure fluctuations, turbulent motions, and the effects of viscosity. It has the form of a diffusion term. The second term on the right of equation (4.31) represents an interaction between the mean and fluctuating motion which leads to a transfer of energy from the mean to the fluctuating motion. It thus represents a production of turbulence energy. The last term in equation (4.31) represents the rate of dissipation of turbulence energy into heat by the action of viscosity.

The first term on the right hand side of equation (4.31) is the only one which requires approximation at this point. The approximation adopted is as follows:-

$$-\overline{u_2(u_j u_j + p/\rho)} = \frac{\nu_T}{\sigma_k}\ \frac{\partial k}{\partial x_2} \quad (4.32)$$

where σ_k is a 'turbulent Prandtl number' for turbulence energy, which is assumed to have a constant value. Such an approximation has previously been proposed independently by a number of workers, e.g. Prandtl (72), Emmons (27). Measurements of $\overline{u_2 u_j u_j}$ and k in the fully turbulent region of the boundary layer (where $\overline{u_2 p/\rho}$ is thought to be negligible) provide some evidence in support of the model, e.g. see references (36) and (89). The lack of

measurements in the sublayer of the boundary layer however precludes direct comparison of the model with experiment for low turbulence Reynolds numbers.

(3) The Equation for Dissipation-Rate of Turbulence Energy

An exact equation for the dissipation-rate of turbulence kinetic energy may be derived by manipulation of the Navier-Stokes equation (2.1). This may be achieved by first differentiating the momentum equation for u_i with respect to x_j, multiplying by $\{2\nu\partial u_i/\partial x_j\}$ and finally averaging. The result is:-

$$\frac{D\varepsilon}{Dt} = \nu \frac{\partial^2 \varepsilon}{\partial x_j \partial x_j} - 2\nu \overline{u_m \frac{\partial u_j}{\partial x_i}} \frac{\partial^2 U_j}{\partial x_i \partial x_m}$$

(1)

$$- 2\nu \frac{\partial U_j}{\partial x_m} \left[\overline{\frac{\partial u_j}{\partial x_i} \frac{\partial u_m}{\partial x_i}} + \overline{\frac{\partial u_i}{\partial x_j} \frac{\partial u_i}{\partial x_m}} \right]$$

(2)

$$- 2\nu \overline{\frac{\partial u_j}{\partial x_i} \frac{\partial u_m}{\partial x_i} \frac{\partial u_j}{\partial x_m}} - 2\nu^2 \overline{\left(\frac{\partial^2 u_j}{\partial x_m \partial x_i} \right)^2}$$

(3) (4)

$$- \frac{\partial}{\partial x_m} \left[\nu \overline{u_m \frac{\partial u_j^2}{\partial x_i}} + \nu \overline{\frac{\partial u_m}{\partial x_i} \frac{\partial p}{\partial x_i}} \right] \qquad (4.33)$$

(5)

To close the equations it is necessary to make closure assumptions for the terms numbered 1 - 5 appearing on the right hand side of equation (4.33). There is no direct experimental evidence about any of the terms 1 - 5 and closure therefore involves a substantial amount of speculation.

Equations for the dissipation rate of turbulence kinetic energy have previously been proposed in various forms by Chou (18), Davidoff (23), Harlow and Nakayama (34) and Lumley (57). In deriving the presently proposed dissipation rate equation, use has been made, where appropriate, of the work of the above authors. The procedure adopted here is that of approximating the unknown terms 1 - 5 in terms of R_{ij} and ϵ by judicious use of a combination of the assumption of similarity of all turbulence microscales and 'flux-gradient' approximations. The approximations are chosen so that their tensor properties conform with those of the exact terms and also so that they reflect the observed property of turbulent motion at high turbulence Reynolds numbers, namely that the motion is <u>not</u> directly effected by molecular viscosity.

The 'flux-gradient' approximation used may be written in the general form:

$$\overline{u_j \phi} = - \alpha \nu_T \frac{\partial \Phi}{\partial x_j} \qquad (4.34)$$

where α is a constant of order unity. ϕ is the fluctuating component and Φ the mean part of the quantity considered. An essential requirement for its use is that Φ should be convected by the mean motion. Such flux approximations are discussed by Hinze (38) p. 24. The approximation of terms through the assumption of microscale similarity is facilitated by the introduction of a dissipation microscale defined by:

$$\overline{\left(\frac{\partial u_i}{\partial x_j}\right)^2} = k/\lambda^2 \quad (\equiv \epsilon/\nu) \qquad (4.35)$$

The assumption of microscale similarity is considered in some detail by Chou (18).

Term 1

This term may be approximated by use of the flux approximation (4.34), whereby:-

$$2\nu \overline{u_m \frac{\partial u_j}{\partial x_i} \frac{\partial^2 U_j}{\partial x_i \partial x_m}} = - F_1 \nu \nu_T \left[\frac{\partial^2 U_j}{\partial x_i \partial x_m}\right]^2$$

The approximated term is of an order comparable with those which have already been neglected in deriving the 'turbulent viscosity' relations (4.29) and (4.32) and so strictly it should also be neglected here. Nevertheless it will for the present be retained; it was found necessary for the prediction of a plausible turbulence energy distribution within the sublayer of the boundary layer.

Term 2

The term is approximated through the assumption of microscale similarity. A term may be constructed so that it conforms with certain properties of the exact term under contraction of the indices.

e.g. $$\delta_{jm} \overline{\frac{\partial u_i}{\partial x_j} \frac{\partial u_i}{\partial x_m}} = \epsilon$$

$$\delta_{ij} \overline{\frac{\partial u_i}{\partial x_j} \frac{\partial u_i}{\partial x_m}} = 0$$

With the above restrictions and assumptions the following approximation results:-

$$2\nu \frac{\partial U_j}{\partial x_m} \left[\overline{\frac{\partial u_j}{\partial x_i} \frac{\partial u_m}{\partial x_i}} + \overline{\frac{\partial u_i}{\partial x_j} \frac{\partial u_i}{\partial x_m}}\right] = F_2 \nu \frac{R_{jm}}{\lambda^2} \frac{\partial U_j}{\partial x_m}$$

$$= F_2 \frac{\epsilon}{k} R_{jm} \frac{\partial U_j}{\partial x_m}$$

(For a detailed derivation of this result, the reader is directed to Chou (18)).

Term 3

This term is not easily approximated by either microscale similarity assumptions or by use of the flux approximation. Davidoff (23) has argued that the term should be negligible. Here, after experimentation with approximations of the form:-

$$\frac{\partial}{\partial x_j} \left[\nu_T \frac{\epsilon}{k} \frac{\partial k}{\partial x_j}\right] \text{ and } \frac{\epsilon}{k} \frac{\partial}{\partial x_j} \left[\nu_T \frac{\partial k}{\partial x_j}\right]$$

which were found to be negligibly small for boundary layer flows, the term was neglected.

Term 4

The term represents the destruction of the dissipation rate by the action of viscosity. It may be approximated through the assumption of microscale similarity, whereby there results:-

$$2\,\nu^2\,\overline{\left[\frac{\partial^2 u_j}{\partial x_i \partial x_m}\right]^2} \;=\; F_3\,\nu^2\,\frac{k}{\lambda^4} \;=\; F_3\,\frac{\epsilon^2}{k}$$

The above result has been derived in a rigorous manner by Chou (18) and Lumley (57).

Term 5

The following approximation was used to represent this term:-

$$\nu\left[\overline{u_m\,\frac{\partial u_j}{\partial x_i}^2} + \nu\,\overline{\frac{\partial u_m}{\partial x_i}\,\frac{\partial p}{\partial x_i}}\right] = -\frac{\nu_T}{\sigma_\epsilon}\,\frac{\partial \epsilon}{\partial x_m}$$

The result was obtained by application of the flux relation (4.34) to the first term in the curly brackets. Strictly it does not apply to the second term. However both terms have similar effects in that they both represent a diffusive transport of dissipation. In the absence of anything better, it seems appropriate to consider their effects simultaneously. The approximation is consistent with that adopted for the turbulence kinetic

energy equation.

After incorporating all the above approximations the proposed form of the dissipation-rate equation may be written:-

$$\frac{D\epsilon}{Dt} = \frac{\partial}{\partial x_m}\left[\nu + \frac{\nu_T}{\sigma_\epsilon}\frac{\partial \epsilon}{\partial x_m}\right] + F_1 \nu \nu_T \left[\frac{\partial^2 U_j}{\partial x_i \partial x_m}\right]^2$$

$$- F_2 \frac{\epsilon}{k} R_{jm} \frac{\partial U_j}{\partial x_m} - F_3 \frac{\epsilon^2}{k} \qquad (4.36)$$

where the terms σ_ϵ, F_1, F_2 and F_3 are functions of the Reynolds number R_T ($\equiv k^2/\epsilon\nu$). The derivation does not suggest the forms of the functions except in that they should not deviate far from unity. The functions must also approach constant values for large values of R_T in order that the model conform with the observed properties of high Reynolds number turbulence, i.e. the motion is uneffected directly by the action of molecular viscosity. At large values of R_T the terms in the above equation in which the molecular viscosity appears explicitly will also be negligibly small.

The dissipation-rate equation proposed above contains similarities to the forms proposed independently by Chou (18), Davidoff (23), Harlow and Nakayama (34) and Lumley (57). For the case of homogeneous turbulence, all the proposed equations reduce to identical forms. The main differences result from the approximation of the terms which reflect the inhomogeneity of the turbulence. For example, Davidoff (23) proposed to obtain the term

representing the diffusive transport of dissipation-rate by turbulent motions by solution of a partial differential equation for that quantity. Harlow and Nakayama (34) used a flux relation such as (4.34) to approximate the diffusive transport of ϵ due to pressure fluctuations in terms of mean pressure gradient (in spite of the fact that pressure is not convected by the mean motion).

When the above dissipation rate equation (4.36) is specialised to plane boundary layer conditions it reduces to:-

$$\frac{D\epsilon}{Dt} = \frac{\partial}{\partial x_2}\left[\left(\nu + \frac{\nu_T}{\sigma_\epsilon}\right)\frac{\partial \epsilon}{\partial x_2}\right] + F_1\, \nu\, \nu_T \left[\frac{\partial^2 U_1}{\partial x_2^2}\right]^2 + F_2 \frac{\epsilon}{k}\, \nu_T \left[\frac{\partial U_1}{\partial x_2}\right]^2 - F_3\, \epsilon^2/k \qquad (4.37)$$

where $\nu_T = F_\mu\, k^2/\epsilon$

The actual forms of the functions and their 'constant' values for high R_T must, however, be determined by recourse to experiment. Here they were established by applying the complete turbulence model, comprising equations (4.29), (4.31) and (4.36) together with the mean momentum and continuity equations to a number of simple flow configurations.

4.52 Determination of the Reynolds Number Functions

(1) The decay of homogeneous isotropic grid turbulence

An estimate of the form of F_3 may be obtained

from the experimental data of Batchelor and Townsend (5 & 6) on the decay of isotropic homogeneous grid turbulence. For this case the turbulence energy and dissipation rate equations reduce to:-

$$\frac{dk}{dt} = -\epsilon$$

$$\frac{d\epsilon}{dt} = -F_3 \frac{\epsilon^2}{k} \qquad (4.38)$$

At large turbulence Reynolds numbers the data indicates that $k \propto t^{-1}$ which requires that $F_3 = 2$. However, in the final stages of decay, i.e. at low Reynolds numbers, the measurements indicate that an exponent of $-5/2$ is appropriate. This latter decay law requires that $F_3 = 1{\cdot}4$. The change-over between the two decay laws occurs quite rapidly at $R_T \left(\equiv \frac{k^2}{\epsilon\nu}\right) \approx 1$. The function F_3 was thus represented by:-

$$F_3 = 2{\cdot}0 \left\{1 - 0{\cdot}3 \exp(-R_T^2)\right\} \qquad (4.39)$$

The similarities between boundary layer (shear flow) and homogeneous isotropic turbulence are perhaps tenuous. This is particularly so for the viscous sublayer of the boundary layer, the structure of which is markedly different from that found in low Reynolds number isotropic turbulence. In view of this we should not be surprised if some modification of the low R_T form of F_3 is subsequently found to be necessary when the model is applied to the sublayer of the boundary layer. In the fully turbulent (high R_T) region of the boundary

layer the similarity may be greater for there 'local isotropy' is thought to prevail. The assumption of 'local isotropy' implies that the dissipation processes in shear flows are overall similar to those arising in isotropic turbulent flows. This is a plausible assumption: at high Reynolds numbers, the main dissipation of turbulence energy occurs in a high wave number (small eddy) range of the turbulence spectrum, whereas the main transfer of energy to the turbulent motions (by the action of the mean strain) occurs in a low wave number (large eddy) range. There usually exists a large separation (in wave number space) between the two ranges and so, to a first approximation, $F_3 = 2{\cdot}0$ may be reasonably expected to apply.

The remaining functions of turbulence Reynolds number may be treated more conveniently if their high and low Reynolds number behaviour is considered separately.

(2) The high Reynolds number form of the model

As was noted above, the functions of the turbulence Reynolds number appearing in equation (4.37) have constant values at high R_T. Moreover, terms in which the molecular viscosity appears explicitly will then be negligibly small and may therefore be neglected. Also we have observed that a constant value of F_3 equal to 2·0 is appropriate for high Reynolds number turbulence. An estimation of the remaining 'constants' may be obtained from consideration of measurements in the turbulent boundary

layer developing in constant pressure along a flat plate. In the near wall, fully turbulent region of the boundary layer the mean velocity profile is found to be described by:

$$U_1 = \sqrt{\frac{\tau_w}{\rho}}/\kappa \ln\frac{\sqrt{\tau_w/\rho}x_2}{\nu} + c \qquad (4.40)$$

and the Reynolds stress is approximately constant and equal to the wall shear stress i.e. $-\rho\,\overline{u_1u_2} = \tau_w$. In addition, the convection of momentum, turbulence energy and dissipation rate are negligible and the turbulence energy is also approximately constant. With the above considerations in mind the turbulence energy and dissipation rate equations reduce to:

$$0 = \nu_T\left[\frac{\partial U_1}{\partial x_2}\right]^2 - \epsilon \qquad (4.41)$$

$$0 = \frac{\partial}{\partial x_2}\left[\frac{\nu_T}{\sigma_{\epsilon_\infty}}\frac{\partial}{\partial x_2}\right] + F_{2_\infty}\frac{\epsilon}{k}\nu_T\left[\frac{\partial U_1}{\partial x_2}\right]^2 - F_{3_\infty}\frac{\epsilon^2}{k}$$

where $\nu_T = F_{\mu_\infty} k^2/\epsilon$

The subscript '∞' denotes the high R_T 'constant' values of the functions.

After noting that $\partial U_1/\partial x_2 = \sqrt{\tau_w/\rho}/\kappa x_2$ the equations may be manipulated to yield the following relations:

$$F_{\mu_\infty} = \left[\frac{\tau_w}{k}\right]^2$$

$$F_{2_\infty} = F_{3_\infty} - \frac{\kappa^2}{\sigma_{\epsilon_\infty} F_{\mu_\infty}} \qquad (4.42)$$

Now $\varkappa$ has a value of about 0·42 and the parameter $\tau/\rho k$ is found to have a constant value of about 0·3 in the fully turbulent region of the boundary layer. On inserting these values and the value of F_3 previously chosen we obtain:

$$F_{\mu_\infty} = \cdot 09 \quad ; \quad F_{2_\infty} \approx 2\cdot 0 - {}^{0\cdot 59}/_{\sigma_\epsilon}$$

A value of $F_{\mu_\infty} = \cdot 09$ is very close to that estimated previously (p 112) from consideration of the return of an initially anisotropic turbulent flow to isotropy in the absence of strain or shear. The fact that closely similar values of F_{μ_∞} arise from consideration of flows of very different character lends support to the validity of the assumptions made thus far.

All that now remains to close the high Reynolds number form of the model is the choice of the values for the 'turbulent Prandtl numbers', σ_k and σ_ϵ. The Prandtl numbers were chosen by reference to computer experiments. The equations (4.31) and (4.36) were solved for the fully turbulent region of the boundary layer for the case of constant pressure plane flow with the aid of the finite-difference procedure of ref. (69) A detailed description of the method of solution will not be given here; suffice it to say that the finite-difference solution was patched onto a 'fully turbulent' one-dimensional solution just outside the viscous sublayer of the boundary layer. The inner boundary conditions for turbulence energy and dissipation rate were thus given by:-

$$k = \left(\frac{\tau_w}{\rho}\right) F_{\mu_\infty}^{-\frac{1}{2}} \quad ; \quad \epsilon = \left(\frac{\tau_w}{\rho}\right)^{3/2} / \kappa x_2$$

The resulting solutions were compared with the H-R_2 correlation of Coles (21) and the measurements of Klebanoff (46) for the plane turbulent boundary layer in zero pressure gradient. The Prandtl numbers, σ_k and σ_ϵ were then adjusted until reasonable agreement with both Coles' correlation and Klebanoff's mean and fluctuating profile data was procured. The set of constants which give 'best' agreement for the high Reynolds number plane turbulent boundary layer in zero pressure gradient are listed below

F_{μ_∞}	F_{2_∞}	F_{3_∞}	σ_{k_∞}	σ_{ϵ_∞}
·09	1·55	2·0	1·0	1·3

The above constants differ only slightly from a set proposed by Hanjalic (36) for a similar (though not identical) turbulence model. Hanjalic applied his model to obtain satisfactory predictions of a wide range of high Reynolds number boundary layer flows.

(3) The Low Reynolds Number Form of the Model

The extension of the model to regions of low turbulence Reynolds number such as exist in the viscous sublayer of the boundary layer is based on less secure

ground than the high Reynolds number form of the model. The viscous sublayer occupies a very thin region adjacent to the wall and is usually only a few thousands of an inch thick; as a result few measurements have been possible. Measurements that do exist indicate that the sublayer (down to $x_2^+ = \frac{1}{2}$ at least) has a strongly three dimensional intermittant structure which is perhaps more akin to an unsteady laminar flow than to turbulent flow. The sublayer is a region of high relative intensity i.e. $\sqrt{\overline{u_1^2}}/U_1$ and strong anisotropy and inhomogeneity in which strong interaction between the mean and fluctuating motion takes place for <u>all</u> scales of the turbulent motion. Thus the assumption which description of turbulence in terms of two scalar quantities, k and ε, implies (namely only small deviations from homogeneity) is not likely to be accurate. For example the model contains the implicit assumption that the two point velocity correlation tensor $\mathcal{R}_{ij} \equiv \overline{u_i(\underline{x})u_j(\underline{x} + \underline{r})}$ varies only slowly with spatial position $\underline{x}$ compared with separation $\underline{r}$ (see reference (18)). This condition is not likely to be satisfied in the large intensity gradients which exist in the sublayer of the boundary layer.

In view of the above facts we should not expect the present turbulence model to be capable of providing a detailed description of the macroscopic properties of the turbulence structure of the sublayer. Nevertheless, we proceed with the task of extending the model to account for the viscous sublayer in the knowledge that considerable

success has already been achieved (by a large number of workers) through use of the Van Driest sublayer mixing length model. The present model is a good deal more sophisticated and should therefore lead to an improvement over the Van Driest formula; we may reasonably expect the model to provide a fairly close description of the overall behaviour of the sublayer.

(4) The Limiting Form of the Model : $R_T \rightarrow 0$

The task of extending the proposed turbulence model so that it may be applied to the sublayer of the boundary layer is most conveniently accomplished if first the asymptotic behaviour as $R_T \rightarrow 0$ is considered. In the sublayer $R_T \rightarrow 0$ as the wall is approached and there is an appreciable region $0 \leq x_2^+ \lesssim 5$ in which inertial forces are negligible. In this viscous region the turbulence energy and dissipation rate equations reduce to:-

$$0 = \nu \frac{d^2k}{dx_2^2} - \epsilon$$

$$0 = \nu \frac{d^2\epsilon}{dx_2^2} - F_{3_o} \frac{\epsilon^2}{k} \qquad (4.43)$$

where the subscript 'o' denotes the low R_T asymptotic value of the function.

Now it is well established that the turbulence energy varies as $(x_2^+)^2$ in the viscous region $x_2^+ \lesssim 5$ and is zero at the wall. It may easily be shown that this implies a value of F_{3_o} equal to zero. If the restriction

of a quadratic variation of turbulence energy is relaxed then $^1/_6 \leq F_{3_o} \leq 1$ must be satisfied if all the terms in the above limiting forms of the equations are to remain bounded at the wall. A value of $F_{3_o} = {}^1/_6$ produces an energy variation proportional to $[x_2^+]^4$; the exponent increases rapidly as F_{3_o} is increased. An unbounded behaviour of any of the terms at the wall is both physically extremely unrealistic and likely to lead to considerable difficulty in the task of obtaining numerical solutions of the equations; it should therefore be avoided.

The need to predict a reasonable energy distribution in the sublayer suggests that F_{3_o} should be a function which has the property of approaching zero rapidly (at least as x_2^{+2}) as the wall is approached. However when F_{3_o} was assumed given by such a function of R_T and the equations solved certain undesirable features arose; mainly a large unrealistic growth in turbulence energy in the sublayer and a spurious behaviour in regions of low R_T away from walls. The approach also resulted in wall boundary conditions for the turbulence energy and dissipation rate equations i.e. $k = \frac{\partial k}{\partial x_2} = 0$ at $x_2^+ = 0$, which were difficult to apply numerically.

At this point the reader is reminded that the above behaviour of F_{3_o} differs from that found in the final stages of decay of isotropic grid turbulence where $F_{3_o} = 1{\cdot}4$ was obtained. It is also in conflict with the derivation of the model which suggested that all the functions, including F_{3_o}, should not deviate far from unity.

The necessity of $F_{3_o} = 0$ in the viscous region $x_2^+ \lesssim 5$ may thus be taken to reflect the limitations of the proposed turbulence model when applied in regions of steep intensity gradients. A systematic extension of the model so that it may be applicable to regions of steep intensity gradients involves modification of most of the approximations and is, at best, an extremely difficult and uncertain task. Here a simpler procedure was adopted whereby a term was added, on an empirical basis, to the turbulence energy equation so that the correct asymptotic behaviour resulted. This path was followed in the belief that events in the region $x_2^+ \lesssim 5$ were not of great significance as far as the mean velocity profile was concerned for there ν is much greater than ν_T. Of course, this is only true providing that events in the region $x_2^+ \lesssim 5$ do not unduly influence the turbulence profiles outside the region as would be the case if ε were allowed to go to infinity at the wall (a result which arises from $F_{3_o} = 1{\cdot}4$ at the wall).

The method adopted to obtain the required additional term is outlined below. First it was noted that at the wall:

$$\text{total dissipation rate} = \nu\{\overline{\left[\frac{\partial u_1}{\partial x_2}\right]^2} + \overline{\left[\frac{\partial u_3}{\partial x_2}\right]^2}\} \qquad (4.44)$$

Now measurements of the instantaneous velocity profile within the sublayer (Bakewell (7)) have shown that at any instant of time the velocity varies linearly with x_2. This finding implies that:-

$$u_1 = a_1(t)\, x_2$$
$$u_3 = a_3(t)\, x_2 \qquad (4.45)$$

where $a_i(t)$ are functions of time whose mean values are zero. With the insertion of equation (4.45) into (4.44) there results:

$$\text{total dissipation rate} = \nu\left[\overline{a_1^2} + \overline{a_3^2}\right] \qquad (4.46)$$

If, further, u_2, the normal component of fluctuating velocity is presumed negligible, we obtain from equation (4.46) the following expression for the variation of kinetic energy near the wall:

$$k = \frac{\overline{u_1^2} + \overline{u_3^2}}{2} = \left[\overline{a_1^2} + \overline{a_3^2}\right]\frac{(x_2)^2}{2} \qquad (4.47)$$

We now construct a term which reduces to the total dissipation at the wall. From equations (4.46) and (4.47) it is readily verified that one such term which satisfies this requirement is:- $2\nu\left[\frac{\partial k^{\frac{1}{2}}}{\partial x_2}\right]^2$ and this was added to the turbulence energy equation to give the correct asymptotic behaviour of the turbulence energy at the wall.

At this point it must be stressed that the above procedure is not the only one possible. It does however provide for a simple but necessary means of modifying the model to procure agreement with experiment within the sublayer of the boundary layer. It has the additional advantage of allowing the application of homogeneous boundary conditions to the turbulence model at the wall,

thus considerably simplifying the task of obtaining numerical solutions of the equations.

The form of the remaining functions were chosen by confining attention to the calculation of constant stress Couette flows. For this flow the mean momentum equation (2.7), the turbulence energy equation (4.31), (with the additional term) and the the dissipation rate equation (4.36) reduce to:

$$0 = \frac{d}{dx_2}\left[(\nu + \nu_T)\ \frac{\partial U_1}{\partial x_2}\right]$$

$$0 = \frac{d}{dx_2}\left[(\nu + \frac{\nu_T}{\sigma_k})\ \frac{dk}{dx_2}\right] + \nu_T\left[\frac{dU_1}{dx_2}\right]^2 - \epsilon - 2\nu\left[\frac{dk^{\frac{1}{2}}}{dx_2}\right]^2$$

$$0 = \frac{d}{dx_2}\left[(\nu + \frac{\nu_T}{\sigma_\epsilon})\ \frac{d\epsilon}{dx_2}\right] + F_1\ \nu\ \nu_T\left[\frac{d^2U_1}{dx_2^2}\right]^2 \qquad (4.48)$$

$$+ F_2\ \frac{\epsilon}{k}\ \nu_T\left[\frac{dU_1}{dx_2}\right]^2 - F_3\ \frac{\epsilon}{k}^2$$

with boundary conditions

$$x_2 = 0 \qquad k = \epsilon = U_1 = 0$$

$$x_2 = x_{2,c} \qquad k = \frac{\tau_w}{\rho}\ F_{\mu_\infty}^{-\frac{1}{2}}$$

$$\epsilon = \left(\frac{\tau_w}{\rho}\right)^{3/2} / \kappa x_{2,G}$$

$$U_1 = U_{1,G}$$

where $x_{2,G}$ denotes the outer boundary of the flow.

Initally the above set of equations (4.48)

were solved numerically with the turbulent viscosity specified by way of the Van Driest formula ($A^+ = 26$) (4.8) rather than by the relation (4.29). This practice enabled attention to be focussed simply on the dissipation rate equation which was then tuned to give a plausible turbulence energy distribution within the viscous sublayer. The turbulence measurements within the sublayer of a pipe flow by Laufer (55) were used to provide a guide to the required energy profile. Close fitting of the data was however thought unwarranted as measurements within the sublayer are of relatively low accuracy and as a result the measured k profile is probably only accurate to within about 20%. In practice the estimation of the functions in the ε equation turned out to be a relatively simple matter for a reasonable k profile could be obtained through choice of a suitable constant value of F_1 alone; the other functions F_2, σ_k and σ_ε could be allowed to retain their 'constant' high R_T values and F_3 given by the isotropic grid turbulence decay result.

On achieving a satisfactory turbulence energy distribution within the sublayer, the 'turbulent viscosity' relation (4.29) was inverted to provide a preliminary estimate of the Reynolds number function F_μ:

$$F_\mu = \varepsilon/k^2 \quad \nu_T \qquad \text{Van Driest}$$

where $F_\mu = F_\mu(R_T)$ and $F_\mu(\infty) = \cdot 09$

Finally the equations were solved using this estimate of F_μ to calculate the 'turbulent viscosity'. Small adjustments were then made to the function until the predicted velocity profile agreed closely with that obtained through use of the Van Driest formula.

This latter task completed the 'derivation' of the turbulence model which may now be applied to the calculation of both the sublayer and fully turbulent regions of the boundary layer. The equations which constitute the turbulence model, together with the mean momentum, continuity and thermal energy equations may thus be restated:-

Mean Momentum

$$\frac{DU_1}{Dt} = -\frac{1}{\rho}\frac{dP}{dx_1} + \frac{\partial}{\partial x_2}\left[(\nu + \nu_T)\frac{\partial U_1}{\partial x_2}\right]$$

Continuity

$$\frac{\partial U_1}{\partial x_1} + \frac{\partial U_2}{\partial x_2} = 0$$

Thermal Energy

$$\frac{D\Theta}{Dt} = \frac{\partial}{\partial x_2}\left[\left(\frac{\nu}{\sigma} + \frac{\nu_T}{\sigma_T}\right)\frac{\partial \Theta}{\partial x_2}\right]$$

Turbulence Energy

$$\frac{Dk}{Dt} = \frac{\partial}{\partial x_2}\left[\left(\nu + \frac{\nu_T}{\sigma_k}\right)\frac{\partial k}{\partial x_2}\right] + \nu_T\left[\frac{\partial U_1}{\partial x_2}\right]^2 - 2\nu\left[\frac{\partial k^{\frac{1}{2}}}{\partial x_2}\right]^2 - \epsilon$$

Dissipation Rate

$$\frac{D\epsilon}{Dt} = \frac{\partial}{\partial x_2}\left[\left(\nu + \frac{\nu_T}{\sigma}\right)\frac{\partial \epsilon}{\partial x_2}\right] + F_1\,\nu\,\nu_T\left[\frac{\partial^2 U_1}{\partial x_2^2}\right]^2 \qquad (4.49)$$

$$+ F_2\,\frac{\epsilon}{k}\,\nu_T\left[\frac{\partial U_1}{\partial x_2}\right]^2 - F_3\,\frac{\epsilon^2}{k}$$

where $\nu_T = F_\mu\, k^2/\epsilon$ $\qquad F_\mu = \exp\{-2.5/(1 + R_T/50)\}$

$F_1 = 2{\cdot}0$

$F_2 = 1{\cdot}55$

$F_3 = 2{\cdot}0\,[1{\cdot}0 - 0{\cdot}3\exp(-R_T^2)]$

$\sigma_T = 0{\cdot}9$

$\sigma_k = 1{\cdot}0$

$\sigma = 1{\cdot}3$

and $R_T \quad k^2/\epsilon\nu$

The above equations (4.49) together with boundary conditions form a closed set which may now be solved.

4.53 The Validity of the Proposed Model

The assumptions contained in the foregoing model are many and are such that it is difficult, if not impossible to establish conditions for their validity. Indeed, in view of the crudity of the assumptions the

relation between the model and 'real' turbulence may be thought tenuous. It is a disappointing feature of the derivation that we were unable to use more of the available experimental information. For example, it is well established that shear flow turbulent motion is dominated by a large eddy structure and that the outer region of the boundary layer is intermittent in nature. Both these features were ignored completely in the derivation. In this respect, however, the present turbulence model is no different from any other model which attempts a practical solution to turbulent shear flow; other proposers of turbulence models have also been unable to use much of the available experimental information. It seems likely that the reason why workers (including the writer) have been unable to utilise more of the available experimental information in framing turbulence models is due to the extremely complex and 'non-local' nature of turbulent motion. At the same time, many of the existing measurements are of a qualitative nature and are thus not of direct use for the task of formulating closure assumptions to the Reynolds equations. Also it has not been found possible to measure many of the important quantities for which assumptions must be made to effect closure of the equations e.g. the pressure-rate of strain correlation $\overline{p \frac{\partial u_i}{\partial x_j}}$. However, even if sufficient experimental information was available for the formulation of a turbulence model which described the detailed (macro and microscopic) nature of the motion then it is probable, in view of the 'non-local'

nature of turbulent motion, that the model would involve integro-differential equations of complexity approaching that of the Navier Stokes equation itself. It would not therefore represent a practical solution to turbulent shear flow.

The requirement that a turbulence model represents a practical solution to turbulent flow and therefore involves a small number (2 to 3) of simple partial differential rate equations necessitates crude physical assumptions regarding the turbulence structure. For practical applications, however, it is necessary only to calculate the behaviour of certain statistical means e.g. U_i, Θ and for this purpose these crude physical assumptions may suffice; it is not necessary to predict the detailed structure of the turbulence.

It must also be remembered that considerable success in the prediction of boundary layer flows has already been achieved with mixing length models. These contain substantially less of the features of turbulence than the present model; indeed they do not recognise turbulence explicitly at all. The present model may certainly be expected to lead to an improvement in predictive ability over mixing length and other simple viscosity models. Its validity and range of applicability may, however, only be established by application of the model to the calculation of boundary layer development and subsequent comparison with experiment.

4.54 The Boundary Conditions and Method of Solution of the Equations.

(1) Smooth Wall Boundaries

The boundary conditions for the turbulence energy, dissipation rate and mean momentum equations at a smooth rigid wall are:-

$$U_1 = 0 \; ; \; U_2 = U_{2,w} \; ; \; k = 0 \; \& \; \epsilon = 0 \qquad (4.50)$$

(2) Free Boundaries

The boundary conditions for the turbulence energy, dissipation rate and mean momentum equations appropriate to a free fluid boundary may be stated:-

$$\begin{aligned} U_{1,G} \frac{dk_G}{dx_1} &= -\epsilon_G \\ U_{1,G} \frac{d\epsilon_G}{dx_1} &= -F_3 \frac{\epsilon_G^2}{k_G} \\ U_{1,G} \frac{dU_{1,G}}{dx_1} &= -\frac{1}{\rho}\frac{dP}{dx_1} \end{aligned} \qquad (4.51)$$

where G subscripts denote conditions outside the free stream boundary of the flow. Equations (4.51) are, of course, the limiting free stream forms of equations (4.49). The free boundary is here defined as that surface beyond which all quantities considered deviate only by a small fixed amount (taken as $\frac{1}{2}\%$) from their respective free stream values. This boundary will not in general coincide with either the 'edge' of the velocity layer or the average position of the interface between rotational and irrotational 'turbulent fluid'.

(3) Axes of Symmetry

At axes of symmetry the following boundary conditions may be imposed on the equations for turbulence energy, dissipation rate and mean momentum:-

$$\frac{\partial k}{\partial x_2} = 0 \; ; \; \frac{\partial \varepsilon}{\partial x_2} = 0 \; \& \; \frac{\partial U_1}{\partial x_2} = 0 \qquad (4.52)$$

(4) Solution of the Equations

For the steady plane flows presently considered the governing set of partial differential equations (comprising equations (4.49)) were solved by means of the finite-difference procedure of ref (69). One hundred cross stream intervals were employed with the finite difference grid compressed near the wall so that about half were distributed within the region where x_2^+ was less than 100. Typically the forward step size was chosen as 0·3 times the local boundary layer thickness. Calculations performed with various other numbers and distributions of cross stream intervals and forward step sizes established that the solutions were of sufficient numerical accuracy.

(5) Initial Profiles

In addition to the boundary conditions discussed in the foregoing paragraph it is necessary to specify the initial profiles of U_1, k, ε and Θ before integration of the equations may be commenced. For the calculations to be presented here estimated 'fully turbulent' profiles were used. In the case of the similar boundary layers

considered, the solution is formally independent of the initial conditions and hence the forms of the initial profiles are unimportant. For the other flows it was usually possible to start the calculations well upstream of the region of interest on which, as a result, the initial conditions had little influence. Measurements of profiles of U_1 and Θ at the initial x_1 station existed for a few cases and these were therefore used whenever available. However in all cases it was necessary to use estimated profiles of the turbulence quantities k and ε. Details of the estimated initial profiles for U_1, Θ, k and ε are given in Appendix

4.55 Presentation and Discussion of Results

(1) The Turbulent Boundary Layer in Zero Pressure Gradient

Figure 4.4 displays the predicted variation of boundary layer shape factor, H and skin friction coefficient, C_f with momentum deficit-thickness Reynolds number R_2. Also shown are the $H \sim R_2$ and $C_f \sim R_2$ correlations of Coles (21) obtained from what he considered to be the most reliable constant pressure plane boundary layer data. For values of R_2 greater than 2500 the predicted values of H and C_f agree with those of Coles' correlation to within 1%. For values of R_2 less than 2500 there is a small but systematic departure of the predictions from the correlation of Coles, the predicted shape factor being too high and the value of C_f too low. (Typically, at R_2 = 1000, the predicted value of H is

about 3% high and the value of C_f is about 9% low.) As far as the shape factor is concerned the differences are probably not significant and can be accounted for by experimental uncertainty. The experimental values of H may also be expected to be influenced by the method of inducing transition from laminar to turbulent flow and probably the predicted values on the initial profiles.

The principal reason for the discrepancy in C_f may be observed in figure 4.5 where mean velocity profiles are plotted for several values of R_2 on $U_1^+ - x_2^+$ axes. The predicted profiles display a detectable Reynolds number dependence in what is normally termed the 'universal' wall region. ($50 \lesssim x_2^+ \lesssim 200$). Now, Coles estimated the local skin friction coefficient by use of a presumed universal semi-logarithmic wall law; indeed his correlation includes a proposal for this law. However if the boundary layer does in fact possess a Reynolds number dependence similar to that predicted, then Coles' values of C_f would be in error by an amount similar to the discrepancy between the prediction and correlation. In the absence of accurate measurements of wall shear stress it is not possible to conclude with certainty whether it is the prediction or the correlation that reflects the true behaviour of the turbulent boundary layer at low Reynolds numbers.

(2) Mean Velocity Profiles

The predicted mean velocity profiles at values

of R_2 ranging between 2,000 and 16,000 are displayed on semi-logarithmic axes in figures 4.6 - 4.9 . Also shown are the mean velocity profile measurements of Wieghardt (88). The agreement between predictions and measurements is in all cases excellent. Wieghardt did not make velocity measurements close to the wall and so a detailed comparison of the predicted and measured profiles within the sublayer and near wall region is not possible. There is, however, some very slender evidence (resting on a single point velocity measurement) to suggest that a discrepancy between measured and predicted velocity profile exists in the near wall region; the predicted profile being slightly too low.

In figure 4.10 the predicted mean velocity profile at R_2 = 7,700 is displayed on linear axes and compared with the measured mean profile of Klebanoff (46). The predictions are again in excellent accord with the measurements.

(3) Fluctuating Quantities

The predicted profiles of turbulence energy, k and Reynolds shear stress, $-\rho\overline{u_1u_2}$, for R_2 equals 7,700, are shown in figure 4.10 . Also shown are the turbulence measurements in a zero pressure gradient boundary layer of Klebanoff (46). The predicted variation of both k and $-\rho\overline{u_1u_2}$ are in good overall agreement with the measurements. In the region close to the wall the predicted turbulence energy is too low by about 8%.

However, in view of the experimental uncertainty of turbulence measurements near walls the discrepancy is probably not significant. At the outer edge of the boundary layer the predicted profiles of k and $-\overline{\rho u_1 u_2}$ do not fall to their free stream values as rapidly as the measurements. This latter discrepancy is not thought to be important since in the outer region ($x_2 > 2{\cdot}0$ ins) the values of k and $-\overline{\rho u_1 u_2}$ are small compared with their maximum values and therefore do not significantly affect the development of the boundary layer.

In figure 4.11 the predicted turbulence energy profile within the sublayer of the boundary layer is shown. Also displayed is the turbulence energy profile taken from the measurements of turbulent pipe flow by Laufer* (55). The total shear stress $(\mu\frac{\partial U_1}{\partial x_2} - \overline{\rho u_1 u_2})$ is approximately constant in the sublayer of a high Reynolds number pipe flow which, in this respect, is similar to the high Reynolds number plane boundary layer. Laufer's turbulence measurements in the sublayer of a pipe flow may therefore be used for the purposes of comparison. The predicted turbulence energy profile in the sublayer lies below the measured profile. The maximum predicted turbulence energy occurs at $x_2^+ \simeq 25$

---

* $\overline{u_2^2}$ & $\overline{u_3^2}$ Klebanoff did not make turbulence measurements deep within the sublayer and indeed utilised Laufer's results to estimate their variation in his boundary layer.

which is at roughly the same position as the measured maximum. Its value is, however, about 20% too low. Nevertheless, in view of the uncertainty in the measurements of k within the sublayer (especially $\overline{u_2^2}$) the predictions are considered to be of acceptable accuracy. Measurements of $\overline{u_1^2}$ (the largest and most accurately measurable component of k) within the sublayer provide an estimate of the accuracy of the measured turbulence energy profile. Measurements in nominally identical flow situations by different workers display a scatter of about $\pm$ 30% in the maximum value of $\overline{u_1^2}$; the sublayer turbulence energy profile is thus probably accurate only to within about 20-25%.

4.56 Accelerated Flows

(1) Similar Boundary Layers

Attention is first directed towards the prediction of the similar hydrodynamic turbulent boundary layers which arise from flow in a plane convergent channel. Although these boundary layers have been discussed in some detail elsewhere in this thesis it is appropriate, at this juncture, to mention that they have profiles which are completely self-preserving and flow parameters K, R_2, H and C_f etc. which are invariant in the flow direction.

In figures 4.12 and 4.13 the predicted variation of momentum Reynolds number R_2 and shape factor, H with acceleration parameter K is shown. Also included in the figures are the experimental results of the present study,

Jones (40), Julien et al (43), the similar boundary layer data of Badri Narayanan and Ramjee (2) and the equilibrium boundary layer data of Herring and Norbury (37). As was noted previously this latter data, although of equilibrium flows is closely representative of a similar boundary layer at $K = 2{\cdot}4 \times 10^{-7}$. For the purposes of comparison the solution appropriate to a laminar flow and that obtained with the standard mixing length model are also displayed.

The agreement between prediction and measurement is on the whole good. The model displays the correct qualitative trend of a reversion from turbulent to laminar flow as K is increased. Indeed above a value of K of $3{\cdot}2 \times 10^{-6}$ no turbulent solution exists. That is to say that if the predictions are started with an initially fully turbulent boundary layer then, on application of the acceleration, a gradual decay to zero of the turbulence results and the mean velocity profile collapses to that appropriate to a laminar flow. This result is in broad agreement with the experimental results although the data is not sufficiently definite to establish accurately the value of K at which degeneration to laminar flow occurs. The predictions of R_2 and H for $K > 10^{-6}$ accord with the measurements to a close degree. For values of K less than 10^{-6} there is, however, some discrepancy; the predicted values of R_2 being too low and the values of H too high by a few percent. Notwithstanding these latter small discrepancies, that the predictions display the observed reversion from turbulent to laminar flow

is an encouraging result; one which it should be noted is not obtained with the standard ($A^+ = 26$) mixing-length model.

Figure 4.14 displays, on semi-logarithmic $U_1^+ \sim x_2^+$ axes, the predicted mean velocity profiles for a range of values of K between 10^{-7} and 3×10^{-6}. Also shown is the 'universal' semi-logarithmic wall law. It may be observed that the predicted profiles show a progressive amount of 'overshoot' above the law of the wall as K is increased. Also as K is increased the division between the fully turbulent and the sublayer regions of the predicted profiles becomes less pronounced. This result is in overall agreement with experiment; measured mean velocity profiles in both similar and non-similar boundary layers in strong acceleration display an 'overshoot' above the law of the wall. Again the result is not predicted by standard mixing length models as is illustrated in figure 4.1.

Figure 4.15 compares the predicted mean velocity profile for $K = 2{\cdot}2 \times 10^{-6}$ with the measurements performed by the writer in an earlier study. There is some discrepancy between the detailed shape of the profiles but the main point to note is the predictions, like the measurements, show that the velocity profile lies considerably above the 'universal' law of the wall. By comparison, predictions obtained with the standard mixing length model, figure 4.1, fell below the logarithmic line.

The predicted mean velocity profiles at $K = 1{\cdot}5 \times 10^{-6}$, $2{\cdot}5 \times 10^{-6}$ and $3{\cdot}0 \times 10^{-6}$ are compared with those measured during the present experimental study in figures 4.16, 4.17 & 4.18. In all three cases some discrepancy between prediction and measurement is evident. For the lowest value of K the boundary layer thickness is correctly predicted. However the predicted profile lies slightly below the measured in the region $\cdot 6 < U_1/U_{1,G} < \cdot 85$ but above it in the region $U_1/U_{1,G} > \cdot 85$. The maximum error in velocity is about 7%. In the case of the other values of K the boundary layer thickness is slightly underestimated but the predicted profiles again lie below the measured profiles in the 'central' region $\cdot 6 < U_1/U_{1,G} < \cdot 9$. The error in predicted velocity appears to increase slightly with K; at $K = 3{\cdot}0 \times 10^{-6}$ the maximum error being about 10%. In the near-wall region, for $U_1/U_{1,G}$ less than 0·6 the predictions and measurements appear to accord reasonably well for all three values of K.

In figures 3.21 & 3.24 the measured turbulence energy, k and Reynolds stress $\overline{u_1 u_2}$ profiles at $K = 1{\cdot}5 \times 10^{-6}$ are compared with the predicted distributions. It was not possible to make turbulence measurements in the near wall region and so comparison of the predictions with the measurements is unfortunately restricted to the outer $4/5$ of the boundary layer. Nevertheless it is evident that the predicted turbulence energy and Reynolds stress agree reasonably with the measurements nearest the wall. In the outer half of the boundary layer the agreement is

less satisfactory as the predicted distributions of k and $\overline{u_1u_2}$ fall off to their free stream values more rapidly than the data indicates. A striking feature of the calculations is the behaviour of the parameter $-\overline{u_1u_2}_{/k}$ which is predicted to be roughly constant over an appreciable region of the boundary layer in which it has a value of about 0·22. This value, which is in good agreement with the measurements in the near wall region is substantially less than the value of 0·3 found in a boundary layer developing in constant pressure. However, in the outer half of the boundary layer the predicted distribution of the parameter $-\overline{u_1u_2}_{/k}$ falls off (as in the case of k and $\overline{u_1u_2}$) more rapidly to its free stream value than the data indicates.

To summarise the predictions of similar boundary layers, it can be stated that the gross features of the flows such as the variation of R_2 and H with K, the thickening of the viscous sublayer and the degeneration to laminar flow for a value of K near $3{\cdot}0 \times 10^{-6}$ are in accord with experimental data. This measure of agreement may be regarded as a major achievement of the model. There are detailed discrepancies in the predicted profile shapes; being most evident in the prediction of the turbulence quantities, k and $\overline{u_1u_2}$. It may, however, be possible to improve these profile predictions simply by a better choice of the empirical constants appearing in the model.* For example, at $K = 1{\cdot}5 \times 10^{-6}$ the

---

* The present experimental results did not become available until the final stages of the present study. Time did not permit further optimisation of the constants.

predicted distributions of k and $\overline{u_1 u_2}$ fall off to their free stream values more rapidly than the data indicates. This indicates that a greater diffusion of k and ε away from the wall is required. This may, perhaps, be brought about by modification of the diffusion terms for k and by, say, reducing the Prandtl numbers σ_k and σ_ε.

However it must be stated that all the constants appearing in the model are interdependent and it is <u>not</u> certain that the agreement of prediction with experiment, for accelerating flows, can be improved without detriment to the constant pressure results. Whether or not this is so may only be determined by further computer experiments. Finally it should be mentioned that modifications to the forms of the functions F_3 and F_μ are <u>not</u> likely to bring improvement to the predictions. Experience with the model has shown that the form of the function F_3 has little effect on boundary layer flows; indeed it could well have been put equal to its high R_T constant value, i.e. $F_3 = 2{\cdot}0$ everywhere. The requirement that the model predict the mean velocity profile in the adjacent wall region of high Reynolds number constant pressure flows imposes a great restraint on (and practically fixes) the form of F_μ.

(2) <u>Non-Equilibrium Flows</u>

In practically occurring flows the boundary conditions are rarely, if ever, such that similar boundary layers arise. It is thus of great practical importance that the model be able to predict the behaviour of non-

equilibrium accelerated boundary layers. With this in mind predictions were obtained and compared with the measurements of heat transfer to accelerated boundary layers by Moretti and Kays (63), Filetti (29) and Kearney et al (45).

In figures 4.19 to 4.25 the predicted variations of Stanton number are compared with the measurements of Moretti and Kays and Filetti. In all these experiments the acceleration is preceded by a development length of between 4 ft and 5 ft in which the free stream velocity is uniform; a step change in wall temperature is applied at x_1 equal to two feet and downstream therefrom the wall temperature is maintained nearly constant.

For Filetti's runs (2 & 3) and Moretti and Kays' run (42) shown in figures 4.19, 4.20 & 4.21, the accelerations were such that the value of K was fairly uniform, with values of about $2{\cdot}0 \times 10^{-6}$ and $3{\cdot}2 \times 10^{-6}$ respectively. In each case there is a marked drop in Stanton number in the region of acceleration and a rise downstream therefrom. The predictions consistently mirror this experimental behaviour though for each test the Stanton numbers are somewhat lower than the measured - even upstream of the acceleration. Indeed, for the data shown in figures 4.19 and 4.21 the largest discrepancy between measurement and prediction (about 15%) occurs in the region 3 ft $< x_1 <$ 4 ft where the pressure gradient is zero. To the writer's knowledge all other theoretical models that have been applied to the prediction of these flows exhibit lower

values of Stanton number than the measured over this region of the flow. In view of this, the present predictions may be deemed to be satisfactory.

For the data shown in figures 4.22, 4.23, 4.24 & 4.25 K varies roughly sinusoidally; the data displayed in figures 4.22, 4.23 & 4.25 has a peak value of K of about 4×10^{-6} and that in figure 4.24 a value of 7×10^{-6}. In figures 4.22, 4.23 & 4.25 the predictions like the measurements, show a rapid falling off in Stanton number in the region of severe acceleration. The predictions, however, display too early a recovery as the acceleration dies away. There is some evidence (figure 4.25) to suggest that the predicted recovery, although taking place too soon is not as rapid as that displayed (when it does occur) by the measurements. A similar behaviour is displayed in figure 4.24 for the more severe of the accelerations. Agreement between measurement and prediction is even better than in figures 4.22, 4.23 & 4.25. At the end of the acceleration the predicted boundary layer reverts towards turbulent more quickly than the measurements suggest.

Figures 4.26 to 4.29 compare boundary layer predictions with the measurements of Kearney et al (45) in strongly accelerated boundary layers with blowing at the wall. In these experiments the acceleration was preceded by a development length of about 1 ft in which the free stream velocity was uniform. The accelerations, applied over $1\frac{1}{2}$ ft, were such that K was fairly uniform with a value of $2{\cdot}5 \times 10^{-6}$. The temperature difference

between the free stream and the wall was maintained nearly constant throughout the test section. Various values and distributions (along the test plate) of the blowing parameter F were studied. The predictions shown in figures 4.26 to 4.29 were all started with the measured mean velocity and temperature profiles at the beginning of the acceleration, the first measuring station.

In figure 4.26 the predicted variation of $C_{f/2}$, R_2 and St is compared with the measurements for a case in which the blowing parameter, F was zero. The predictions are in good agreement with experiment. The predicted skin friction coefficient remains roughly constant, as do the measurements, throughout the acceleration; the predicted values being about 4% too low. The predicted variation of R_2 is also in close accord with the measurements with some small deviation (10% maximum) occurring towards the end of the acceleration. The Stanton number decreases smoothly in the region of acceleration and here the predictions and measurements also closely agree. However, as the acceleration dies away the predicted Stanton numbers do not rise as suddenly as the data indicates; the maximum discrepancy being about 15%.

The data shown in figure 4.27 is of an accelerated boundary layer to which blowing at the wall is applied; the value of F is maintained constant and equal to ·004 throughout the test section. The agreement between the predictions and the measurements is not as

good as in the previous case . The predicted values of $C_{f/2}$ show a slight decrease through the region of acceleration whereas the measurements display a small increase. The predicted variation of R_2 is in quite close accord with the measurements with a small deviation occurring at the end of the acceleration. Discrepancies also exist between the predicted and measured Stanton numbers. The measured St values decrease smoothly through the acceleration; the predicted values do also but at too great a rate. Some explanation for the discrepancies that exist for this case may be found in the fact that the data probably represents a difficult case to predict since K and F produce opposing effects in accelerating flows. For example a positive value of F tends to increase St whereas K tends to produce a decrease; a fine balance between these effects probably exists. It should also be mentioned that the mixing-length-A^+-correlation model of Kearney et al does not predict this case accurately.

In figures 4.28 and 4.29 predictions and measurements are shown of accelerated boundary layers in which a step in blowing is applied about half way through the acceleration. In figure 4.29 the blowing (with F = ·004) is applied over the initial region of the flow (and removed about half way through the acceleration) whereas in figure 4.28 the blowing is applied over the latter half of the flow.

Figure 4.29 shows a measured Stanton number variation which falls smoothly in the initial region of acceleration until the step in blowing parameter is reached whereupon it rises sharply. Downstream of the step the Stanton number continues to fall until the end of the acceleration whereafter a rise occurs. In figure 4.28 the measurements show a smooth decrease in Stanton number in the initial half of the acceleration. At the step in blowing parameter F a sudden fall in Stanton number occurs and this is subsequently followed, at the end of the acceleration region by a small increase. In both cases (figures 4.28 and 4.29) the enthalpy deficit thickness Reynolds number R_Δ increases monotonically through the flow. For both the flows shown in figures 4.28 and 4.29 the predictions accord reasonably well with the measurements although (as in the previous cases) the predicted Stanton numbers do not rise quite as rapidly at the end of the acceleration as the measurements indicate. There is also some discrepancy (about 10% maximum) between the predicted and measured values of R_Δ shown in figure 4.29 . However, this is not considered to be significant as Kearney et al used the two-dimensional integrated thermal energy equation to calculate the experimental values of R_Δ, which are thus likely to be of questionable accuracy. Notwithstanding these detailed discrepancies, the overall agreement is good; a satisfactory result considering the sudden changes in boundary conditions which were applied to these flows.

4.57 Concluding Remarks

1. In this section a new turbulence model has been presented in which a description of turbulence is provided through solution of partial differential equations for turbulence kinetic energy and dissipation rate of turbulence energy. The model is such that it may be applied to the calculation of both the fully turbulent and the viscous sublayer regions of the boundary layer. This latter feature was achieved through the inclusion of terms which represent the direct influence of molecular viscosity on the turbulence structure in the near-wall region.

2. The model has been applied to the prediction of the turbulent boundary layer developing in constant pressure and to a number of strongly accelerated flows. For some of these latter boundary layers blowing at the wall was present. Some discrepancies between experiment and prediction have emerged, but overall the model has been shown to be remarkably successful in predicting the hydrodynamic and thermal consequences of acceleration. The model appears to offer substantially greater predictive accuracy than has so far been achieved with the mixing length and other simple 'turbulent viscosity' models.

3. For the future, some improvement (although probably small) in predictive accuracy may be possible by a better choice of the empirical constants appearing in the model. Any further optimisation of these constants

should, however, be performed through examination of a slightly wider range of plane boundary layer flows than presently considered with perhaps consideration being given to equilibrium boundary layers in mild adverse pressure gradient. It must be recognised, however, that the model is relatively insensitive to the choice of constants and any improvements are thus likely to be small. Improvement in the low Reynolds number form of the model may perhaps be achieved if, say, the 'turbulent Prandtl' numbers, σ_k and σ_ϵ are made functions of the Reynolds number ($k^2/\epsilon\nu$) rather than given constant values.

4. In many practically occurring strongly accelerated flow situations large temperature gradients also exist. These variations in temperature produce associated gradients in fluid properties e.g. density and molecular viscosity. The model, in its present form, may be applied to the prediction of these flows. Of course, to obtain accurate predictions some further development of the model will in all probability be necessary. Further testing of the model is therefore required to establish its applicability to flows with large fluid property variations.

CHAPTER V

Conclusions

The aims of the present study which were set out in the Introduction of this thesis have, for the most part, been achieved. The main findings have been outlined at the end of each chapter and so all that remains is to summarise the outcome of the research.

5.1 The Experimental Programme

Three 'constant K' turbulent boundary layers have been set up and studied experimentally. The values of K considered were $1{\cdot}5 \times 10^{-6}$, $2{\cdot}5 \times 10^{-6}$ and $3{\cdot}0 \times 10^{-6}$ respectively. Mean velocity profile measurements in these boundary layers displayed a thickening of the viscous sublayer (in x_2^+ co-ordinates) and the division between the fully turbulent and the sublayer regions of the boundary layer became progressively less pronounced as K was increased; indeed, at K equals $3{\cdot}0 \times 10^{-6}$ no division could be identified. Also observed with increasing K was the progressive deviation of the measured velocity profiles from the semi-logarithmic law of the wall. An implication of this result is that turbulent flow calculation procedures which use the semi-logarithmic law as part of the solution (e.g. by patching a finite difference solution of the boundary layer equations onto a semi-log-law near the wall) may be expected to yield results which become increasingly in error with increasing

accelerations. The above results are in accord with the findings of other workers in studies of arbitrarily developing accelerated flows.

The measurements of fluctuating quantities yield results which illustrate some important differences between the turbulence structure of low Reynolds number accelerated boundary layers and that normally found in high Reynolds number flows.

5.2 The Theoretical Contribution

The main outcome of the theoretical work has been the provision of a turbulence model which is applicable to both the fully turbulent and the viscous sublayer regions of the turbulent boundary layer. The model involves solution of partial differential rate equations for turbulence kinetic energy and dissipation rate of turbulence kinetic energy. It contains a number of empirical constants but it is emphasised that these have all been obtained by reference to high Reynolds number constant pressure boundary layer flows. The model, when applied to the calculation of a range of accelerated boundary layer flows, led to hydrodynamic and heat transfer predictions which were in close overall agreement with experiment. It thus offers substantial improvement in predictive accuracy over simple mixing length models which fail completely to predict the consequences of strong accelerations.

5.3 Suggestions for Further Work

Although the proposed model was remarkably successful in predicting the overall behaviour of boundary layers undergoing laminarisation, comparisons with the results of the present experimental study have revealed certain detailed discrepancies. These are most evident in the predicted profiles of turbulence energy and shear stress. However, due to considerable delay by the manufacturers in delivery of a fan the results of the experimental study did not become available until the final stages of the programme. At this late stage it was not practicable to embark upon a programme of modification of the model. Nevertheless, some suggestions have been made as to how the predictions may be improved and these should be investigated.

In principle the model in its present form may be applied to boundary layer flows in which large fluid property variations arise due to, say, large temperature differences. The application of the model to these flows appears worthwhile, though small adjustments will in all probability be necessary to obtain accurate predictions. The model may also be profitably applied to the calculation of low Reynolds number turbulent pipe and channel flows.

From the experimental viewpoint there is a general shortage of data regarding low Reynolds number turbulent flows. The task of devising and refining a turbulence model for low Reynolds number shear flow would have been substantially aided if measurements of

all the components of $\overline{u_i u_j}$ had been available for a range of similar turbulent boundary layers encompassing accelerations upto the point at which complete degeneration to laminar occurs. The physical dimensions of the present apparatus precluded such measurements. In the future detailed turbulence measurements in accelerated boundary layers could be made by either utilising a working fluid with a larger viscosity than air (e.g. water or glycerine) or by using much lower velocities than presently used; either methods would yield boundary layers which were much thicker, although in neither case can it be said that the attendant experimental difficulties are trivial.

Other simpler low Reynolds number turbulent flows could perhaps be studied to advantage. For example, measurements performed in a low Reynolds number turbulent flow under the action of pure shear or strain would certainly be of aid in devising low Reynolds number turbulence models. In any case more quantitative measurements of low Reynolds number turbulence particularly within the viscous sublayer of the boundary layer are certainly required.

Nomenclature

Symbol	Meaning	Equation of First Appearance
A^+	a function appearing in the Van Driest near wall mixing length formula	4.8
A_s^+	A^+ for a similar boundary layer	4.13
A_μ	constant in turbulence energy equation	4.19
A_D	constant in turbulence energy equation	4.19
a_1, a_2, a_3 & a_4	constants in algebraic length scale equation	4.20
$a_{\ell j}^{mi}$	coefficient of dimensions (velocity)^2 : a function of turbulence	4.22
$a_i(t)$	non-dimensional coefficient, a function of time	4.45
$C_{f/2}$	skin friction coefficient, $\tau_w / \rho U_{1,G}^2$	2.10
C	constant in semi-logarithmic law of the wall	3.3
C_p	specific heat at constant pressure	
C_D, C_μ	constants in the turbulence energy equation	4.19
C_1, C_2	non-dimensional functions of R_T	4.22
c	a constant in lag equation for A^+	4.14
D_v	Van Driest damping function	4.10
d	height of Stanton tube	3.6
E	D.C. voltage signal from hot-wire anemometer	3.8
e	fluctuating voltage signal from hot-wire anemometer	

Symbol	Meaning	Equation of First Appearance
F	surface mass transfer parameter, $U_{2,w}/U_{1,G}$	2.10
$F\{n_1\}$	spectral density of $\overline{u_1^2}$	3.10
F_1, F_2 & F_3	functions of R_T appearing in dissipation rate equation	4.36
F_μ	function of R_T in 'turbulent viscosity' formula	4.27
$f\{\eta\}$	$U_1/U_{1,G}$	2.12
$f\{x_2^+\}$	'law of the wall'	3.1
f	frequency	3.9
$G\{f\}$	frequency spectrum of $\overline{u_1^2}$	3.9
H	shape factor, δ_1/δ_2	2.10
h_o	height at entrance to plane convergent channel	3.12
K	acceleration parameter $\frac{\nu}{U_{1,G}^2}\frac{dU_{1,G}}{dx_1}$	
k	turbulence kinetic energy, $\frac{\overline{u_i u_i}}{2}$	2.6
L	a turbulence length scale	
L_{x_1}	length scale representative of large eddy size	3.13
ℓ	distance between entrance and line of intersection of planes forming convergent channel	3.11
ℓ_m	mixing length	4.6
ℓ, ℓ_D	algebraic length scales in turbulence energy equation	4.19
ℓ_ϵ	dissipation length scale, $\frac{k^{3/2}}{\epsilon}$	4.29
M	'matching' function	4.10

Symbol	Meaning	Equation of First Appearance
m^+	non-dimensional surface mass transfer, $U_{2,w}/U_\tau$	
N	constant in 'turbulent viscosity' formula	4.16
n_1	wave number in direction 1	3.10
n	constant in laminarisation parameter	
P, $\overline{P}$, P_s	mean static pressure	
P_{tot}	total pressure	3.5
P	constant in hot-wire anemometer response equation	3.8
p	fluctuating component of pressure	
Δp	Stanton tube reading	3.6
p^+	non-dimensional pressure gradient, $\frac{\nu}{\rho U_\tau^3}\frac{dP}{dx_1}$	
Q	constant in hot-wire anemometer response equation	3.8
$\dot{q}''_w$	wall heat flux	
R_{ij}	Reynolds stress tensor, $\overline{u_i u_j}$	2.5
R_2	momentum-deficit-thickness Reynolds number, $\delta_2 U_{1,G}/\nu$	2.10
R_Δ	enthalpy-deficit-thickness Reynolds number, $\Delta U_{1,G}/\nu$	2.11
R'_t	turbulence Reynolds number, $\frac{k^{\frac{1}{2}}\ell}{\nu}$	4.19
R_T	turbulence Reynolds number, $k^2/\nu\epsilon$	
$\mathcal{R}_{ij}$	two-point velocity correlation tensor, $\overline{u_i(\underline{x})u_j(\underline{x}+\underline{r})}$	

Symbol	Meaning	Equation of First Appearance
$\underline{r}$	vector separation with components r_1, r_2 and r_3	
St	Stanton number, $\frac{q_w}{\rho U_{i,G}(\Theta_G - \Theta_w)}$	
$S\{\eta\}$	$\overline{u_1 u_2}/U_{1,G}^2$	2.12
S_{ij}	twice the mean rate of strain	4.2
T	temperature	
t	time	
U_i, $\overline{U_i}$	mean velocity components ($i = 1$, 2 and 3)	
U_τ	wall friction velocity, $\sqrt{\tau_w/\rho}$	3.1
U_o	velocity outside boundary layer at entrance to plane convergent channel	3.11
U_c	convection velocity	3.10
ΔU	'strength of the wake'	3.4
U_1^+	non-dimensional velocity, U_1/U_τ	3.2
u_i	fluctuating velocity component ($i = 1$, 2 and 3)	
u_i'	r.m.s. of fluctuating velocity	
$w\{x_2/x_{2,G}\}$	the law of the wake	3.1
x_i	co-ordinate axes ($i = 1$, 2 and 3)	
x_1	co-ordinate in the mean flow direction	
x_2	co-ordinate normal to the wall and mean flow direction	
x_3	co-ordinate parallel to the wall and normal to the mean flow direction	

Symbol	Meaning	Equation of First Appearance
x_2^+	non-dimensional distance normal to the wall, $x_2 U_{\tau/\nu}$	3.2
x_1'	distance from entrance to plane convergent channel	3.11
α	molecular thermal diffusivity	2.9
β	Clauser equilibrium parameter, $\frac{\delta_1}{\tau_x} \frac{dP}{dx_1}$	
γ	intermittency factor	4.16
Δ	enthalpy-deficit thickness, $\int_0^\infty \frac{U_1}{U_{1,G}} \left(\frac{\Theta - \Theta_G}{\Theta_w - \Theta_G} \right) dx_2$	
δ	boundary layer thickness	
δ_1	displacement thickness $\int_0^\infty (1 - U_1/U_{1,G}) dx_2$	
δ_2	momentum-deficit thickness, $\int_0^\infty \frac{U_1}{U_{1,G}} (1 - U_1/U_{1,G}) dx_2$	
δ_{ij}	Kronecker tensor	
ϵ	dissipation rate of turbulence kinetic energy	4.22
η	similarity variable, $\frac{U_{1,G} x_2}{\nu}$	
Θ	mean thermal energy	2.9
θ	fluctuating component of thermal energy	2.9
κ	von Karmen constant ($\approx$ .4)	3.1

Symbol	Meaning	Equation of First Appearance
Λ_1	integral length scale of turbulence in direction 1	
λ	constant in mixing length constant	4.10
λ	turbulence microscale, $\sqrt{\frac{\nu k}{\epsilon}}$	
μ	dynamic molecular viscosity	
ν, ν_T	kinematic molecular and 'turbulent' viscosities respectively	
π	3.14159	
ρ	density	
σ	molecular Prandtl number	
σ_T	'turbulent' Prandtl number for thermal energy	4.11
σ_k	'turbulent' Prandtl number for turbulence energy	4.19
σ_ϵ	'turbulent' Prandtl number for dissipation rate of turbulence energy	4.36
τ	total shear stress, $(\mu\frac{\partial U_1}{\partial x_2} - \rho\overline{u_1 u_2})$	
τ_t	turbulent shear stress, $(-\rho\overline{u_1 u_2})$	

Subscripts

G	denotes free stream conditions
max	refers to maximum
min	refers to minimum
o	refers to limiting value of zero
w	denotes wall conditions
∞	refers to limiting value of infinity

Superscripts

-	denotes time averaged properties
+	denotes 'law of the wall' non-dimensional co-ordinates

References

1. Amsden, A.A. and Harlow, F.H., "The SMAC method : a numerical technique for calculating incompressible fluid flows." Los Alamos Scientific Laboratory, LA-4370 (1970).

2. Badri Narayanan, M.A. and Ramjee, V., "On the criteria for reverse transition in a two-dimensional boundary layer flow." Report No. AE 68 FM 1 Dept. of Aero. Engr., Indian Inst. of Science (1968).

3. Back, L.H., Cuffel, R.F. and Massier, P.F., "Laminarisation of a turbulent boundary layer in a nozzle flow - boundary layer and heat transfer measurements with wall cooling." Paper presented at ASME-AIChE Conference, Minneapolis, U.S.A., ASME Paper No. 69-HT-56 (1969).

4. Back, L.H., Massier, P.F. and Gier, H.L., "Convective heat transfer in a convergent-divergent nozzle." Int. J. Heat Mass Transfer 7, 549 (1964).

5. Batchelor, G.K. and Townsend, A.A., "Decay of turbulence in the initial period." Proc. Roy. Soc. A 193 (1948).

6. Batchelor, G.K. and Townsend, A.A., "Decay of turbulence in the final period." Proc. Roy. Soc. A 190 (1948).

7. Bakewell, H.P., "Viscous sublayer and adjacent wall region in turbulent flow." Physics of Fluids 10 (1969).

8. Beckwith, I.E. and Bushnell, D.M., "Detailed description and results of a method for computing mean and fluctuating quantities in turbulent boundary layers." NASA TN D-4815 (1968).

9. Boldman, D.R., Schmidt, J.F. and Gallagher, A.K., "Laminarisation of a turbulent boundary layer as observed from heat-transfer and boundary layer measurements in conical nozzles." NASA TN D-4788 (1968).

10. Bradshaw, P., Ferriss, D.H. and Atwell, N.P., "Calculations of boundary layer development using the turbulent energy equation." J. Fluid Mech., 28, 593 (1967).

11. Bradshaw, P., "The effect of wind-tunnel screens on nominally two-dimensional boundary layers." J. Fluid Mech., 22, 679 (1965).

12. Bradshaw, P., "A compact null-reading, tilting U-tube micromanometer with a rigid liquid container." J. of Scientific Instruments, 42, 677 (1965).

13. Bradshaw, P., "A note on reverse transition." J. Fluid Mech., 35, 387 (1969).

14. de Bray, R.G., "Some investigations into the spanwise non-uniformity of nominally two-dimensional incompressible boundary layers downstream of gauze screens." A.R.C. Rpt No. 29-271 (1967).

15. Caldwell, G.L. and Seban, R.A., "Flow and heat transfer in a laminarising turbulent boundary layer." ASME paper 69-HT-10 (1969).

16. Cebeci, T., Smith, A.M.O. and Mosinskis, G., "Solution of the incompressible turbulent boundary layer equations with heat transfer." J. Heat Transfer, 92, 133 (1970).

17. Champagne, F.H., Sleicher, C.A. and Wehrmann, O.H., "Turbulence measurements with inclined hot wires." J. Fluid Mech., 28, 153 (1967).

18. Chou, P.Y., "On velocity correlations and the solution of the equations of turbulent fluctuations." Quart. Appl. Math., 3, 38 (1945).

19. Chou, P.Y., "Pressure flow of a turbulent fluid between two infinite parallel planes." Quart. Appl. Math., 3, 198 (1945).

20. Coantic, M., "A study of turbulent pipe flow and of the structure of its viscous sublayer." 4th Euromech Colloquium (1967).

21. Coles, D.E., "The turbulent boundary layer in a compressible fluid." Rand. Rep. R403 (1962).

22. Daly, B.J., and Harlow, F.H., "Transport theory of turbulence." Los Alamos Sci. Lab. Rept. LA-DC-11304 (1970).

23. Davidoff, B.I., "On the statistical dynamics of an incompressible turbulent fluid." Dokl AN SSSR, 136, 47 (1961).

24. Deardorff, J.W., "A numerical study of three-dimensional turbulent channel flow at large Reynolds numbers." J. Fluid Mech., 41, 453 (1970).

25. Donaldson, C.D. and Rosenbaum, H., "Calculation of turbulent shear flows through closure of the Reynolds equation by invariant modeling." Aero. Res. Assoc. of Princeton, Rpt. 127 (1968).

26. Van Driest, E.R., "On turbulent flow near a wall." J. Aero. Sci. 23, 1007 (1957).

27. Emmons, H.W., "Shear flow turbulence." Proc. 2nd U.S. Nat. Cong. Appl. Mech. ASME (1954).

28. Escudier, M.P., "The distribution of the mixing length in turbulent flows near walls." Mech. Eng. Dept., Imperial Col., Rep. TWF/TN/1 (1965).

29. Filetti, E.G., University of Stanford unpublished report, data quoted by Moretti and Kays (ref. 63) (1965).

30. Glushko, G.S., "Turbulent boundary layer on a flat plate in an incompressible fluid." IZV. Akad. Nauk SSSR, Mekh, No 4 (1965).

31. Gosman, A.D., Pun, W.M., Runchal, A.K., Spalding, D.B. and Wolfshtein, M.W., "Heat and mass transfer in recirculating flows." Academic Press, London (1969).

32. Harlow, F.H. and Hirt, C.W., "Generalised transport theory of anisotropic turbulence." University of California Rept. LA-4086 (1969).

33. Harlow, F.H. and Romero, N.C., "Turbulence distortion in a non-uniform tunnel." Los Alamos Sci. Lab. Rept. LA-4247 (1969).

34. Harlow, F.H. and Nakayama, P.I., "Transport of turbulence energy decay rate." Los Alamos Sci. Lab. rept. LA-3854 (1968).

35. Harlow, F.H. and Nakayama, P.I., "Turbulent transport equations." Physics of Fluids, 10, 2323 (1967).

36. Hanjalic, K., "Two dimensional asymetrical turbulent flow in ducts." Ph.D. thesis, University of London (1970).

37. Herring, H.J. and Norbury, J.F., "Experiments on equilibrium turbulent boundary layers in favourable pressure gradients." J. Fluid Mech., 27, 541 (1967).

38. Hinze, J.O., "Turbulence: An introduction to its mechanism and theory." McGraw-Hill, New York, 1959.

39. Hudimoto, B., "Momentum equations for the boundary layer and their application to the turbulent boundary layer." Mem. Fac. Eng., Kyoto Univ., 13, 162 (1951).

40. Jones, W.P., "Strongly accelerated turbulent boundary layers." M.Sc. Thesis, Imperial College (1967).

41. Jones, W.P. and Launder, B.E., "On the prediction of laminarescent turbulent boundary layers." ASME paper 69-HT-13 (1969).

42. Jones, W.P. and Launder, B.E., "The prediction of laminarisation with a two-equation model of turbulence." Paper submitted to Int. J. Heat Mass Transfer (1970).

43. Julien, H.L., Kays, W.M. and Moffat, R.J., "The turbulent boundary layer on a porous plate: experimental study of the effects of a favorable pressure gradient." Rept HMT-4 Mech. Eng. Dept., Stanford University (1969).

44. Kays, W.M., Moffat, R.J. and Thielbahr, W.H., "Heat transfer to the highly accelerated turbulent boundary layer with and without mass addition." Int. J. Heat Mass Transfer, 13, 499 (1970).

45. Kearney, D.W., Moffat, R.J. and Kays, W.M., "The turbulent boundary layer: experimental heat transfer with strong favorable pressure gradients and blowing." Rept. HMT-12, Mech. Eng. Dept., Stanford University (1970).

46. Klebanoff, P.S., "Characteristics of turbulence in a boundary layer with zero pressure gradient." NACA TN 3178 (1954).

47. Kolmogorov, A.N., "Equations of turbulent motion of an incompressible fluid." Itv. Ak. Nauk SSSR (1942). Translation from Russian by D.B. Spalding, Imperial College, 1968)

48. Kolovandin, B.A. and Vatutin, I.A., "On statistical theory of non-uniform turbulence." Int. seminar on Heat and Mass transfer, Herceg Novi, Yugoslavia (1969).

49. Launder, B.E., "Laminarisation of the turbulent boundary layer by acceleration." M.I.T. Gas Turbines Lab. Rept. No. 77 (1964).

50. Launder, B.E., "Laminarisation of the turbulent boundary layer in severe acceleration." J. Appl. Mech., 31, 707 (1964).

51. Launder, B.E. and Stinchcombe, H.S., "Non-normal similar boundary layers." Imperial College, Mech. Eng. Dept. Rept. TWF/TN/21 (1967).

52. Launder, B.E. and Jones, W.P., "Sink flow turbulent boundary layers." J. Fluid Mech., 38, 817 (1969).

53. Launder, B.E. and Jones, W.P., "On the prediction of laminarisation." ARC Rept. No. 1036 (1969).

54. Launder, B.E. and Jones, W.P., "A note on Bradshaw's hypothesis for laminarisation." ASME paper 69-HT-12 (1969).

55. Laufer, J., "The structure of turbulence in fully developed pipe flow." NACA Rept. 1174 (1954).

56. Loyd, R.J., Moffat, R.J. and Kays, W.M., "The turbulent boundary layer on a porous plate: an experimental study of the fluid dynamics with strong favorable pressure gradients and blowing." Rept. HMT-13 Mech. Eng. Dept., Stanford University (1970).

57. Lumley, J.L., "Towards a turbulent constitutive equation." J. Fluid Mech., 41, 413 (1970).

58. Lundgren, T.S., "Distribution functions in the statistical theory of turbulence." Physics of Fluids, 10, 969 (1967).

59. McMillan, F.A., "Experiments on pitot tubes in shear flow." ARC Rept. No. 3028 (1956).

60. McMillan, F.A., "Viscous effects on flattened pitot tubes at low speed." J. Aero. Soc., 58 (1954).

61. Mellor, G.L. and Gibson, D.M., "Equilibrium turbulent boundary layers." Mech. Eng. Rept. FLD-13, Princeton University (1963).

62. Mellor, G.L. and Herring, H.J., "Two methods of calculating turbulent boundary layer behaviour based on numerical solutions of the equations of motion." Proceedings of AFOSR-IFP Stanford Conference (1968).

63. Moretti, P.M. and Kays, W.M., "Heat transfer to a turbulent boundary layer with varying surface temperature - an experimental study." Int. J. Heat Mass Transfer, 8, 1187 (1965).

64. Nee, V. and Kovasznay, L.S.G., "Simple phenomenological theory of turbulent shear flows." Physics of Fluids, 12, 473 (1969).

65. Ng. K.H. and Spalding, D.B., "Some applications of a model of turbulence for boundary layers near walls." Mech. Eng. Dept., Imperial College, Rept. B1/TN/14 (1969).

66. Nikuradse, J., "Gesetzmassigkeiten der turbulenten stromung in glatten Rohren." VDI-Forschungsheft 356 (1932).

67. Patel, V.C., "Calibration of the Preston tube and limitations on its use in pressure gradients." J. Fluid Mech. 23, 185 (1965).

68. Patel, V.C. and Head, M.R., "Reversion of turbulent to laminar flow." J. Fluid Mech., 34, 371 (1968).

69. Patankar, S.V. and Spalding, D.B., "Heat and Mass transfer to boundary layers." Morgan Grampian, London (1967).

70. Powell, T.E. and Strong, A.B., "Calculation of the two-dimensional turbulent boundary layer with mass addition and heat transfer." Proceedings of the 1970 Heat transfer and Fluid Mechanics Institute (1970).

71. Prandtl, L., "Bemerkungen zur Theorie der freien Turbulenz." ZAMM 22, 241 (1942).

72. Prandtl, L. and Wieghardt, K., "Uber ein neues Formelsystem für die ausgebildete Turbulenz." Nach. Akad. Wiss. Göttingen, Math-phys (1945).

73. Preston, J.H., "The minimum Reynolds number for a turbulent boundary layer and the selection of a transition device." J. Fluid Mech., 3, 373 (1958).

74. Reynolds, O., "Scientific papers of Osborne Reynolds." Cambridge, London, 1901 (1874).

75. Reynolds, W.C., "Computation of turbulent flows-state of the art, 1970." Rept. MD-27 Dept. of Mech. Eng., Stanford Univ. (1970).

76. Rodi, W. and Spalding, D.B., "A two-parameter model of turbulence and its application to free jets." Warme-und Stuffubertragung 3, 85 (1970).

77. Rotta, J., "Statistische theorie nighthomogener turbulenz." Zeitschrift für Physik, I: 129, 547 ; II : 131, 51 (1951).

78. Senoo, Y., "The boundary layer on the end wall of a turbine nozzle cascade." J. Heat Transfer 80, 1711 (1958).

79. Sergienko, A.H. and Gretsov, V.K., "Transition from a turbulent into a laminar boundary layer." Sov. Phys. Dokl 4, 275 (1959).

80. Schraub, F.A. and Kline, S.J., "A study of the structure of the turbulent boundary layer with and without longitudinal pressure gradient." Rept. MD-12, Mech. Eng. Dept., Stanford University (1965).

81. Sternberg, J., "Transition from a turbulent to a laminar boundary layer." U.S. Army Ballistics Res. Lab. Rept. 906 (1954).

82. Thielbahr, W.H., Kays, W.M. and Moffat, R.J., "The turbulent boundary layer: experimental heat transfer with blowing, suction and favorable pressure gradient." Rept. HMT-5, Mech. Eng. Dept., Stanford Univ. (1969).

83. Townsend, A.A., "The structure of turbulent shear flow." Camb. Univ. Press (1956).

84. Townsend, A.A., "Self-preserving flow inside a turbulent boundary-layer." J. Fluid Mech., 22, 773 (1965).

85. Tucker, H.J. and Reynolds, A.J., "The distortion of turbulence by irrotational plane strain." J. Fluid Mech., 32, 657 (1968).

86. Wolfshtein, M., "The velocity and temperature distribution in one-dimensional flow with turbulence augmentation and pressure gradient." Int. J. Heat and Mass Transfer, 12, 301 (1969).

87. Wolfshtein, M., "Convection processes in turbulent impinging jets." Ph.D. thesis, London University (1967).

88. Wieghardt, K., "Uber die Wandschubspannung in turbulenten Reibungsschichten bei veränderlichem Aussendruck." ZW.B, KWI, Göttingen, U & M 6603 (1943).

89. Wygnanski, I.and Fiedler, H.E., "Some measurements in the self-preserving jet." Boeing Sct. Res. Lab. Doc. D1-82-0712 (1968).

90. Zaric, Z., "Turbulent heat transfer in a divergent-convergent channel." J.S.M.E. Semi-Int. Sym., Tokyo (1967).

Appendix 1 : Analysis of the electrical signals obtained from a linearised hot-wire anemometer

Introduction

The equations which govern the response of a hot-wire anemometer have been derived by Champagne and Sleicher (17). They applied the equations (which include the effects of the tangential velocity component as well as the non-linearities caused by high turbulence intensity) to an idealised X-wire array the two wires of which were aligned so that their normals were inclined at $+45^{\circ}$ and -45° to the flow direction. The two wires were also assumed to have identical response equations.

In the present work, in order to obtain measurements close to the wall, it was necessary to position the X-probe so that it formed an angle of about 5° with the wall; the wire normals were thus inclined at angles of $+50^{\circ}$ and -40° to the flow direction. Also in practice it is seldom possible to adjust the gains of the two linearisers so that the response equations of the two wires are identical. The equations which govern the response of this 'non-ideal' X-wire array are thus presented. For reasons of practicability the analysis is restricted to low turbulence intensities.

The linearised constant temperature anemometer

The output voltage of a linearised constant temperature hot-wire anemometer is given by:-

$$E\{t\} = P + G\, U_{eff}\{t\} \qquad \text{(A.1.1.)}$$

$E(t)$ is the total output voltage, $U_{eff}(t)$ is the total effective 'cooling' velocity and P and G are constants which depend upon the wire resistance, geometry, temperature and linearisers settings. Now according to Champagne and Sleicher the effective cooling velocity for a wire inclined so that its normal forms an angle α with the mean flow direction is given (to first order) by:-

$$U_{eff} = U_m \cos\alpha \left\{1 + \tfrac{1}{2}k^2\tan^2\alpha - {}^1/_8 k^4\tan^4\alpha\right\} \times \left\{1 + \frac{u_m}{U_m} + a\,\frac{u_n}{U_m}\right\} \qquad \text{(A.1.2)}$$

where $a = [\tan\alpha \left\{1 - k^2(1 + \tfrac{1}{2}\tan^2\alpha) + \tfrac{1}{2}k^4\tan^2\alpha(1 + \tfrac{3}{4}\tan^2\alpha)\right\}] / (1 + \tfrac{1}{2}k^2\tan^2\alpha - {}^1/_8 k^4\tan^4\alpha)$

U_m is the mean velocity, u_m is the fluctuating component of velocity in the flow direction, u_n is the component of fluctuating velocity normal to the flow direction in the plane of the X-array and k represents the fraction of the velocity component, parallel to the wire, that effects the wire cooling.

Following the findings of ref (17) a value of k of 0.2 was adopted for the hot-wires used in the present study.

Now equations (A.1.1) and (A.1.2) may be combined to yield:-

$$\overline{E} + e = P + QU_m\{1 + \frac{u_m}{U_m} + a\frac{u_n}{U_m}\} \qquad (A.1.3)$$

where $Q = G\cos\alpha\{1 + \frac{1}{2}k^2\tan^2\alpha - \frac{1}{2}k^4\tan^4\alpha\}$

$\overline{E}$ is the average (D.C.) output voltage and e is the fluctuating component of voltage. If equation (A.1.3) is averaged then there results:-

$$\overline{E} = P + QU_m \qquad (A.1.4)$$

The 'constants' P and Q must be determined by calibration of the hot-wire with respect to, say, a pitot-tube.

Equations (A.1.4) and (A.1.3) may be manipulated to yield:-

$$e = Q\,(u_m + a\,u_n) \qquad (A.1.5)$$

The single 'normal' hot wire

For a single hot-wire aligned normal to the flow direction 'α' and thus 'a' are both zero. Equations (A.1.4) and (A.1.5) then yield the following expressions for the mean velocity and the turbulence intensity in the flow direction:-

$$U_1 = (\overline{E} - P)/Q$$

$$\sqrt{\overline{u_1^2}} = \sqrt{\overline{e^2}}/Q \qquad (A.1.6)$$

The X-hot-wire probe

The equations (A.1.4) and (A.1.5) may be used to evaluate the electrical signal obtained from an X-wire aligned to the flow direction as shown below:-

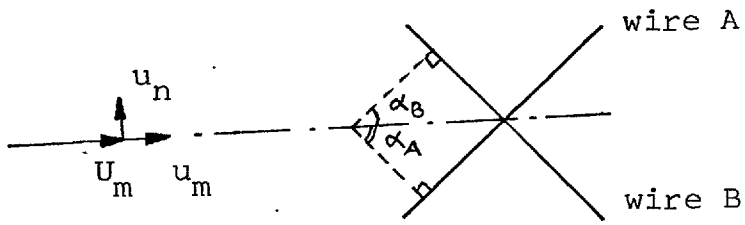

By applying equations (A.1.4) and (A.1.5) to the above X-wire array we obtain, after some manipulation:-

$$\left(\frac{\overline{e_A}}{Q_A}\right)^2 = \overline{u_m^2} + a_A^2\,\overline{u_n^2} + 2\,a_A\,\overline{u_n u_m}$$

$$\left(\frac{\overline{e_B}}{Q_B}\right)^2 = \overline{u_m^2} + a_B^2\,\overline{u_n^2} + 2\,a_B\,\overline{u_n u_m} \qquad \text{(A.1.7)}$$

$$\left(\frac{\overline{e_A + e_B}}{Q_A + Q_B}\right)^2 = \overline{u_m^2} + \left(\frac{Q_A a_A + Q_B a_B}{Q_A + Q_B}\right)^2 \overline{u_n^2}$$

$$+ 2\,\frac{(Q_A a_A + Q_B a_B)}{(Q_A + Q_B)}\,\overline{u_n u_m}$$

where the subscripts A and B denote the values of 'Q' and 'a' appropriate to the wires A and B respectively. The equations (A.1.7) may be solved to yield values of $\overline{u_m^2}$, $\overline{u_n^2}$ and $\overline{u_m u_n}$ from measured values of $\overline{e_A^2}$, $\overline{e_B^2}$ and $\overline{(e_A + e_B)^2}$.

Appendix 2 : Initial profiles for the predictions

Before numerical solution of the boundary layer equations may be commenced it is necessary to specify the initial profiles of all the dependent variables. Where experimental profiles were not available it was thus necessary to use estimated 'starting' profiles. The following initial profiles were therefore assumed:-

(1) Mean velocity

For the 'starting' profile of mean velocity it was assumed:-

$$U_1 = U_{1,G}\, Z^n \quad \text{for } Z \geq Z_J$$

and $$U_1 = U_\tau x_2^+ \quad \text{for } Z < Z_J$$

where $$Z = x_2/x_{2,G} \quad \text{and} \quad Z_J = \left[\frac{U_{1,G}\, x_{2,G}}{\nu} \cdot C_f/2 \right]^{\frac{1}{n-1}}$$

the boundary layer thickness, $x_{2,G}$ and exponent n were obtained from estimated values of R_2 and H.

i.e. $$n = (H - 1)/2$$

$$x_{2,G} = \frac{\nu R_2}{U_{1,G}} \frac{(H+1)H}{H-1}$$

Because of the linear profile for $Z < Z_J$ these latter expressions are only approximate. Nevertheless they should be of sufficient accuracy for the present purpose.

(2) Turbulence kinetic energy

The initial profile of turbulence kinetic energy was assumed given by:-

$$k = a_o + a_1 Z + a_2 Z^2 + a_3 Z^3 \qquad x_2^+ \geq 25$$

$$k = (x_2^+)^2 \{b_o + b_1 x_2^+\} \qquad x_2^+ < 25$$

The quantities a_o, a_1, a_2, a_3, b_o and b_1 appearing in the above equation were evaluated by imposing the following conditions on the k profile

$$\text{at } x_2^+ = 25,\ k = 3.3 \frac{\tau_w}{\rho} \text{ and } \frac{dk}{dZ} = 0$$

$$\text{and at } Z = 1,\ k = k_G \text{ and } \frac{dk}{dZ} = 0$$

(3) Dissipation rate of turbulence kinetic energy

For the initial profile of dissipation rate it was assumed that:

$$\epsilon = k^{3/2}/\ell$$

where ℓ was given by:-

$$\frac{\ell}{x_{2,G}} = \frac{\kappa}{(F_{\mu,\infty})^{.75}} Z(1 - \tfrac{1}{2}Z)$$

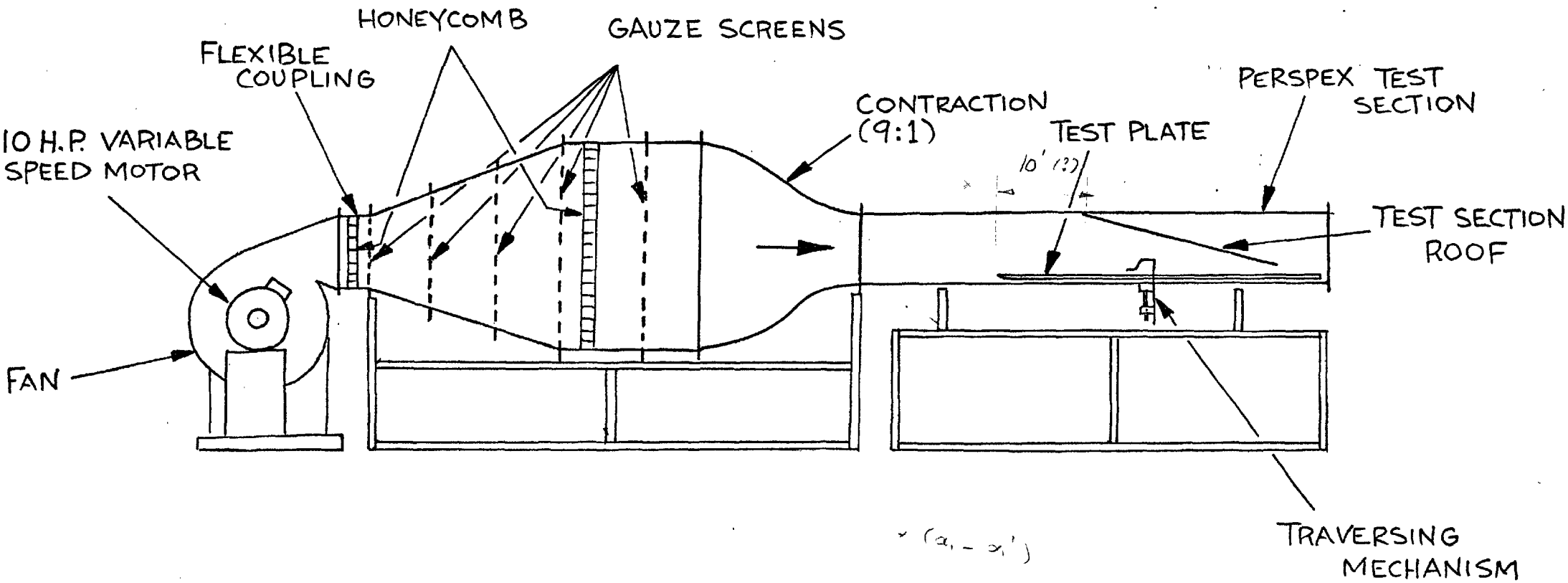

FIG. 3.1 : SCHEMATIC OF APPARATUS

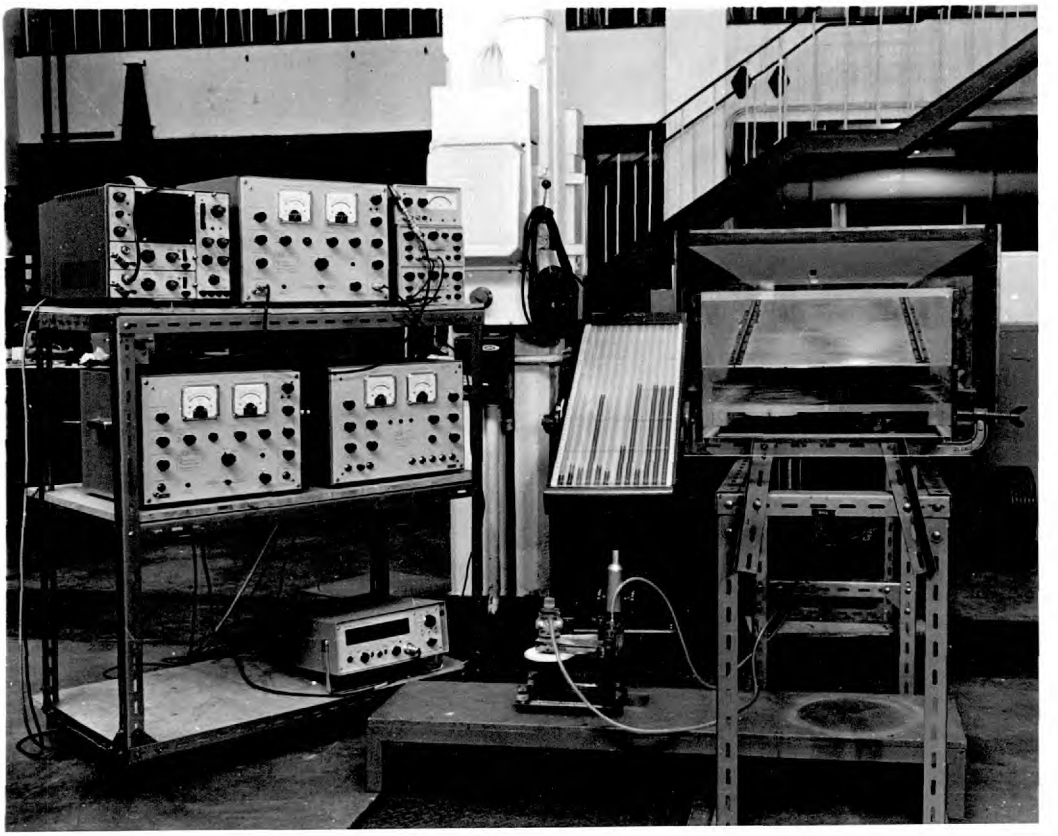

Fig. 3.2(a) Hot-wire signal processing equipment.

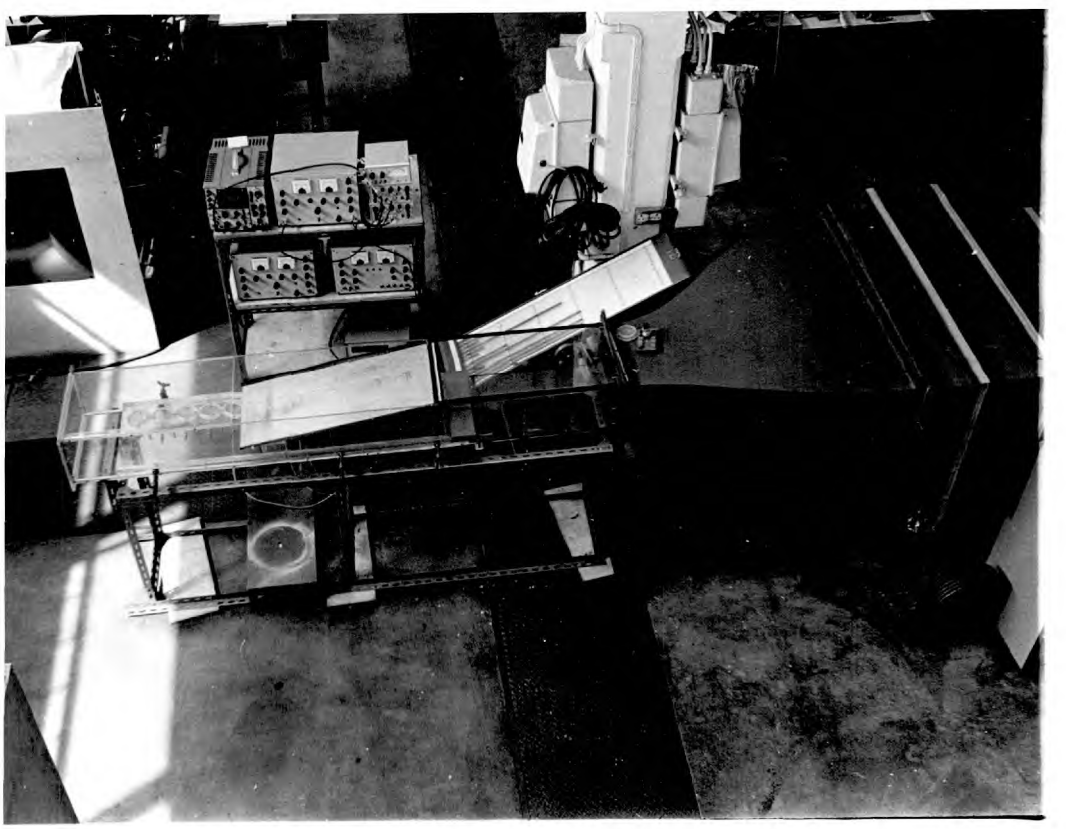

Fig. 3.2(b) General layout of apparatus

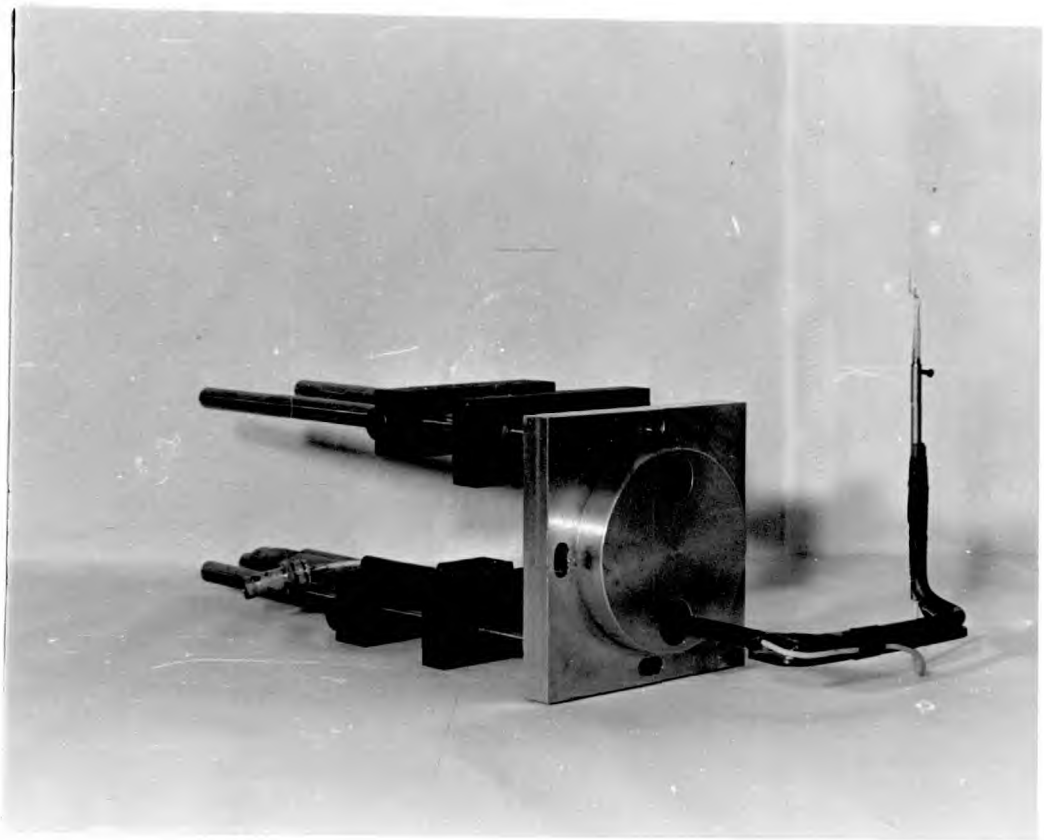

Fig 3.3(a) Traversing mechanism

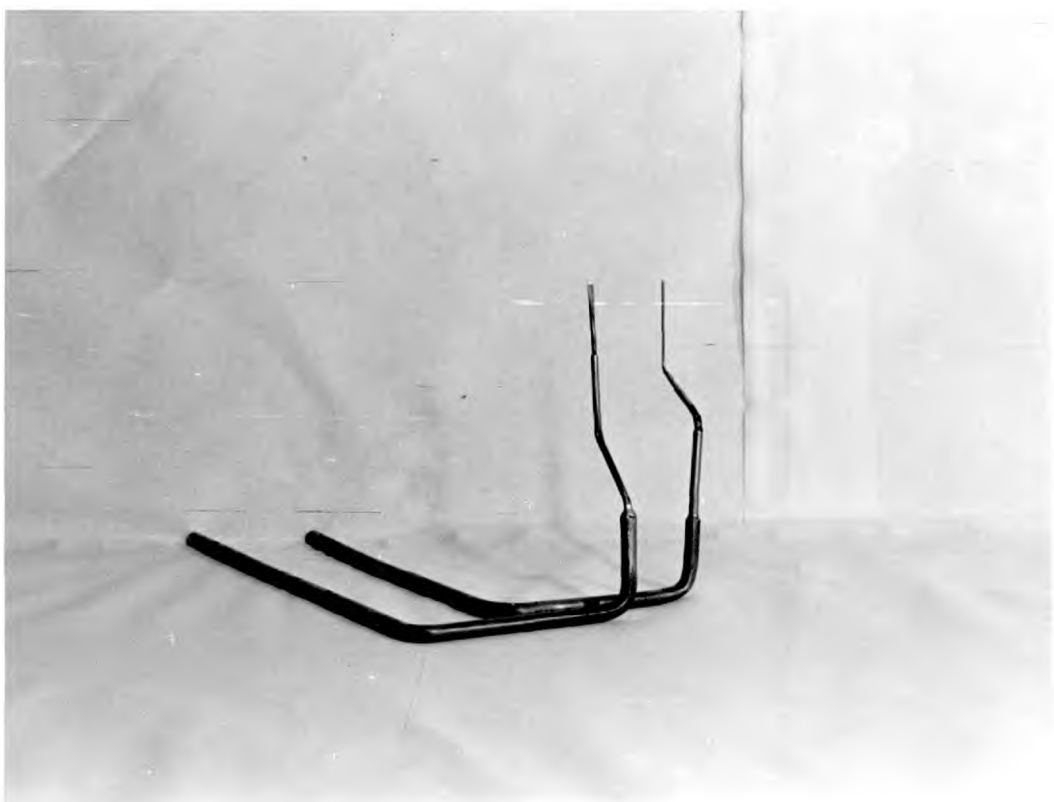

Fig 3.3(b) Flattened tip pitot and Preston tubes.

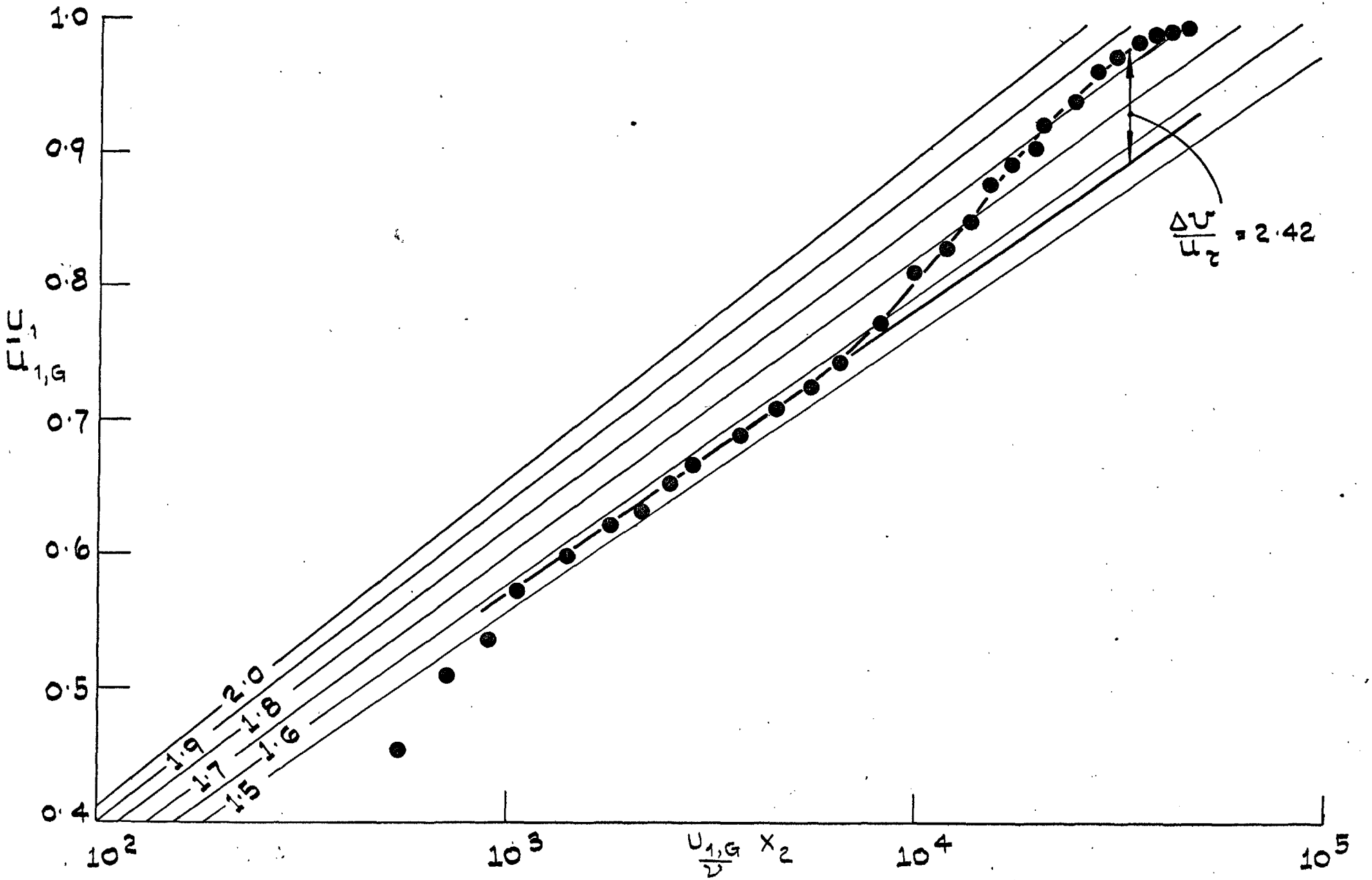

FIG. 3.4: BOUNDARY LAYER IN ZERO PRESSURE GRADIENT. MEAN VELOCITY PROFILE $R_2 = 3806$

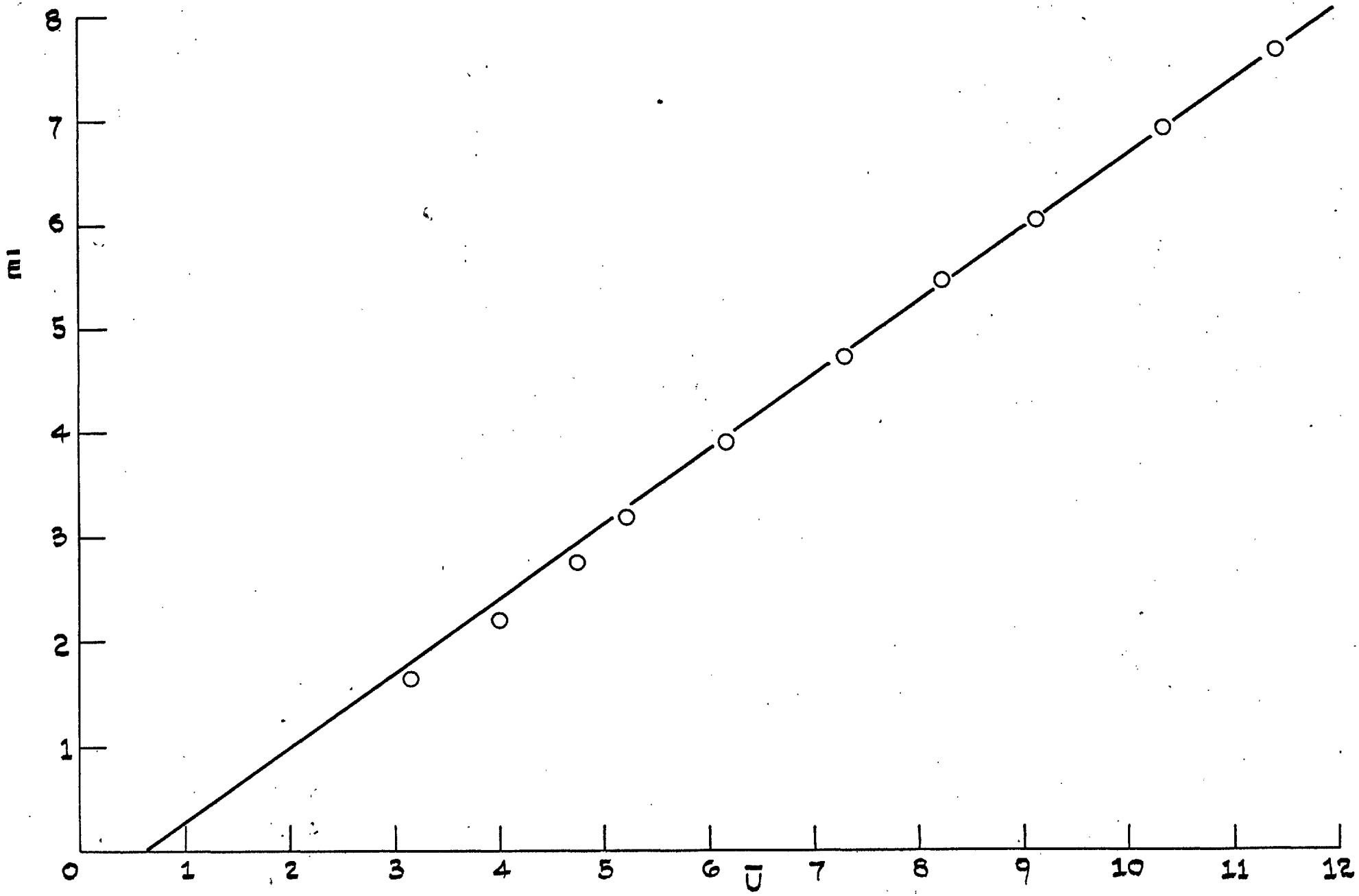

FIG. 3.5: CALIBRATION CURVE: DISA BOUNDARY LAYER HOT-WIRE PROBE.

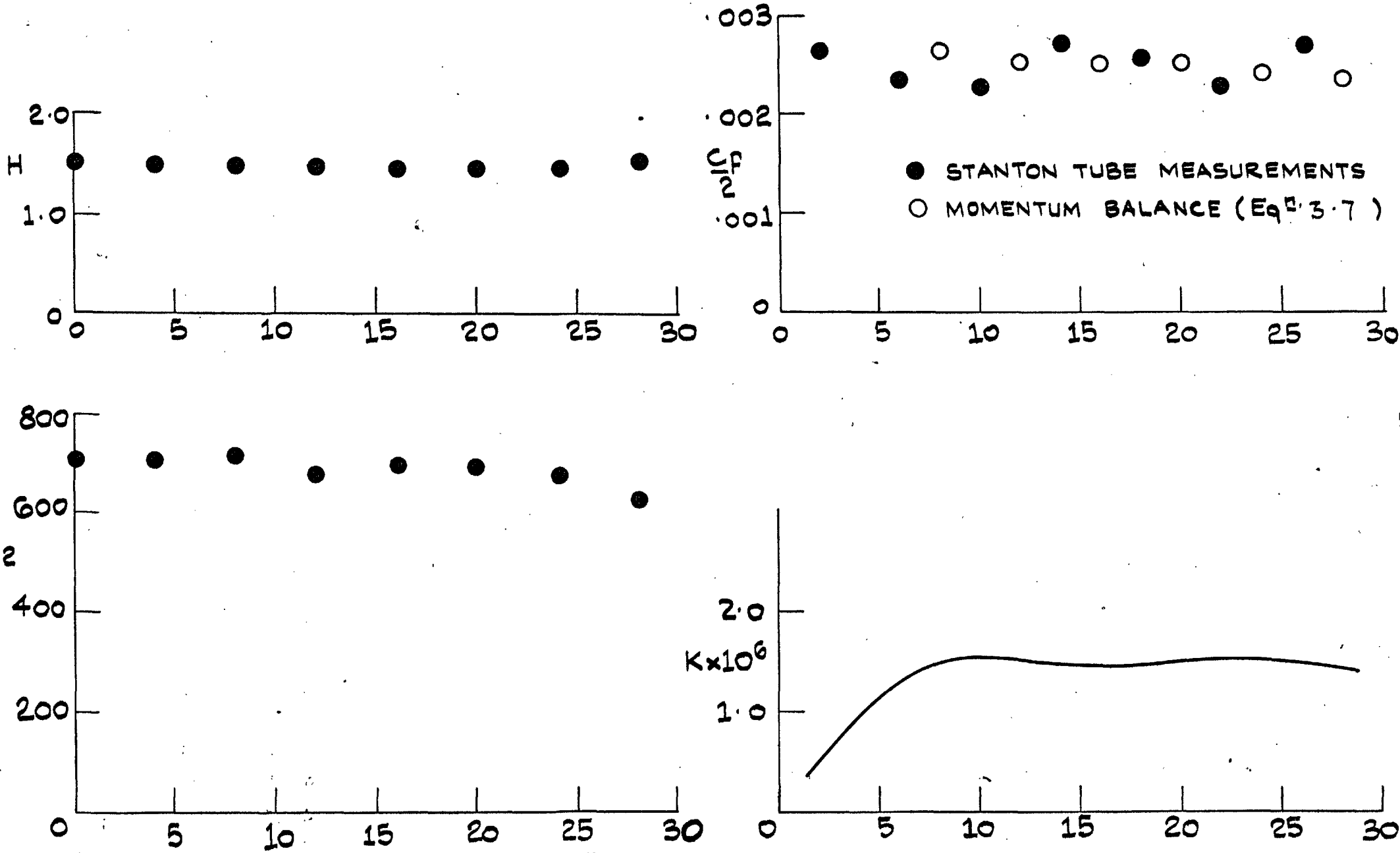

FIG. 3.6: 'BOUNDARY LAYER IN A PLANE CONVERGENT CHANNEL: VARIATION OF R_2, H, $C_f/2$ & K THROUGH THE ACCELERATION.

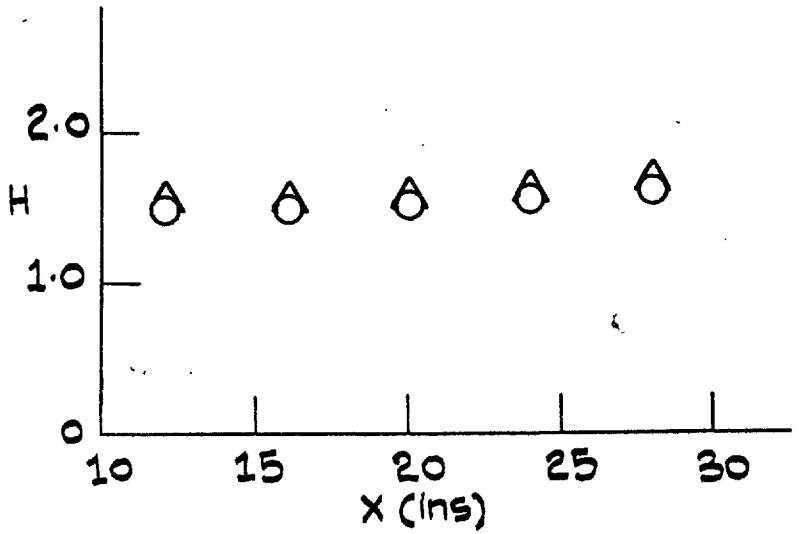

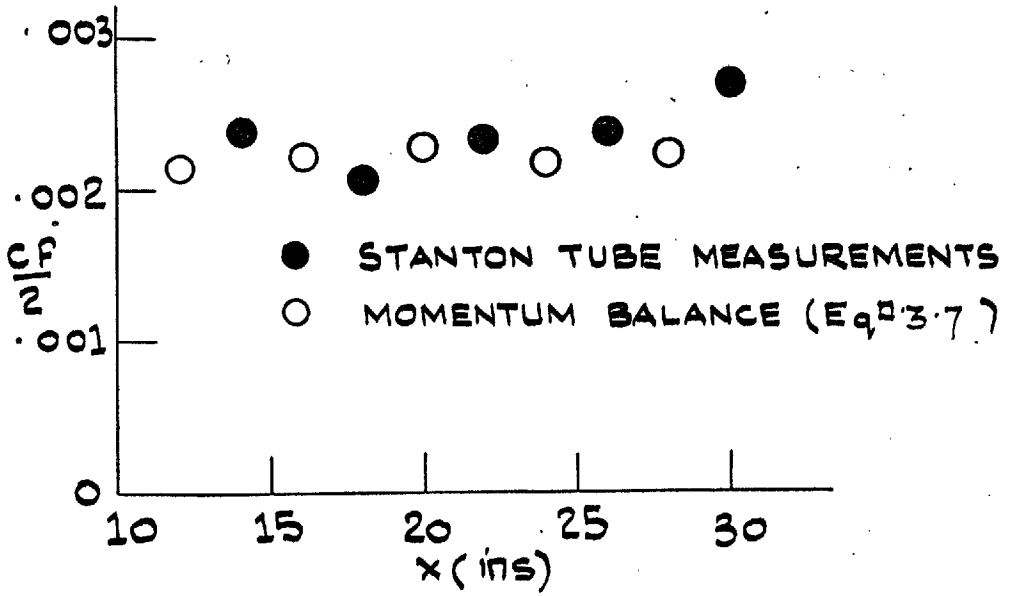

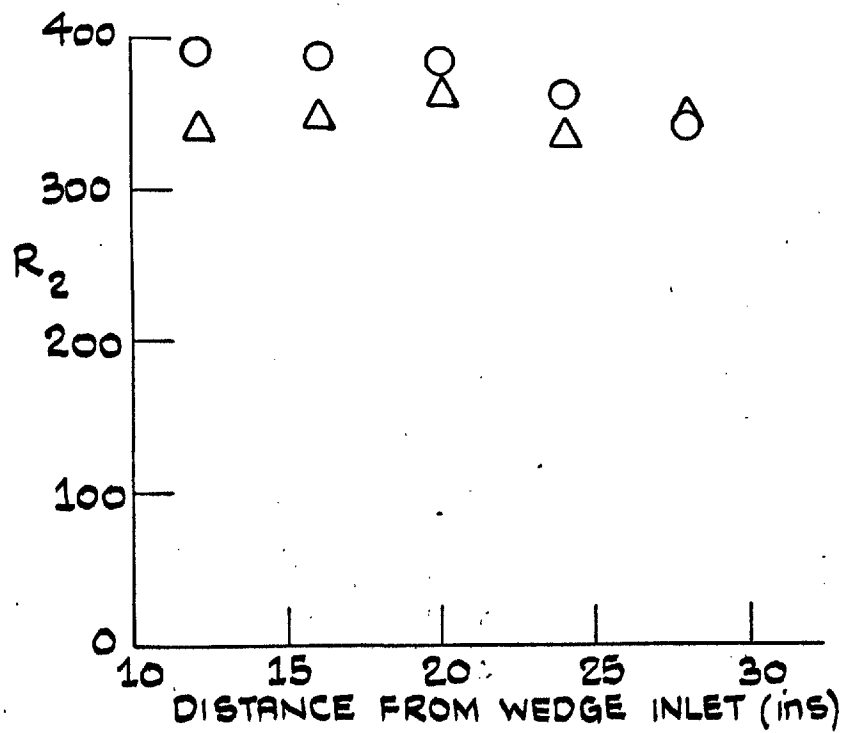

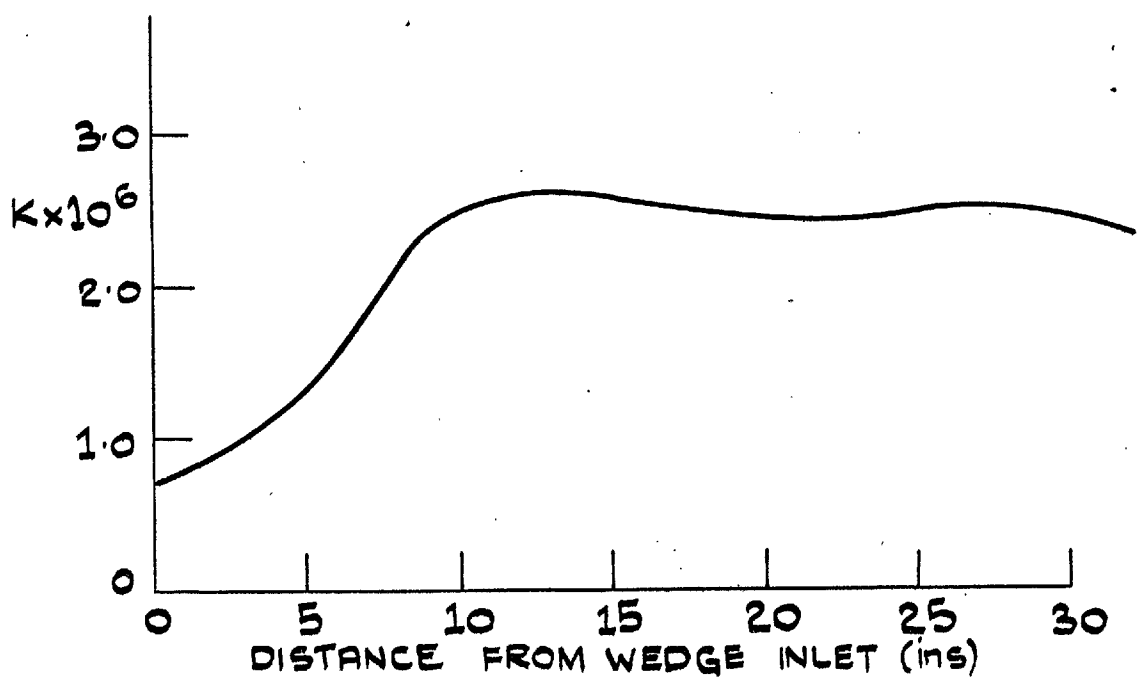

FIG. 3.7: BOUNDARY LAYER IN A PLANE CONVERGENT CHANNEL VARIATION OF R_2, H, $C_f/2$ & K THROUGH THE ACCELERATION.

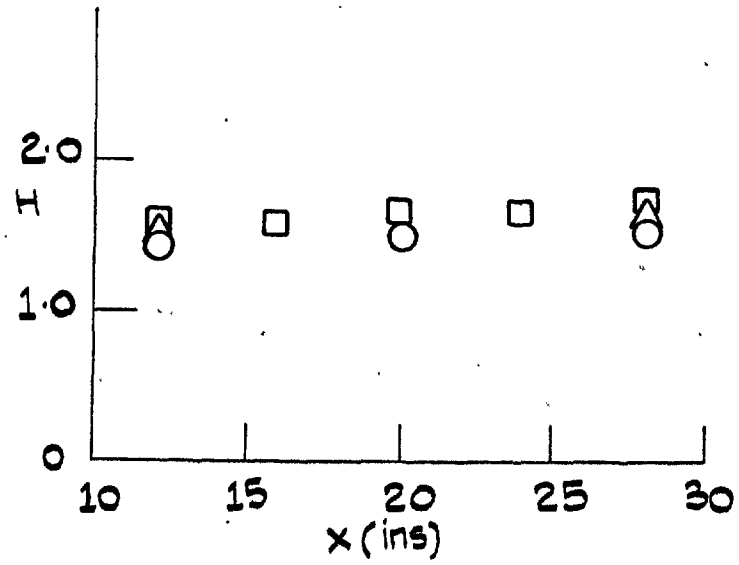

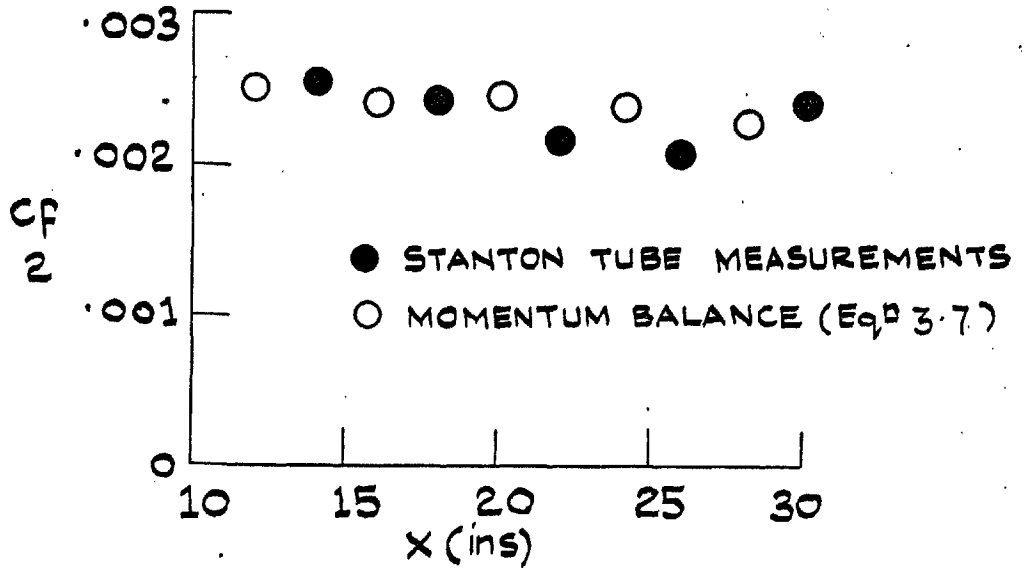

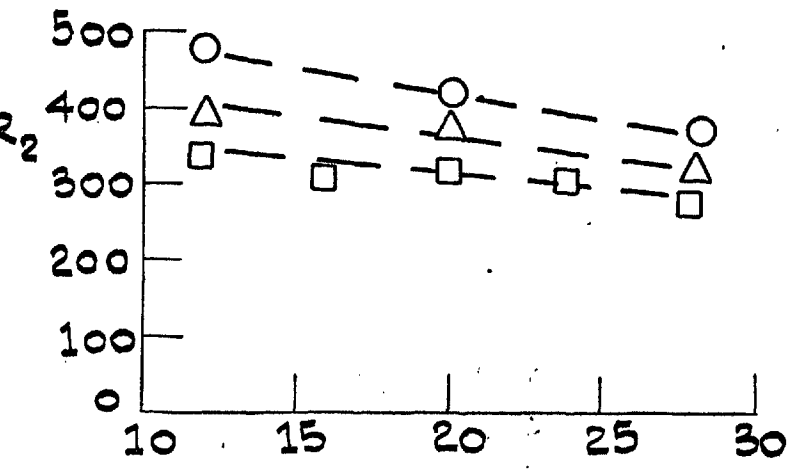

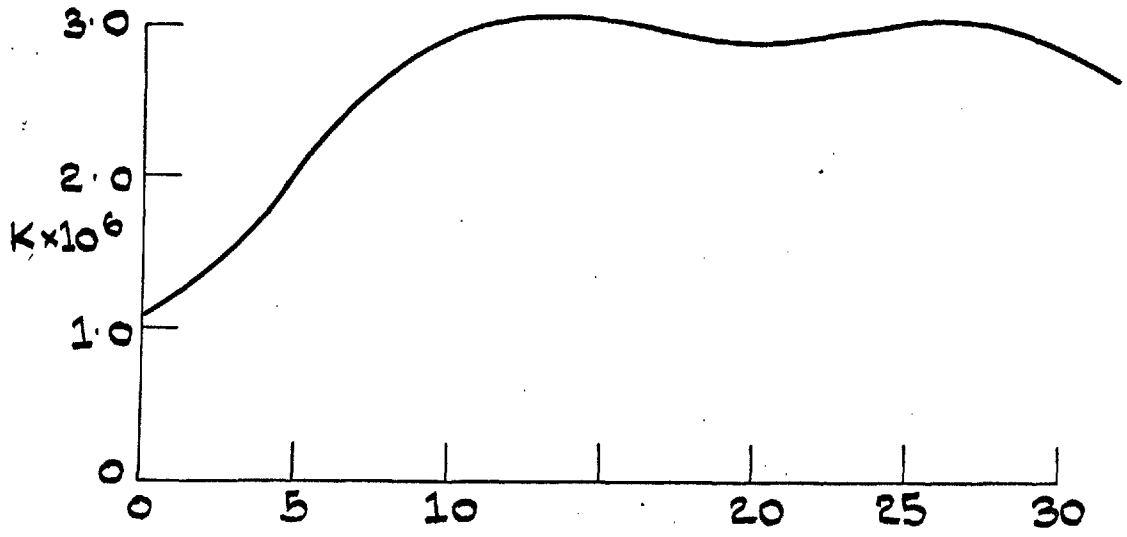

FIG. 3.8: BOUNDARY LAYER IN A PLANE CONVERGENT CHANNEL: VARIATION OF R_2, H, $C_f/2$ & K

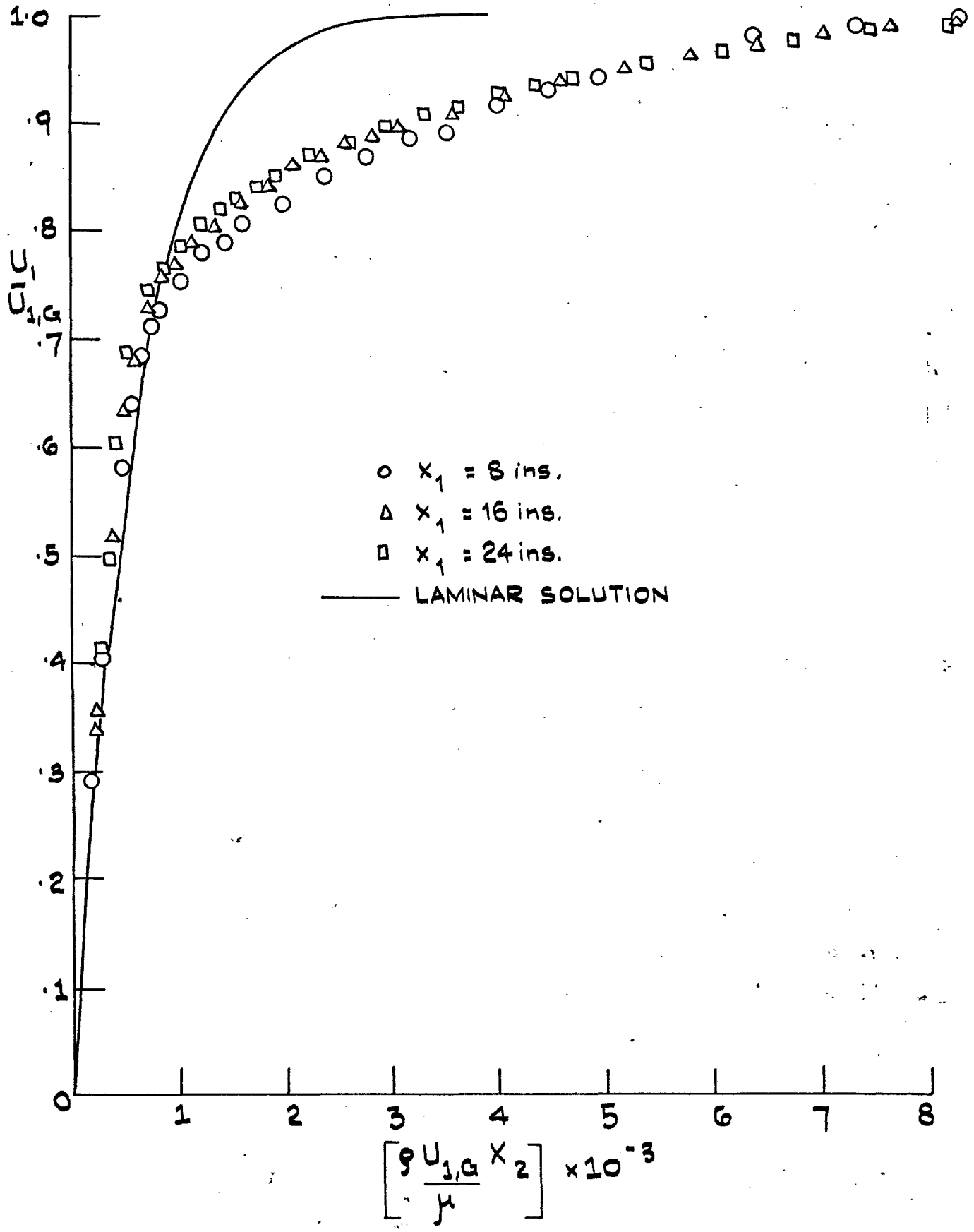

FIG.3.9: 'CONSTANT K' BOUNDARY LAYER: MEAN VELOCITY PROFILE
$K = 1 \cdot 5 \times 10^{-6}$

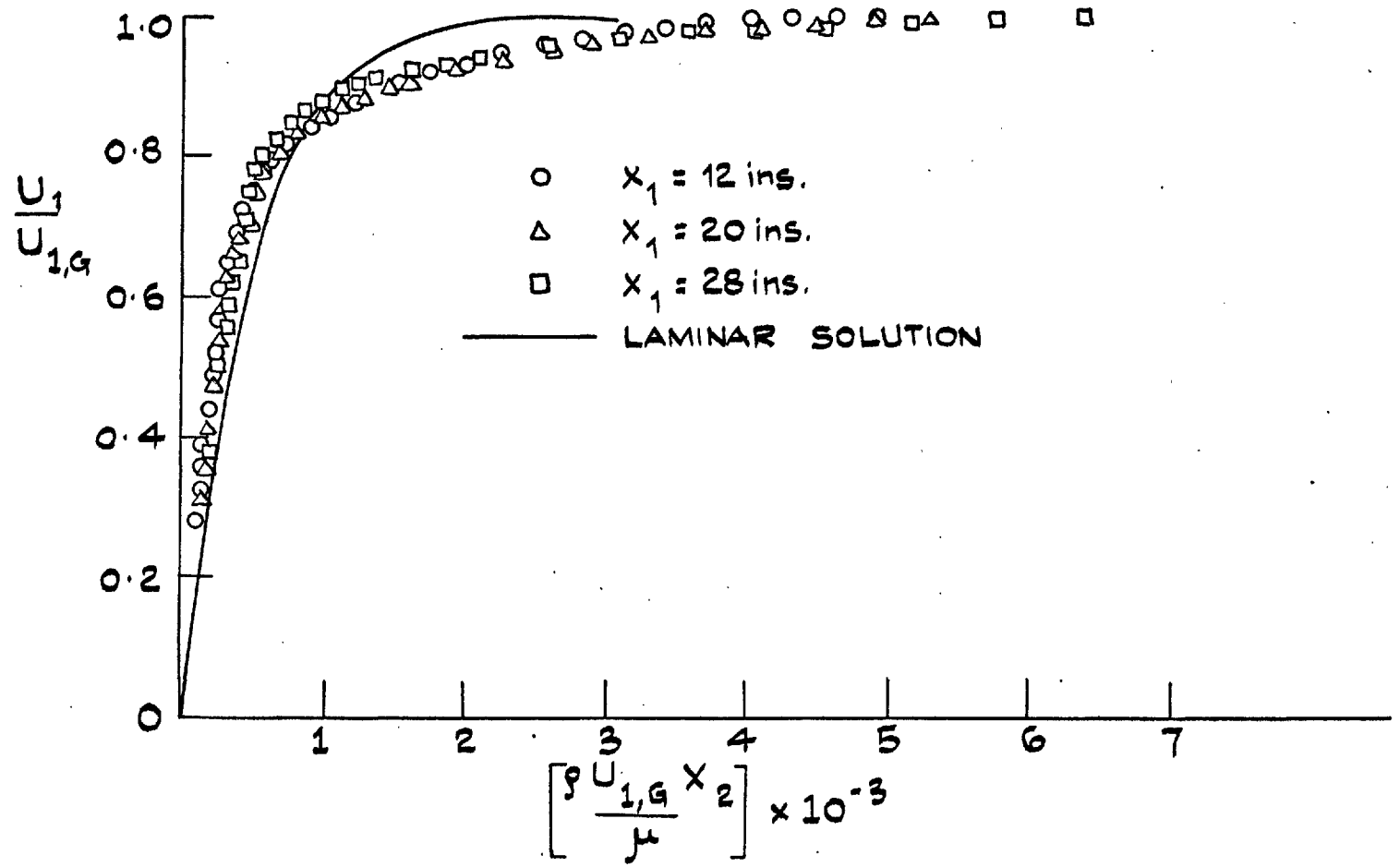

FIG. 3.10 : 'CONSTANT K' BOUNDARY LAYER: MEAN VELOCITY PROFILES, $K = 2{\cdot}5 \times 10^{-6}$

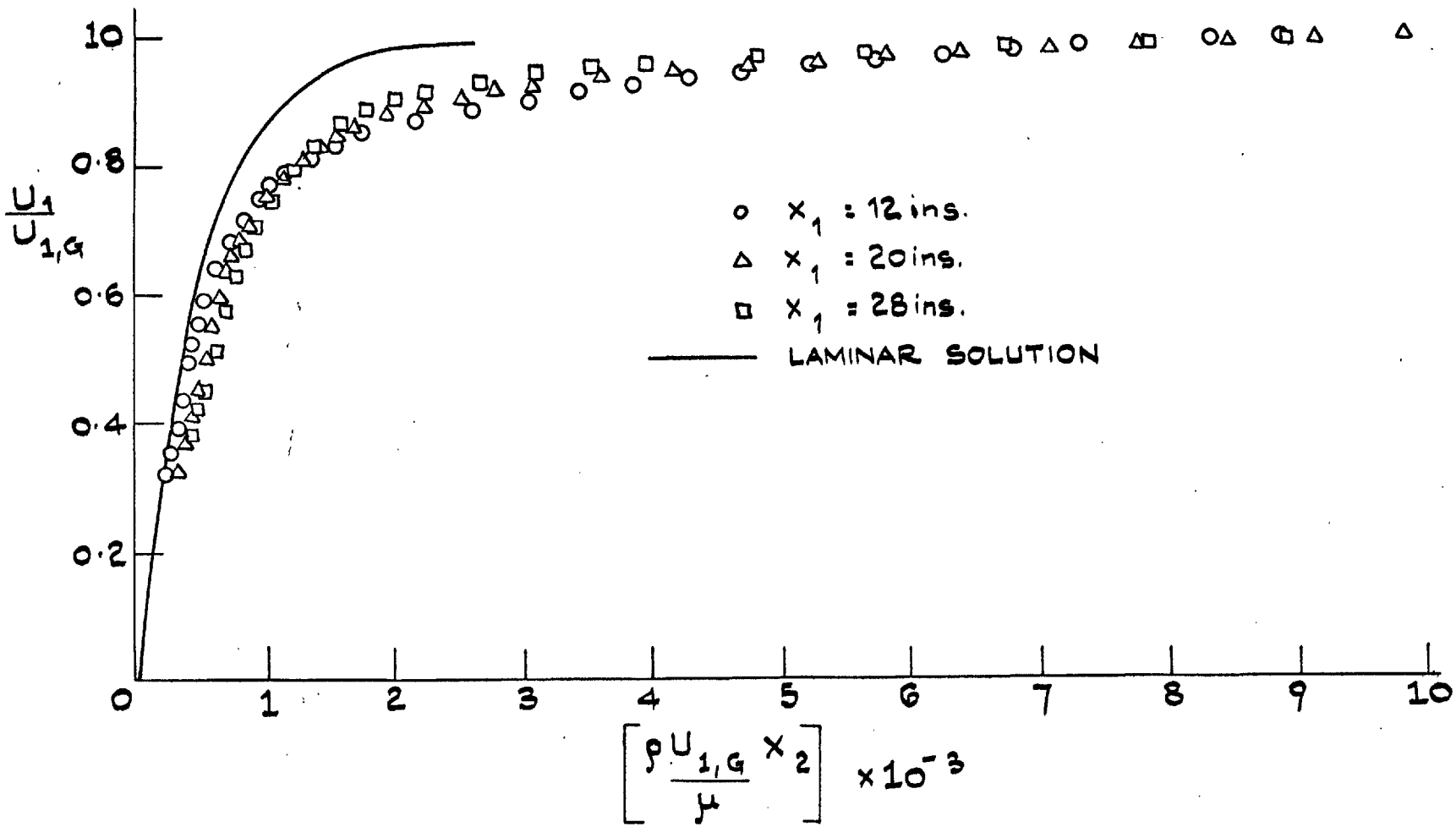

FIG. 3.11: 'CONSTANT K' BOUNDARY LAYER: MEAN VELOCITY PROFILES, $K = 3.0 \times 10^{-6}$

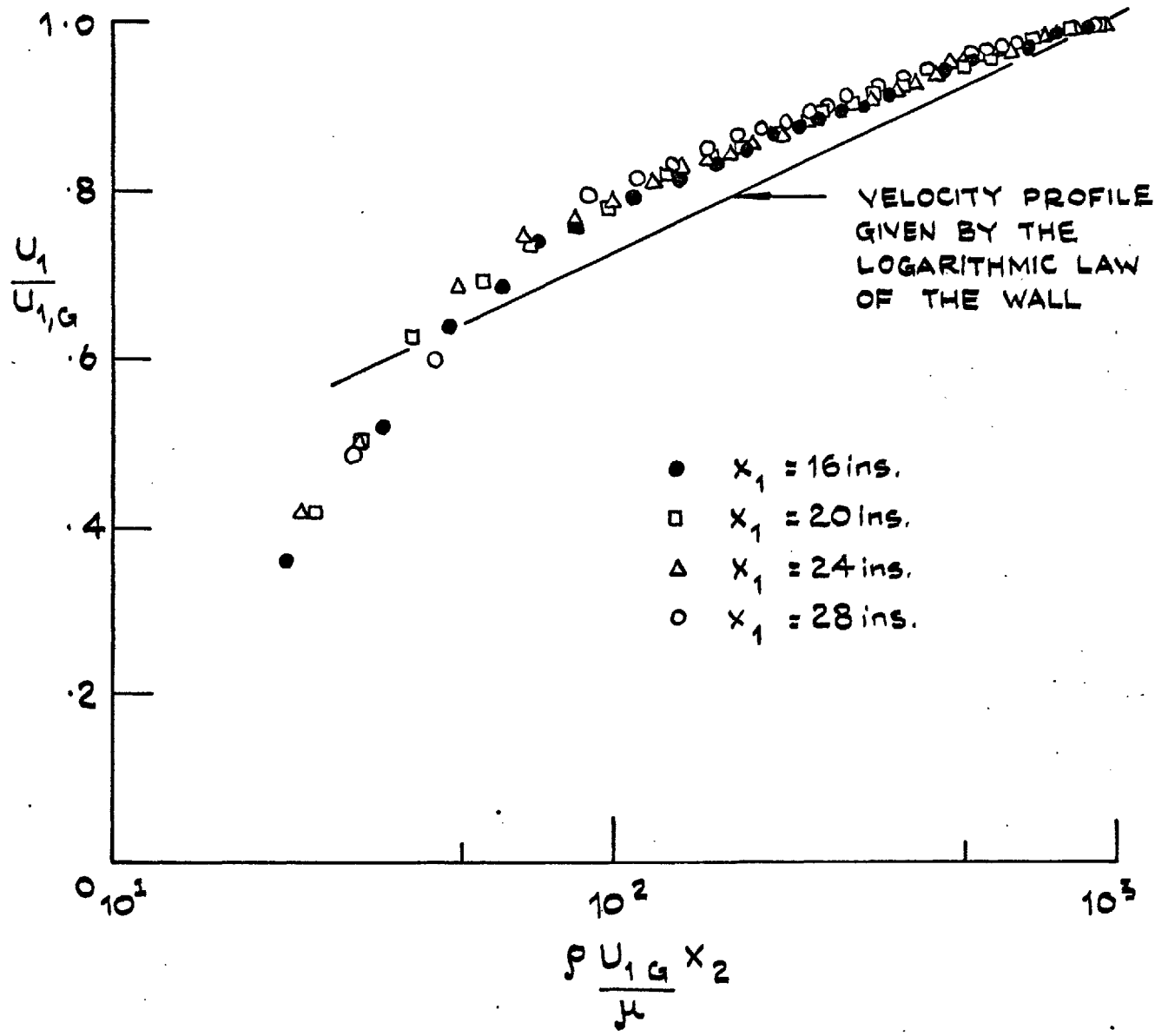

FIG. 3·12: 'CONSTANT K' BOUNDARY LAYER: MEAN VELOCITY PROFILES, $K = 1.5 \times 10^{-6}$

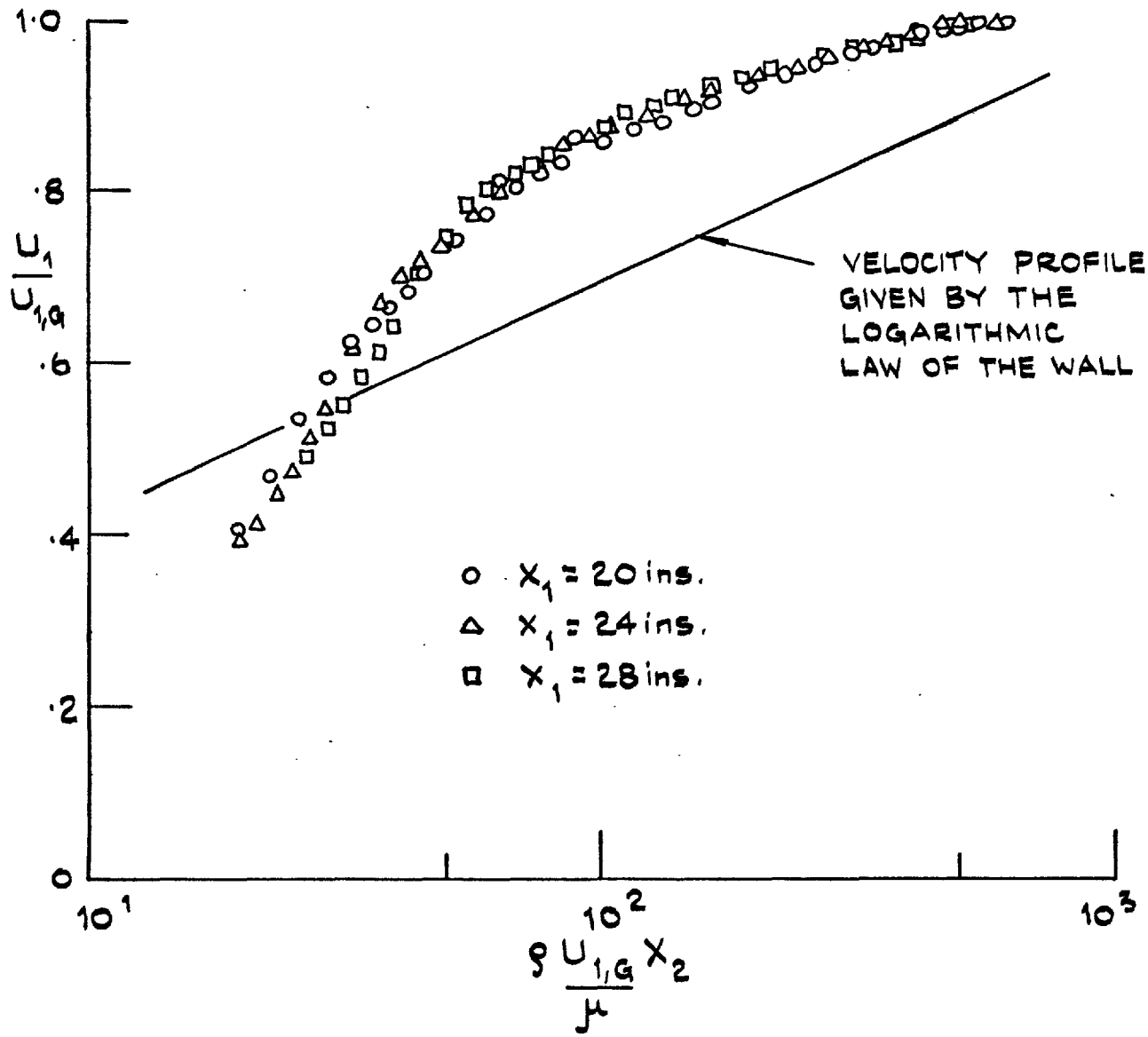

FIG. 3.13: 'CONSTANT K' BOUNDARY LAYER: MEAN VELOCITY PROFILES, $K = 2.5 \times 10^{-6}$

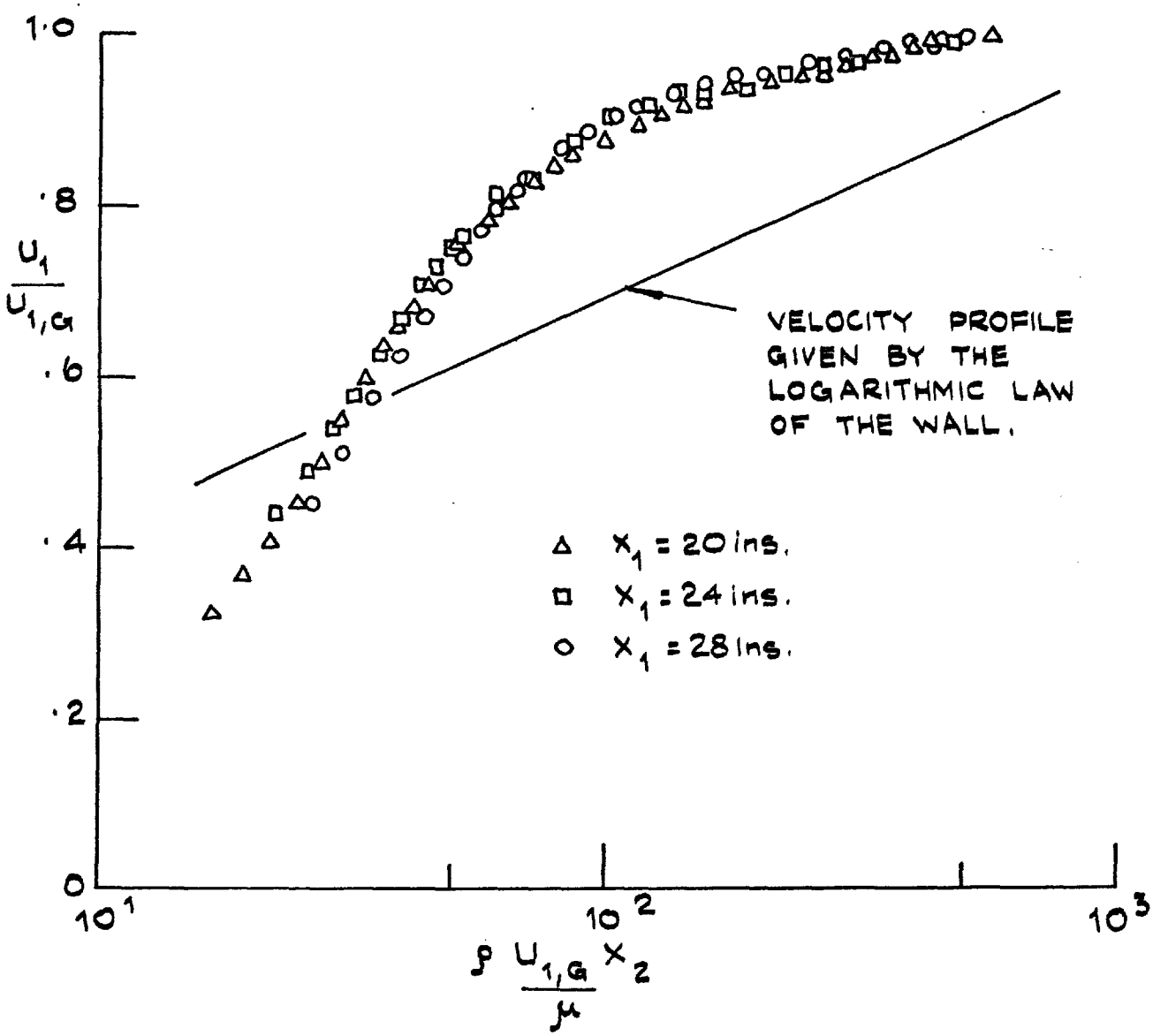

FIG. 3·14: `CONSTANT K' BOUNDARY LAYER: MEAN VELOCITY PROFILES, $K = 3.0 \times 10^{-6}$

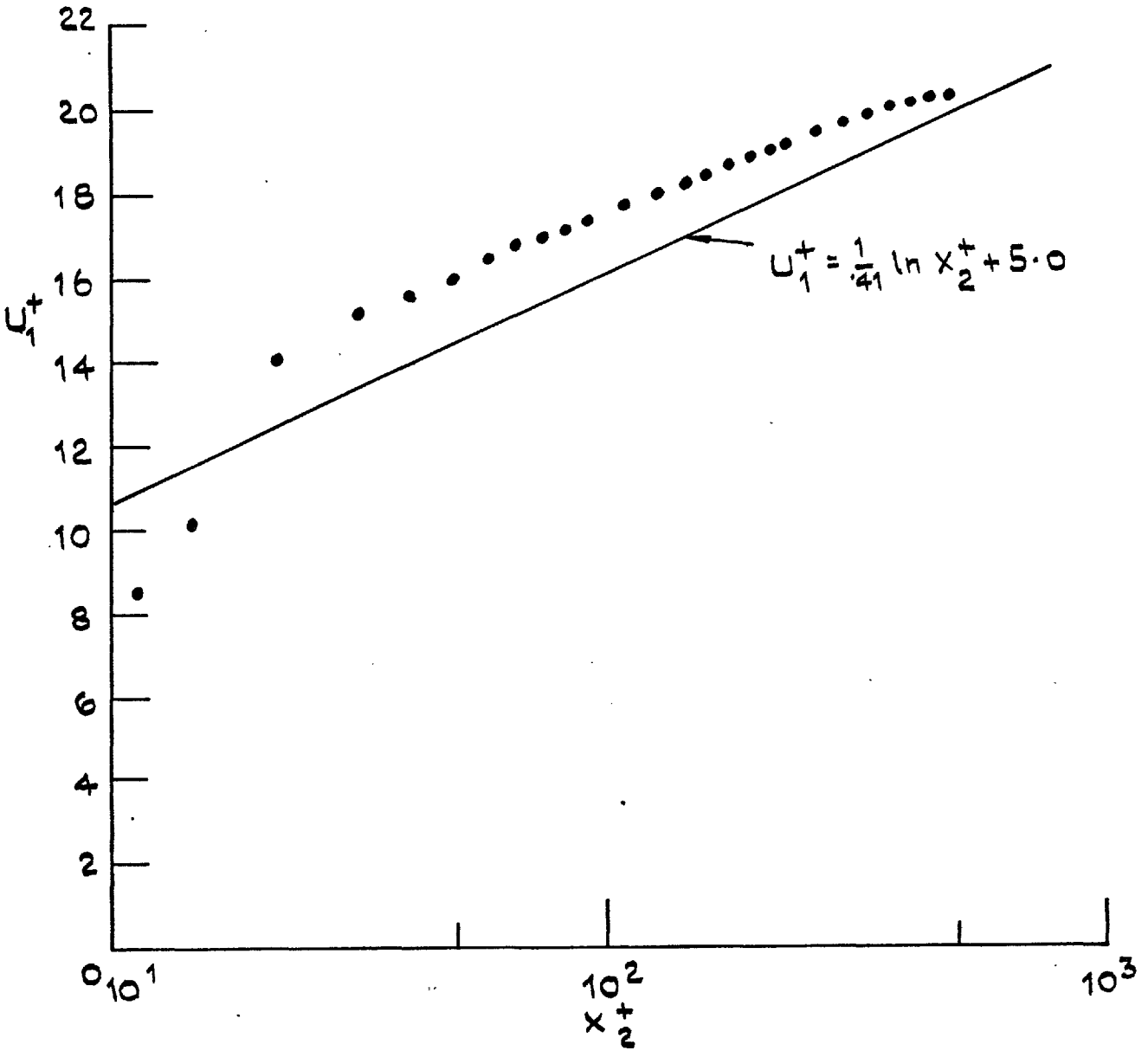

FIG. 3.15: 'CONSTANT K' BOUNDARY LAYER, $K = 1.5 \times 10^{-6}$ MEAN VELOCITY PROFILE IN UNIVERSAL CO-ORDINATES.

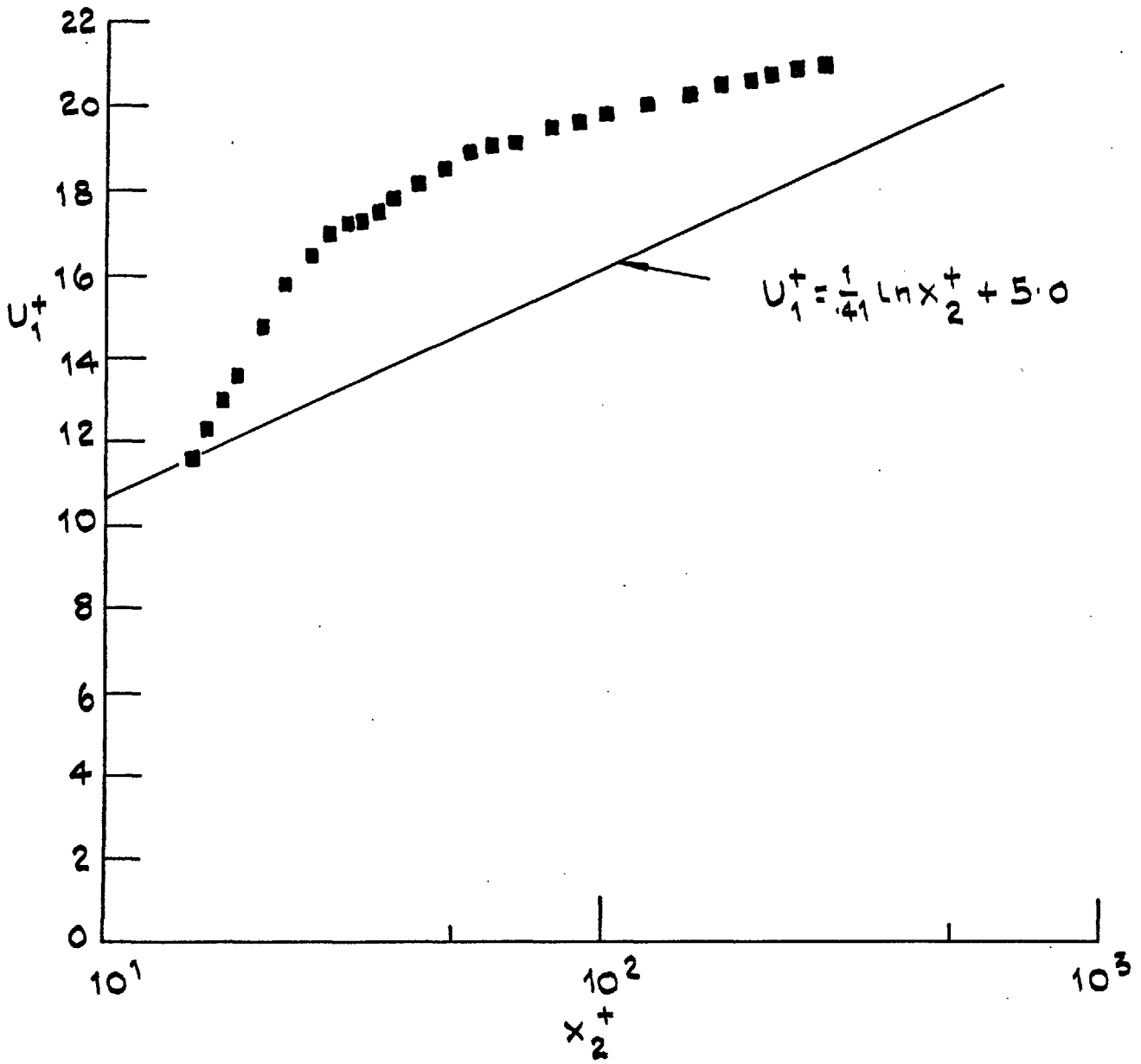

FIG. 3.16: 'CONSTANT K' BOUNDARY LAYER, $K = 2.5 \times 10^{-6}$ MEAN VELOCITY PROFILE IN UNIVERSAL CO-ORDINATES.

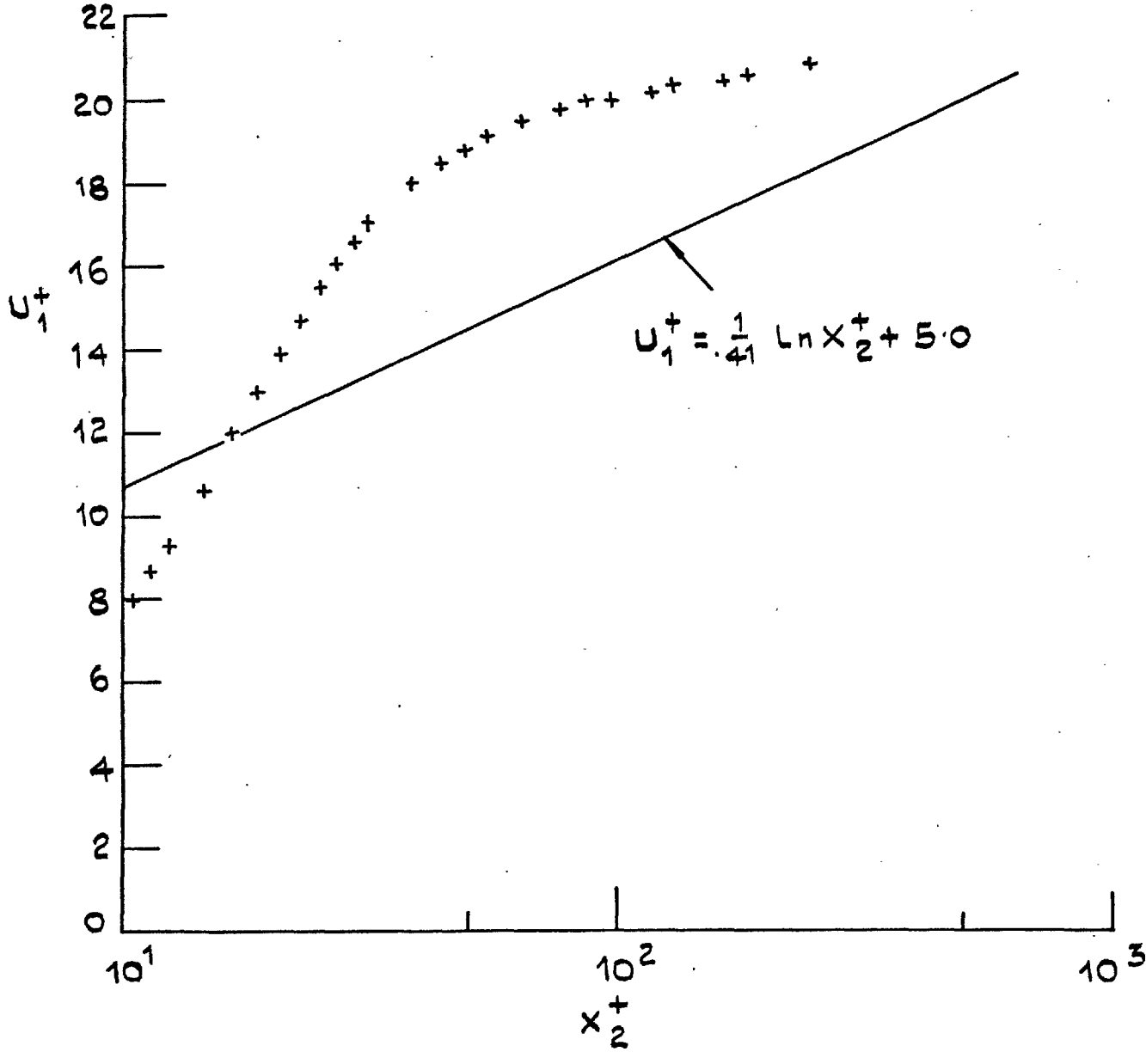

FIG. 3.17: 'CONSTANT K' BOUNDARY LAYER, $K = 3.0 \times 10^{-6}$ MEAN VELOCITY PROFILE IN UNIVERSAL CO-ORDINATES.

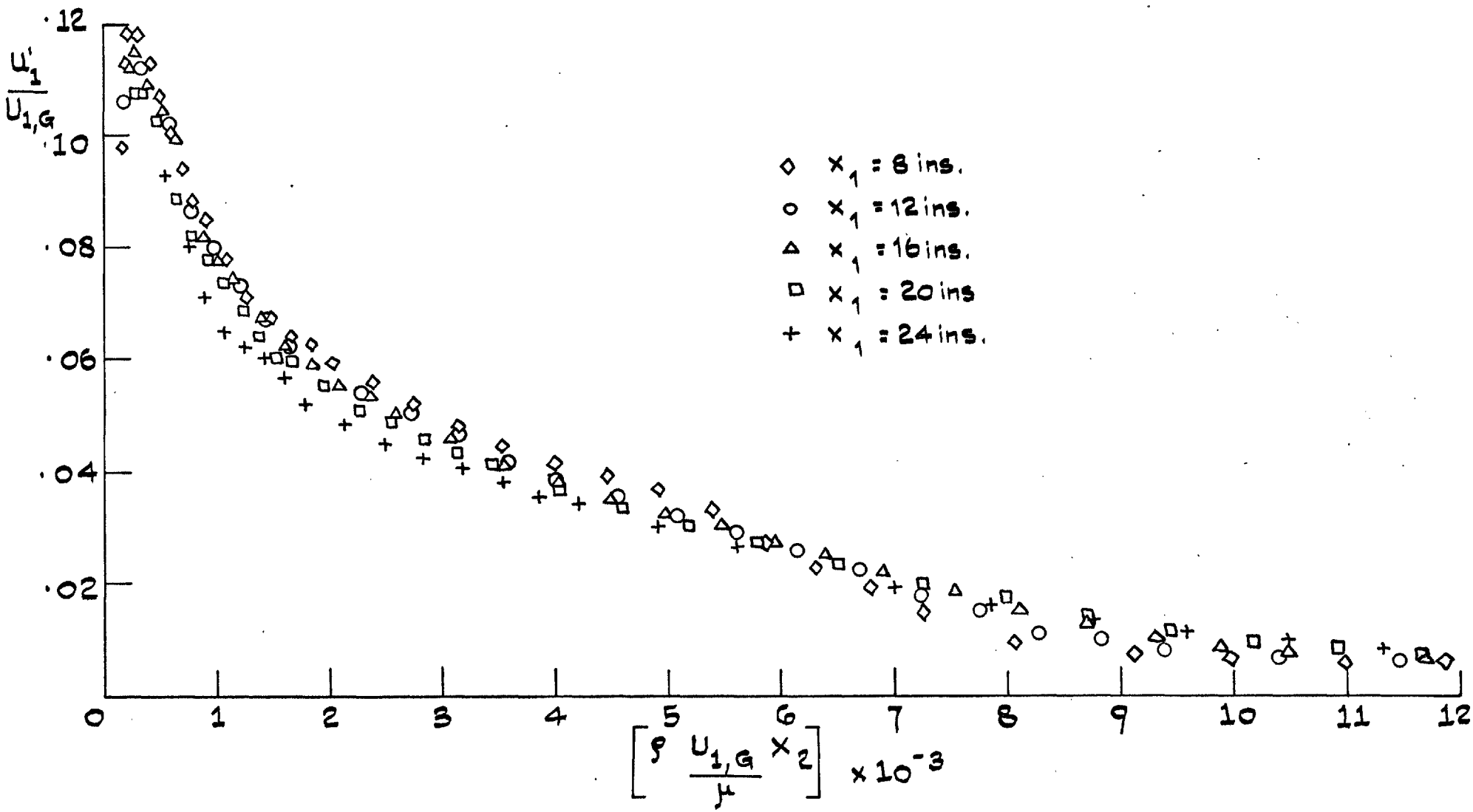

FIG. 3.18: 'CONSTANT K' BOUNDARY LAYER LONGITUDINAL TURBULENCE INTENSITY PROFILES, $K = 1.5 \times 10^{-6}$

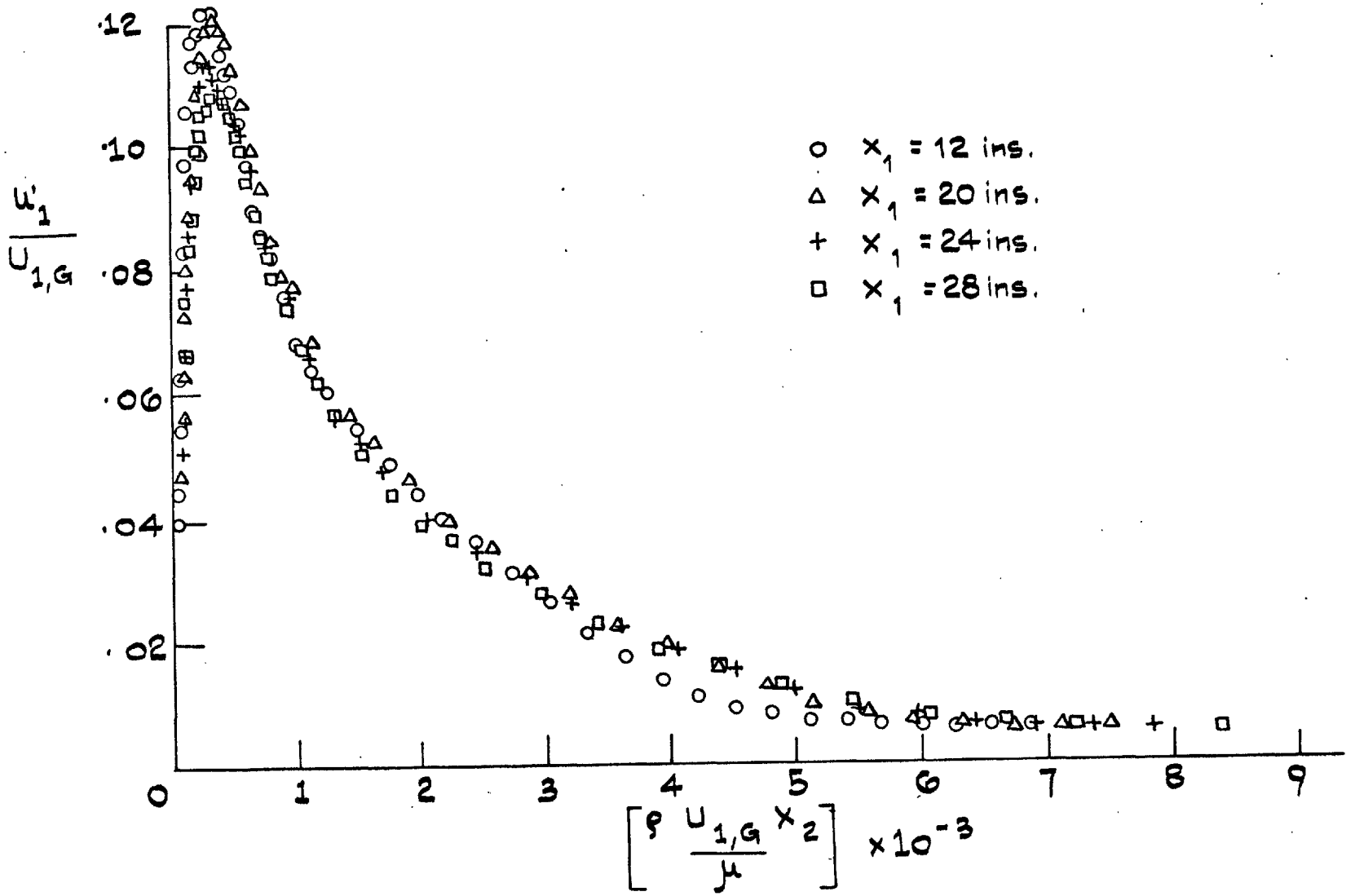

FIG. 3·19: 'CONSTANT K' BOUNDARY LAYER: LONGITUDINAL TURBULENCE INTENSITY PROFILES, $K = 2{\cdot}5 \times 10^{-5}$

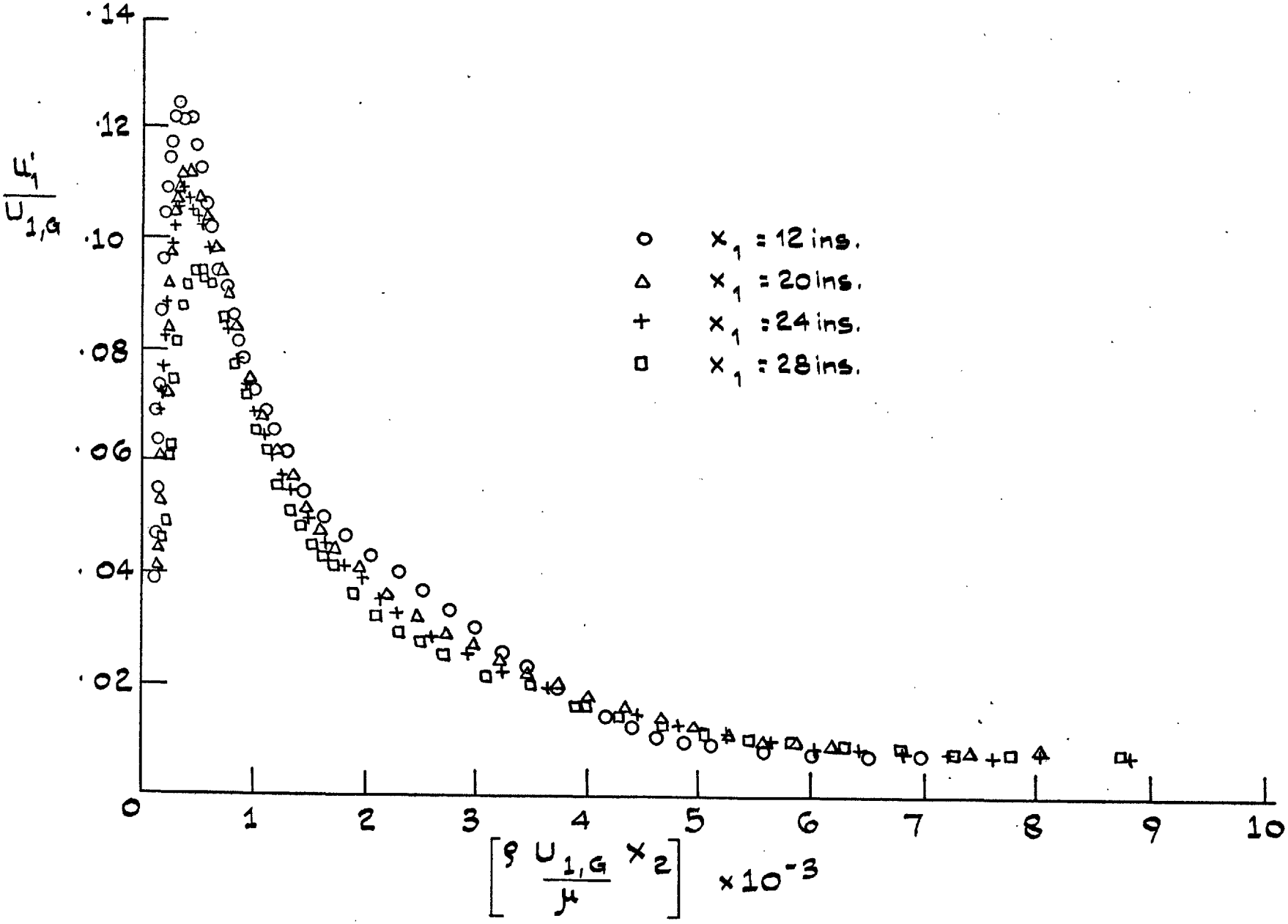

FIG. 3.20: 'CONSTANT K' BOUNDARY LAYER: LONGITUDINAL TURBULENCE INTENSITY PROFILES, $K = 3.0 \times 10^{-6}$

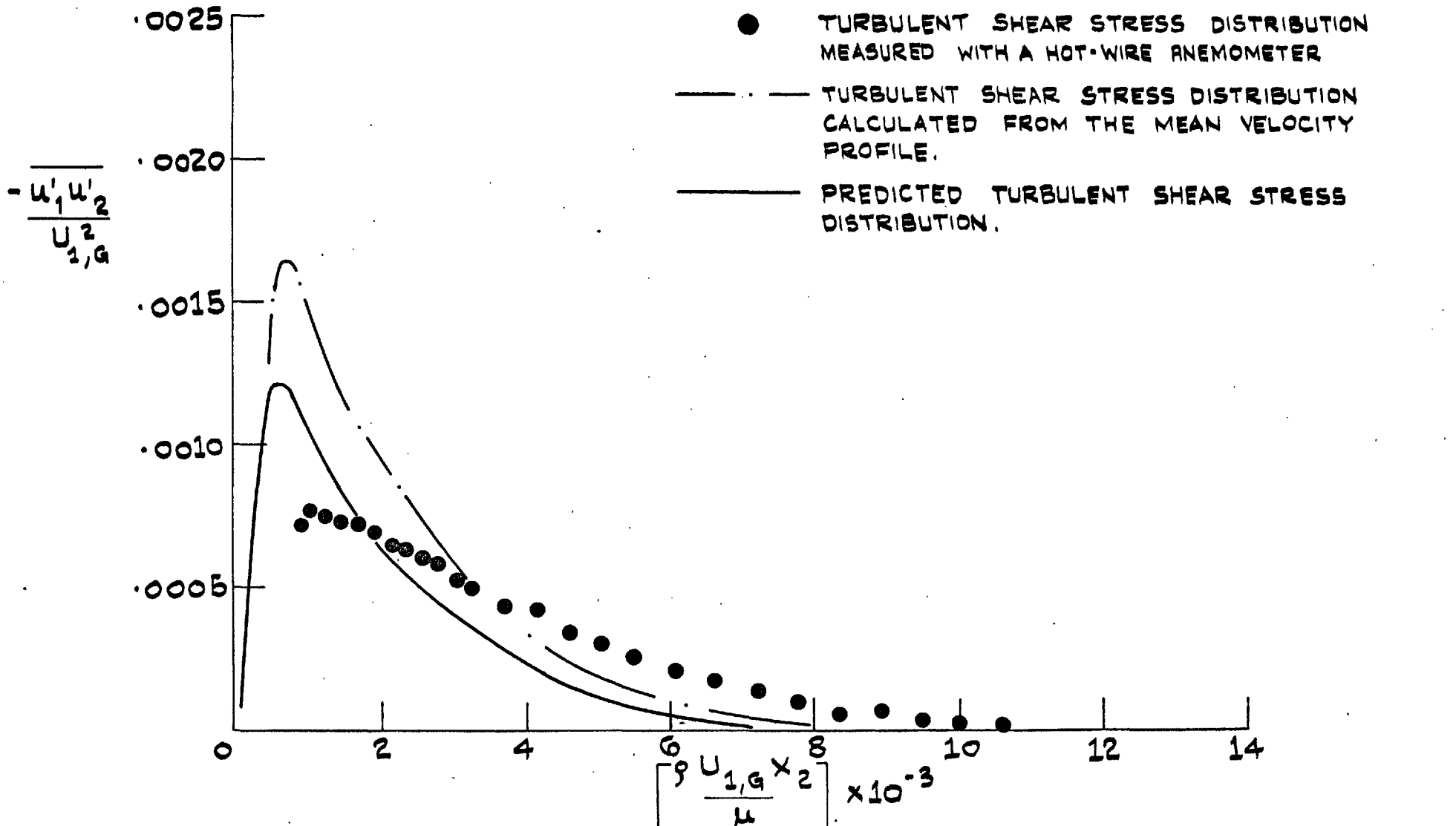

FIG. 3.21: 'CONSTANT K' BOUNDARY LAYER: $K = 1{\cdot}5 \times 10^{-6}$ TURBULENT SHEAR STRESS PROFILE. $x_1 = 513{\cdot}0$ ins

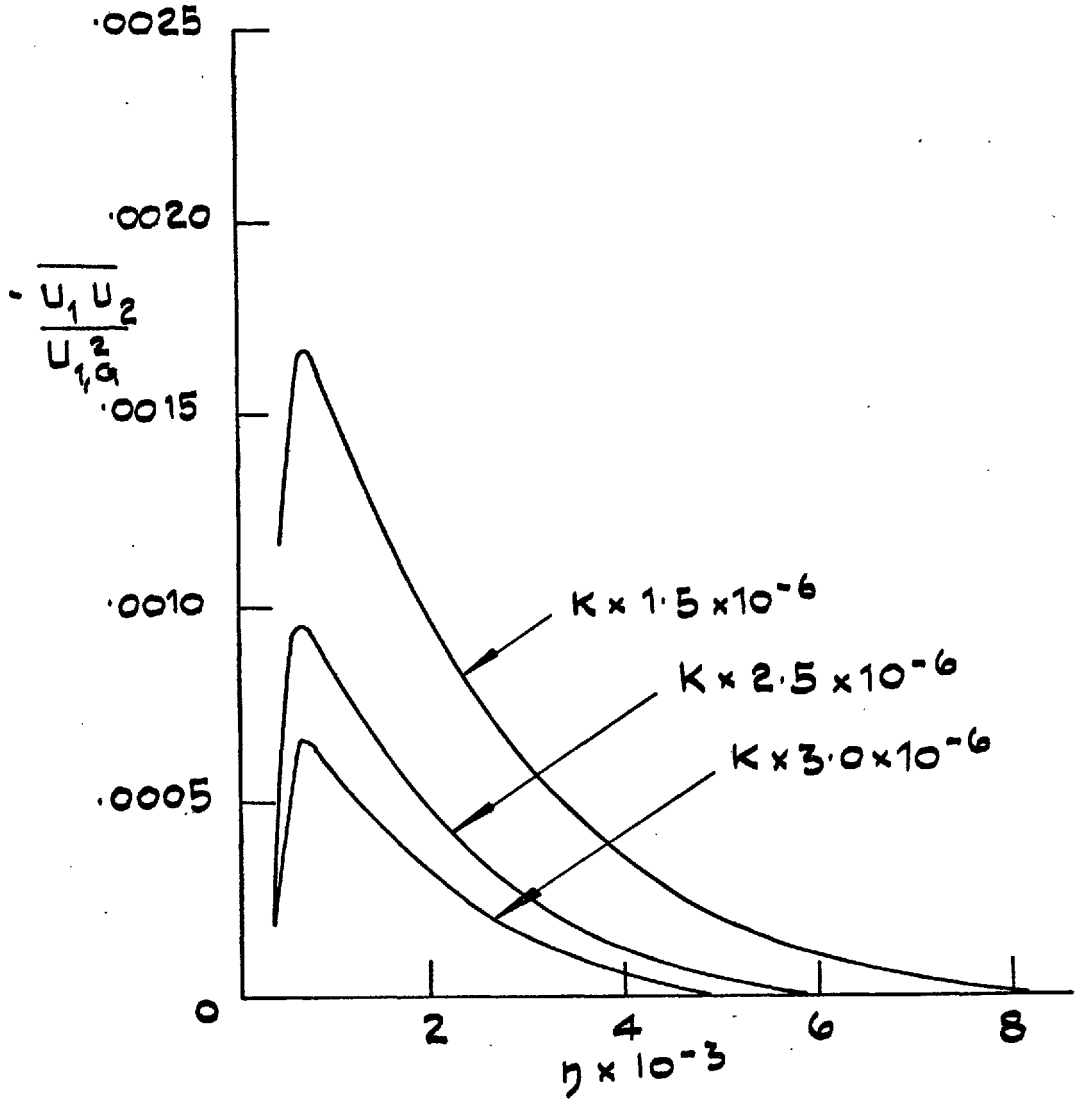

FIG. 3.22: 'CONSTANT K' BOUNDARY LAYERS: TURBULENT SHEAR STRESS PROFILES (CALCULATED FROM MEASURED MEAN VELOCITY PROFILES).

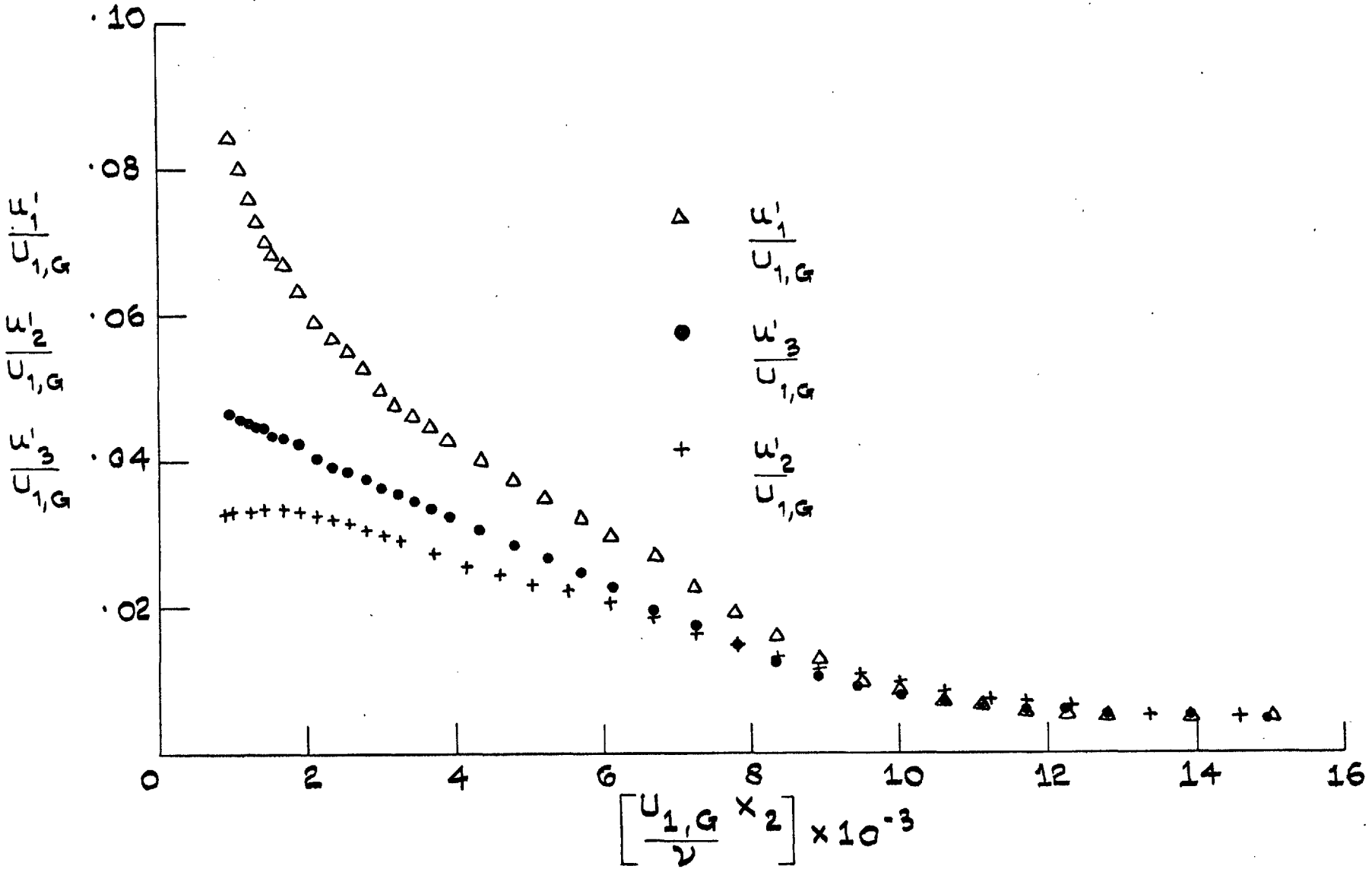

FIG. 3.23: 'CONSTANT K' BOUNDARY LAYER, $K = 1.5 \times 10^{-6}$
TURBULENCE INTENSITY PROFILES $x_1 = 12$ ins.

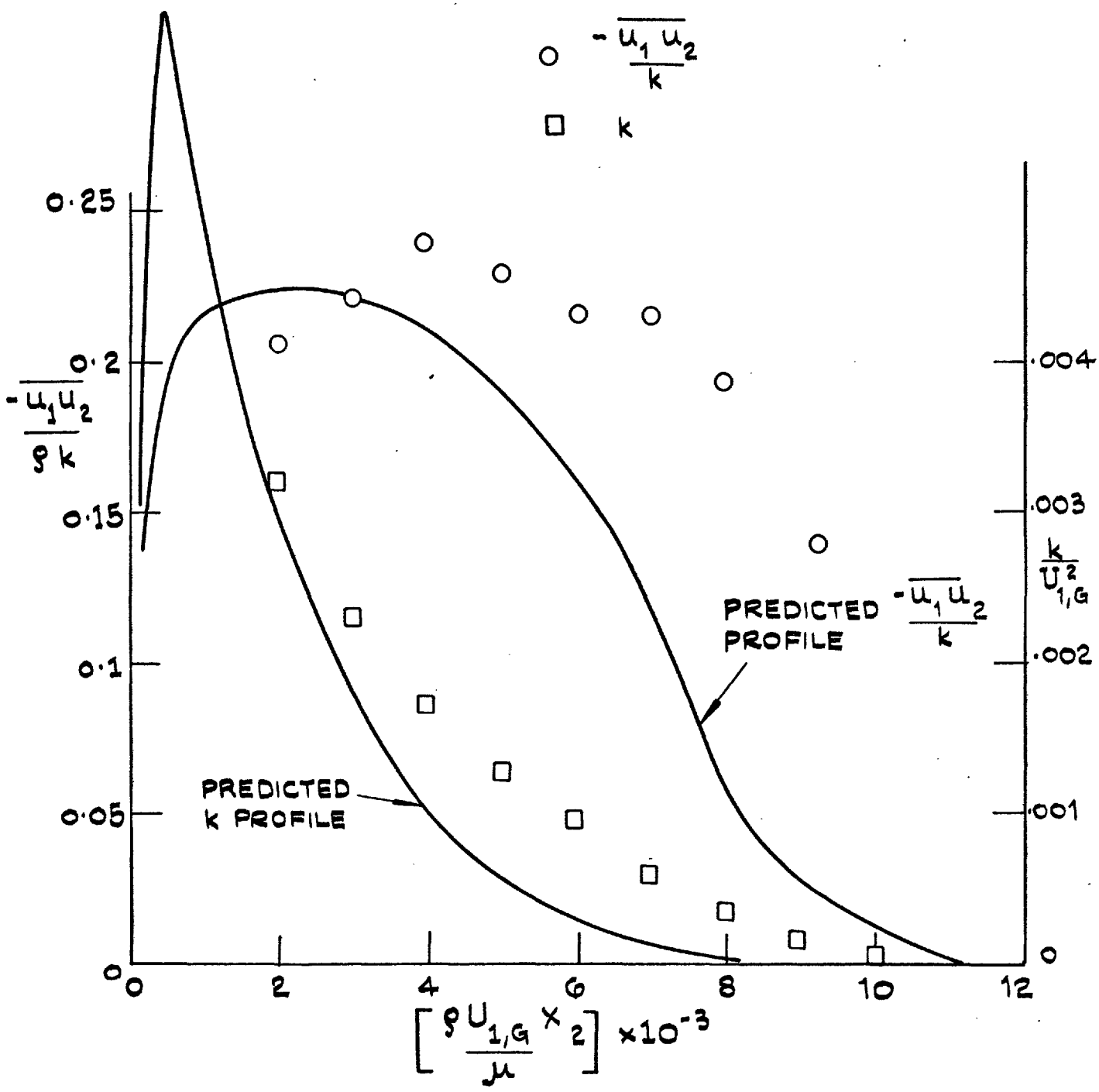

FIG. 3.24: 'CONSTANT K' BOUNDARY LAYER, $K = 1{\cdot}5 \times 10^{-6}$ PROFILES OF TURBULENCE ENERGY AND STRUCTURE PARAMETER $-u_1 - u_2 / k$. $x_1 = 12$ ins.

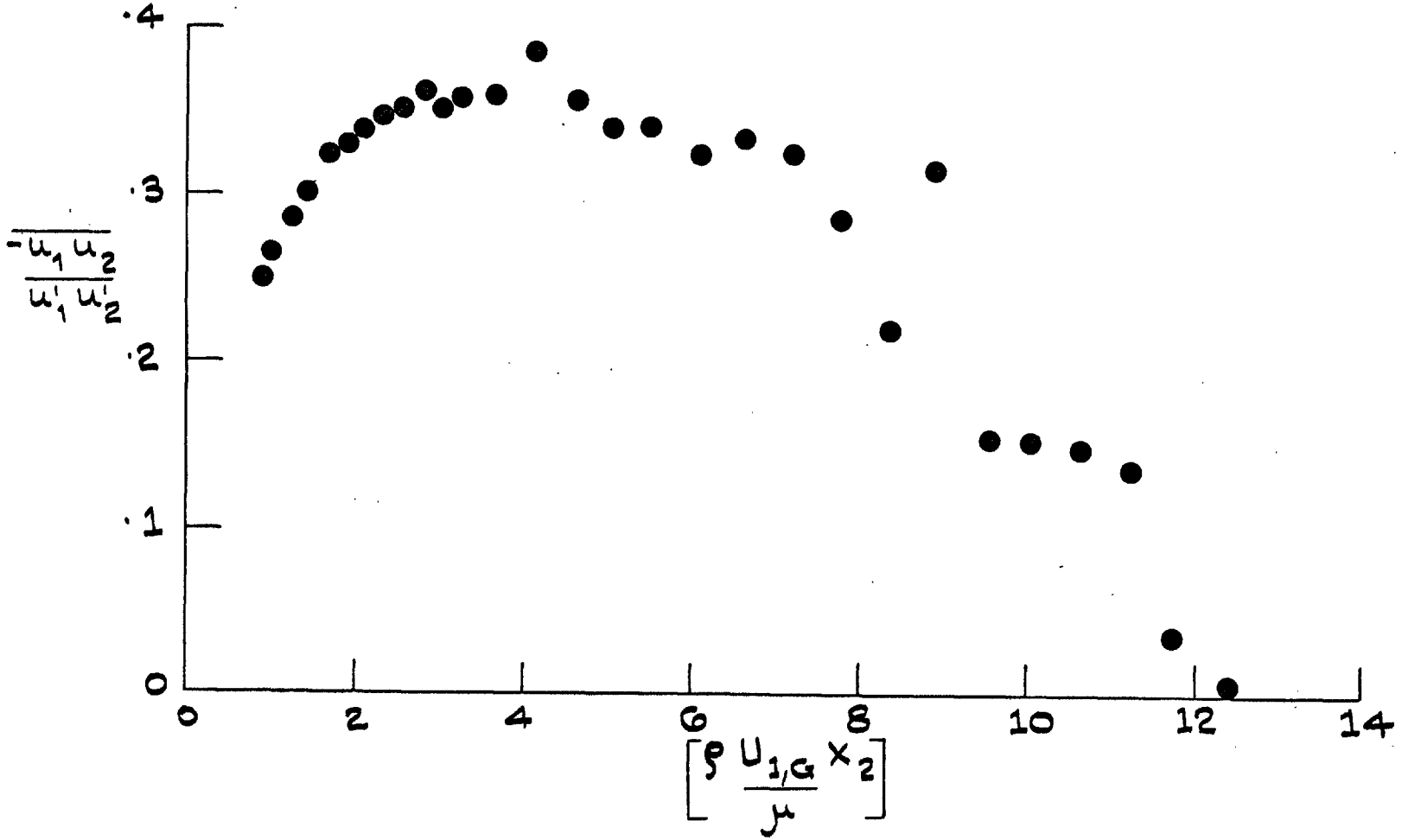

FIG. 3.25: 'CONSTANT K' BOUNDARY LAYER, $K = 1.5 \times 10^{-6}$

VARIATION OF COEFFICIENT OF CORRELATION ACROSS THE LAYER, $x_1 = 12$ ins.

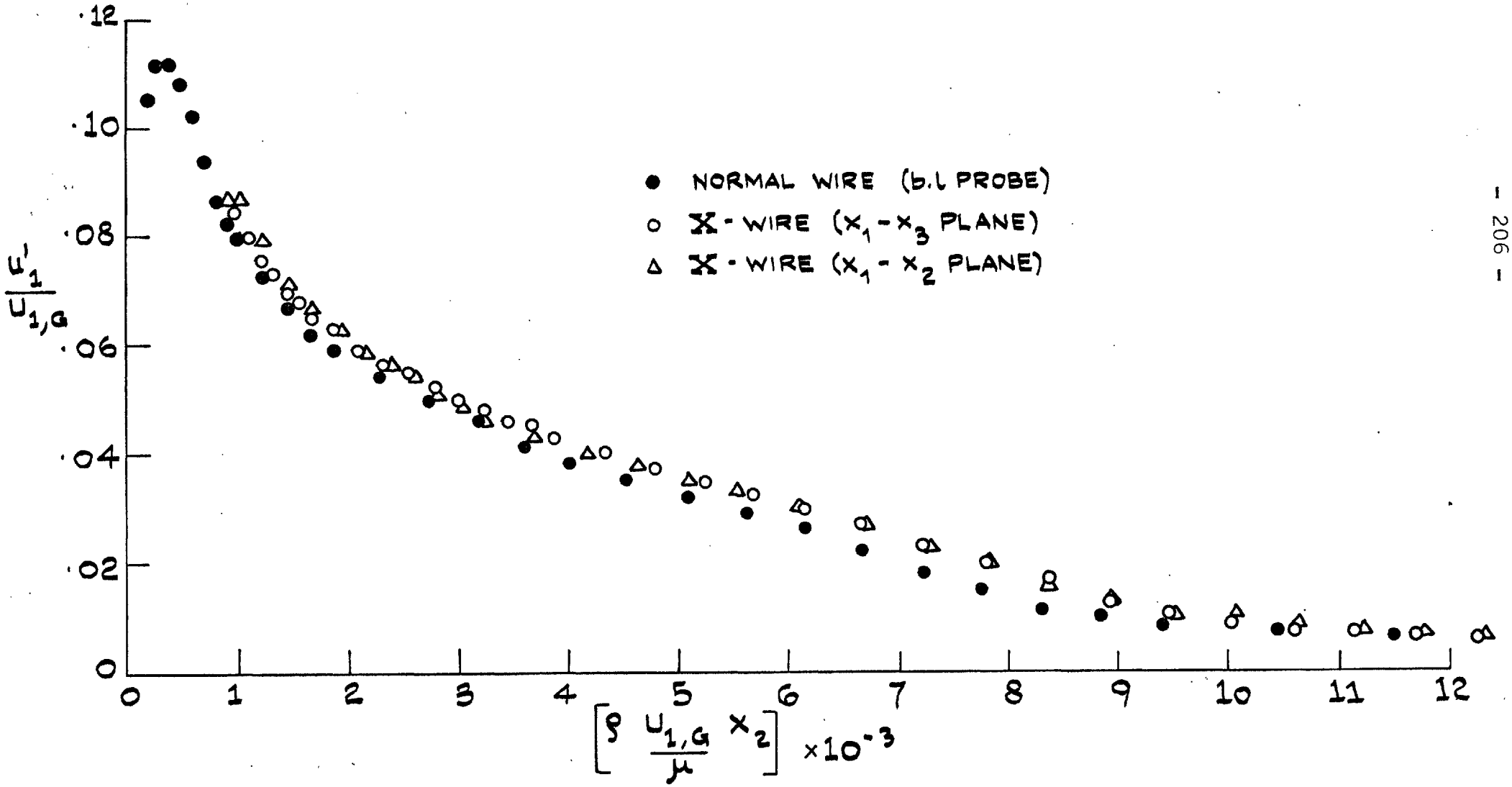

FIG. 3·26: 'CONSTANT K' BOUNDARY LAYER, $K = 1{\cdot}5 \times 10^{-6}$ LONGITUDINAL TURBULENCE INTENSITY, X_1 = 12 ins

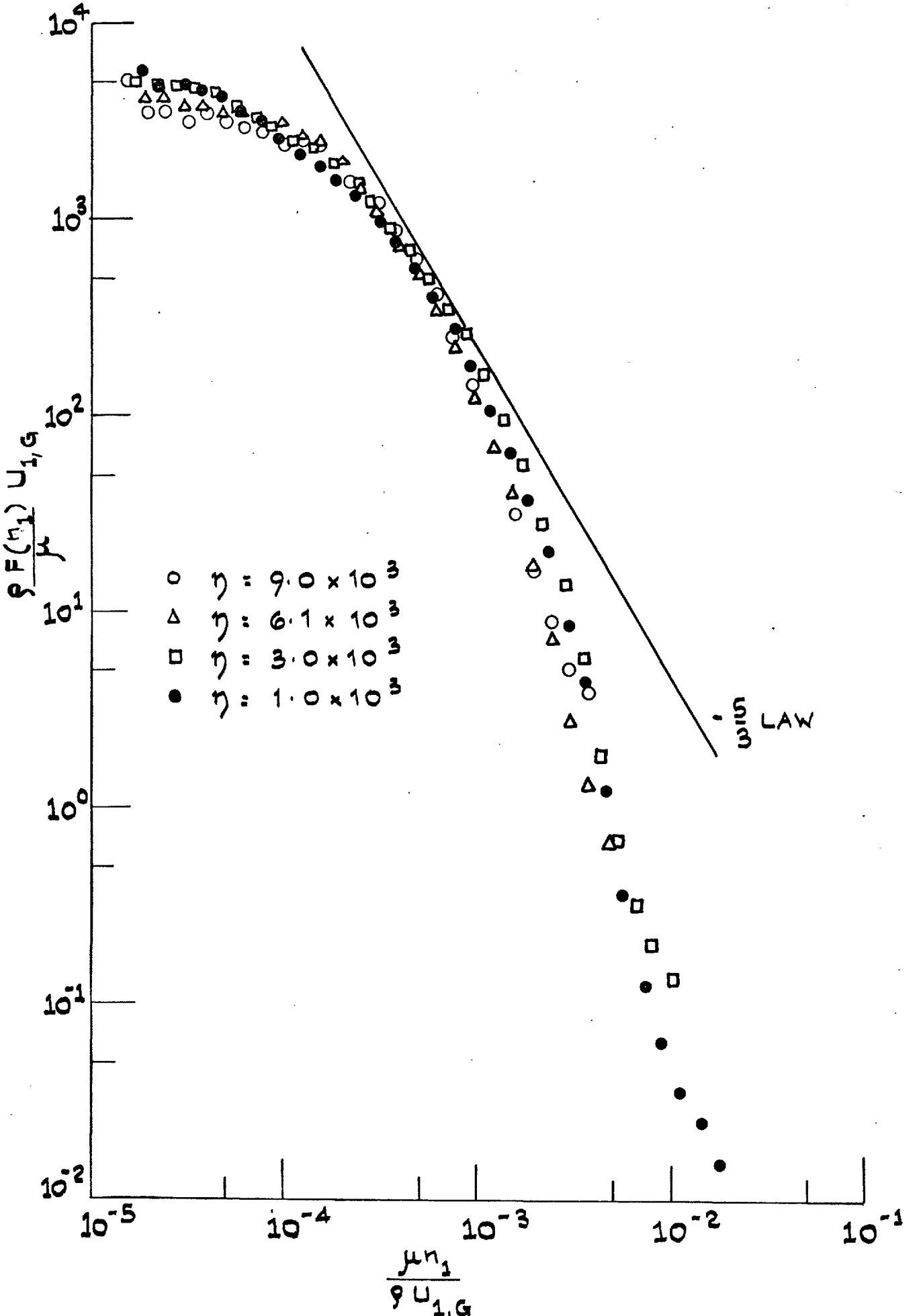

FIG. 3.27: 'CONSTANT K' BOUNDARY LAYER, $K = 1.5 \times 10^{-6}$
SPECTRA OF LONGITUDINAL TURBULENCE

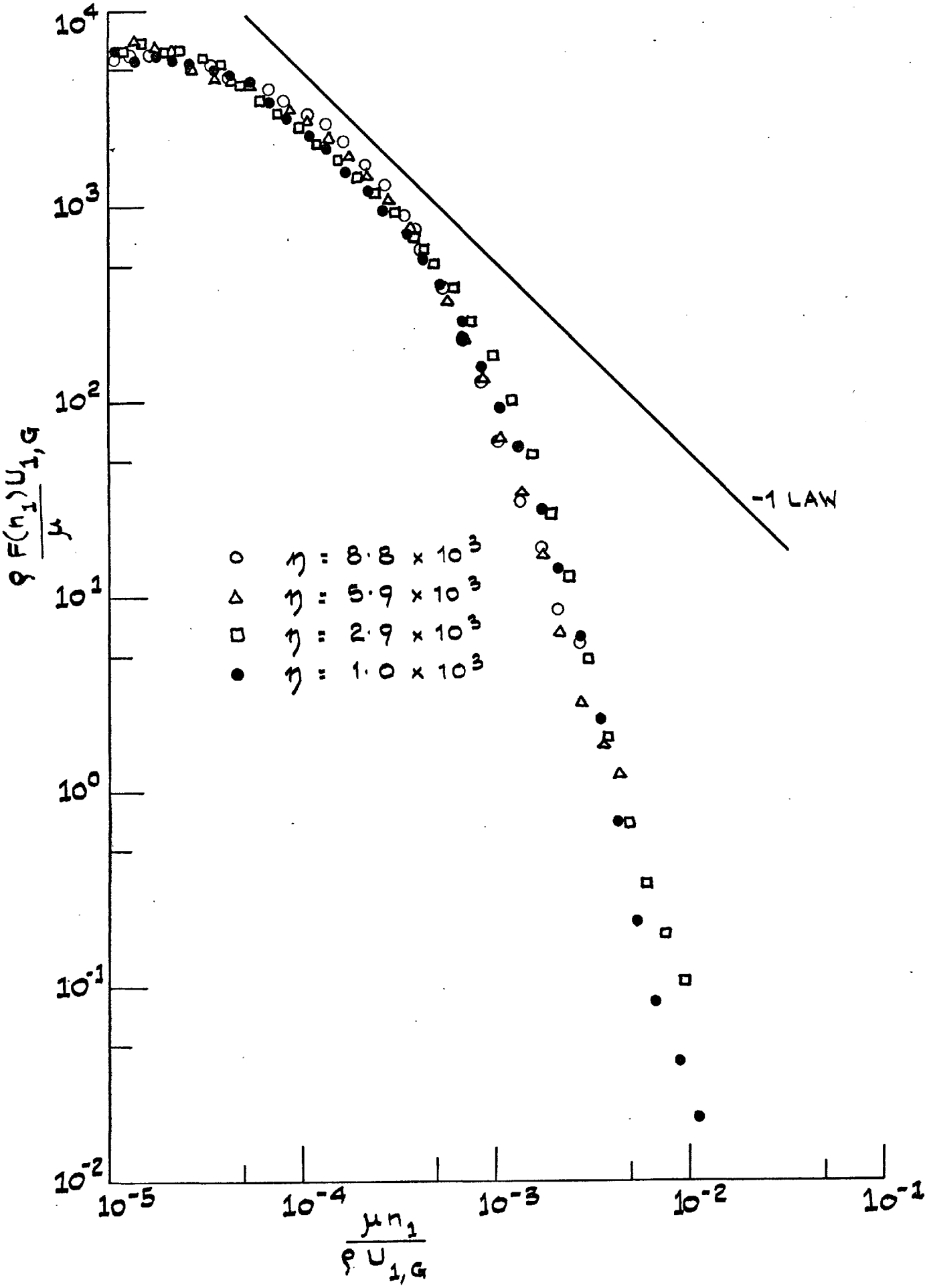

FIG. 3·28: SPECTRA OF LONGITUDINAL TURBULENCE INTENSITY: $K = 1.5 \times 10^{-6}$, $X_1 = 20$ ins.

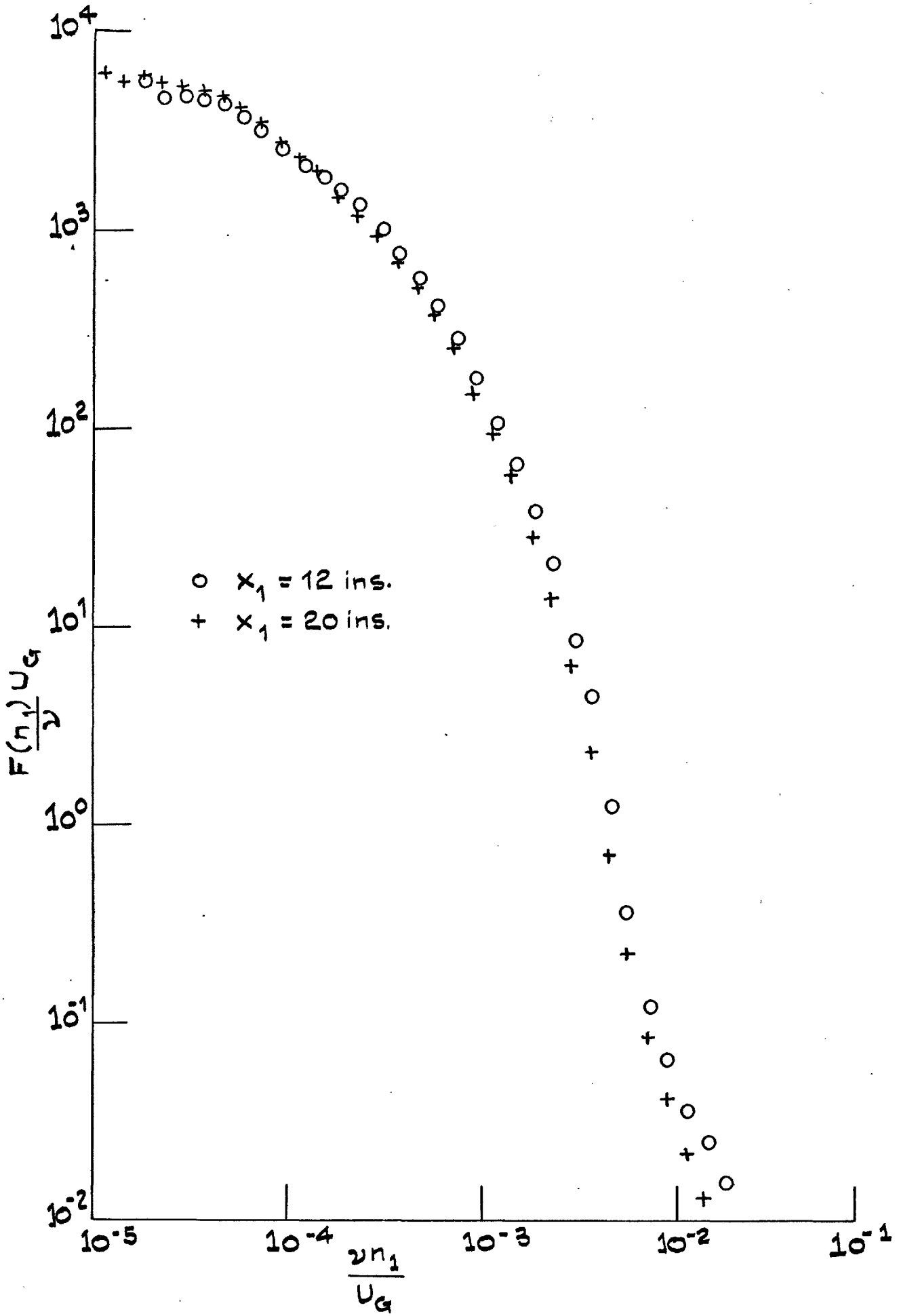

FIG. 3.29: SPECTRA OF LONGITUDINAL TURBULENCE INTENSITY: $K = 1.5 \times 10^{-6}$, $\eta = 1.0 \times 10^3$

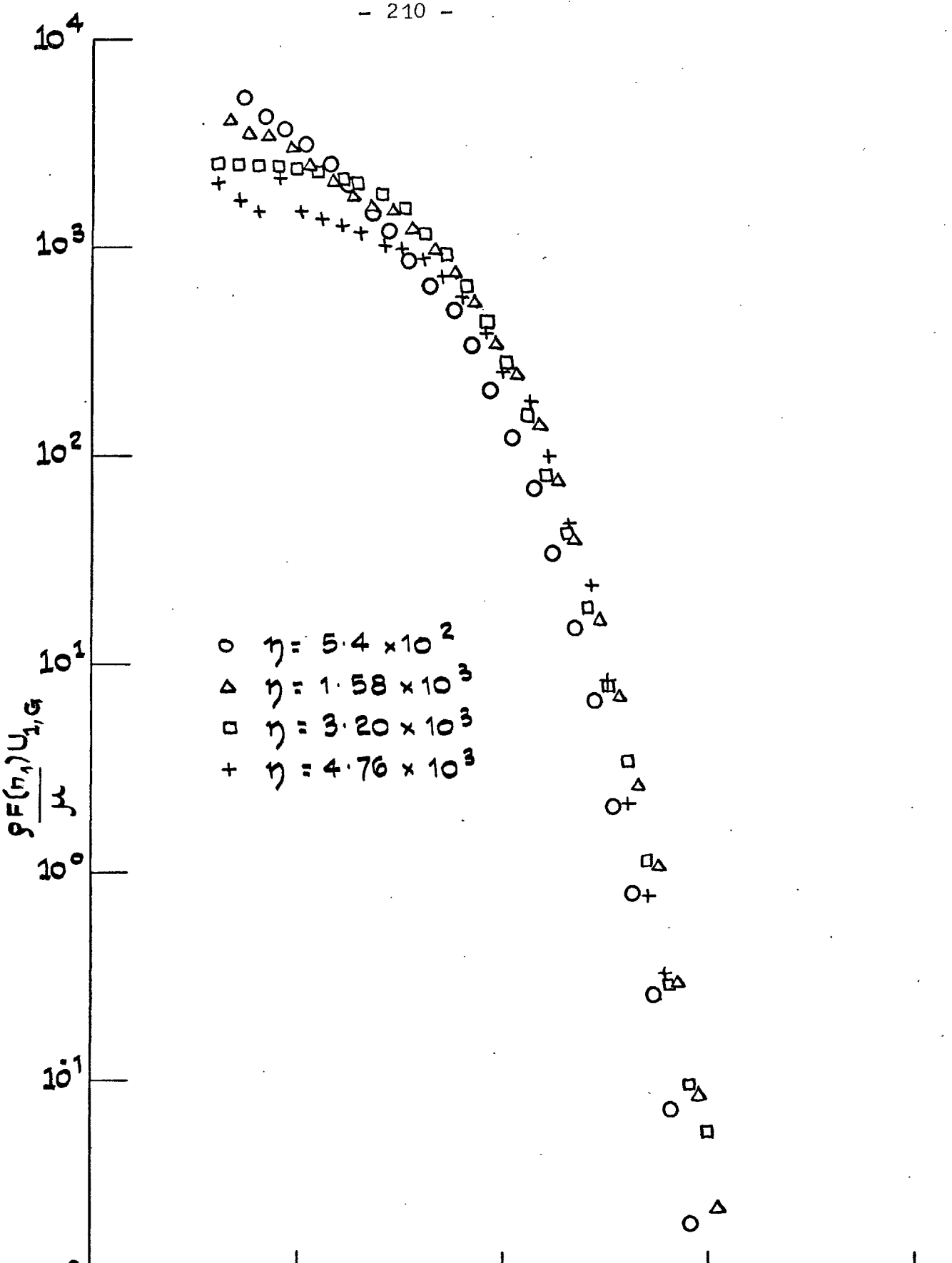

FIG. 3·30: SPECTRA OF LONGITUDINAL TURBULENCE INTENSITY: $K = 2.5 \times 10^{-6}$, $X_1 = 16$ ins

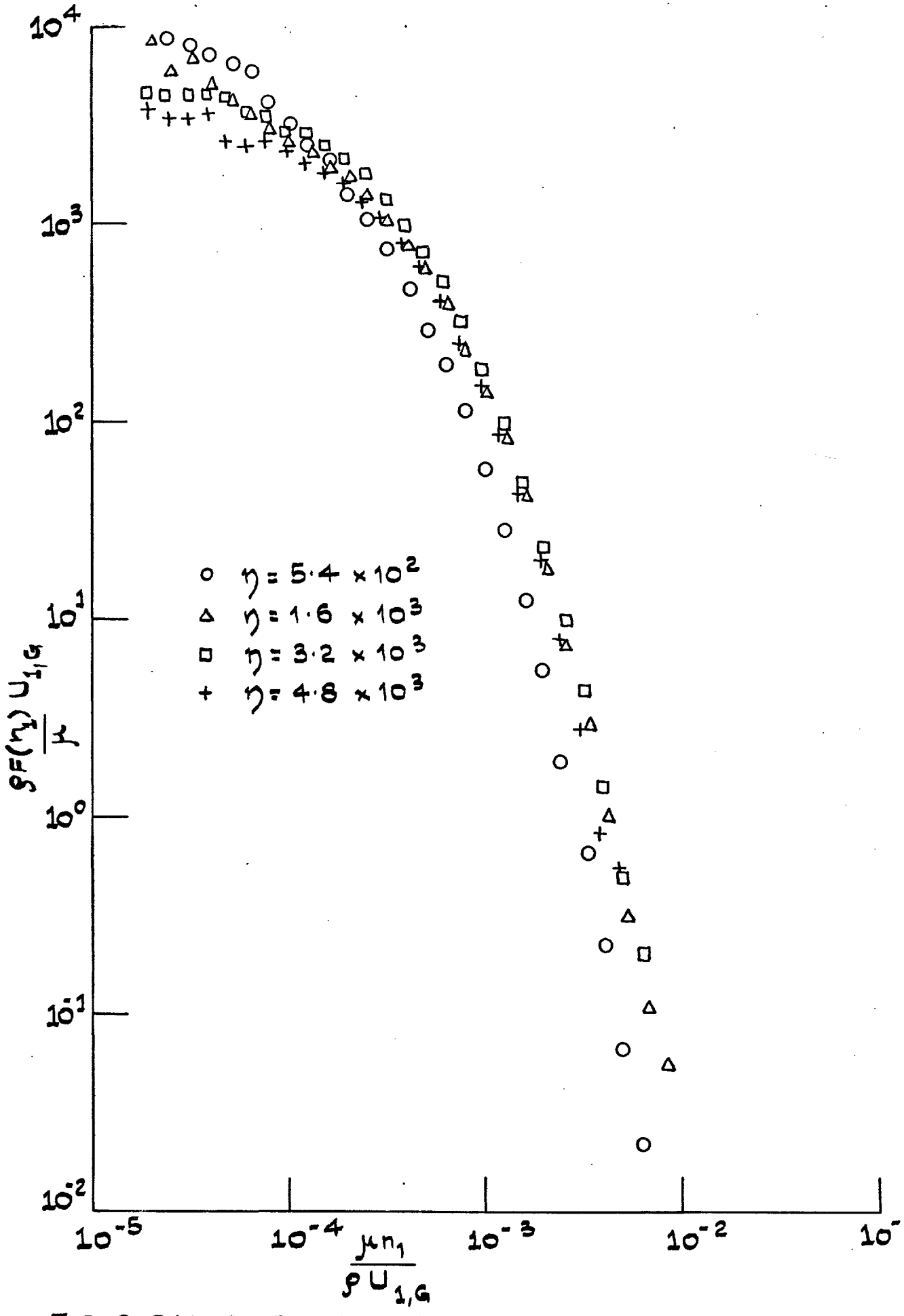

FIG. 3.31: SPECTRA OF LONGITUDINAL TURBULENCE INTENSITY $K = 2.5 \times 10^{-6}$, $X_1 = 24$ ins.

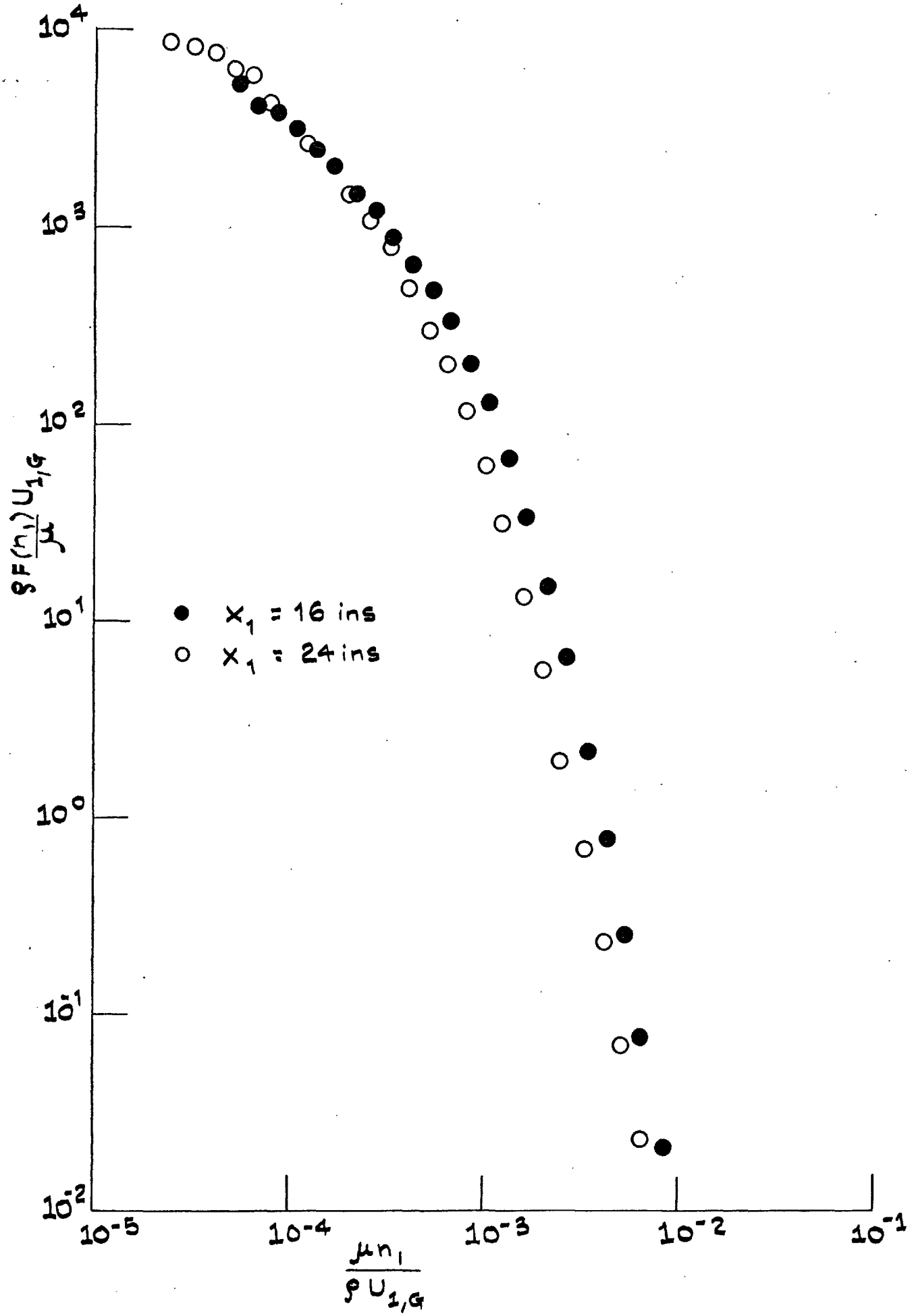

FIG. 3.32: SPECTRA OF LONGITUDINAL TURBULENCE INTENSITY : $K = 2.5 \times 10^{-6}$, $\eta = 5.4 \times 10^2$

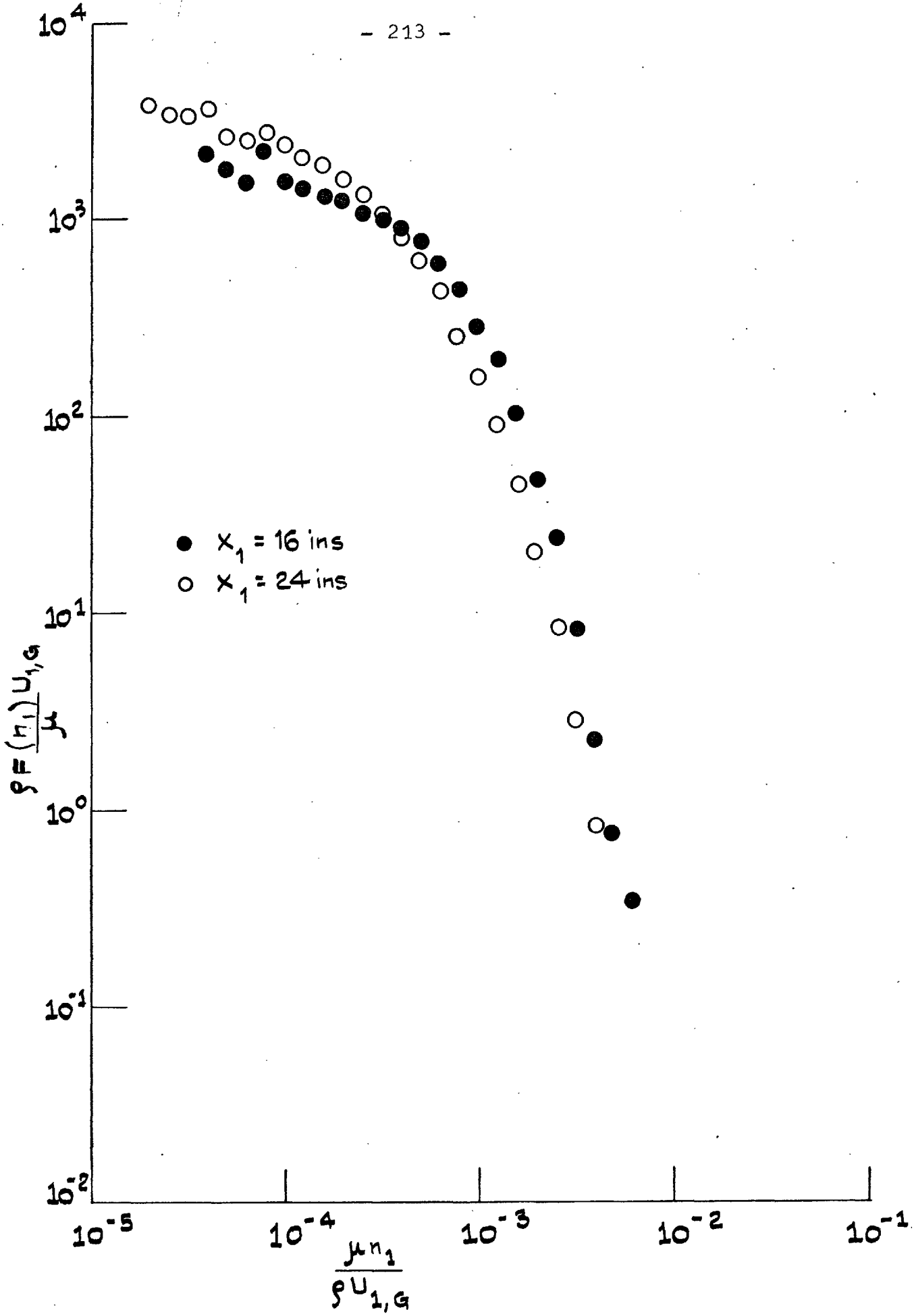

FIG. 3·33: SPECTRA OF LONGITUDINAL TURBULENCE INTENSITY: $K = 2.5 \times 10^{-6}$, $\eta = 4.8 \times 10^3$

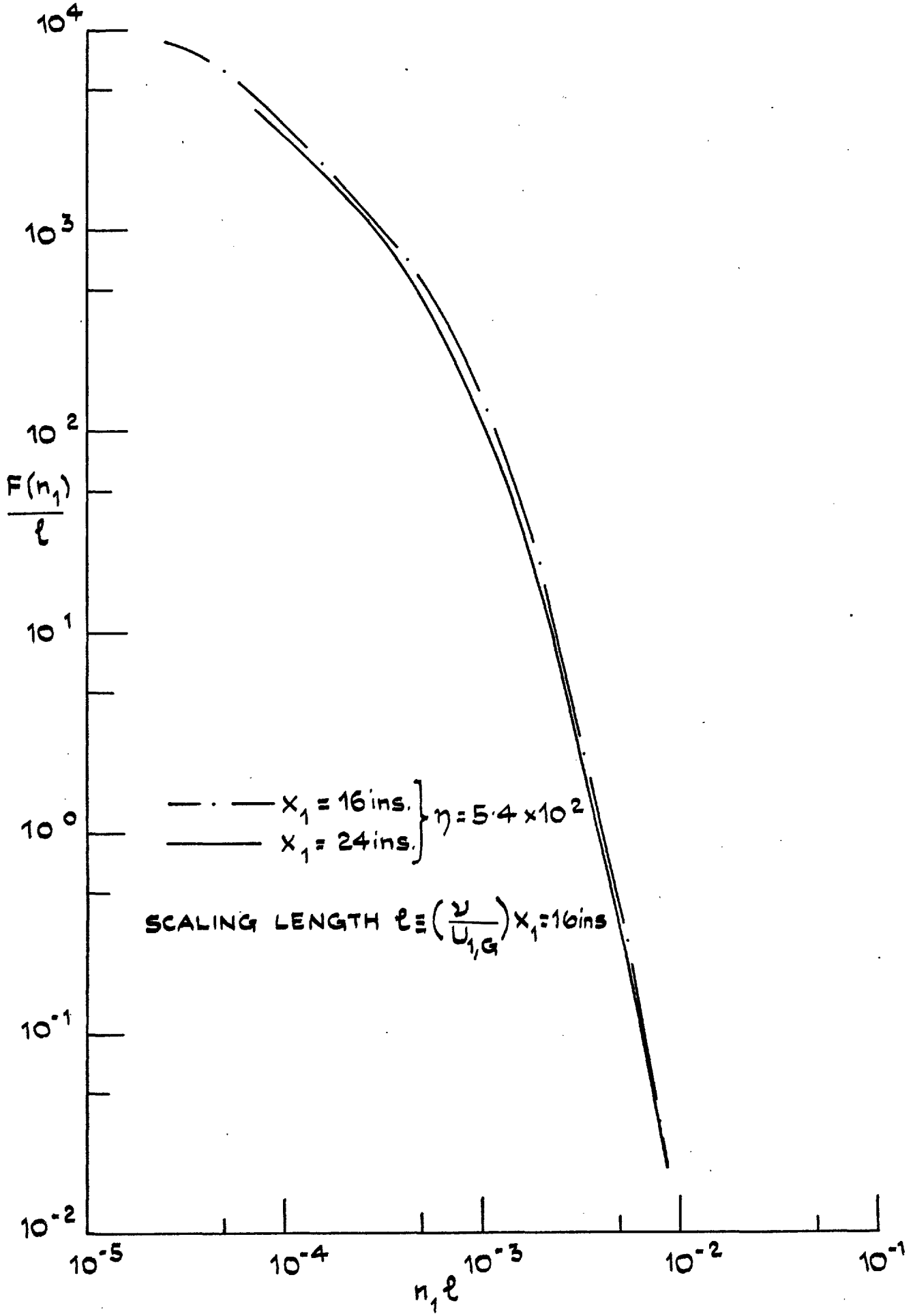

FIG. 3·34 : SPECTRA OF LONGITUDINAL TURBULENCE INTENSITY AT TWO X_1 - STATIONS NORMALISED WITH THE SAME LENGTH SCALE $K = 2{\cdot}5 \times 10^{-6}$

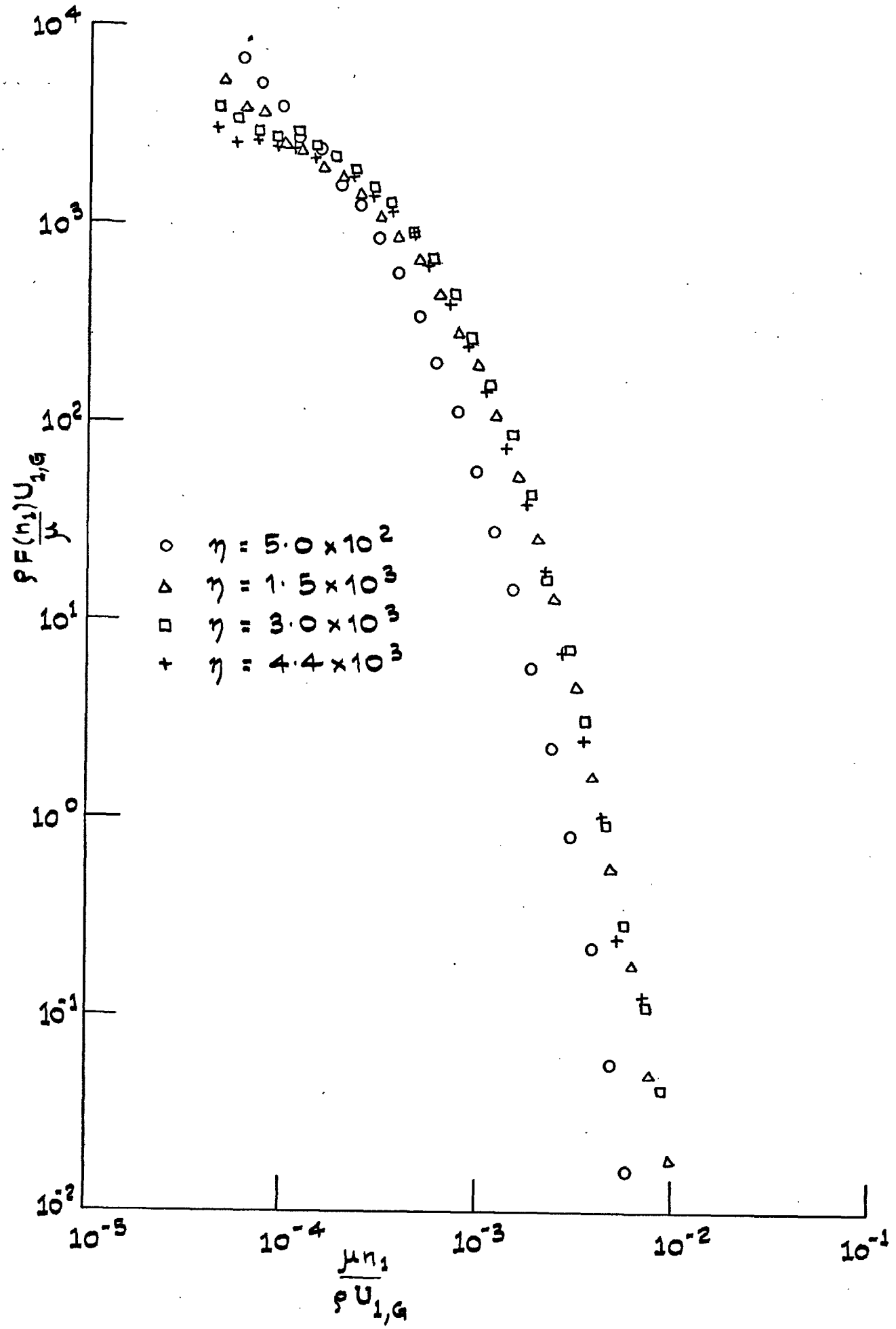

FIG. 3.35: SPECTRA OF LONGITUDINAL TURBULENCE INTENSITY: $K = 3.0 \times 10^{-6}$, $X_1 = 16$ ins.

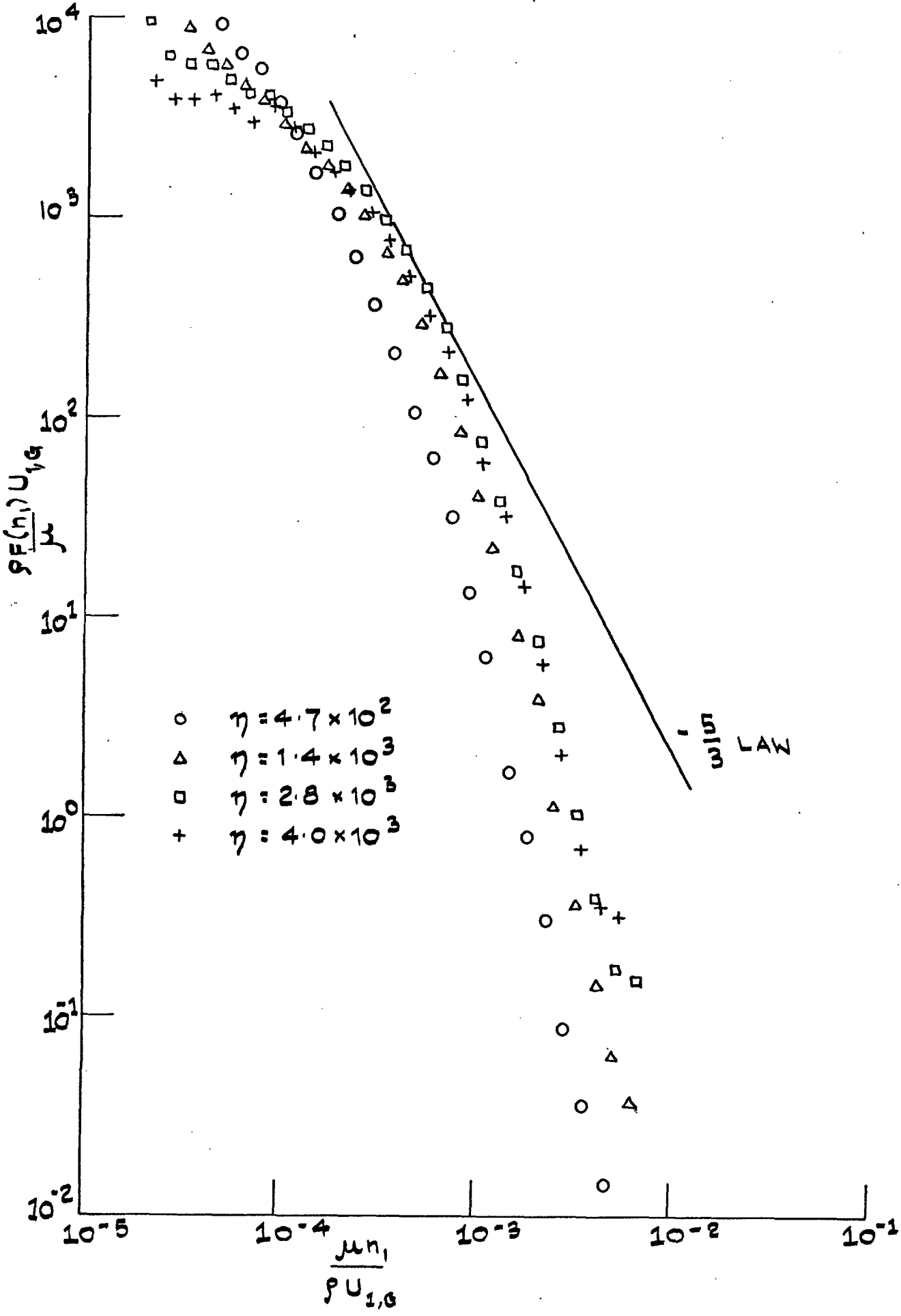

FIG. 3.36: SPECTRA OF LONGITUDINAL TURBULENCE INTENSITY: $K = 3.0 \times 10^{-6}$, $x_1 = 24$ ins

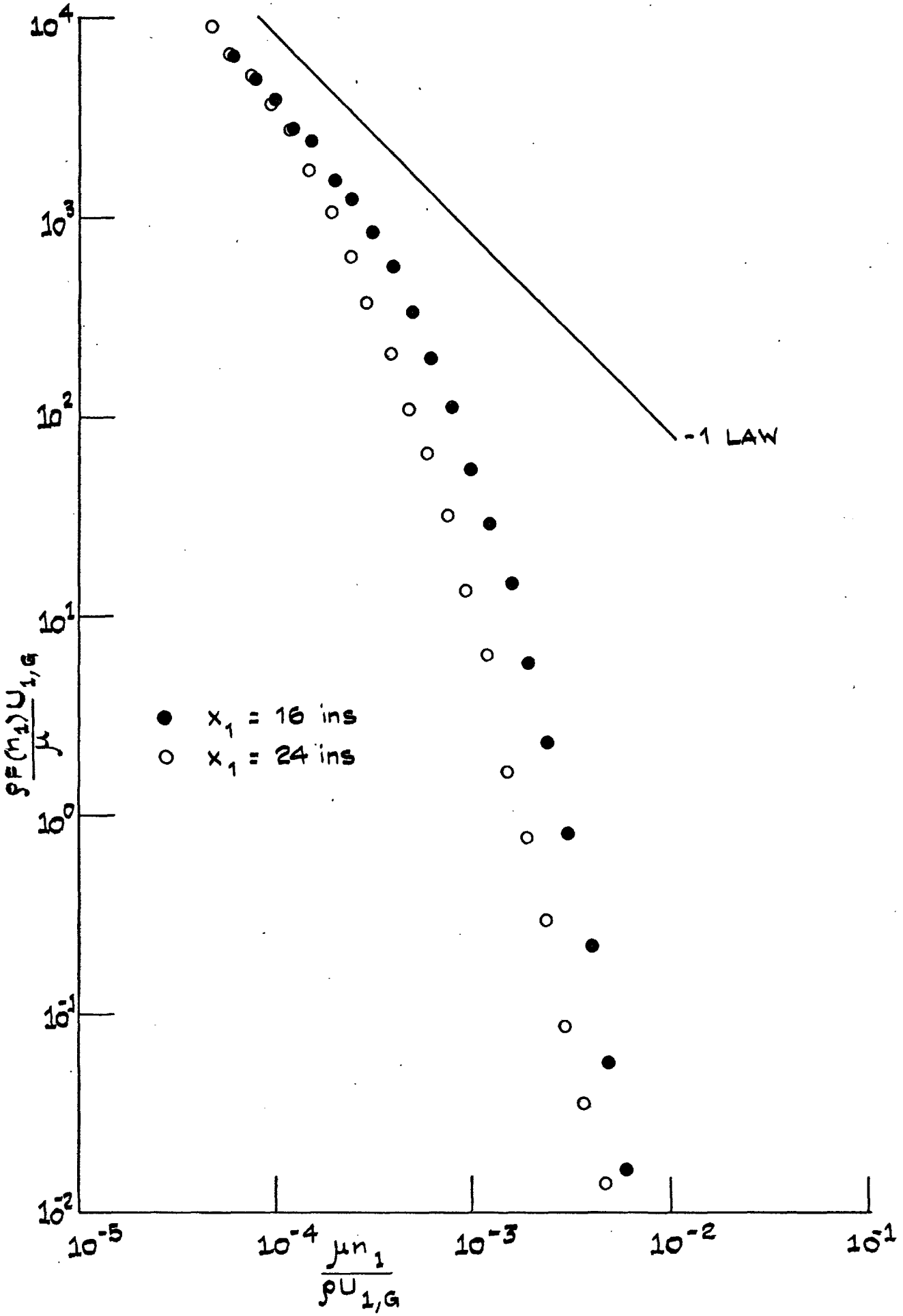

FIG. 3.37: SPECTRA OF LONGITUDINAL TURBULENCE INSENSITY : $K = 3.0 \times 10^{-6}$, $\eta = 5.0 \times 10^2$

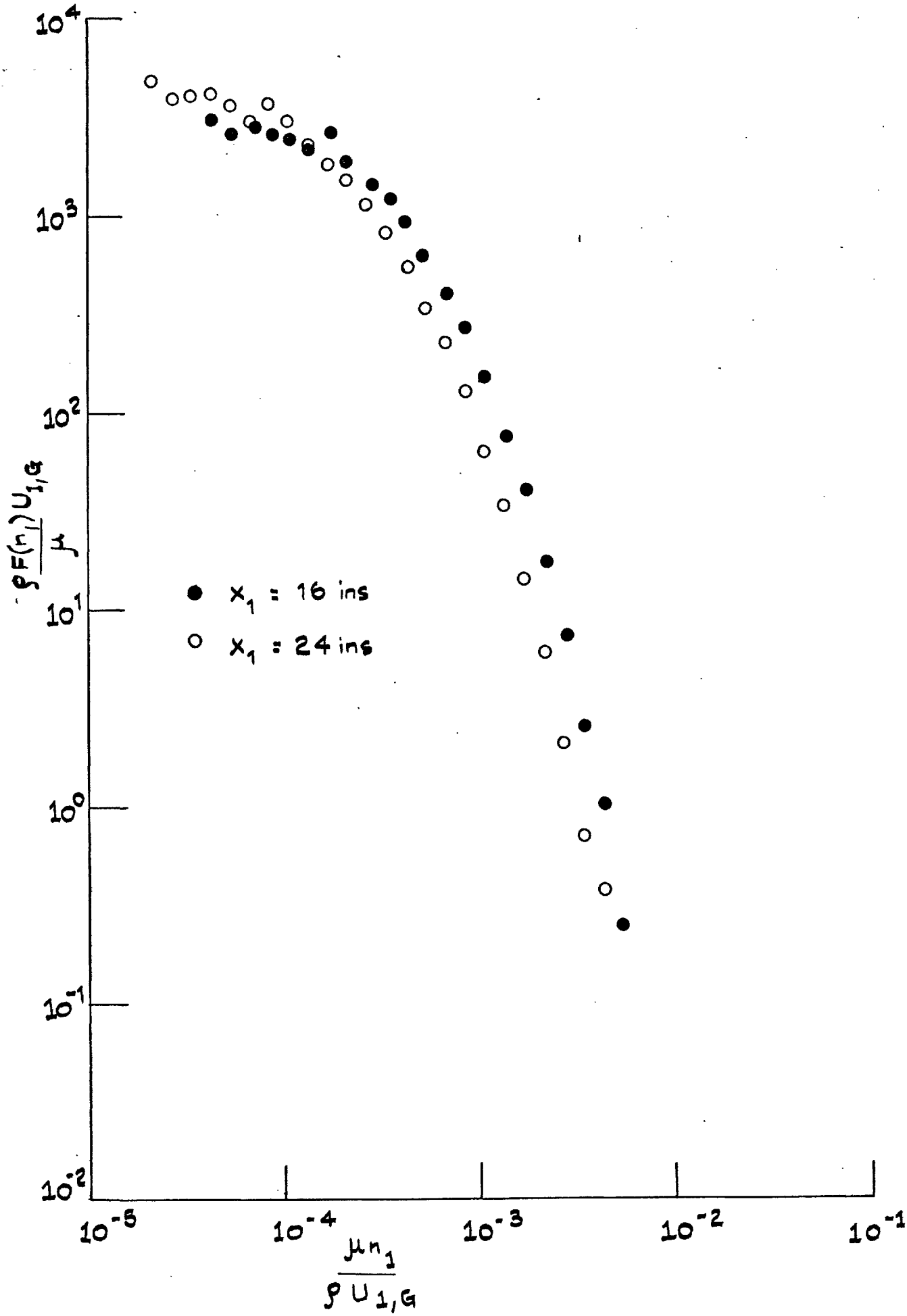

FIG. 3.38: SPECTRA OF LONGITUDINAL TURBULENCE INTENSITY : $K = 3.0 \times 10^{-6}$ $\eta = 4.4 \times 10^{-6}$

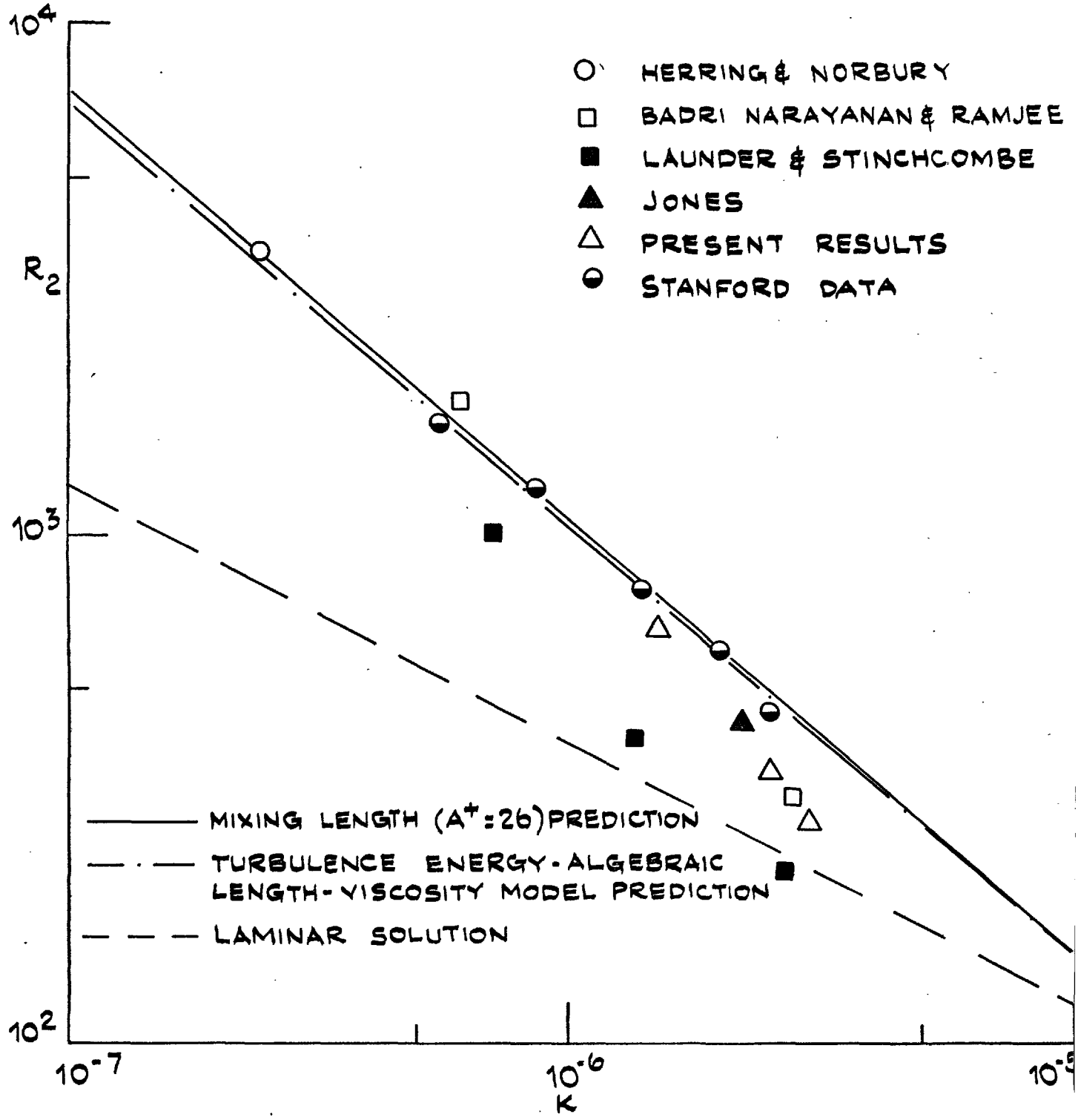

FIG. 3·39: 'CONSTANT K' BOUNDARY LAYER: VARIATION OF R_2 WITH K.

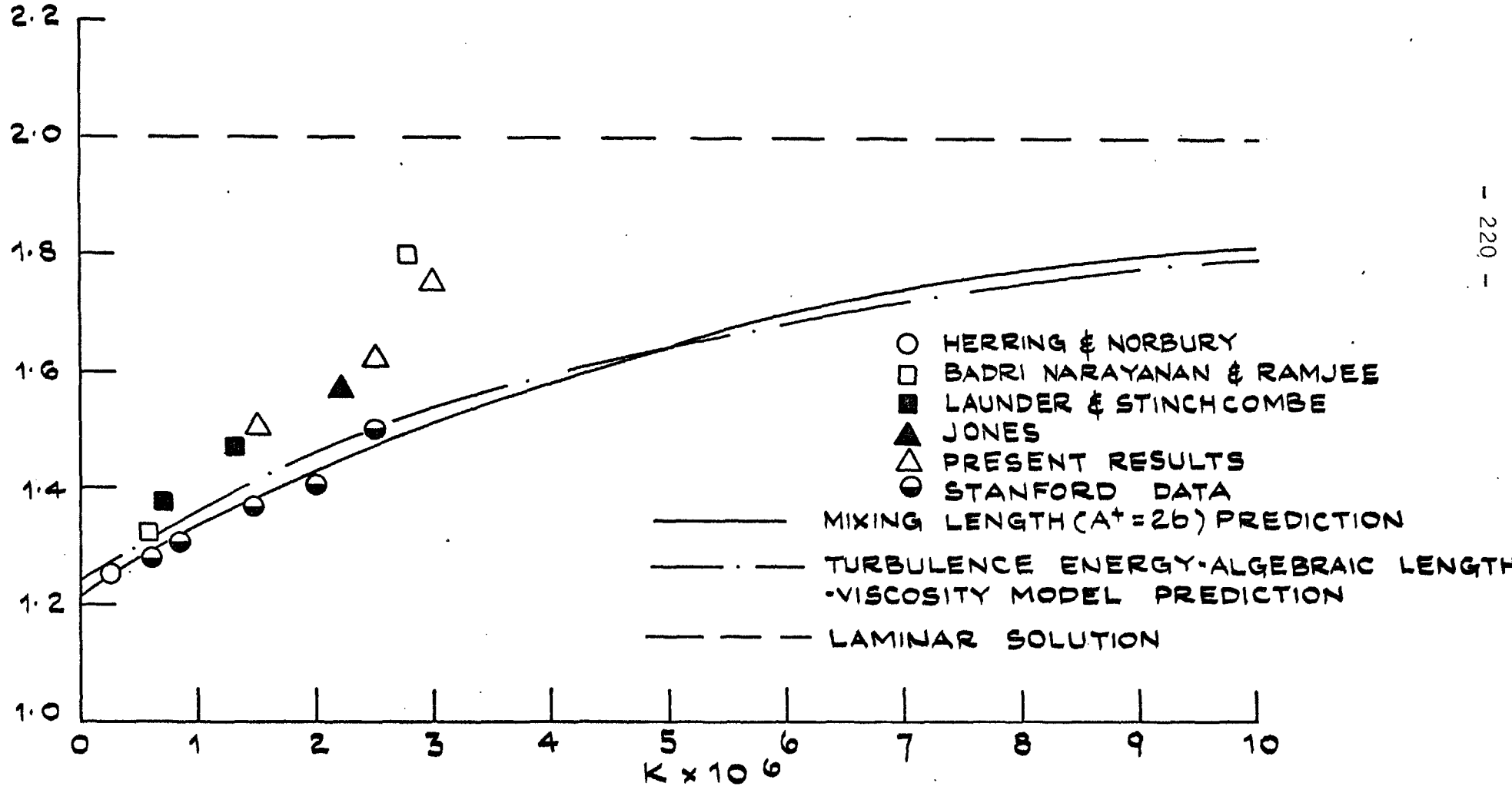

FIG. 3.40: 'CONSTANT K' BOUNDARY LAYER: VARIATION OF H WITH K

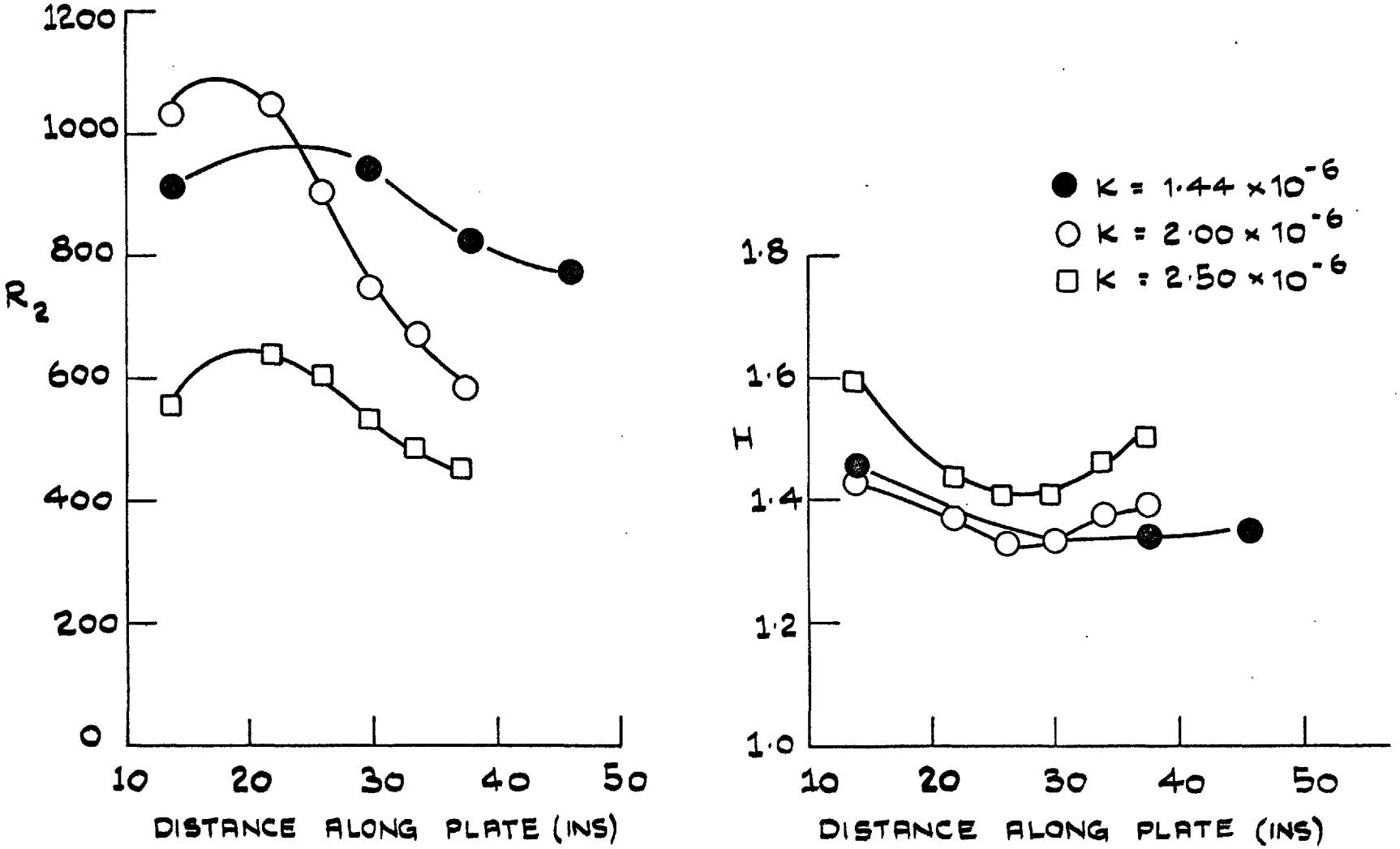

FIG. 3.41 : STANFORD GROUP 'CONSTANT K' BOUNDARY LAYER DATA : VARIATION OF INTEGRAL PARAMETERS THROUGH THE ACCELERATION.

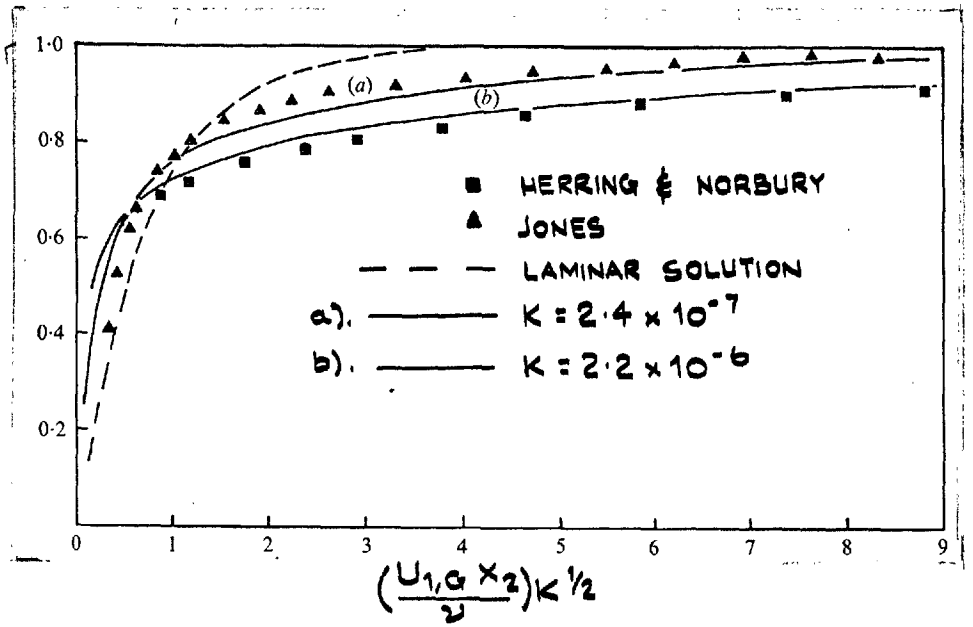

a). MEAN VELOCITY PROFILES FOR 'CONSTANT K' BOUNDARY LAYERS

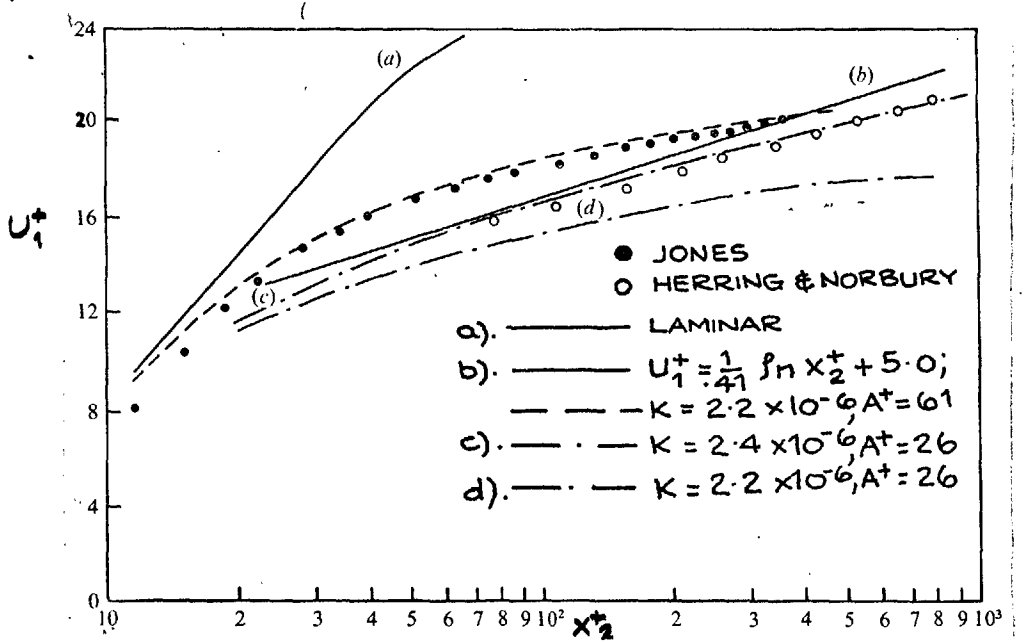

b). MEAN VELOCITY PROFILES.

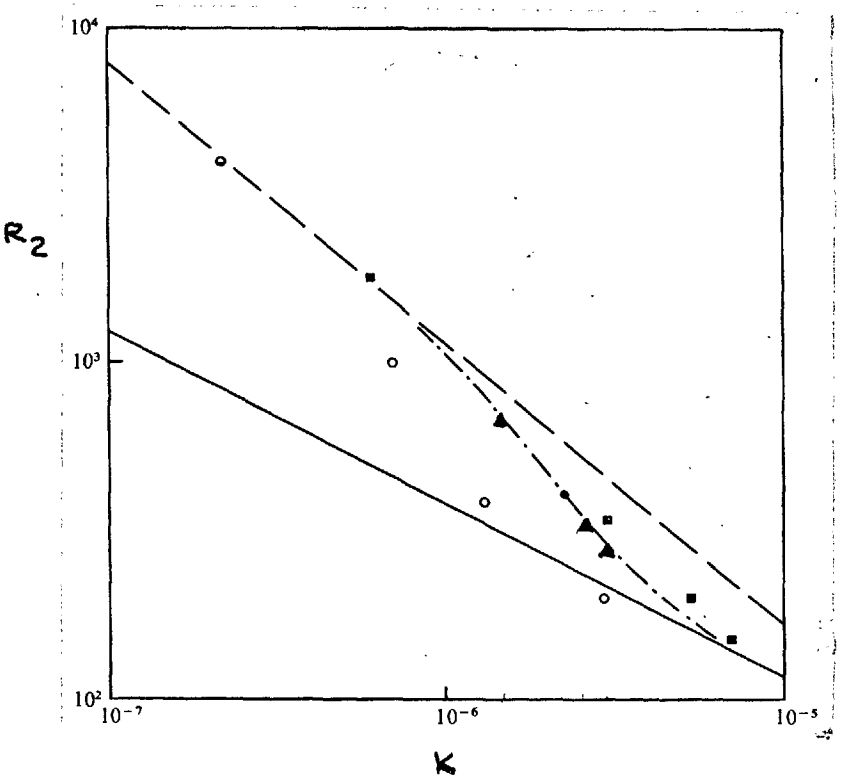

c). VARIATION OF R_2 WITH K.
HERRING & NORBURY; BADRI NARAYARIAN;
LAUNDER & STINCHCOMBE; JONES;
LAMINAR SOLUTION,
TURBULENT SOLUTION, A⁺ = 26
TURBULENT SOLUTION, A⁺ = f(p⁺)

FIG. 4.1.

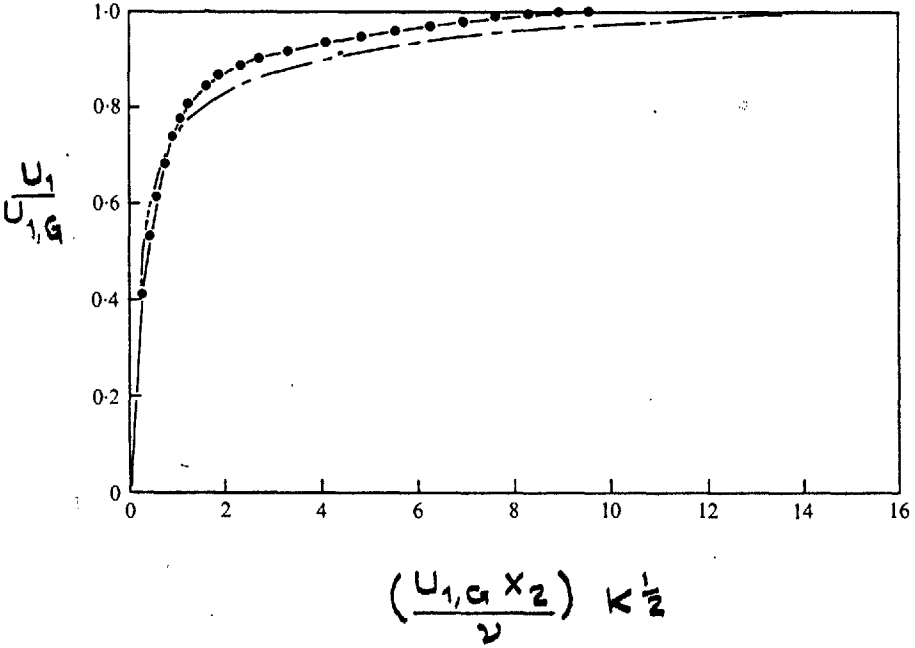

a). MEAN VELOCITY PROFILES, EXPERIMENTAL AND PREDICTED SOLUTION TO 'CONSTANT K' BOUNDARY LAYER, $K = 2{\cdot}2 \times 10^{-6}$.

- ● JONES
- ——— $A^+ = 61$
- —·— $A^+ = 26$

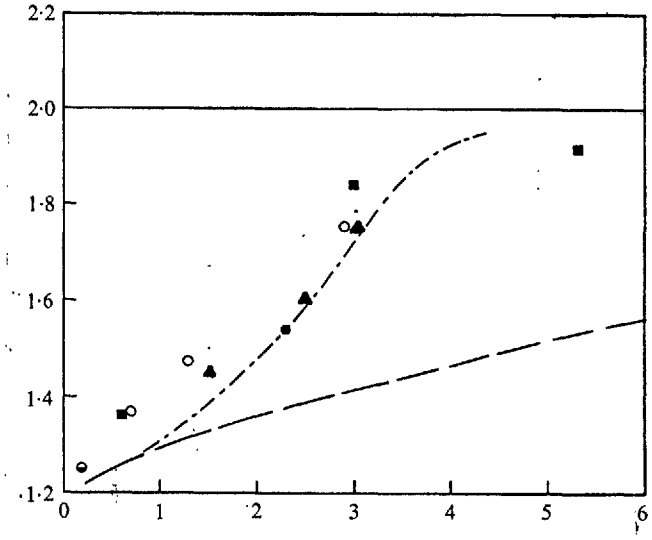

b). VARIATION OF SHAPE FACTOR WITH K

- ■ BADRI NARAYANAN;
- o LAUNDER & STINCHCOMBE;
- ● JONES;
- ⊖ HERRING & NORBURY;
- ▲ PRESENT RESULTS;
- ——— LAMINAR SOLUTION
- —·— $A^+ = F(p^+)$
- — — $A^+ = 26$

FIG. 4.2.

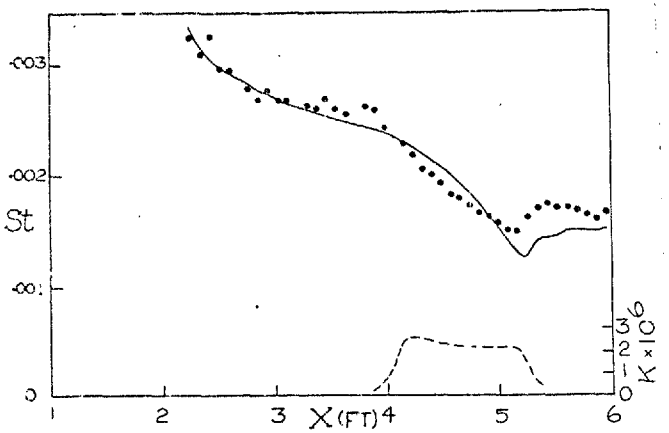

a) St vs x: Filetti Run 3

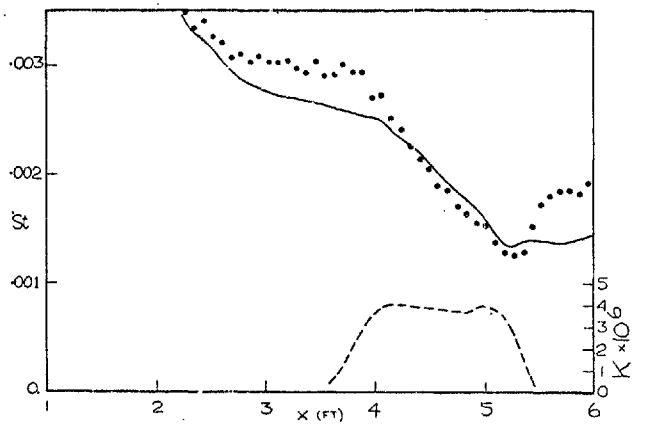

c) St vs x: Moretti and Kays run 42

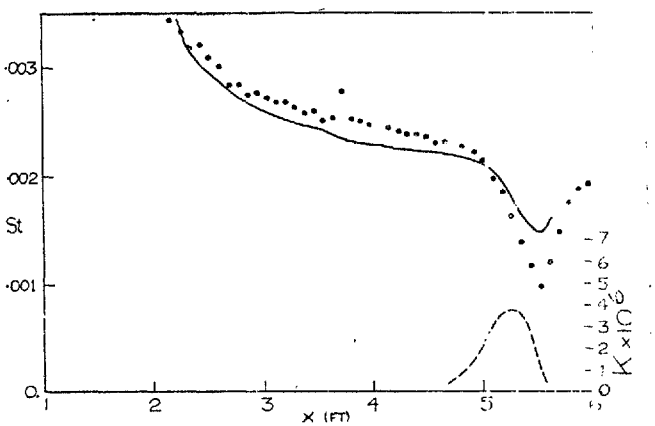

e) St vs x: Morette and Kays run 12

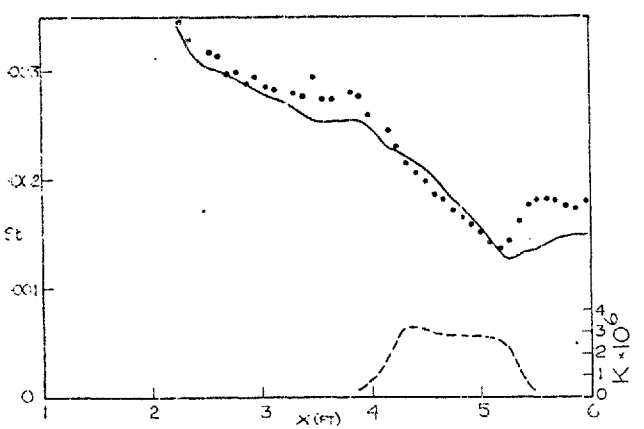

b) St vs x: Filetti Run 2

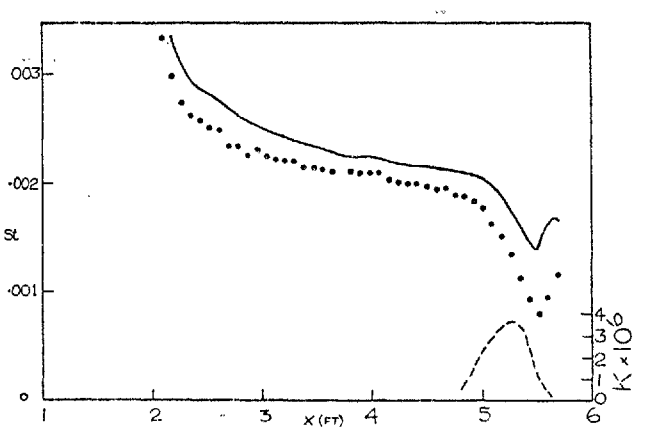

d) St vs x: Moretti and Kays run 10

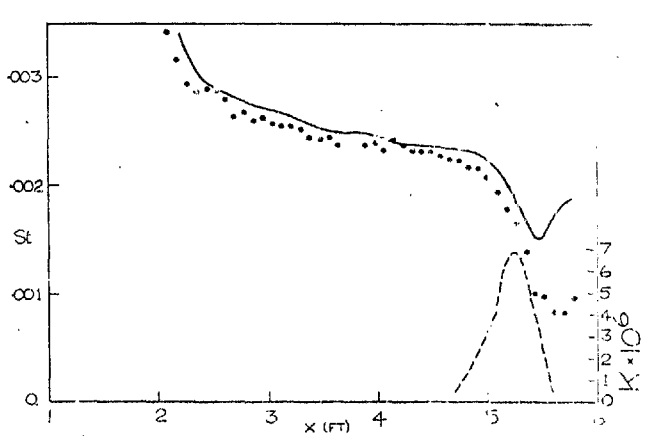

f) St vs x: Morette and Kays run 11

FIG. 4·3

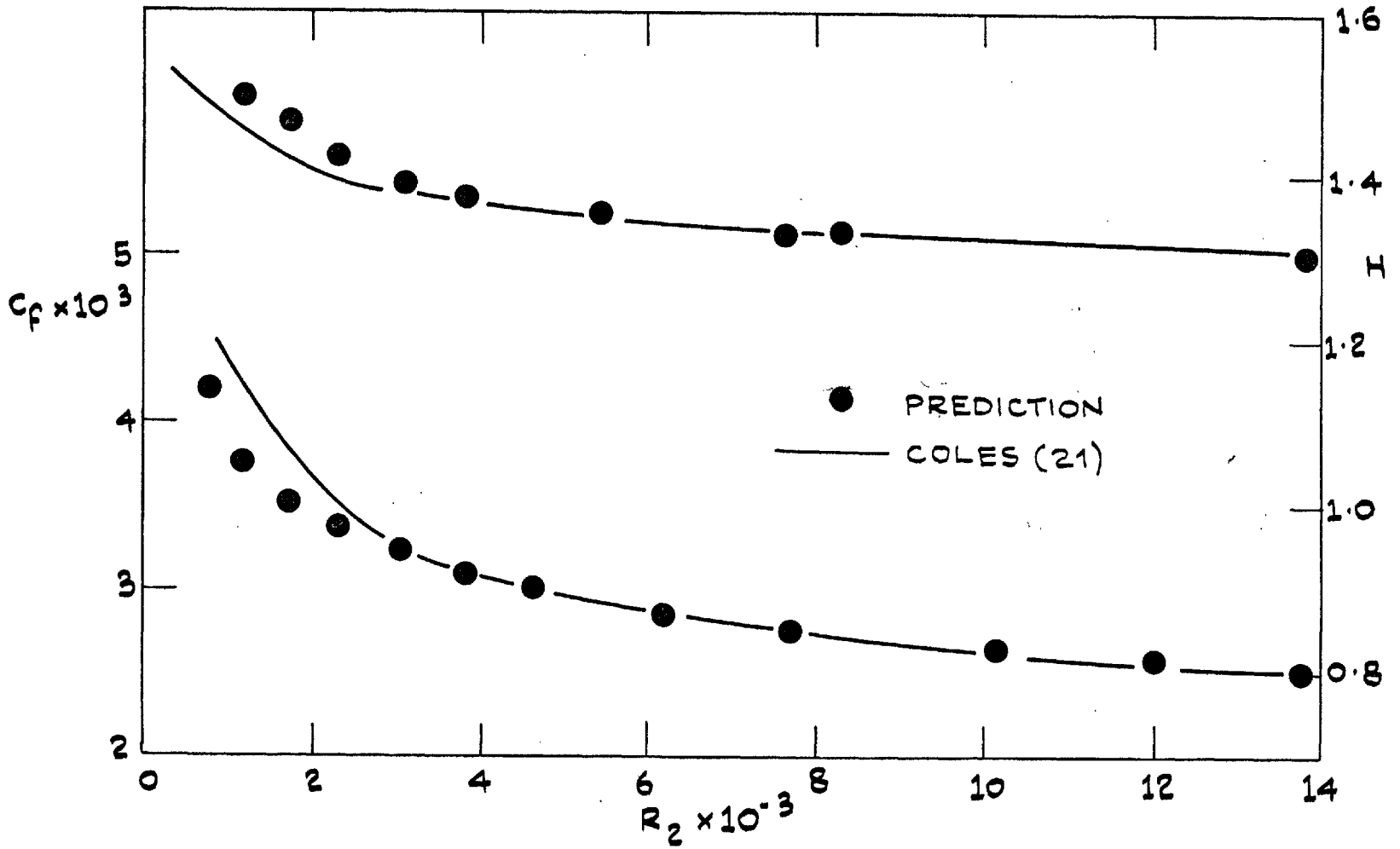

FIG. 4.4: BOUNDARY LAYER IN ZERO PRESSURE GRADIENT
VARIATION OF H AND CF WITH R_2

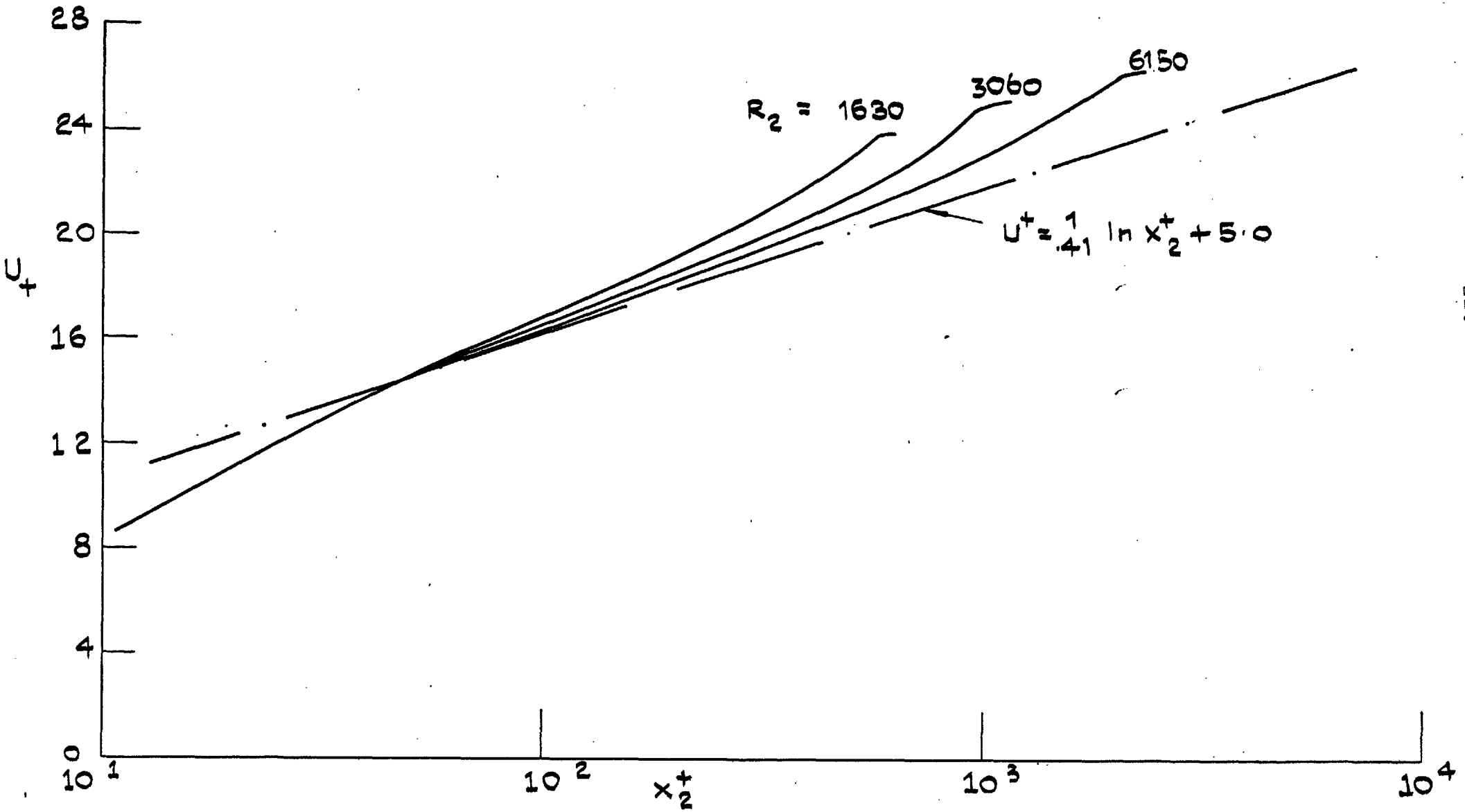

FIG.4.5: BOUNDARY LAYER IN ZERO PRESSURE GRADIENT, MEAN VELOCITY PROFILES IN UNIVERSAL CO-ORDINATES.

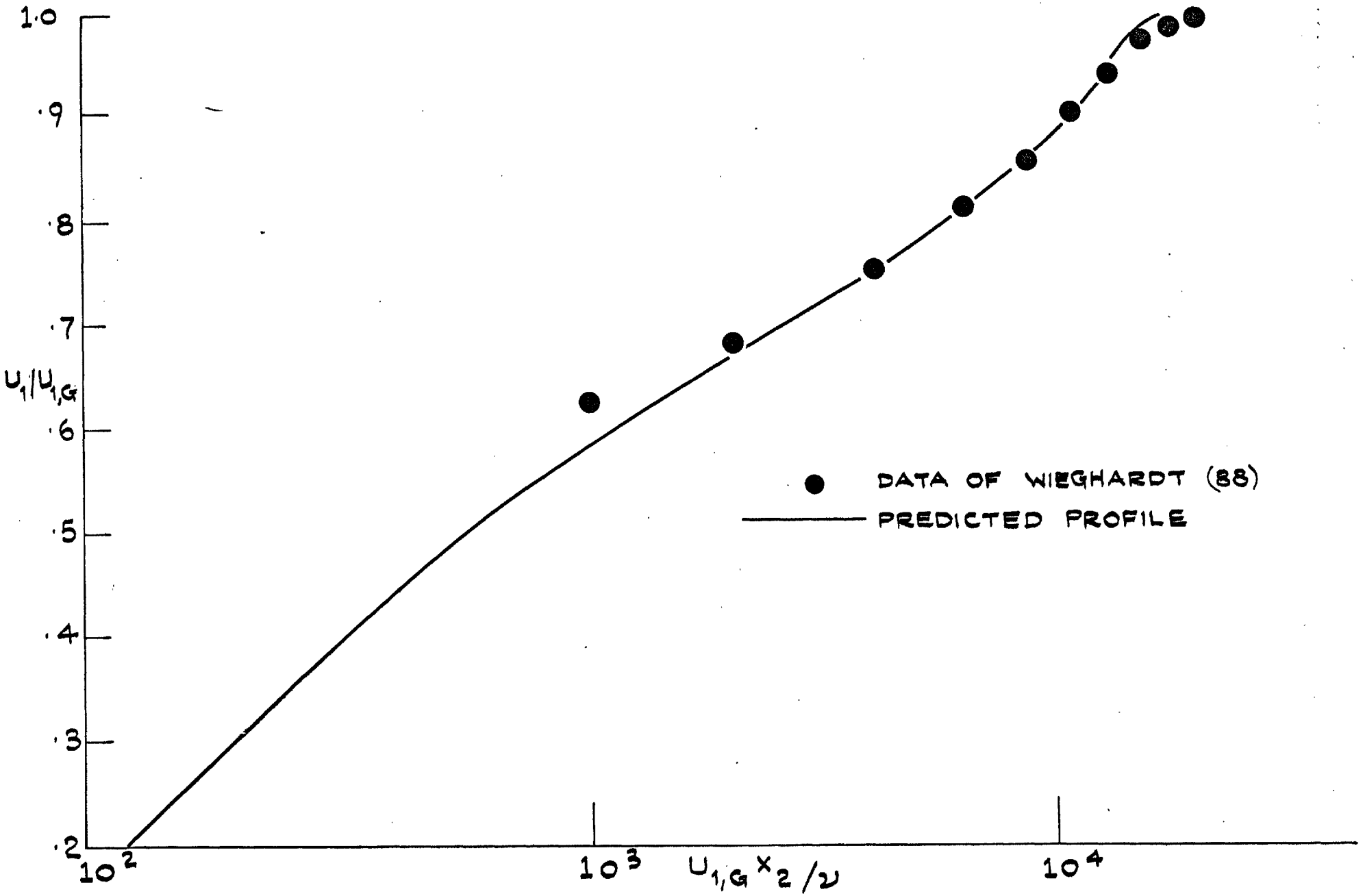

FIG.4.6: BOUNDARY LAYER IN ZERO PRESSURE GRADIENT: MEAN VELOCITY PROFILE $R_2 = 2000$.

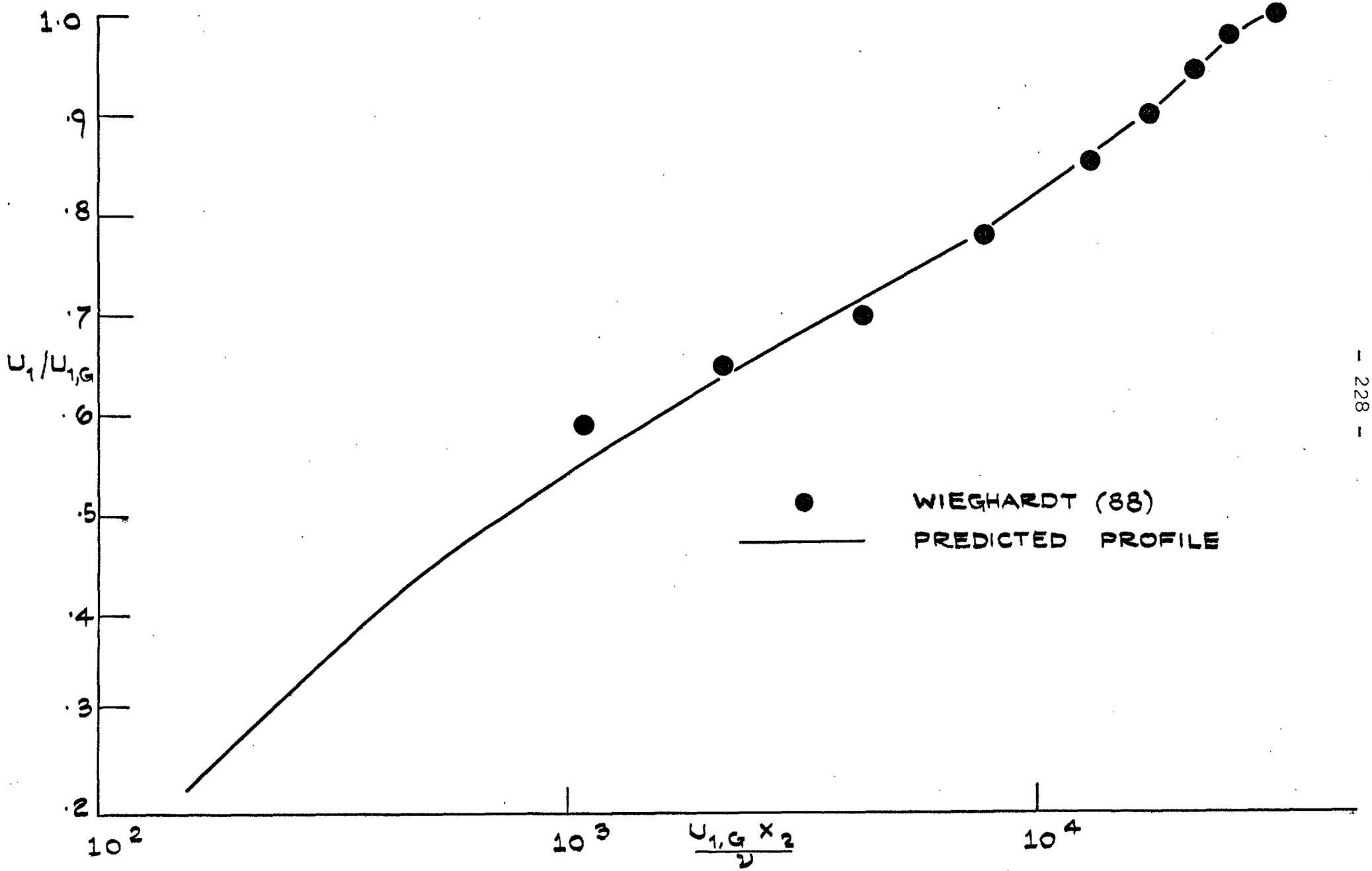

FIG. 4.7: BOUNDARY LAYER IN ZERO PRESSURE GRADIENT MEAN VELOCITY PROFILE, $R_2 = 3470$.

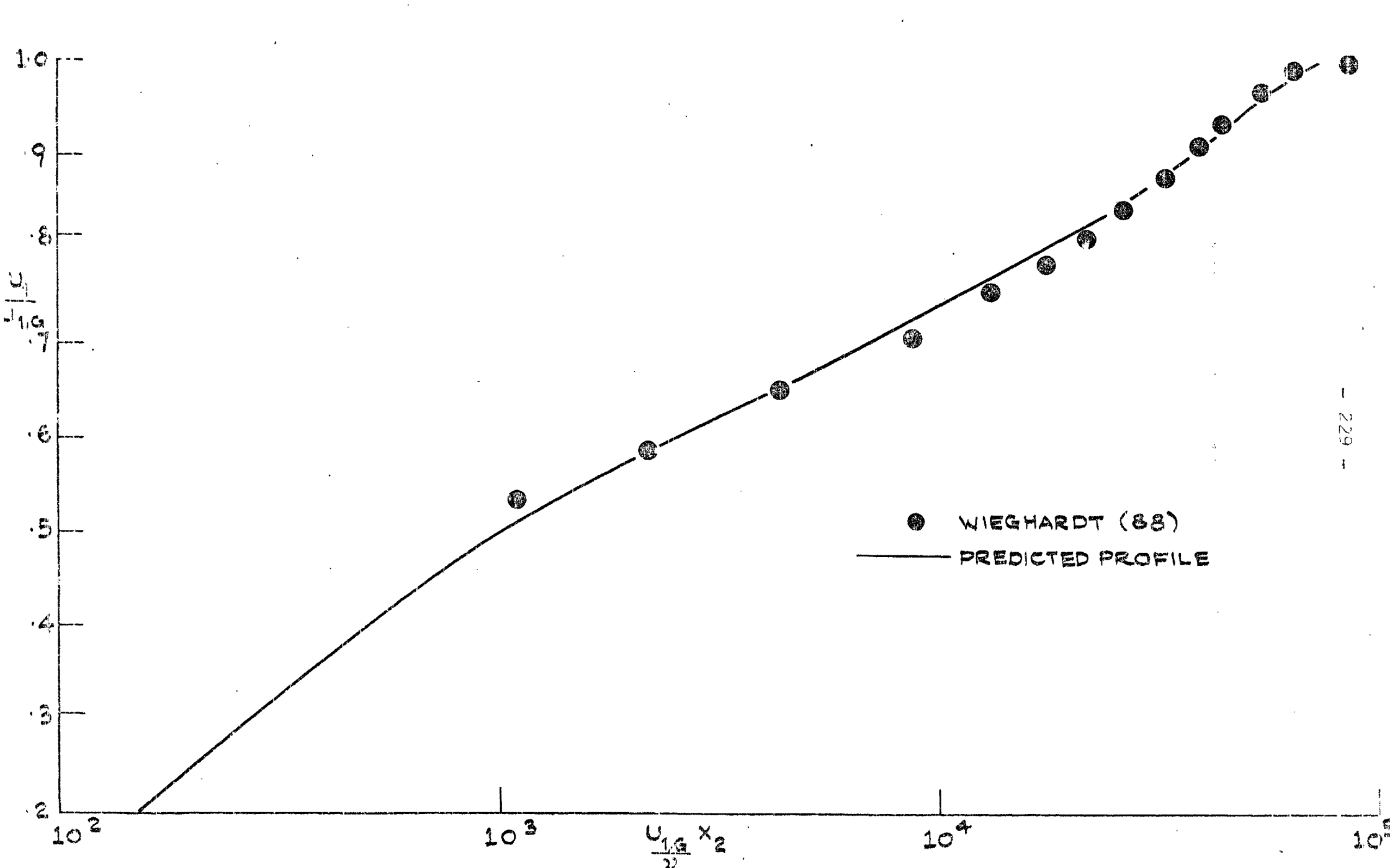

FIG. 4.8: BOUNDARY LAYER IN ZERO PRESSURE GRADIENT, MEAN VELOCITY PROFILE, R_{x_2} = 7280

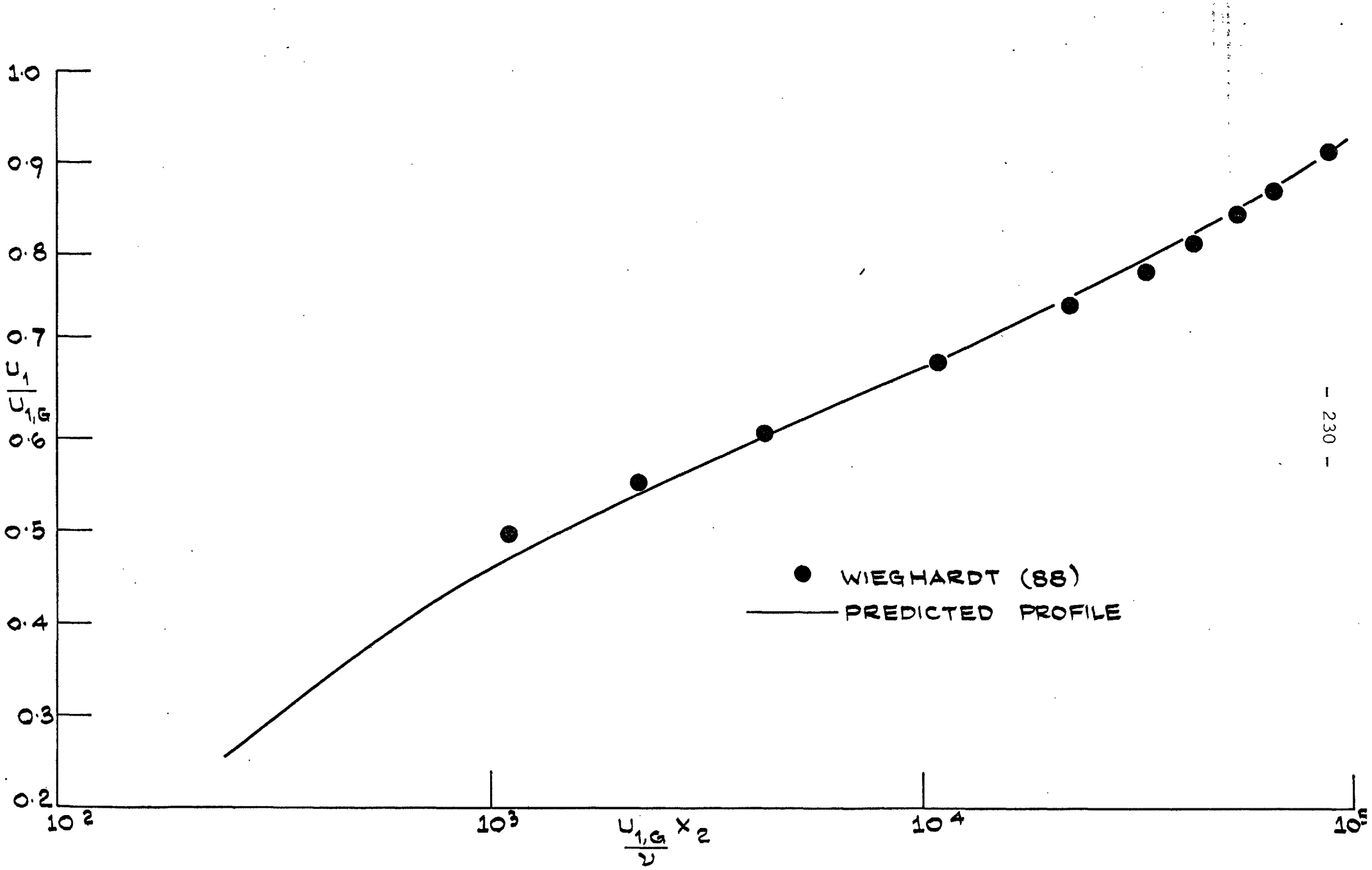

FIG. 4.9: BOUNDARY LAYER IN ZERO PRESSURE GRADIENT, MEAN VELOCITY PROFILE, $R_2 = 15,900$

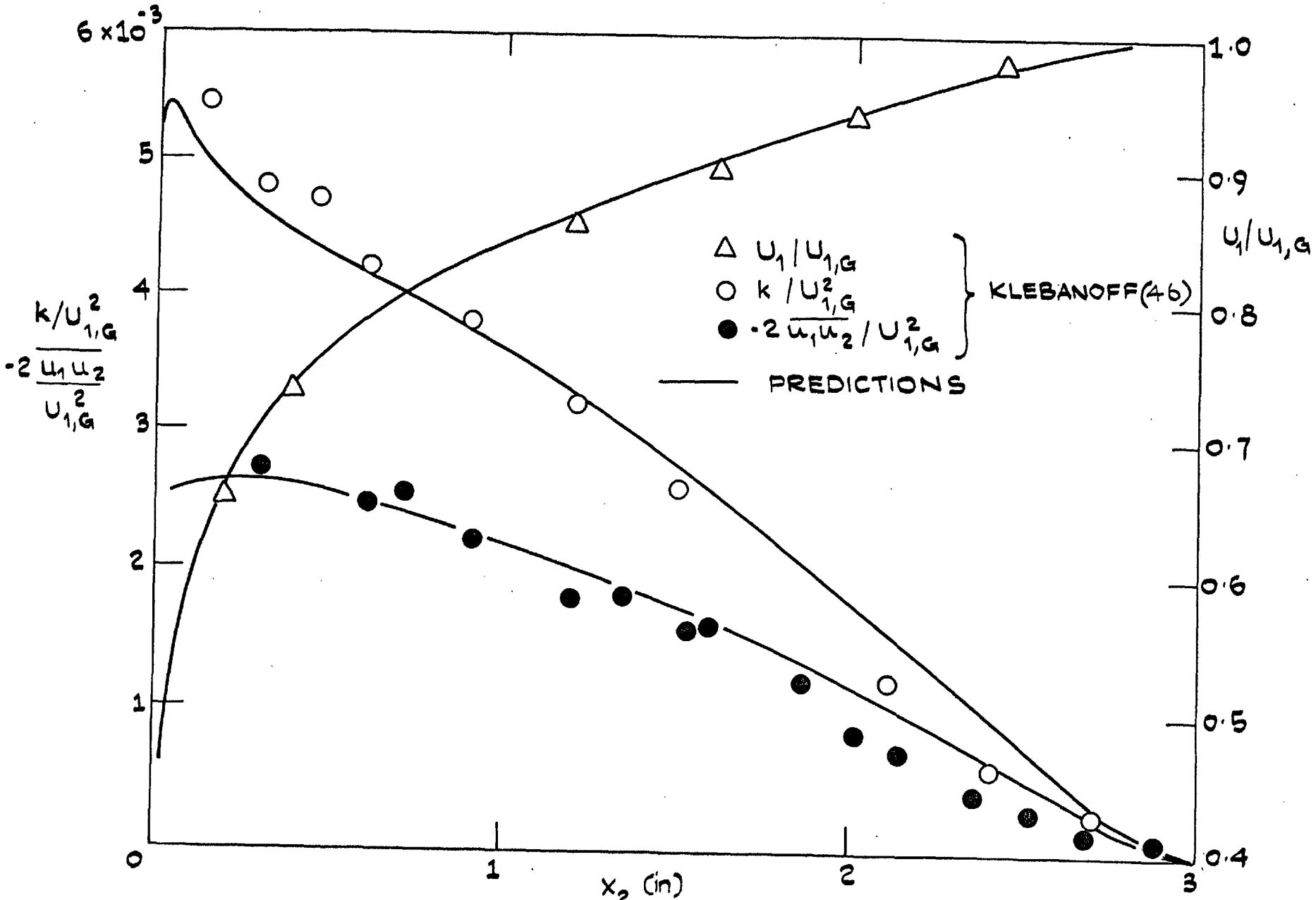

FIG. 4.10: BOUNDARY LAYER IN ZERO PRESSURE GRADIENT. PROFILES OF MEAN VELOCITY, TURBULENCE ENERGY AND SHEAR STRESS.

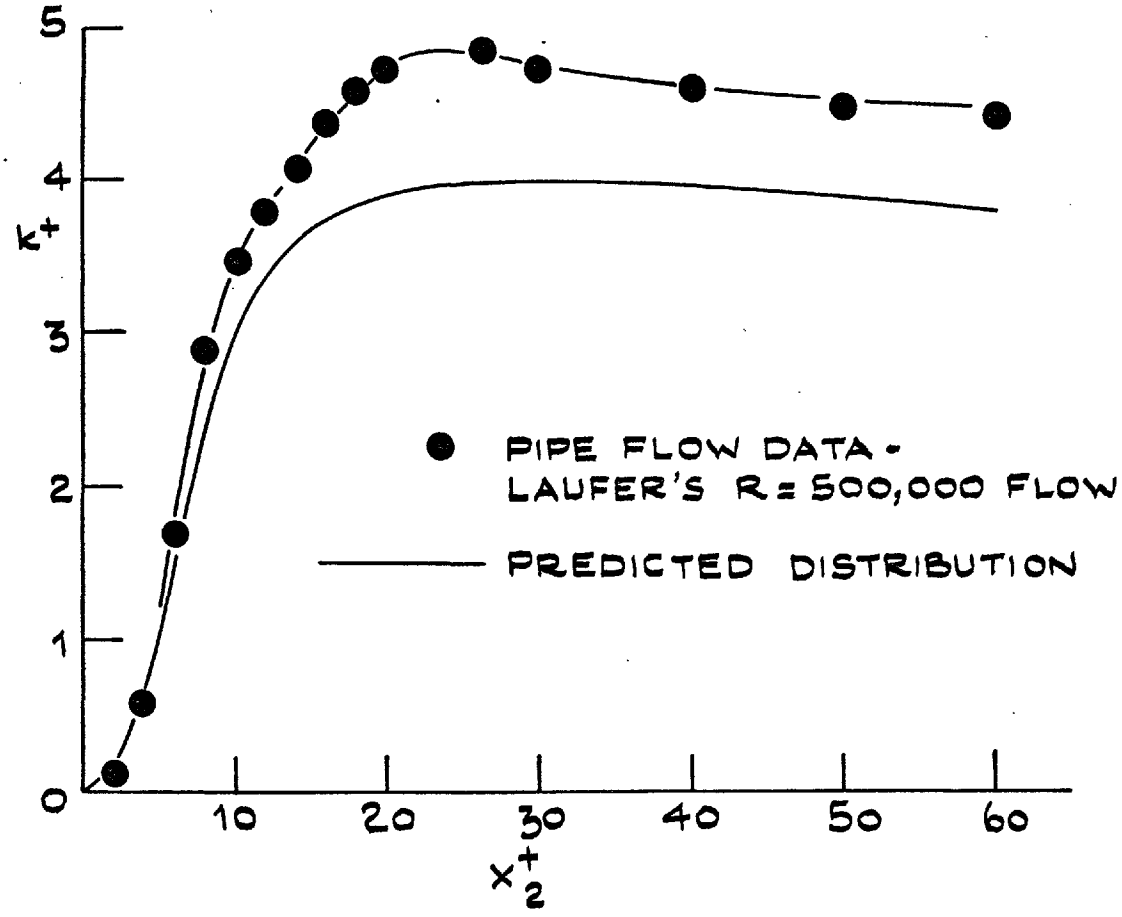

FIG. 4·11: TURBULENCE KINETIC ENERGY WITHIN THE VISCOUS SUBLAYER

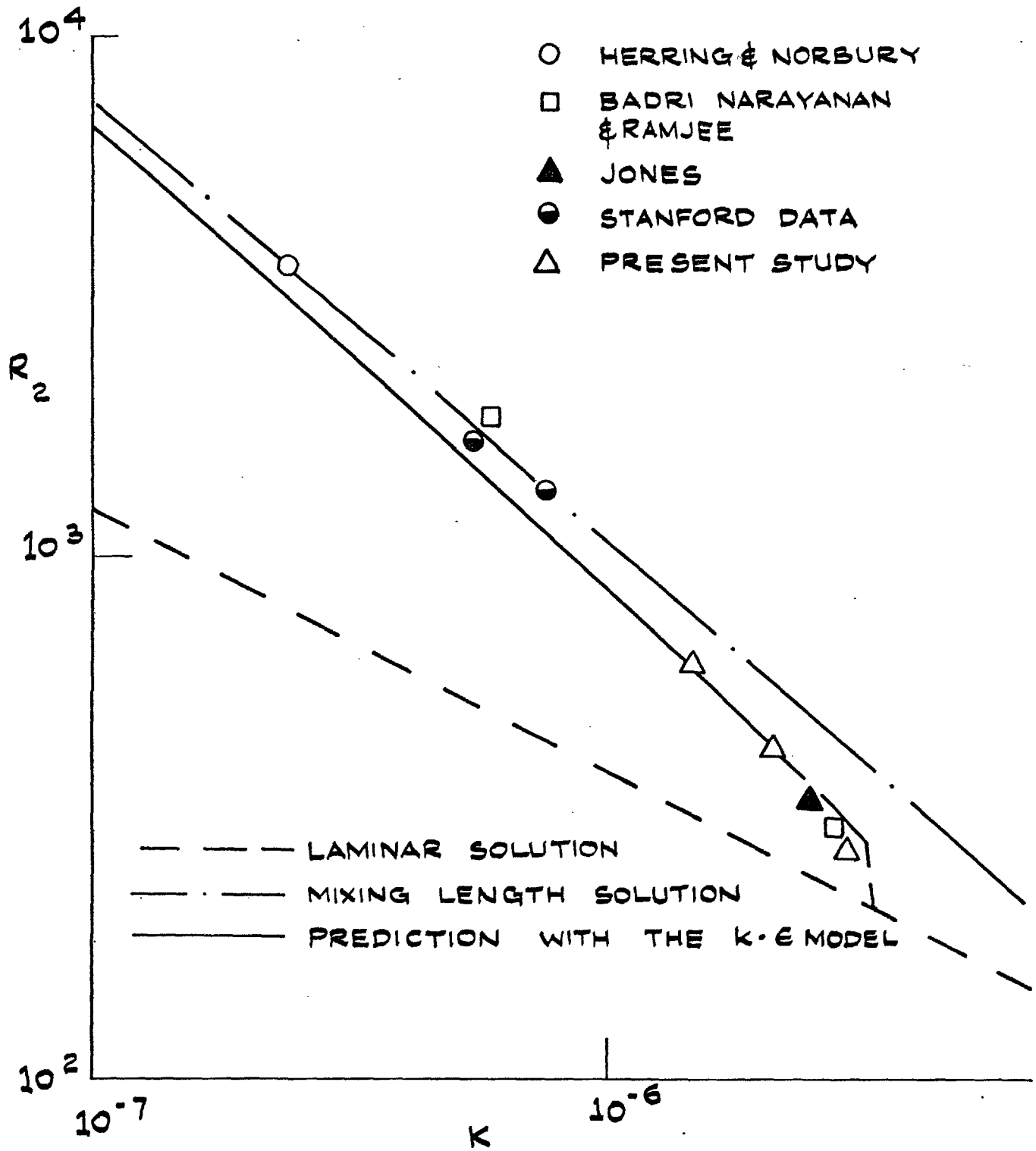

FIG.4.12: 'CONSTANT K' BOUNDARY LAYER. VARIATION OF R_2 WITH K.

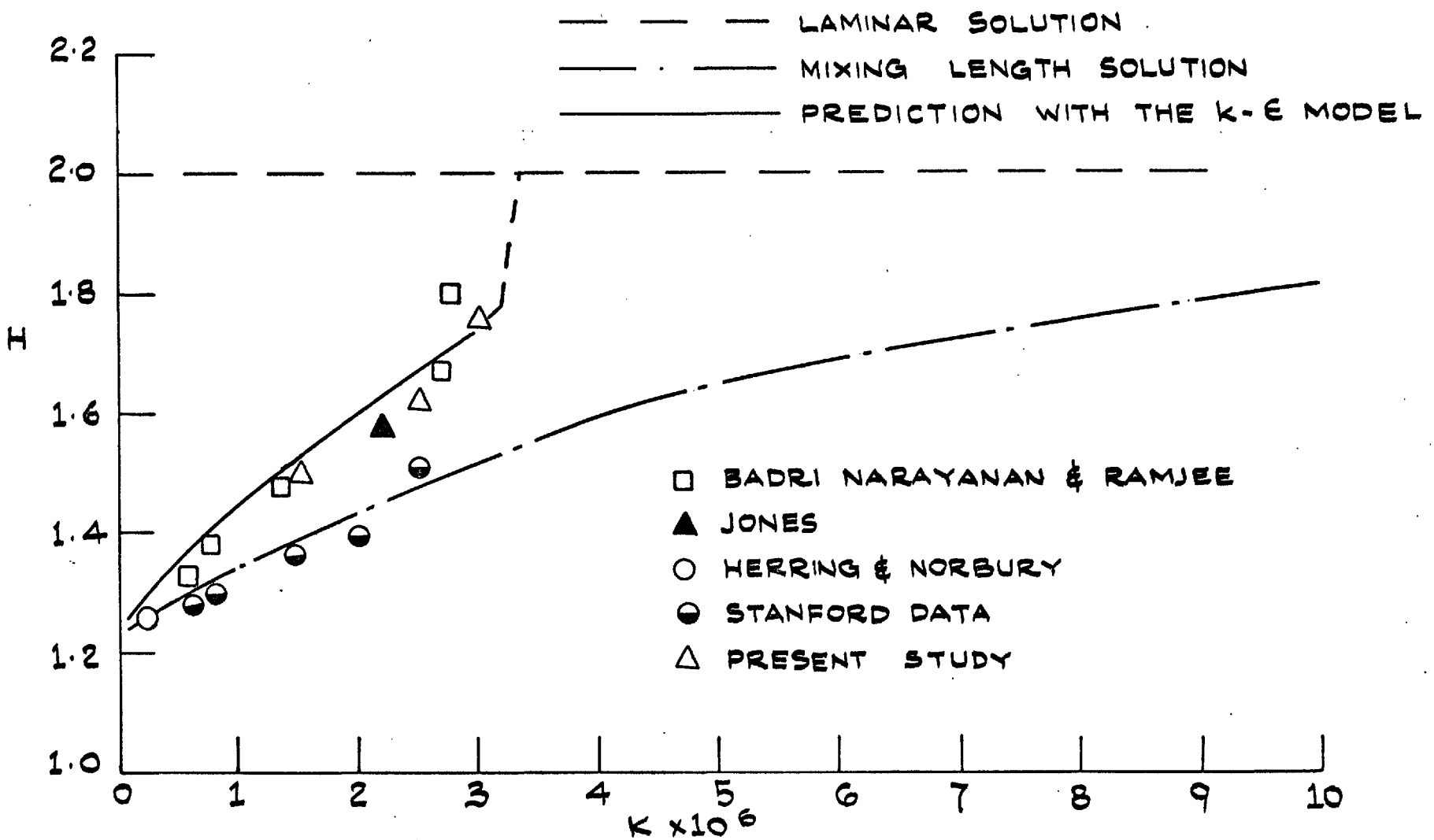

FIG. 4·13: 'CONSTANT K' BOUNDARY LAYER VARIATION OF H WITH K

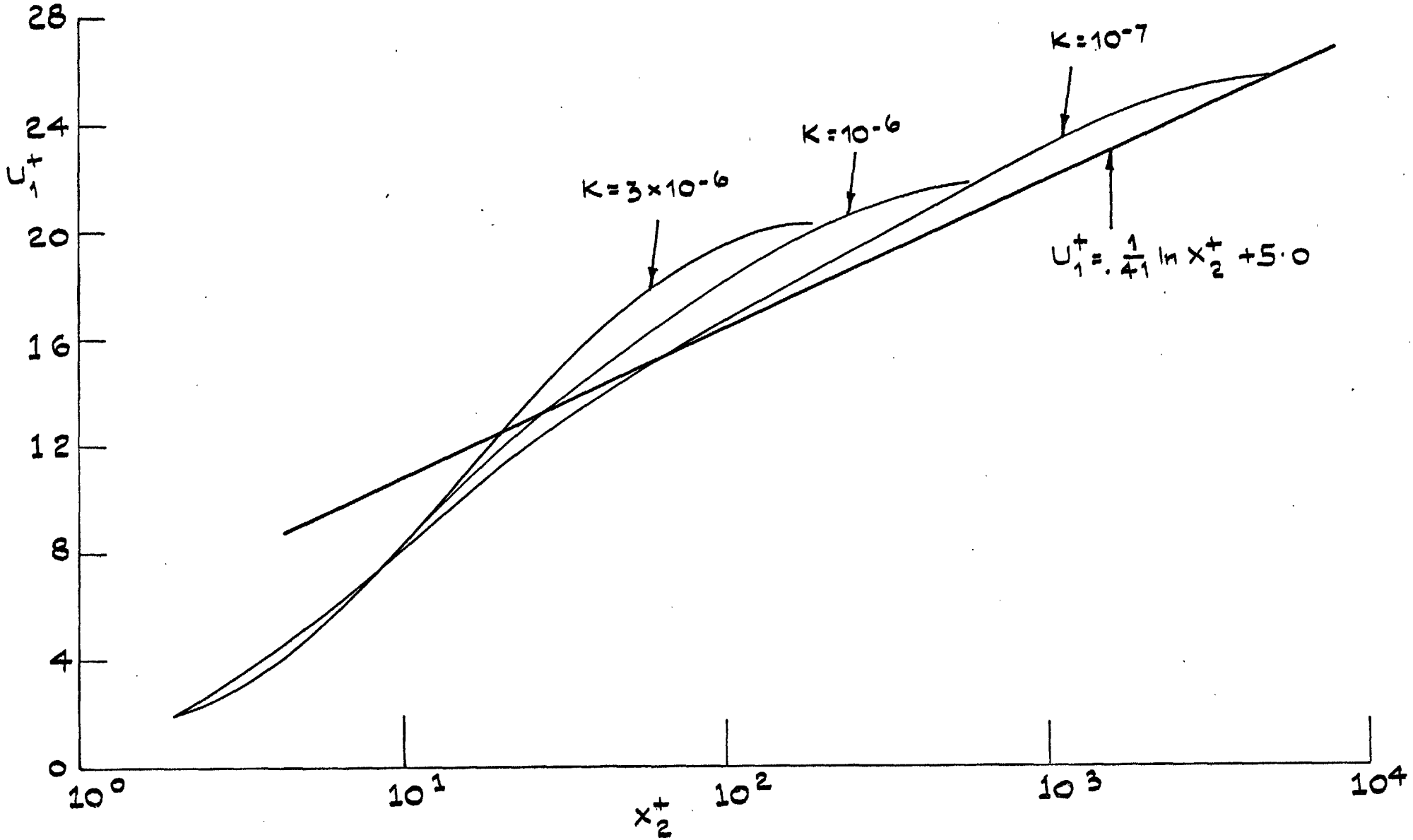

FIG. 4.14: 'CONSTANT K' BOUNDARY LAYERS PREDICTED MEAN VELOCITY PROFILES.

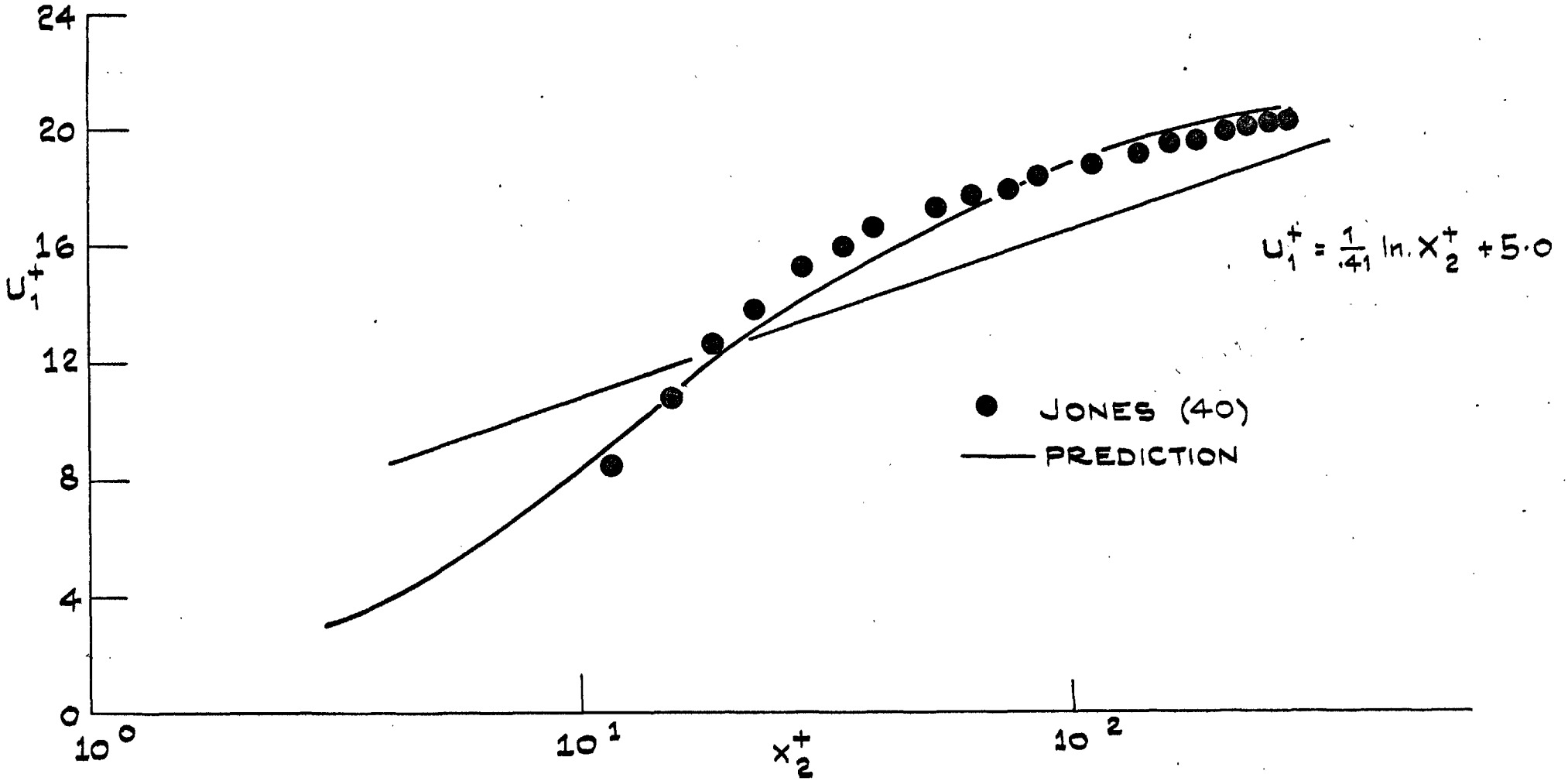

FIG. 4·15: 'CONSTANT K' BOUNDARY LAYER MEAN VELOCITY PROFILE, $K = 2.2 \times 10^{-6}$

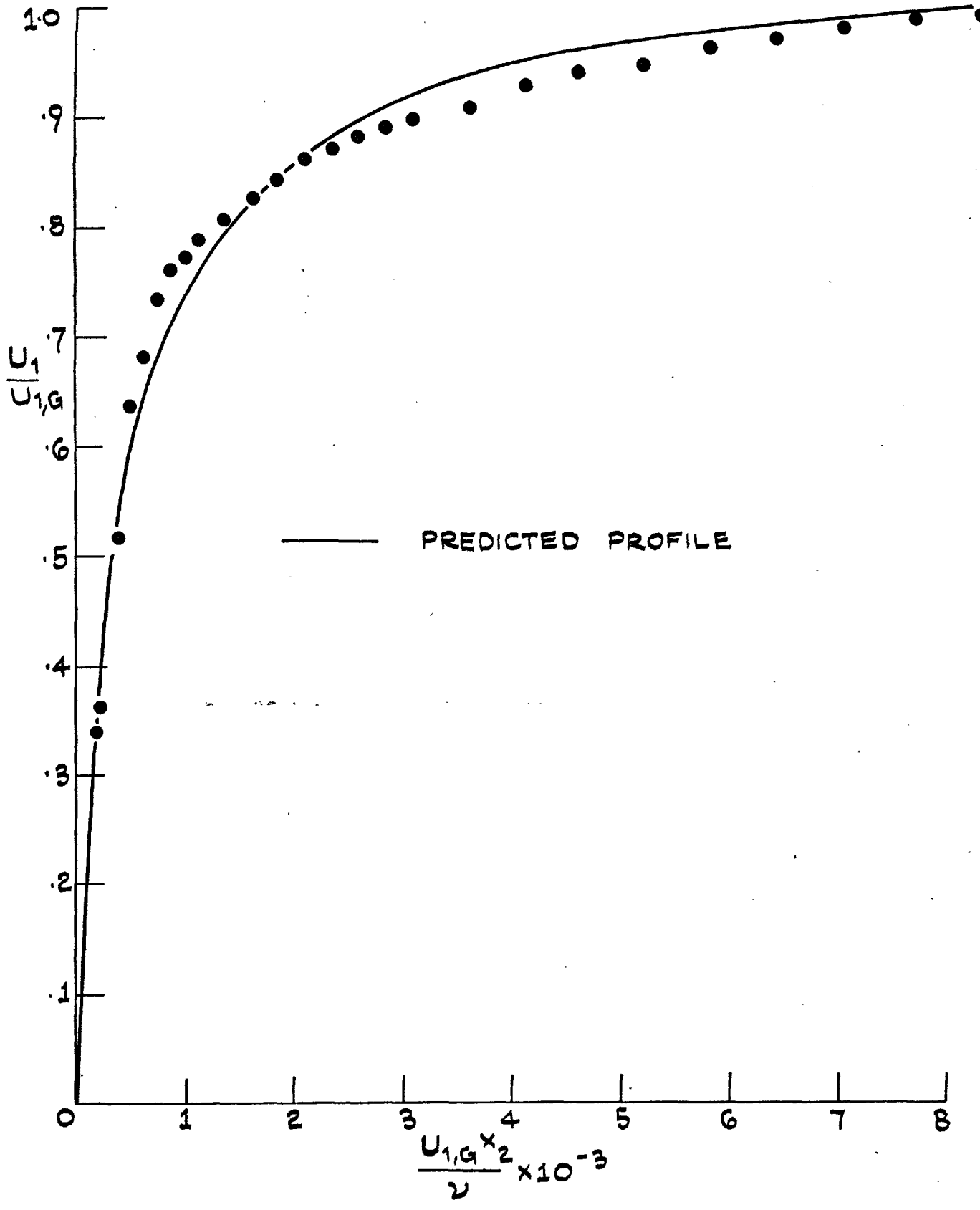

FIG. 4·16 : 'CONSTANT K' BOUNDARY LAYER MEAN VELOCITY

$K = 1{\cdot}5 \times 10^{-6}$

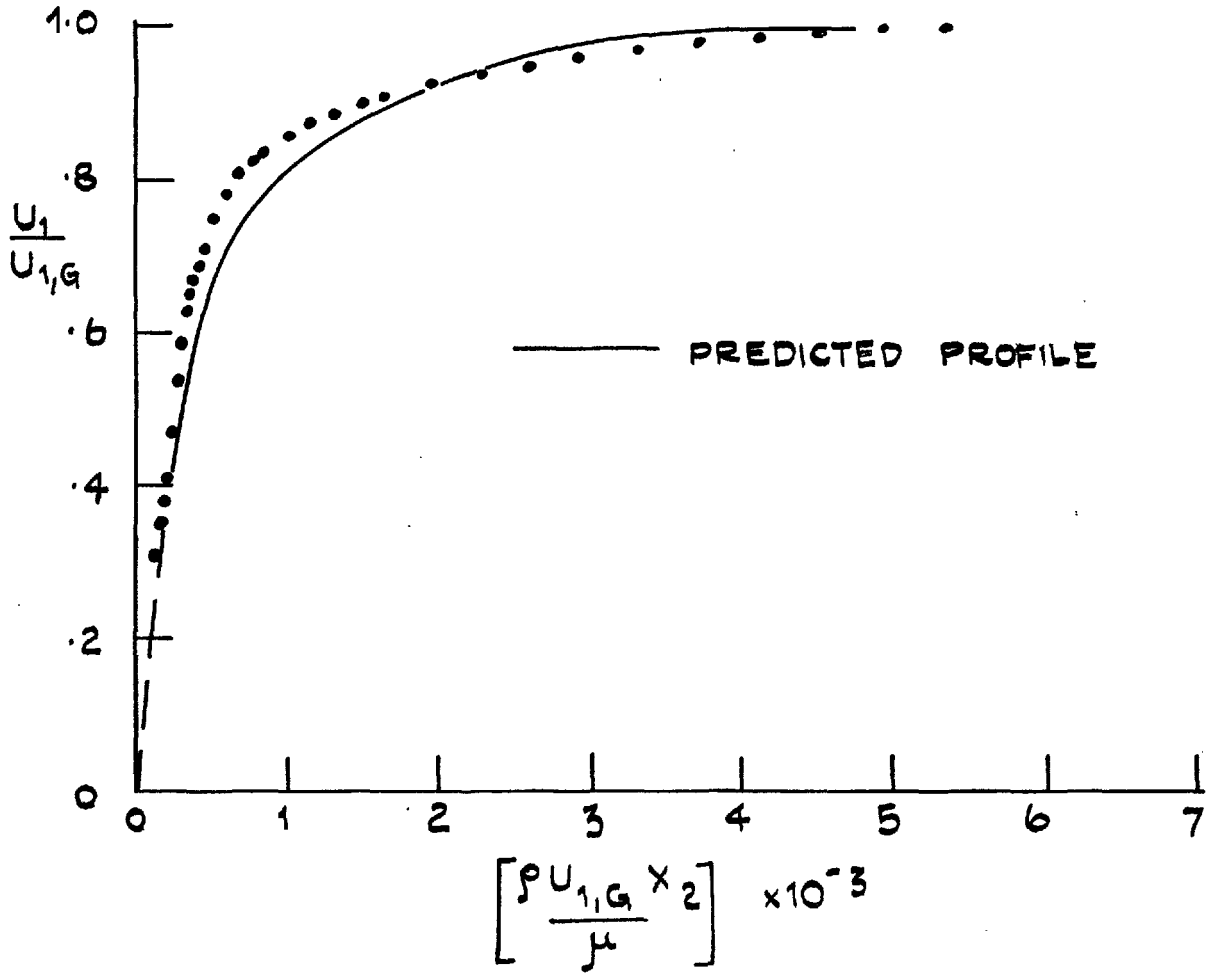

FIG. 4·17: 'CONSTANT K' BOUNDARY LAYER MEAN VELOCITY PROFILE, $K = 2{\cdot}5 \times 10^{-6}$

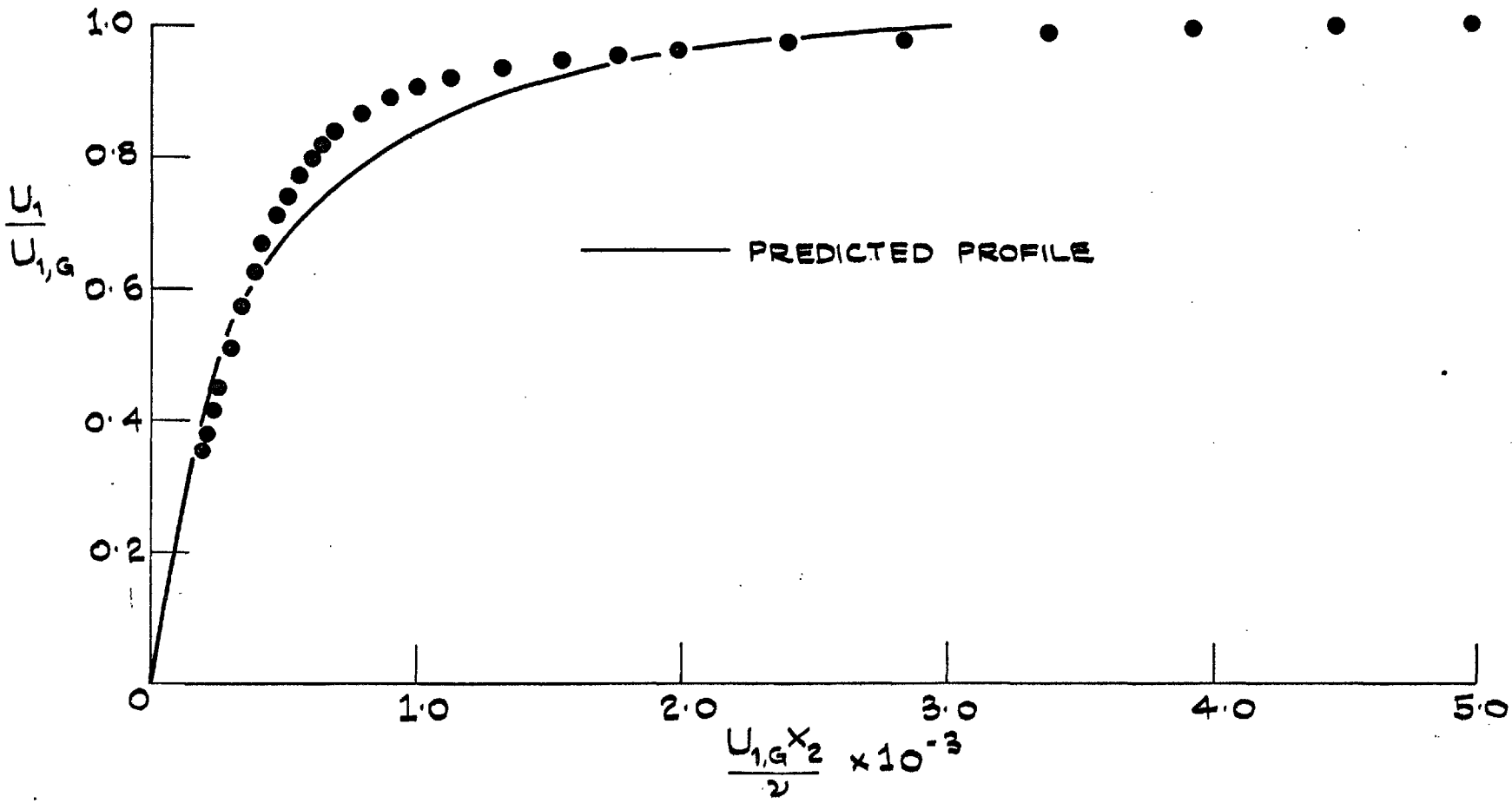

FIG. 4·18: 'CONSTANT K' BOUNDARY LAYER MEAN VELOCITY PROFILE, $K = 3{\cdot}0 \times 10^{-6}$

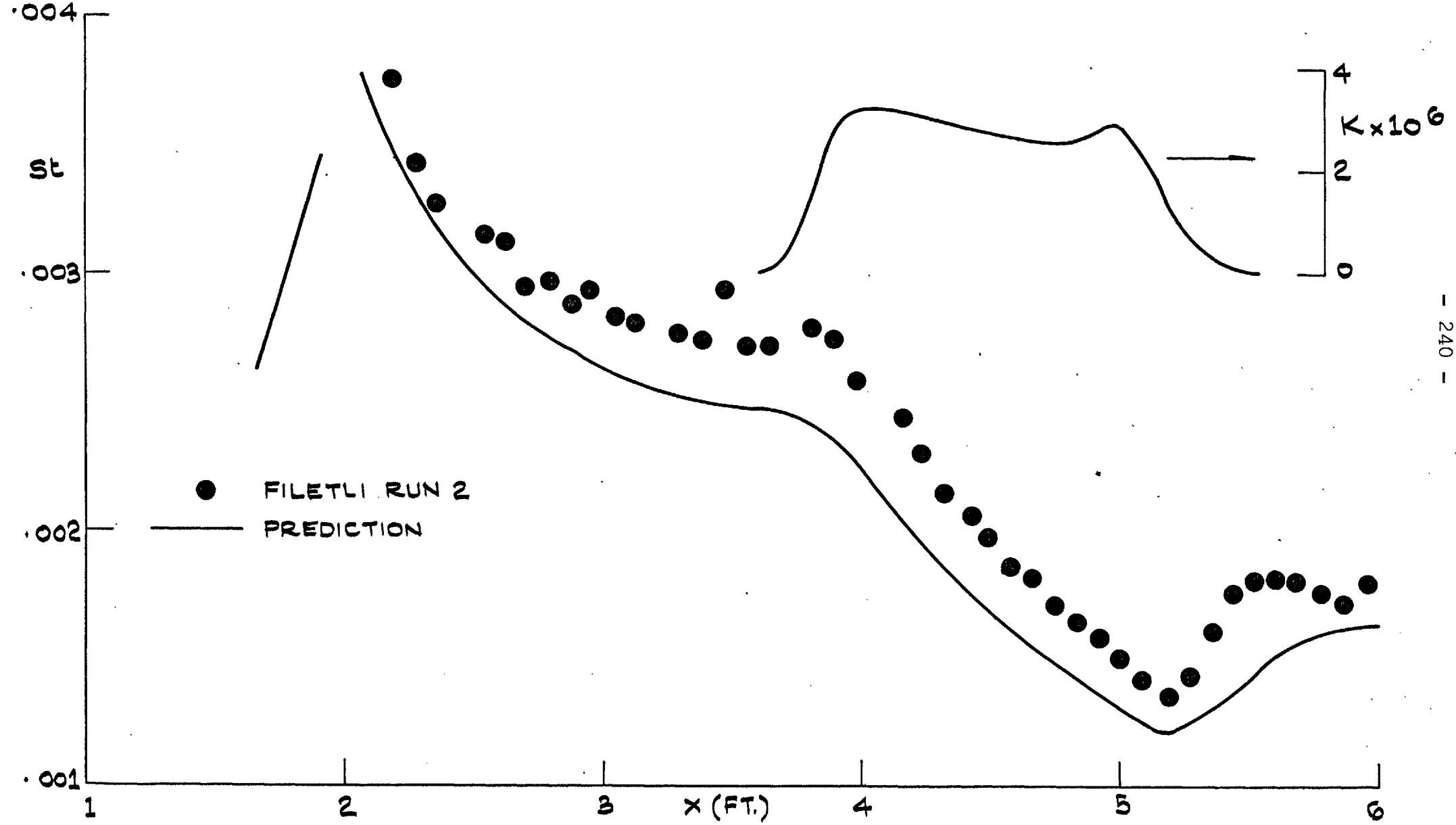

FIG. 4·19 : VARIATION OF St WITH X_1

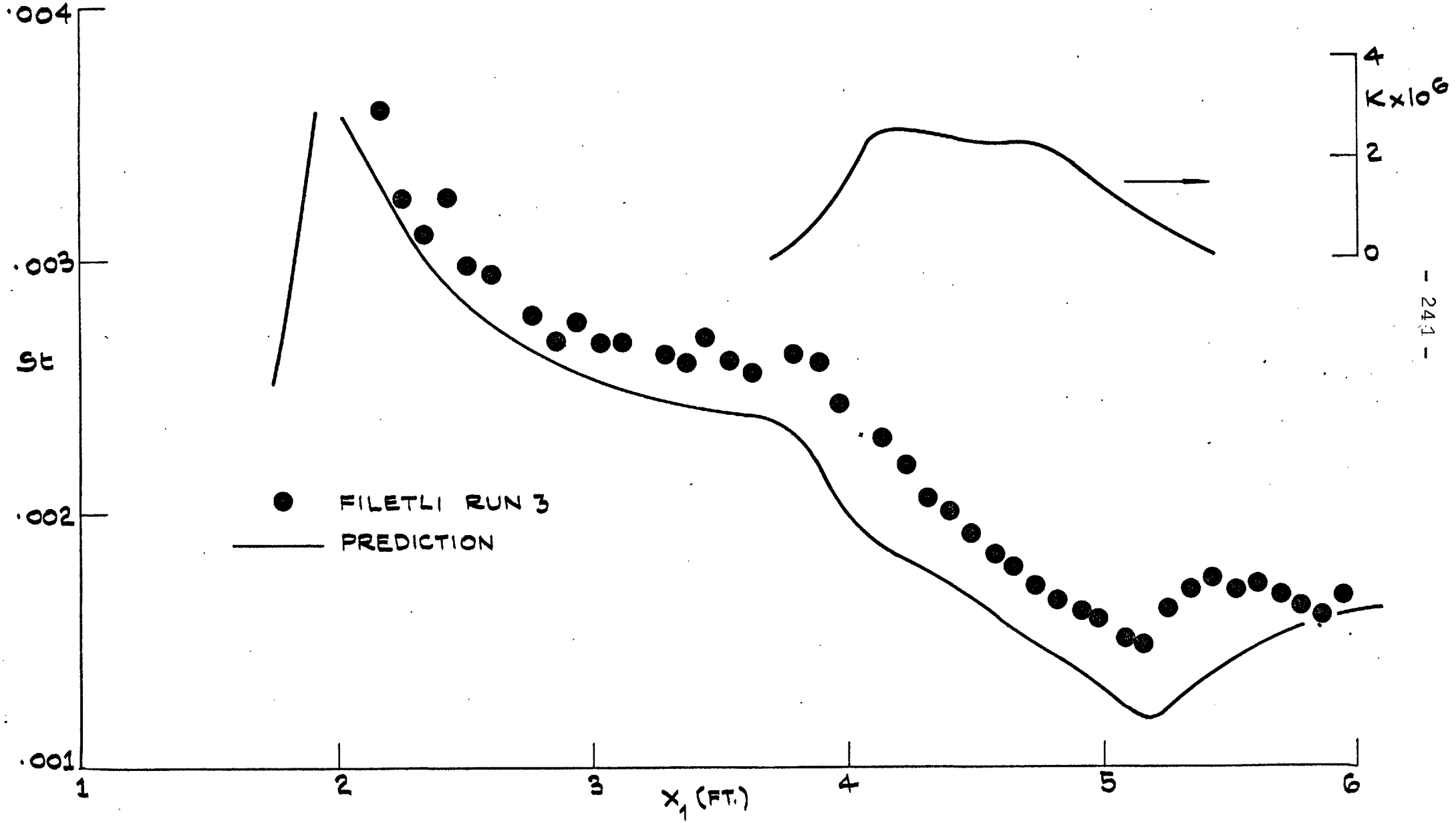

FIG. 4.20: VARIATION OF St WITH X_1

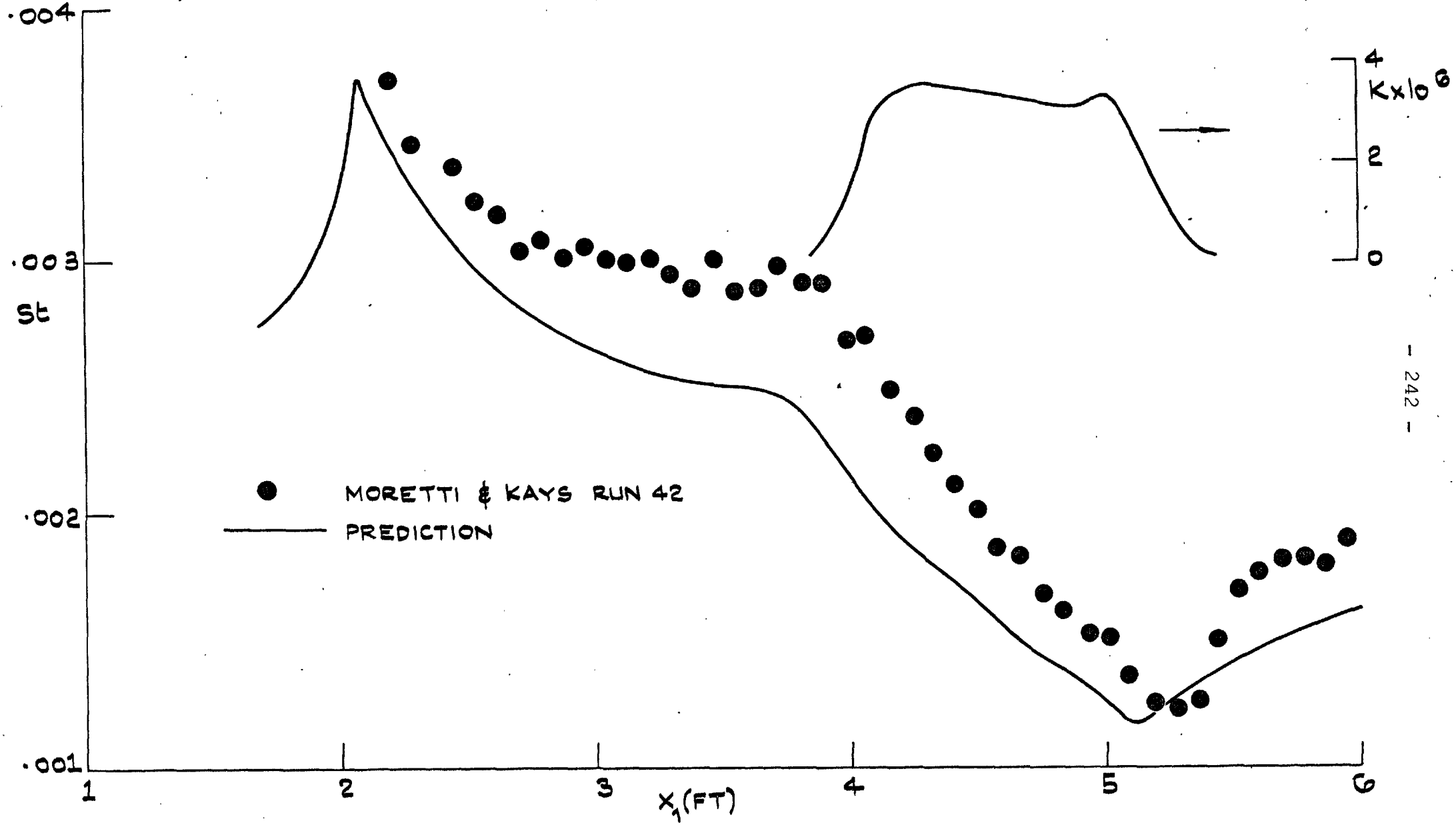

FIG. 4.21: VARIATION OF St WITH X_1

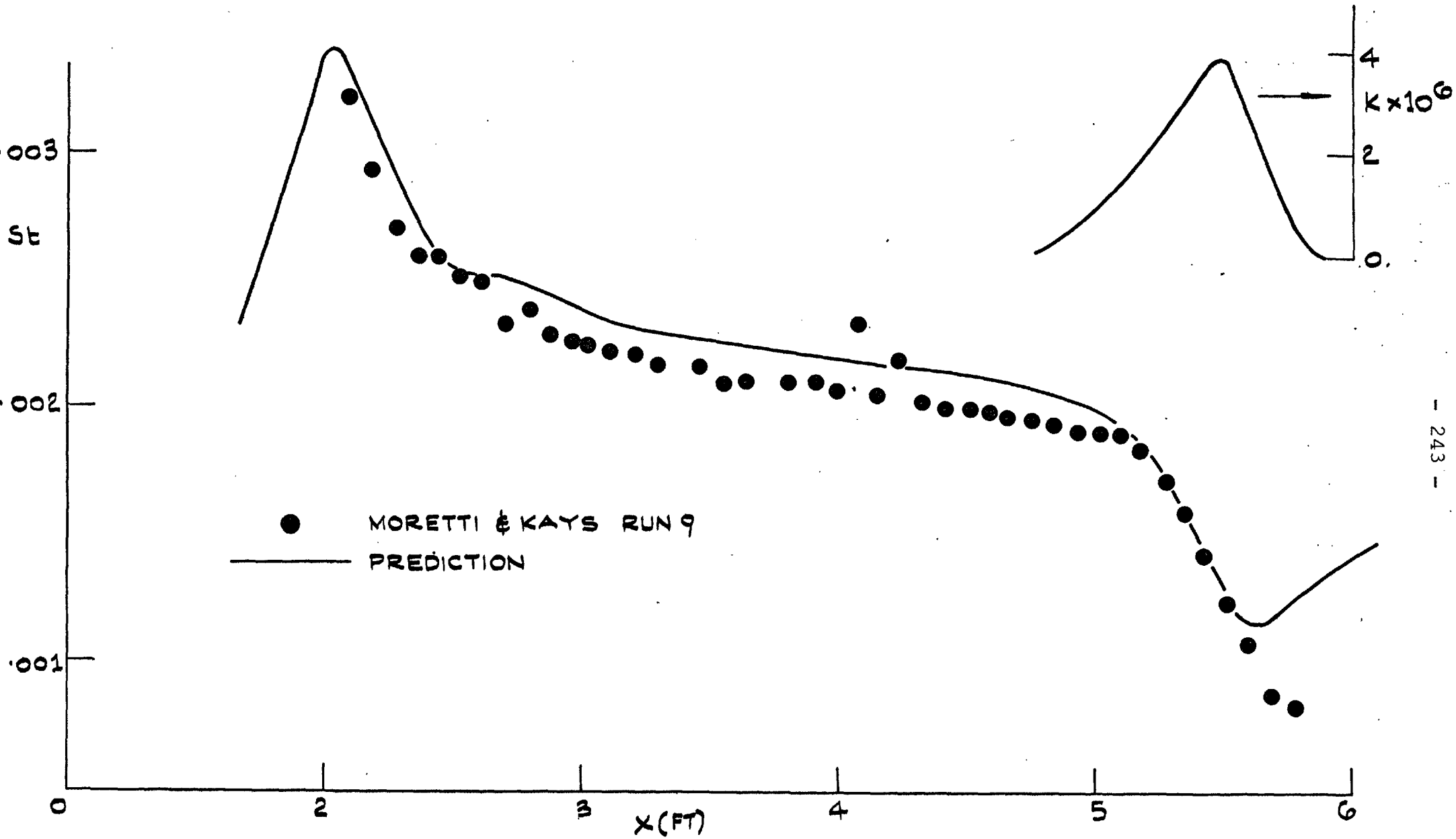

FIG. 4·22 VARIATION OF St WITH X_1

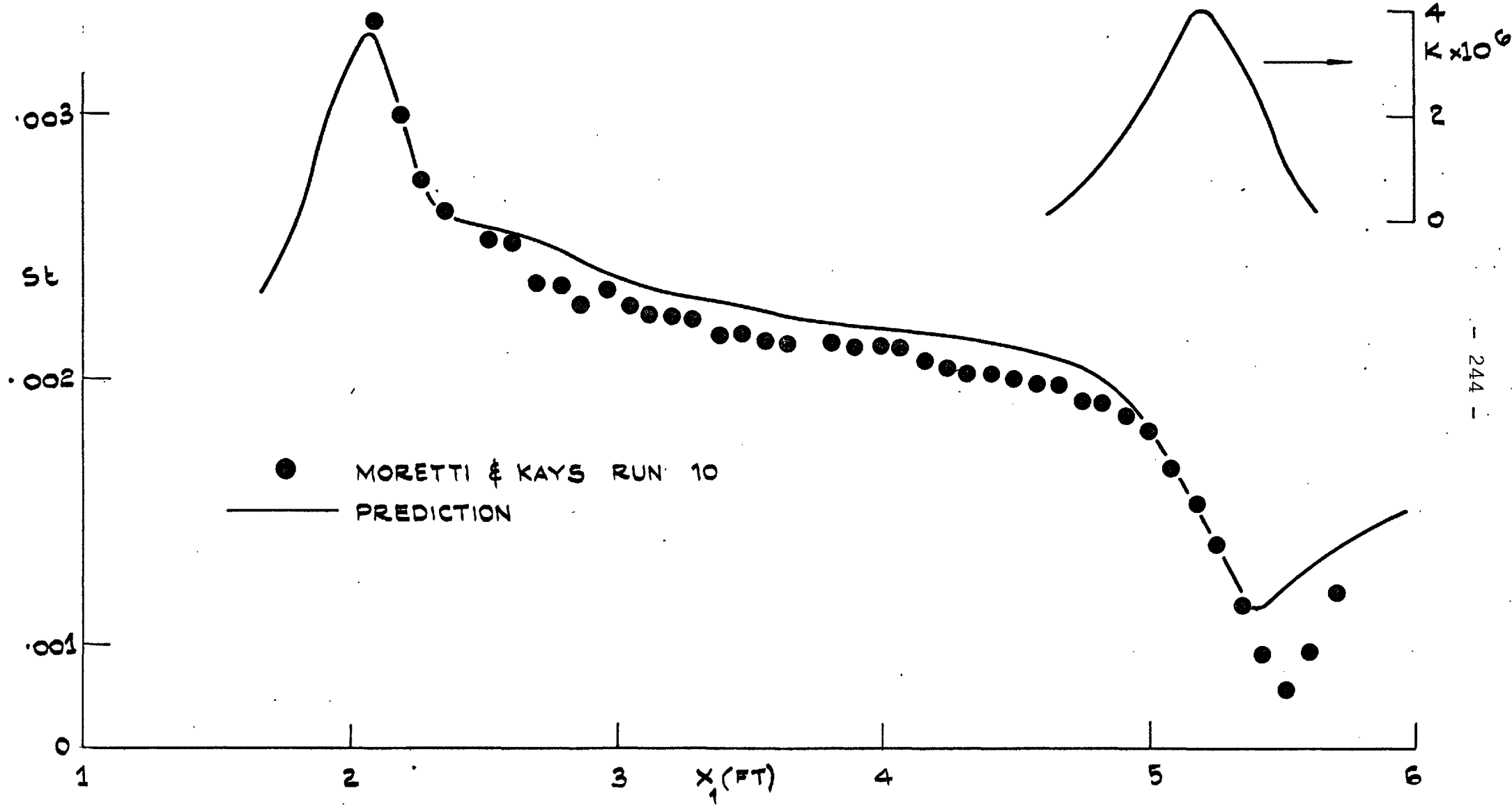

FIG. 4·23: VARIATION OF St WITH X_1

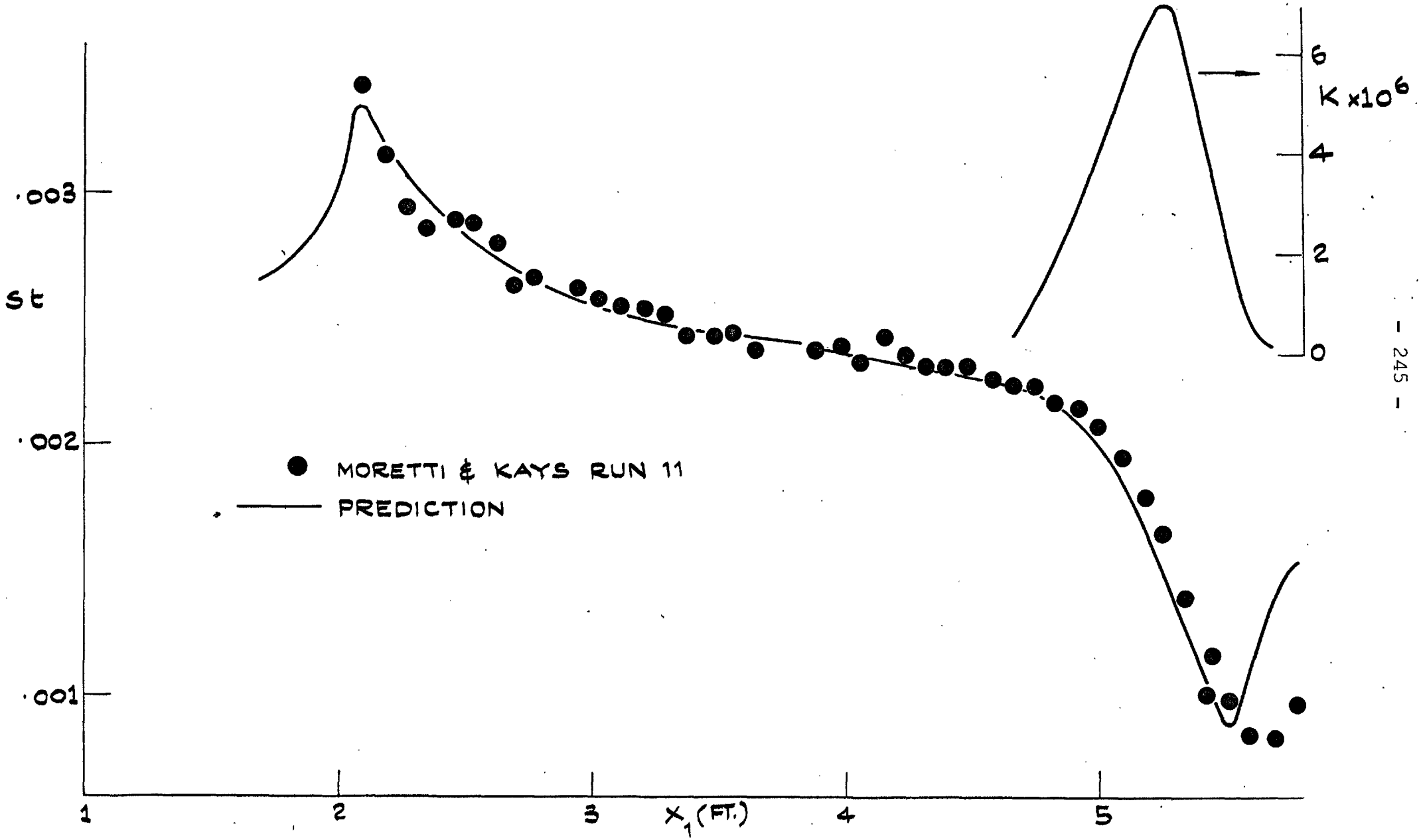

FIG. 4.24: VARIATION OF St WITH X_1

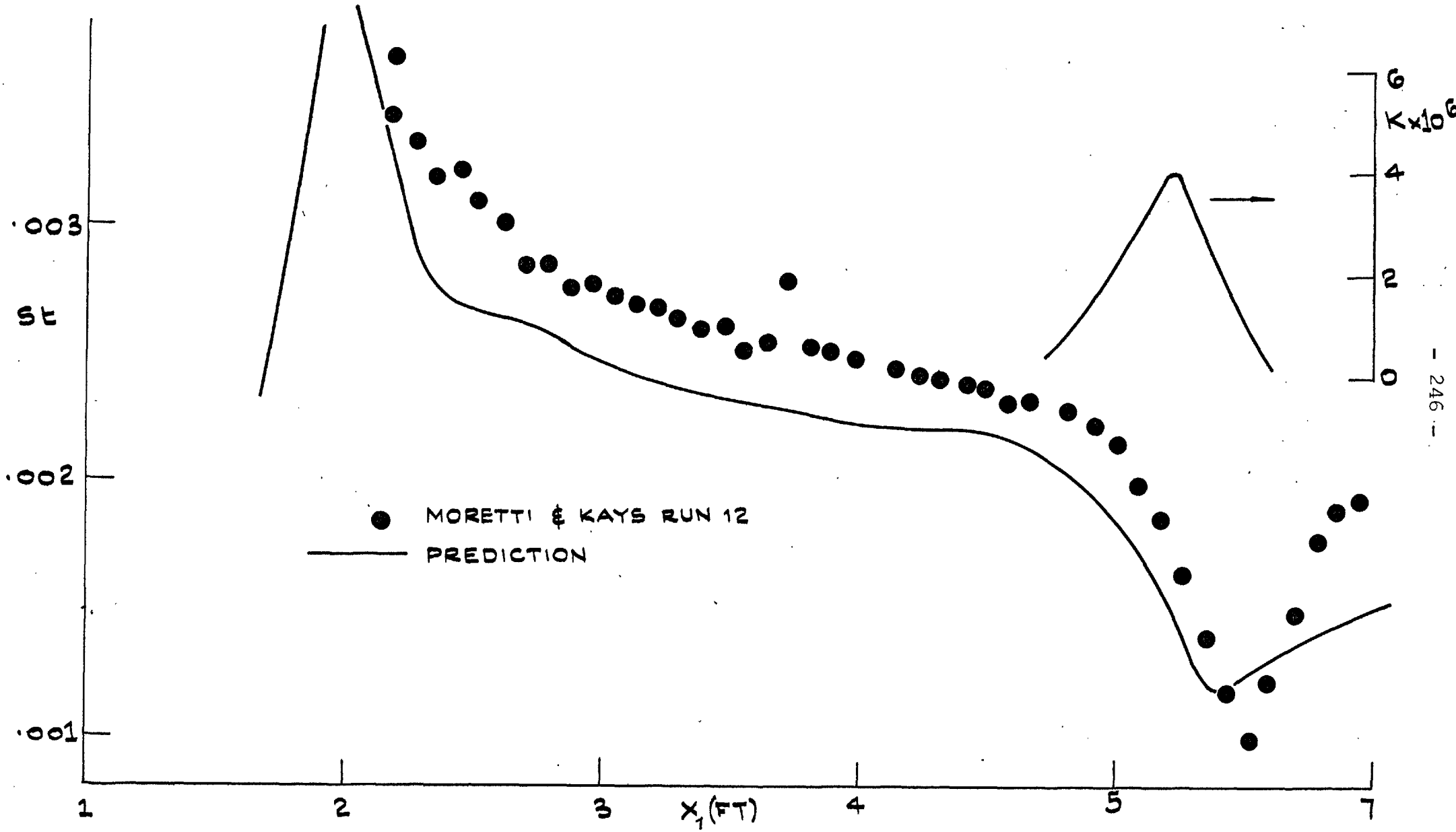

FIG. 4·25: VARIATION OF St WITH X_1

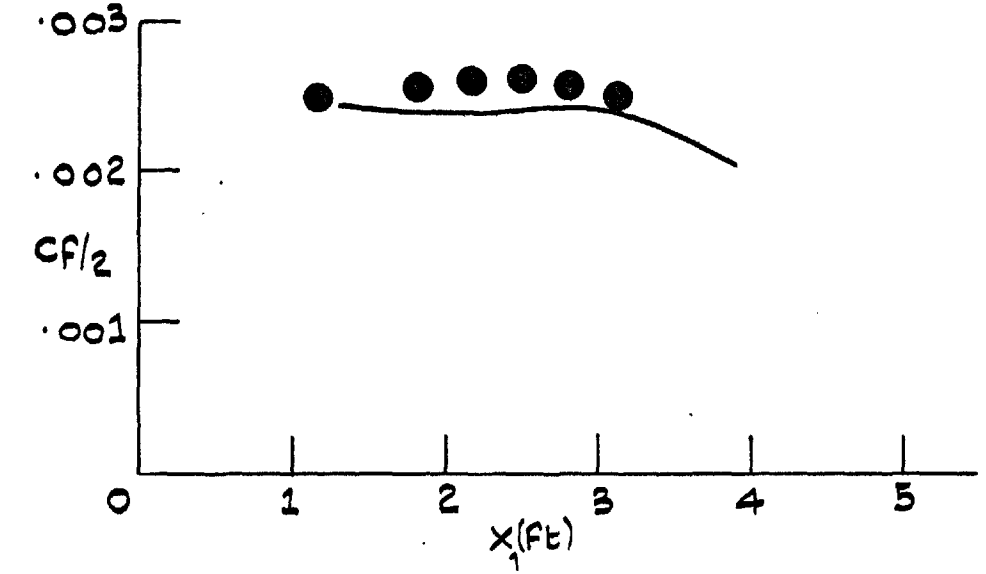

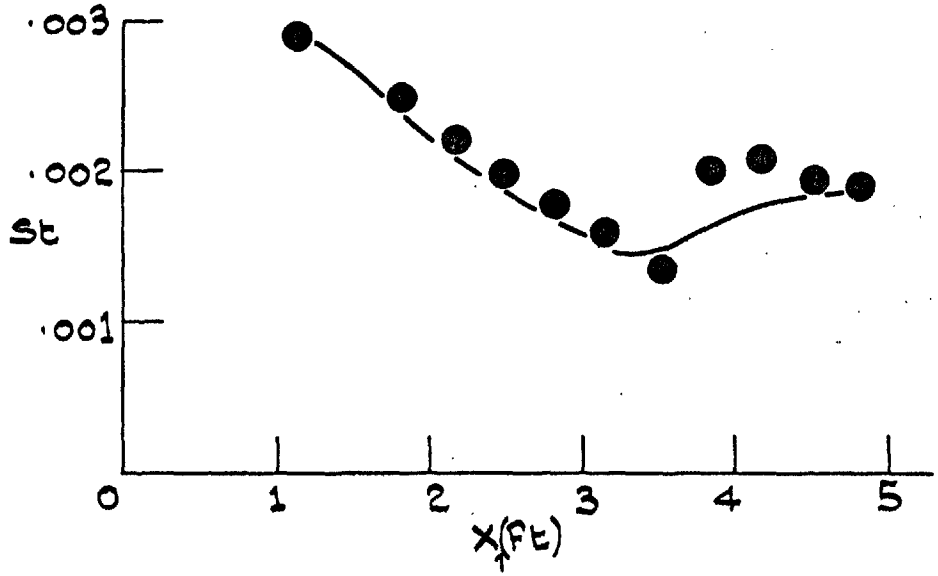

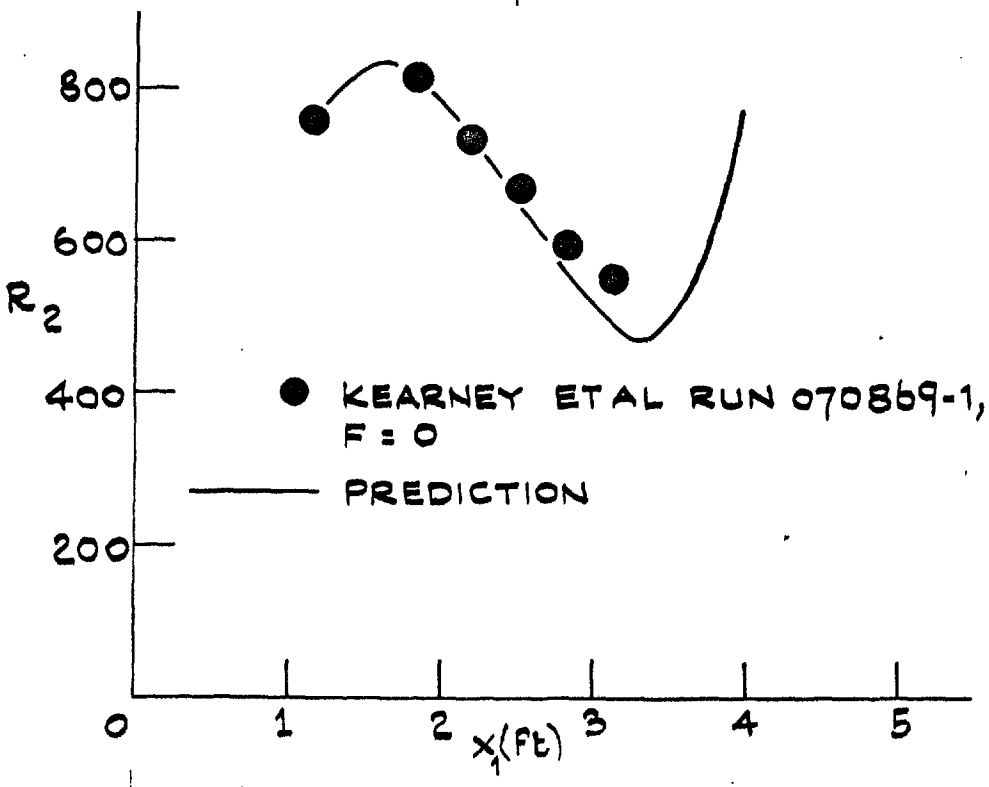

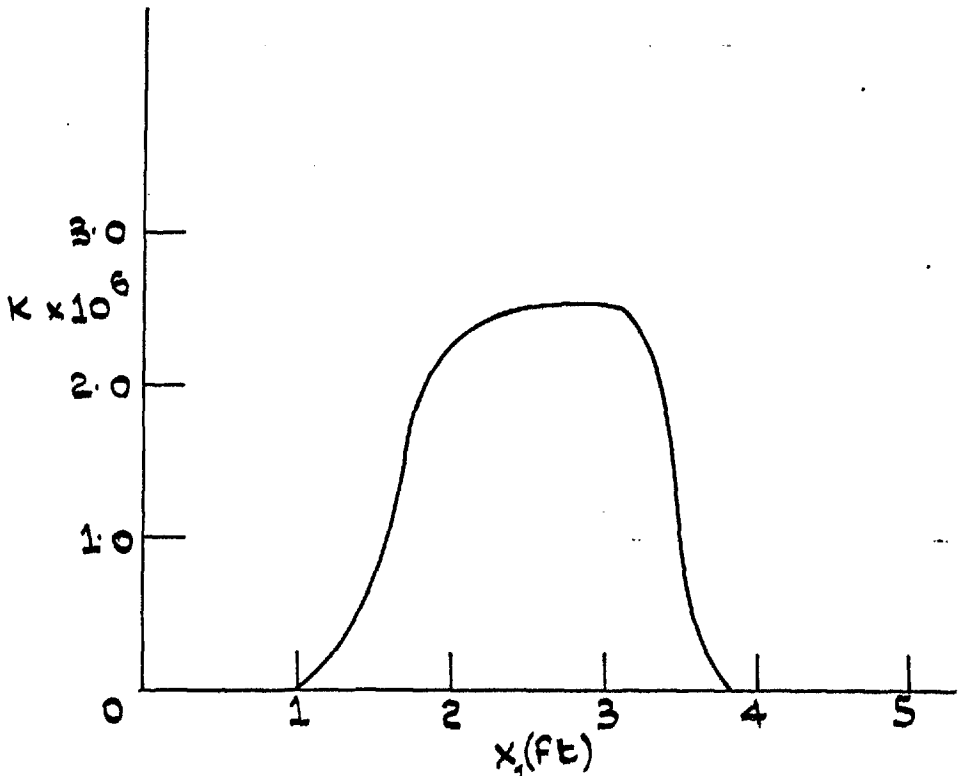

FIG. 4·26: ACCELERATED BOUNDARY LAYER WITH HEAT TRANSFER

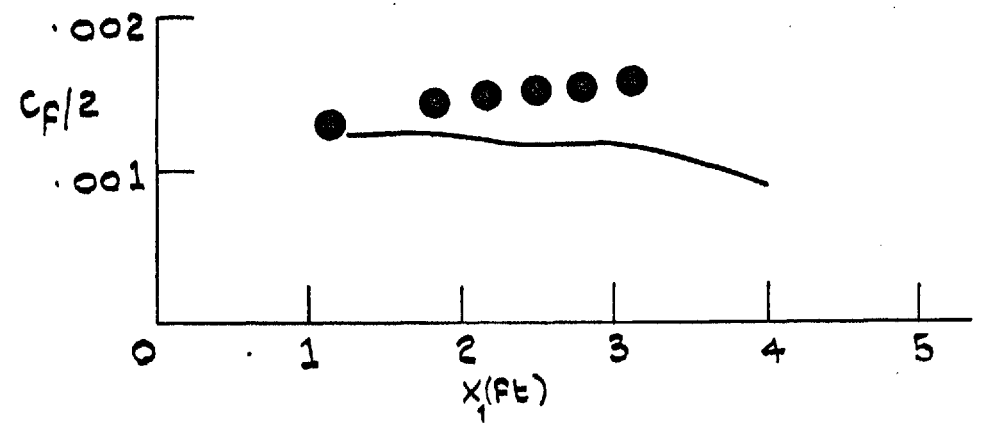

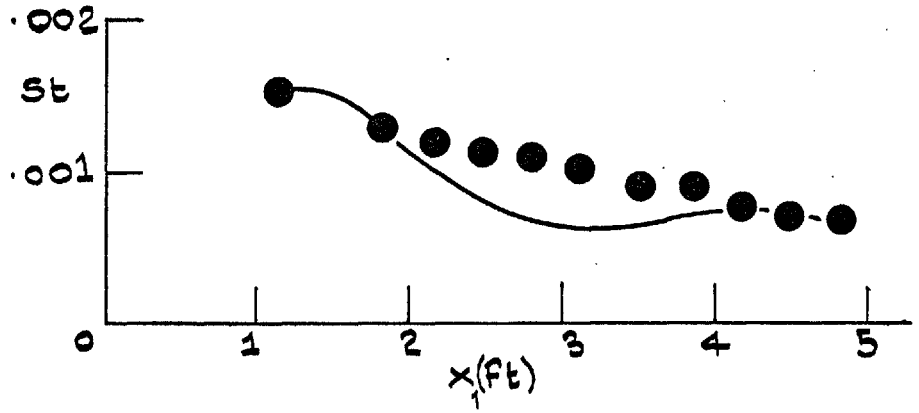

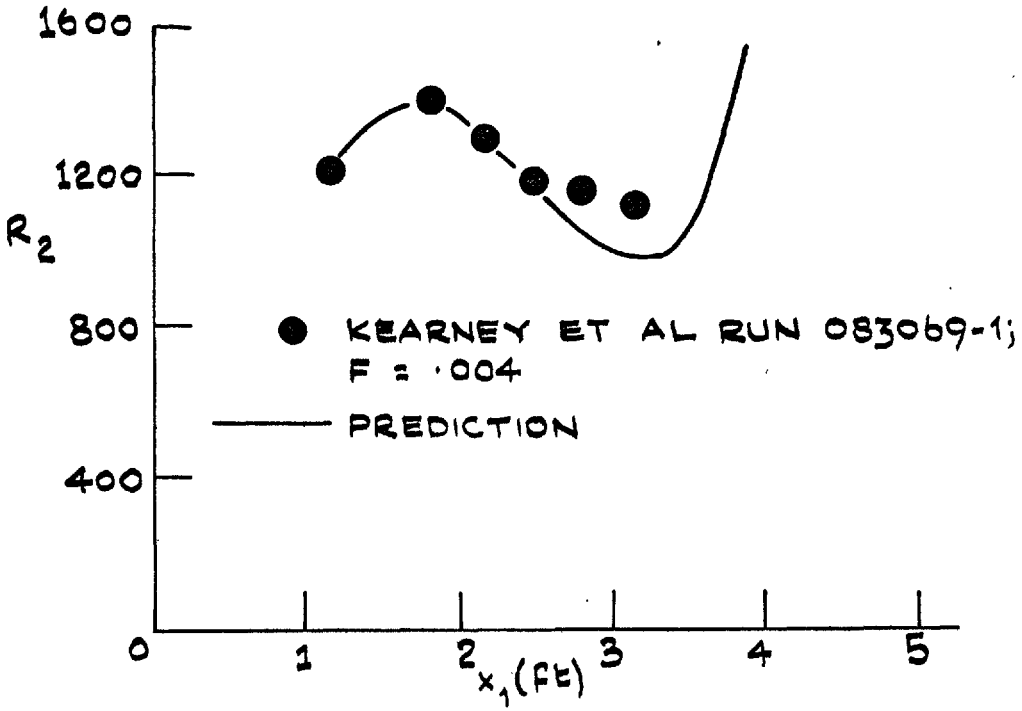

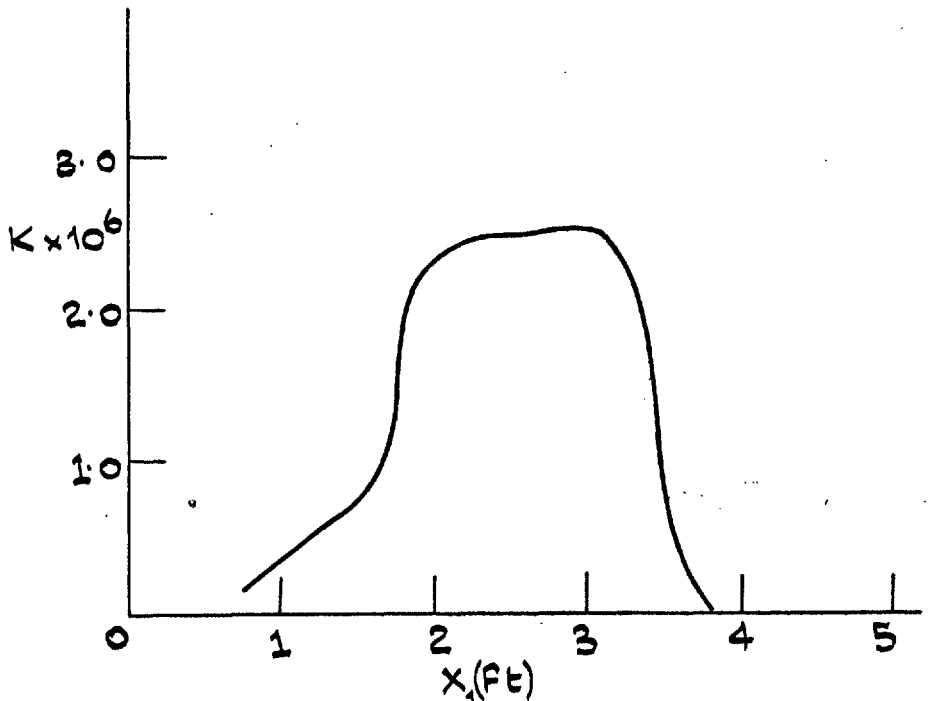

FIG. 4·27: ACCELERATED BOUNDARY LAYER WITH HEAT AND MASS TRANSFER.

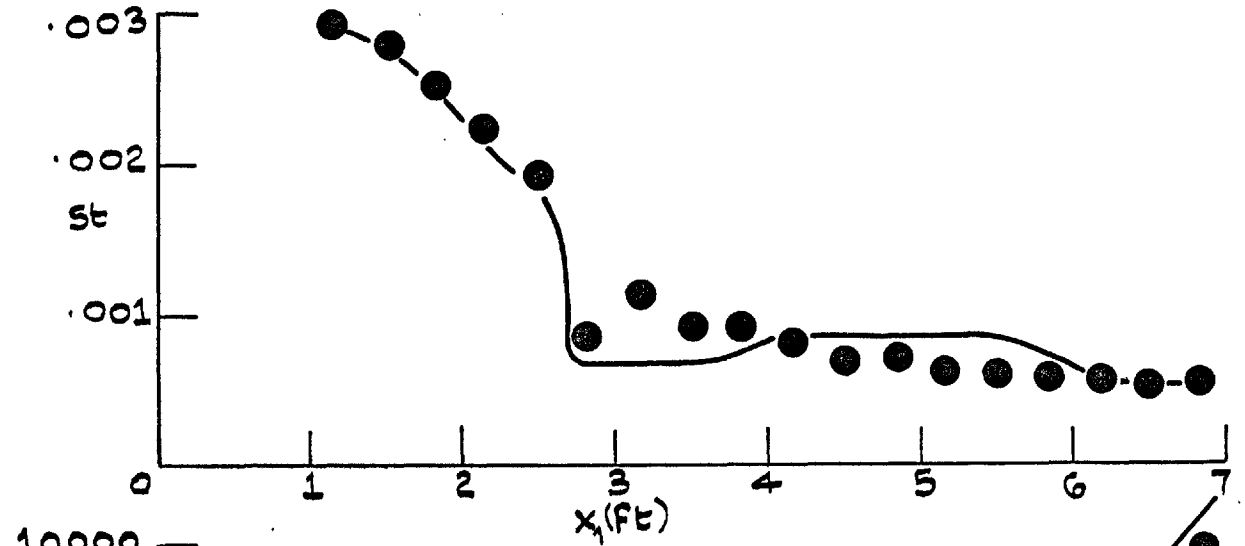

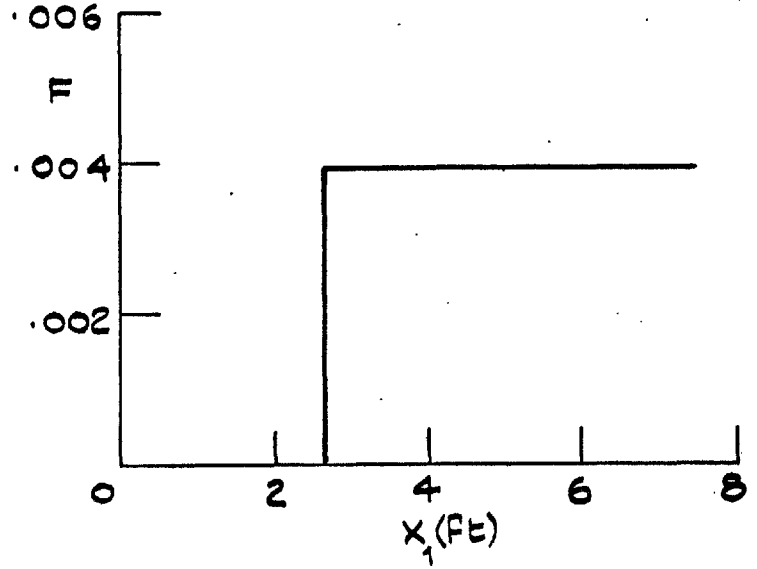

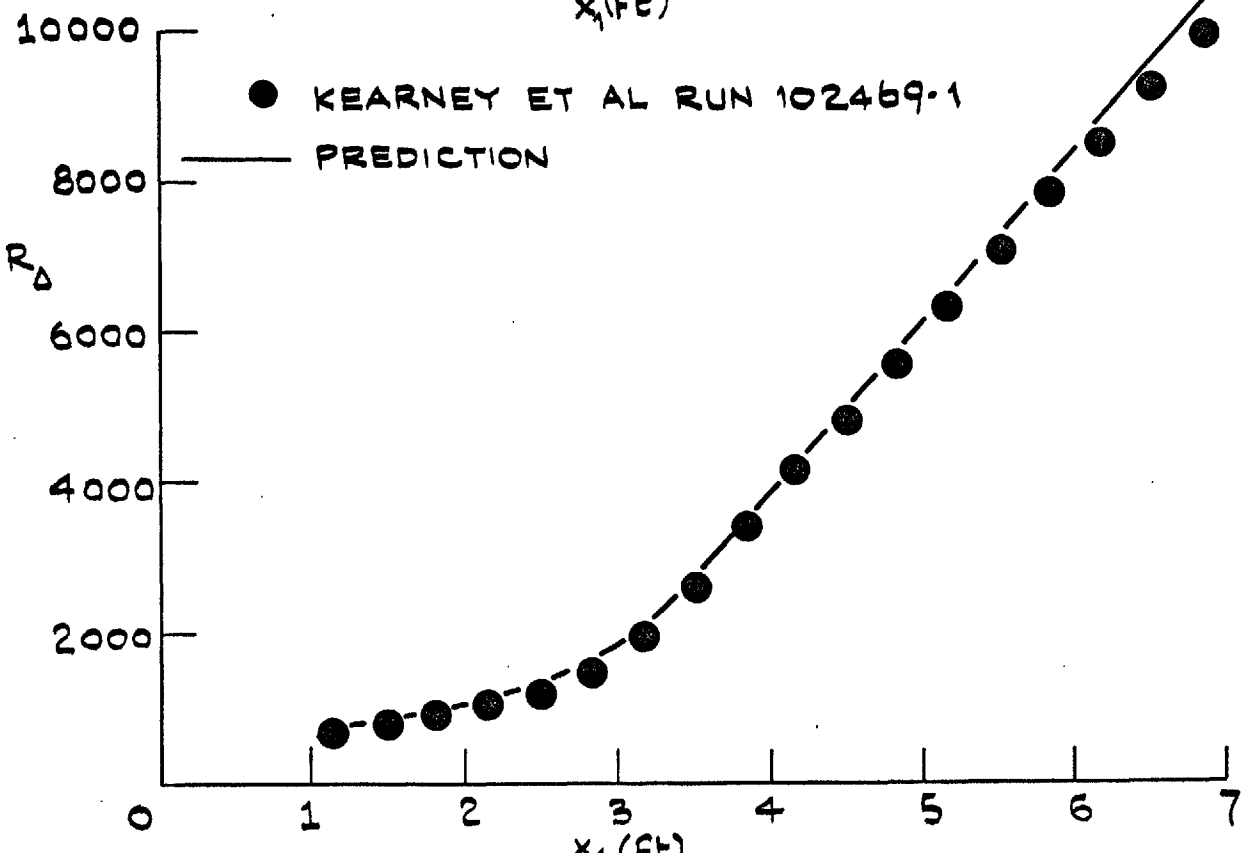

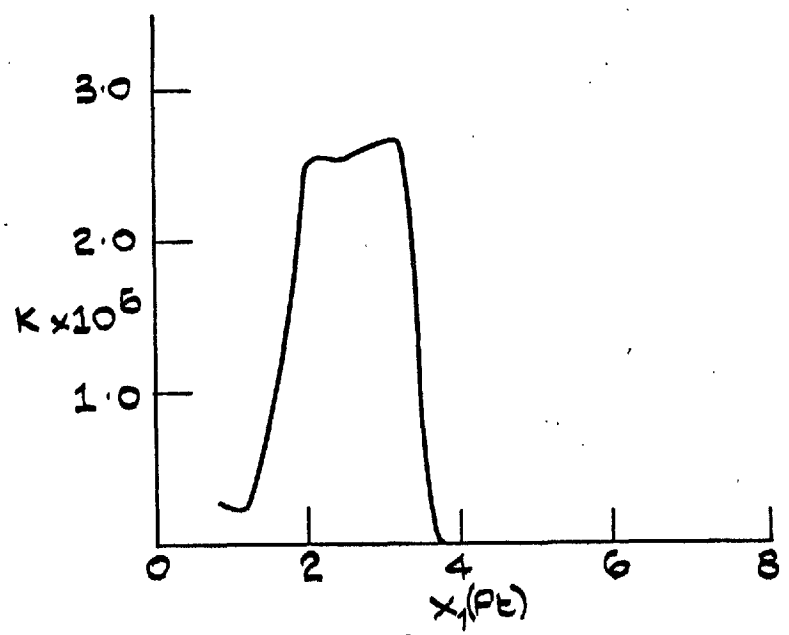

FIG.4.28: ACCELERATED BOUNDARY LAYER WITH HEAT AND MASS TRANSFER

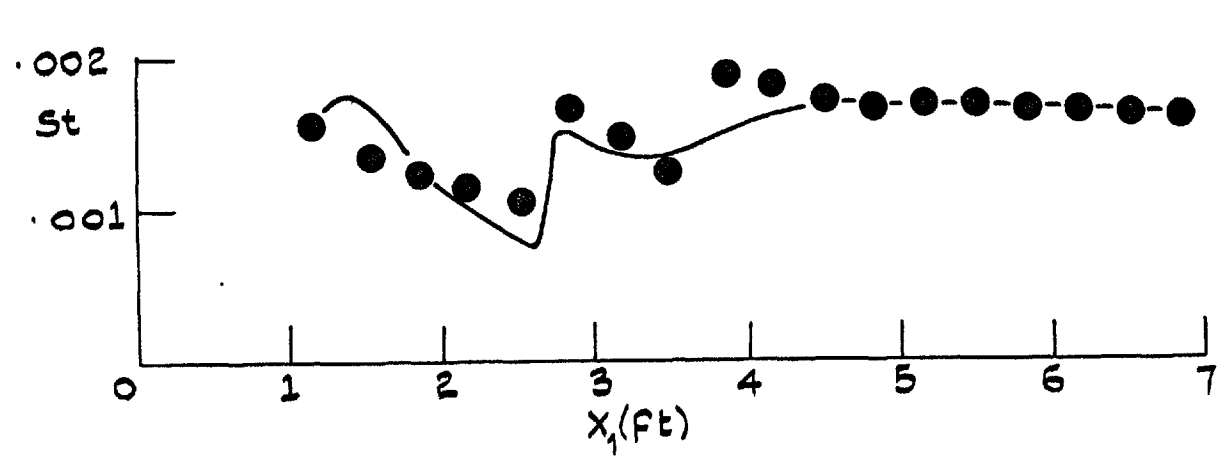

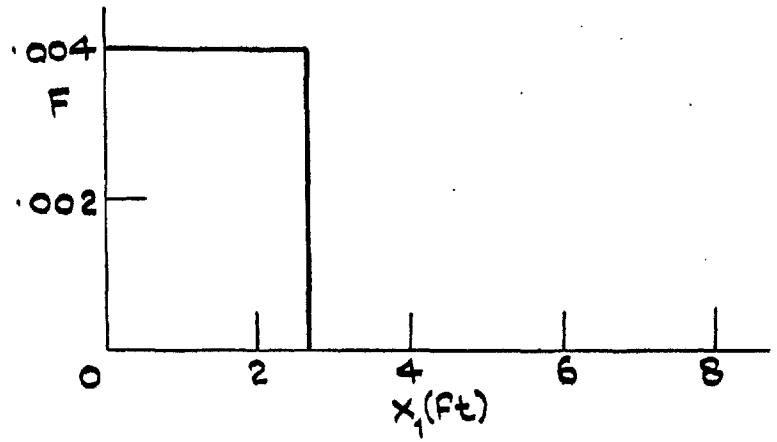

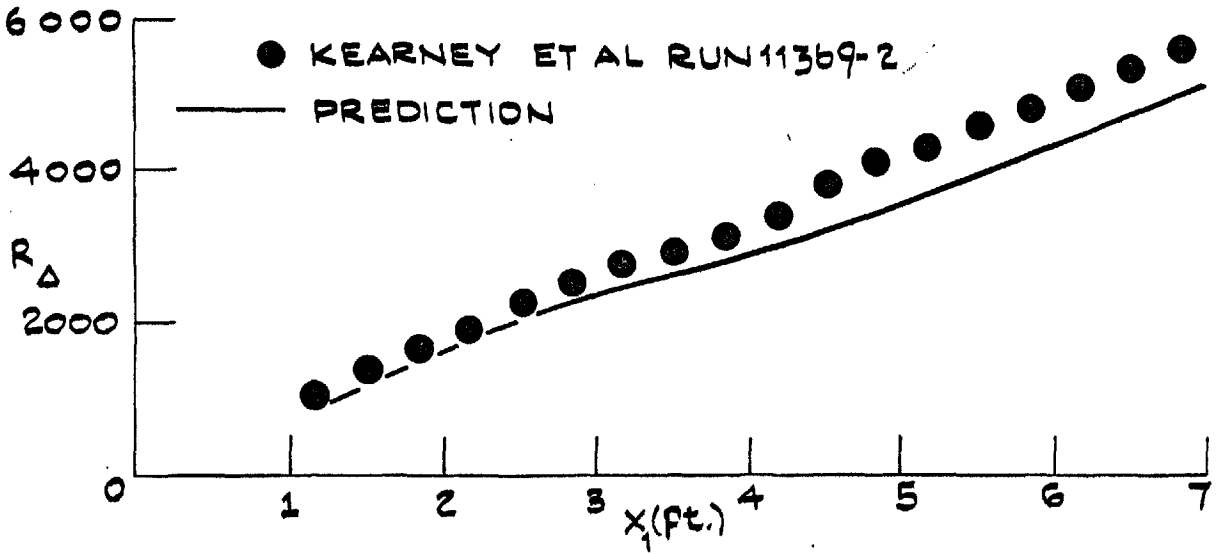

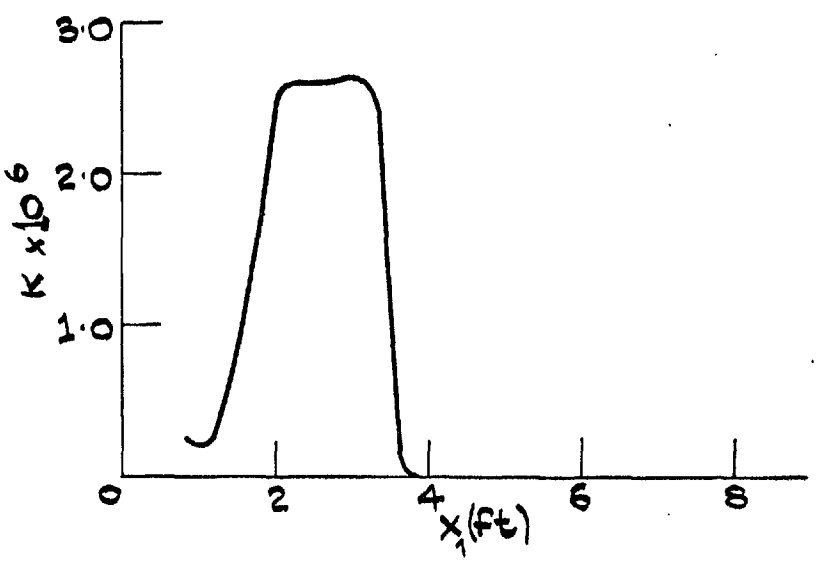

FIG. 4.29: PREDICTION OF HEAT TRANSFER DATA